Controls on the Coastal Environment and Their Changes under Climate Change: A Case Study for the Island of Okinawa in the Western Pacific

Ph.D. Thesis

Takeharu Ikema

July 2008

Department of Geography
The University of Sheffield

Acknowledgement

I would like to express my gratitude to all those who gave me the possibility to complete this thesis. I thank the Okinawa International Exchange and Human Resources Development Foundation for giving me the scholarship and their support for the stay abroad. I would like to thank Dr. Gong Ping Yeh from Fermilab, USA and Prof. Hayao Miyagi from the University of the Ryukyus, Japan who wrote the reference to the Department of Geography of the University of Sheffield.

I am deeply indebted to my supervisors Dr. Robert Bryant and Prof. Grant Bigg not only for their insightful and professional support for the research work but also encouragement that helped me in all the time of research and writing of this thesis. Discussions with them were highly valuable and stimulating.

My family in Okinawa supported the stay in UK. Their sincere encouragement and patience enabled me to complete this work.

Contents

List of Figures

Chapter 1

Chapter 2

Chapter 3

Chapter 4

Chapter 5

Chapter 6

Chapter 7

Appendix

List of Tables

Chapter 2

Chapter 3

Chapter 4

Chapter 5

Chapter 6

List of Acronyms

ARA: accumulated rainfall amount

AVHRR: Advanced Very High Resolution Radiometer

BOD: biological oxygen demand

CCW: Chinese Coastal Water

Chl-a: Chlorophyll-a

CDOM: coloured dissolved organic matter

CT: Category of Typhoon strength

D1: Domain 1 for EOF analyses

D2: Domain 2 for EOF analyses (sub domain of D1)

D3: Domain 3 for EOF analyses (sub domain of D2)

EAM: East Asian Monsoon

ECS: East China Sea

ENSO: El Niño – Southern Oscillation

FOC: Frequency of Occurrence

IPCC FAR: Intergovernmental Panel on Climate Change Forth Assessment Report

IPCC TAR: Intergovernmental Panel on Climate Change Third Assessment Report

KBC: Kuroshio Branch Current

KC: Kuroshio Current

LGM: Last Glacial Maximum

MODIS: Moderate Resolution Imaging Spectrometer

MOI: Monsoon Index

MCSST: multi-channel SST

NLSST: non-linear SST

OC4: Ocean Chlorophyll 4 (SeaWiFS algorithm to estimate chlorophyll-a concentration)

OGB: Okinawa General Bureau

OI: Optimum Interpolation

OPG: Okinawa Prefectural Government

OR: Ordinary Rainfall

SeaWiFS: Sea-viewing Wide Field-of-view Sensor

SLP: sea level pressure

SOI: Southern Oscillation Index

SPSS: Suspended Particle in Sea Sediments

SR: southern region

SS: suspended sediments

SSH: Sea Surface Height

SST: Sea Surface Temperature

T300: Typhoon event that approached the Island of Okinawa less than 300 km from Okinawa

TAR: IPCC Third Assessment Report

TE: T300 that involved the Island of Okinawa by their east sector

TN: total nitrogen

TN100: Number of Typhoons that approached the Island of Okinawa less than 100 km from Okinawa

TP: total phosphorus

TR300: Typhoon rainfall brought by T300

TSWC: Tshusima Warm Current

TW: T300 that involved the Island of Okinawa by their west sector

TWC: Taiwan Warm Current

W5: 5 grid cells on the West coast off the Island of Okinawa

YRW: Yangtze River Water

YSCW: Yellow Sea Cold Water

YSWC: Yellow Sea Warm Current

Abstract

Coastal environments are increasingly under threat due to the climate impacts associated with global warming and increasing terrestrial impacts through coastal development and inappropriate land management. As a result, a third of the world's coral reefs are facing the threat of extinction. In order to conserve and manage coral reef ecosystems, it is important to accurately assess the interactions of natural and anthropogenic (including climatic) stresses that are operating.

In this study, key controls on the coastal environment that affect the coral reefs around the Island of Okinawa, and changes in key controls under climate change, were investigated. Two satellite remote sensing data products were used to observe properties in coastal zone: (1) the AVHRR sea surface temperature (SST) for 1985 – 2006 and (2) the SeaWiFS ocean colour using the version 4 algorithm (OC4) to estimate sediment or nutrient loadings for 1998 – 2006. Empirical orthogonal function (EOF) analyses were employed at different scales, ranging from the large scale of the East China Sea to a small scale of the Island of Okinawa. It was found that solar radiation is the dominant control on the SST variability at all scales. For OC4, the 1st mode revealed that the winter East Asian Monsoon (EAM) is a primary control at all scales. Around Okinawa it was found that the winter EAM had a greater influence on OC4 as the terrestrial impact from the Yangtze River becomes less influential. Along the western coastal zone of Okinawa, it was found that the winter EAM is linked to sediment removal, and terrestrial impact is a secondary control on OC4 variability via river run-off. It was also found that the SST anomaly is strongly influenced by the outer ocean SST, indicating a larger scale control. Typhoons were found to be an important factor for OC4 anomalies.

An analysis using a probability distribution function of daily rainfall data in Okinawa (1982 – 2005) revealed that heavy rainfall has a statistically significant increasing trend due to more rainfall provided by a typhoon, rather than a rising number of strong typhoons approaching the Island. This suggests that sediment delivery to the coastal zone has been increasing, providing a combined climate/terrestrial, impact to the coastal environment. Although typhoons and heavy rainfall are episodic events, the lack of appropriate land management may delay natural recovery of the coastal ecosystem around the western Pacific, degrade its resilience, and lead to permanent change into a barren ecosystem. Given the negative impacts of warming ocean environment, typhoons' heavy rainfall, and sediment delivery, actions are needed both globally and locally to improve the marine environment.

Chapter 1 Introduction

1.1 Challenges Facing the Coral Reefs in the Western Pacific

Mankind obtains great benefit from coral reefs which: (1) provide living-space and subsistence fisheries for millions of people, who have developed unique cultures based around reef resources; (2) provide a livelihood for many people in the tropical and subtropical regions who obtain a considerable proportion of their food and earnings from the products of coral reefs or from reef-related activities e.g., tourism; (3) are particularly important geographic components of many countries as they support islands, protect fragile coastlines from wave and current erosion, permit the growth of mangroves and wetlands; (4) constitute a valuable resource for research as they have the highest diversity of any marine ecosystems (Wilkinson and Buddemeier, 1994). Although coral reefs comprise 600,000 km^2, less than 0.2 % of the ocean floor, it is estimated that more than 90 % of marine species are directly or indirectly dependent on them (UNEP, 2004). The economic value of coral reefs is estimated between US$100,000 to US$600,000 per km^2 (UNEP World Conservation Monitoring Centre, 2006).

About 40 % of the world's population lives within 60 km of the coast (UNEP, 2004). The coastal zone is an important sphere which supports humanity, and coral reef ecosystems also provide significant resources for people. However, coral environments are facing challenges from the serious threat of climate change and increasing human impacts. With such an integrated effect ranging from global to local, it is vital to understand their impacts. If multiple scale management for the coastal environment are not implemented without understanding the threats imposed by climate and humans, serious implications for sustainable development and loss of biodiversity may be expected.

In this chapter, basic biology of coral reefs, their relation to climate, increasing climatic and terrestrial impacts on coral reefs are introduced. Given the problems of coral reef environment with social importance, research aims and objectives are discussed.

1.1.1 Coral Biology

The majority of hermatypic corals (reef building corals) are found within tropical and subtropical waters. Hermatypic corals contain photosynthetic dinoflagellates (zooxanthellae) from the Symbiodinium genus. These are located in the gut lining and may number up to 30,000 cells/mm^3. In essence, the coral polyp provides: protection, living space and nutrients (CO_2, NO^{3-}, NH^{4+}), and the zooxanthellae provide: oxygen, food (e.g. glucose, amino acids), and

increased calcification. Coral colour is related to the existence of zooxanthellae pigments, so expulsion under conditions causing stress results in loss of pigment, or coral 'bleaching'. Hermatypic coral reefs typically occur between 30 °N and 30 °S latitudes (red dots in Fig. 1.1). The distribution and functioning of these coral reefs can be characterised as follows (Wilkinson and Buddemeier, 1994):

(1) reefs cover 600,000 km^2, (less than 0.2 %) of the global ocean floor (see Fig. 1.1).
(2) they are bounded by 20 °C isotherm, and tolerate water temperatures in the 18 – 40 °C range; with optimum growth at 23 – 29°C,
(3) they require salinity of 25 – 40 ppt,
(4) they require submersion – so are restricted to below low tide,
(5) they require low turbidity to allow high light levels and no clogging of polyp feeding mechanism.

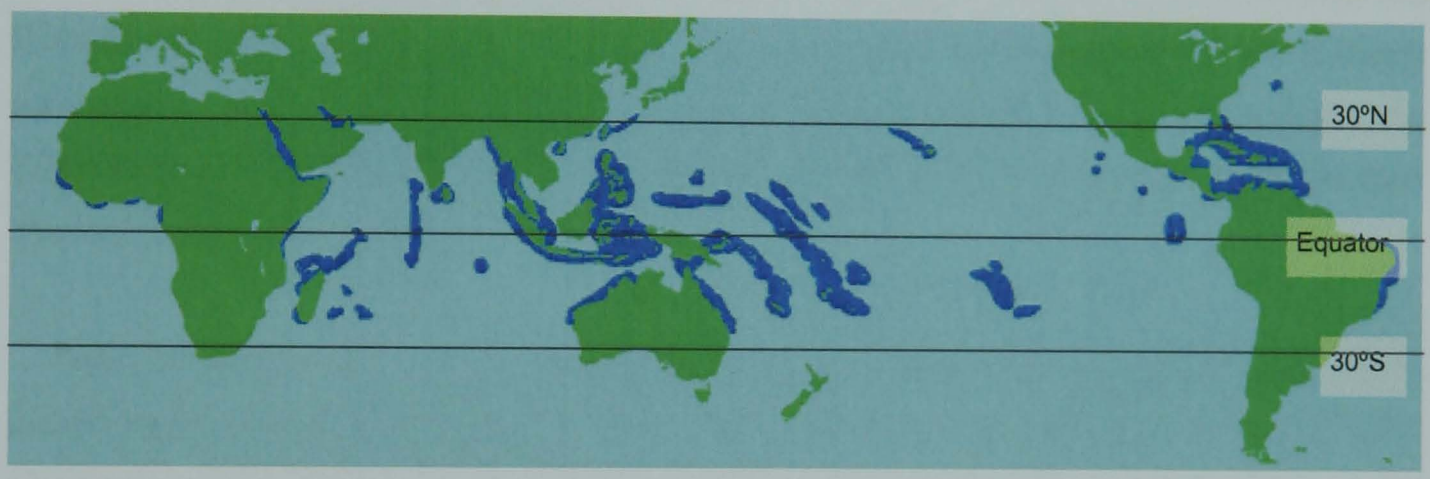

Fig. 1.1. Map of coral reefs (blue) in the world (World Wide Fund for Nature Japan, http://www.wwf.or.jp/shiraho/nature/nature1.htm).

As seen from Fig. 1.1, coral reef distribution is limited to warm water (tropical and subtropical) environments. However, any change in the optimum temperature range may significantly impact on corals growth, and cause stress to the delicate endosymbiotic relationship between coral polip and zooxanthellae. Transient temperature increases of only 1-2 °C above the local average maximum may prove lethal to many corals (Jokiel and Coles, 1990), and even smaller increase may result in bleaching (Glynn, 1993). Overheated corals also expel most of their zooxanthella and become pale or white (bleached). Because zooxanthellae require light for photosynthesis, coral reef communities are limited to shallow water. Light requirements and adaptation in corals are such that maximum rates of calcification and photosynthesis can be sustained down to depths of 20 m in clear water (Falkowski et al., 1990). Light penetration is significantly reduced by turbidity, so that the depth range of reef communities can be significantly reduced where water clarity is affected by either local organic productivity or suspended sediments (Chou, 1991). There are at least three adverse effects that

sediments may impact on corals via: (1) reef location on unconsolidated sediment which forms an unstable substrate for new coral settlement or reef formation, (2) acute stress from the smothering effects of rapid sediment deposition by terrestrial run-off and resuspension, and (3) chronic stress from an enhanced suspended load which reduces water clarity and light levels, hampering photosynthetic activities (McLaughlin et al., 2003). In addition, salinity levels below about 20 ppt for longer than 24 hours can be lethal for corals and most other reef organisms. Variations in salinity are not an issue for most oceanic reefs, but may control reef development in restricted lagoons where freshwater run-off or ground water discharge may be intense (Simith and Buddemeier, 1992).

1.1.2 Global Loss of Coral Biodiversity and Coral Bleaching

The full extent of the biodiversity of a coral reef is often difficult to assess because of the enormous number of different species packed into small areas (Norris, 1993; Wilkinson and Buddemeier, 1994). For the example of the Great Barrier Reef, there are more than 400 different coral species, about 4000 shells and thousands of different sponges, worms, crustaceans and echinoderms: within this ecosystem there are at least 1500 species of fish (Great Barrier Reef Marine Park Authority, 1989).

These invaluable coral reefs are showing sings of rapid degradation at a global scale due to human impact and climate change. In the report of *Status of Coral Reefs of the world: 2004* (Wilkinson, 2004), it was estimated that 20% of the world's coral reefs have been destroyed and show no immediate prospects of recovery; 24% of the world's reefs are under imminent risk of collapse through human pressures; and a further 26% are under a longer term threat of collapse. In the next three decades 60 % of the world's coral reefs are considered at a significant risk of being lost (UNEP, 2004). To date, the majority of damage to coral reefs around the world has been through direct anthropogenic stress (Alcala et al., 1987; Grigg and Dollar, 1990; Wilkinson, 2002, 2004). The major causes of damage are excessive pollution from industrial and agricultural waste, and poor land-use practices which increase sediment and nutrient delivery to the coastal zone. As outlined above, high sediment loadings will impose acute stress on coral communities because of the smothering effects of rapid sediment deposition. Frequent loadings will therefore lead to chronic stress resulting from low light levels, hampering photosynthetic activities. Coral reefs subjected to high nutrient levels may also deteriorate due to increased turbidity from plankton within the photic zone, reduced coral recruitment, and overgrowth by filamentous algae. The growth of reefs often diminishes significantly along a gradient from oligotrophic to eutrophic conditions within affected coastal zones (Hallock, 1988).

Apart from anthropogenic impacts, coral reef growth is fundamentally linked to climate. For example, reefs often grow over previous reefs that have been killed off during massive sea level falls during ice ages. The stony corals gradually build up the calcium carbonate framework until the reef reaches the sea surface, where atmospheric exposure limits further upward growth (Wilkinson and Buddemeier, 1994). Therefore, coral reefs will respond to climate and climate change. Although climate change will directly stress coral reefs, reefs may change their spatial distribution rather than disappear entirely (Hughes et al., 2003). However, present rates of change in climate are likely to have serious impacts on coral and on those who significantly depend on coral reefs. For example, increased sea temperatures (e.g. El Nino) cause coral bleaching. If thermal stress is severe and prolonged, most of the corals may die due to lack of nutrient and food supply from zooxanthella (Yamazato, 1999; Hughes et al., 2003). Episodes of bleaching have already increased greatly in frequency and magnitude over the past 30 years (e.g. Hoegh-Guldberg, 1999). Furthermore, tropical cyclones are an important factor that can both cause physical damage to and influence the structure of coral reefs (Massel and Done, 1993). Therefore, changes in the distribution, frequency, or intensity of tropical cyclones may also have major effects on the structure and growth rate of coral reefs (Lough, 1994). In fact, strong storm occurrence has been reported to be in an increasing trend over 1970 – 2004 over the western Pacific (Webster et al., 2005).

It is not only the direct influences of climate change but also the interactions of these impacts combined with anthropogenic activities that will most likely lead to a synergistic increase in the global change in coral reef distribution and survival. Changes in weather patterns and associated increases in rainfall for example, will dramatically change the flux of nutrients, contaminants and sediments to coasts, and make coral reefs more vulnerable to climate and anthropogenic activities on adjacent coasts and in drainage basins (Wilkinson and Buddemeier, 1994). Consequently, it may be possible that acute stress events will become so large and so frequent that they block effective coral recovery, leading to widespread coral mortality. Unfortunately, human pressures are increasing. Poor land management practices are causing more release of sediment, nutrients and other pollutants to the coastal zone, and coral reefs around the world are expected to continue to decline (Wilkinson, 2004).

1.1.3 Coral Reefs of the Western Pacific

Among the coral reefs in the world, the reefs in the western Pacific should serve as a primary focus with respect to both understanding and mitigating against losses of coral reef biodiversity (Wilkinson and Buddemeier, 1994; Wilkinson, 2002, 2004). In particular, Southeast Asia harbours the highest diversity and productivity of corals and associated organisms in the world's

oceans (Veron, 1993; Burke et al., 2002). Fig. 1.2 shows the global distribution of reef-building corals species, and indicates that the highest diversity occurs in Southeast Asia. The coral reefs in Southeast Asia occupy 32.3 % of the global total of coral reef area. The potential economic value of well-managed coral reefs in this region is estimated at 42.5 % of the global total of US$29.8 billion attributed to coral reef values (Wilkinson, 2004). However, human pressures are also both serious and increasing in Southeast Asia; 88 % of coral reefs in are at medium to very high threat from human impacts (Wilkinson, 2002). By far the most serious human threats are destructive practices e.g., dynamite and poison fishing, and overfishing in general, followed by coastal development, and increased sedimentation and pollution (Wilkinson, 2002). Although active management initiatives are being implemented throughout the region, threats to coral reefs remain high and are dominated by the impact of anthropogenic these factors (Wilkinson, 2004). Under such situations, an extensive monitoring effort to establish a regional standardisation of methods, data archiving, analysis, and interpretation are required to conserve coral reefs in Southeast Asia (Wilkinson, 2004).

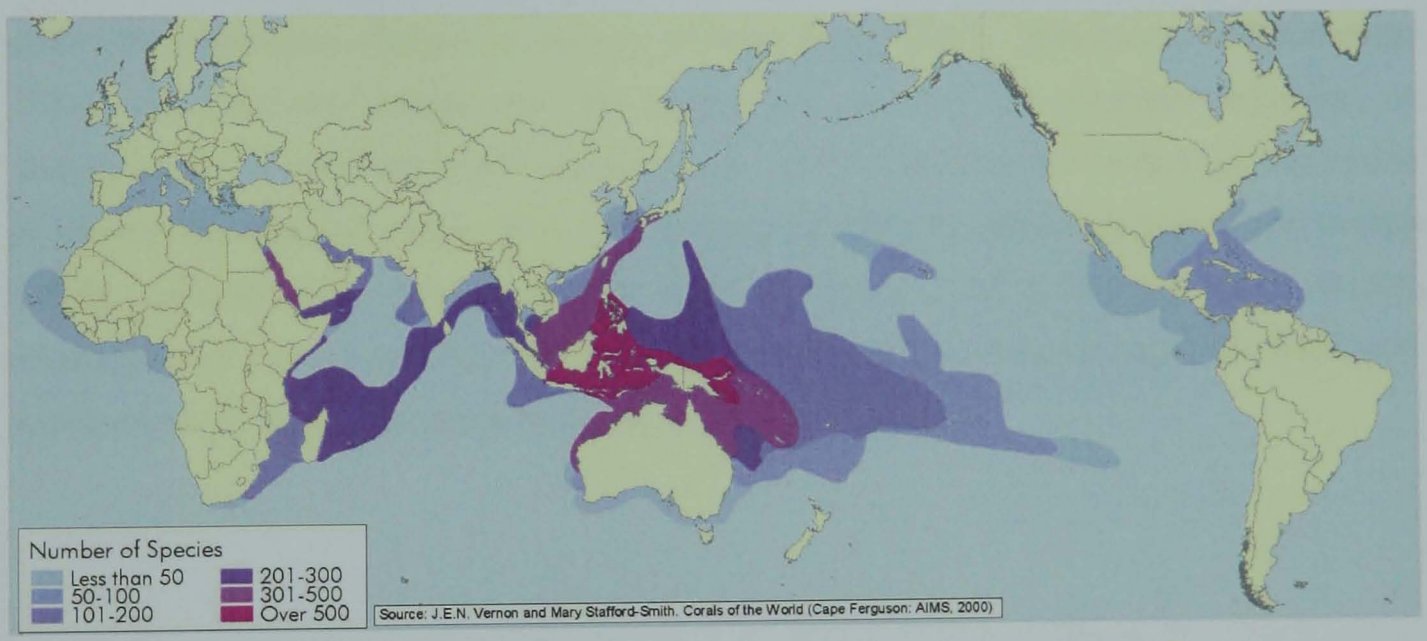

Fig. 1.2. Patterns of diversity in reef-building corals (from Burke et al., 2002).

Coral reefs in East and North Asia (China, Taiwan and Japan) in the western Pacific lie just north of the global centre of biodiversity of coral reefs in Southeast Asia; those of Japan and Taiwan are, in particular, influenced by the Kuroshio Current which carries coral larvae from this centre (Wilkinson, 2002). Biodiversity is therefore higher in the southern part of this region. Well developed coral reefs occur off all the southern Ryukyu Islands of Japan. Under the influence of the Kuroshio Current, a wide range of coral reefs around these Islands exhibit some of the highest biodiversities in the world, with notable and rare endemic species (Roberts et al., 2002). However, sedimentation from terrestrial run-off also represents a serious threat to these corals. Nearly 80 % of the reefs in East and North Asia have been damaged from human impacts and there has been no change since 2002 (Wilkinson, 2004).

In the western Pacific, the main factors controlling regional climate is the Asian monsoon, which provides seasonal wind and rainfall over Asia and the western Pacific. In the ocean, the temperature is strongly affected by El Niño-Southern Oscillation (ENSO) which impacts coral reefs. Coral bleaching in this region often correlates with abnormally high seawater temperatures or prolonged summer peak seawater temperatures, frequently during El Niño years (Brown and Odgen, 1993). Interactions between these climate effects with anthropogenic activities are likely to produce a combined and enhanced impact on coral reefs. Under a range of climate change scenarios reported by IPCC Fourth Assessment Report (Solomon et al., 2007), there are likely to be more severe stresses on coral growth in the future; with rapid changes in weather patterns being predicted (i.e. direct changes to rainfall, tropical cyclones and seawater temperature). These effects operate from global to local scales. Therefore, it is very important to assess the combined impact of these effects in order to suggest better management and conservation of coral reefs. However, research into assessing the combined role of climate and local factors affecting coral reefs is extremely rare. Most coral reef research is *parochial* and *short-term* in nature (e.g., Nakano, 2002; Tada et al., 2003), and provides little insight into global or longer-term changes or forcing (Hughes et al., 2003). Wilkinson and Buddemeier (1994) state that the management and conservation of reefs are extremely dependent on identifying and controlling chronic (long-term i.e., climate) stresses, and on accurate assessment of interactions between climate and anthropogenic stresses. For the coral reefs of the western Pacific, understanding climate and anthropogenic effects are therefore the major research challenges that exist at present, and our ability to tackle these research issues will have direct implications for better management of coral reefs in the future.

1.2 Research Questions

As described above, the growth of coral reefs has been inherently and intricately linked with climate. Changes in climate will affect coral reefs in the future as they have been shown to be important in the past during the formation phases of major global reefs. A major question at present is the degree to which both climate and anthropogenic factors affect the coastal environment that impact coral reefs, and how climate change will interact with the anthropogenic effects to increase their impact on coral reefs. In many respects, this is also a problem of scale, as what is true in terms of long-term global averages (representing climate change) may bear little relationship to what is happening now at any particular location (e.g. the western Pacific)

The problems of understanding the factors affecting coral reef biodiversity and growth are also scale-related (Hatcher et al., 1987). Long-term scales (e.g., seasonal cycles including monsoons) are important in the structuring of coral reefs. Short-term scales are also important because coral reefs are also strongly influenced by events such as daily tidal cycles and storms. Climate change obviously occurs at a long-term scale, and it is anticipated that there will be changes in the intensity and distribution of tropical cyclones (Houghton et al., 2001). It has also been predicted that the geographic range of tropical cyclone storms will expand polewards, and that their frequency and intensity will also increase (Ryan et al., 1992). Areas presently in or adjacent to zones of tropical cyclones may therefore experience increases in storm damage. Such regions may also experience increased rainfall that will enhance terrestrial run-off, loaded with both sediment and nutrients, to coral reefs. The impact on coral reefs through anthropogenic effects (e.g., poor land management) may belong to the short-term scale. However, sediment and nutrient delivery have components related to both climate processes and anthropogenic effects; particularly in the islands of the western Pacific where human stresses (population expansion and increased pressure on resources) are high. Therefore, climate and both regional and local controls on coral mortality are likely to interact strongly. *What is needed therefore is a detailed understanding of the degree to which both climate and anthropogenic impacts on coral reefs will change in response to climate change.* Focusing on the western Pacific, where coral reef biodiversity and economic value are high, the following research questions are raised:

Question 1

What are the key climatic and terrestrial, including anthropogenic controls on the coastal zone of the western Pacific at both regional and local scales for the period of available satellite data (1985-2006 for the SST and 1998 – 2005 for the ocean colour in this study), and to what extent do the key controls contribute to observed variability of the coastal zone for the period of available data in this study (1982 – 2005)?

Question 2

To what extent do extreme events e.g., typhoons impact on the coastal zone?

Question 3

What long-term changes in key climatic controls are linked to climate change; winds for 1988 – 2005 and rainfall for 1982 – 2005 in this study?

Question 4

What are the implications of changes in key climatic controls for coral reefs in the western Pacific?

To answer these questions, a case study will be undertaken in a region where both representative climate and terrestrial controls are found for the western Pacific. In this thesis, the Island of Okinawa, Japan, in East Asia was chosen for a case study as the Island is under the influence of the East Asian Monsoon and of regular typhoon visits. In addition, the coral reefs around the Island have been damaged through soil run-off and the impact of sediment which has been a major coastal environmental problem in the Island (Omija, 1987, 1992, 2002). In order to monitor sediment impacts on coral reefs in Okinawa, a local standardised monitoring of sediments has been established, and extensive records have been collected around the Island. These data provide important records to enable evaluation of the terrestrial impact on the coastal zone. Moreover, through the influence of the Kuroshio Current connecting oceans in Southeast Asia, coral reefs around Okinawa have high biodiversity that needs to be conserved (Robert et al., 2002; Wilkinson, 2004).

1.3 A Case Study: The Island of Okinawa

The Island of Okinawa is the main Island of the Ryukyu Islands in East Asia, and is located at about 26 °N and 127 °E; forming the most southwestern part of Japan in the western Pacific (Fig. 1.3). The Ryukyu Islands are the only subtropical islands in Japan under the administrative district of the Okinawa Prefectural Government (OPG). Other major islands, Miyako, Ishigaki and Iriomote, lie further south of the Island of Okinawa. There are 160 islands (49 inhabited and 111 uninhabited: Statistics Bureau, 2000) in total within the OPG, stretching for about 1100 km, and forming the eastern boundary of the East China Sea (ECS) along with Amami Island of Kagoshima Prefecture. The climate over Okinawa is greatly influenced by one of the most distinct monsoon systems in the globe; the East Asian Monsoon (EAM). The word "monsoon" originates in the Arabic word "*mausim*" which means season (Webster, 1987a), so the EAM brings alternating wind systems over East Asia. The winter EAM originates in the huge anticyclonic Siberian High, providing northwesterlies in Japan and northeasterlies in central and eastern Asia. The summer EAM develops over the warm Pacific Ocean, bringing southwesterlies over central and eastern Asia, with rainfall. On the Island of Okinawa, strong, cold and dry northeasterlies prevail during winter, and weak, warm and moist southeasterly flows during summer, the latter providing the rainy season. Throughout the year, the Kuroshio Current (KC) flows in the Okinawa Trough west of Okinawa, bringing warm water from the

central North Pacific as an extension of the North Equatorial Current. This warm current is also a very important factor that renders the climate of Okinawa as subtropical. On the Island of Okinawa, an annual mean temperature reaches 23 °C, with a maximum of 29 °C in July and minimum of 17 °C in January (climatology at Naha City, south Okinawa, derived from the data provided by the *Japan Meteorological Agency* for 1982 – 2006). In addition to the rainy season brought by the summer EAM, typhoons during summer and autumn supply considerable rainfall to Okinawa.

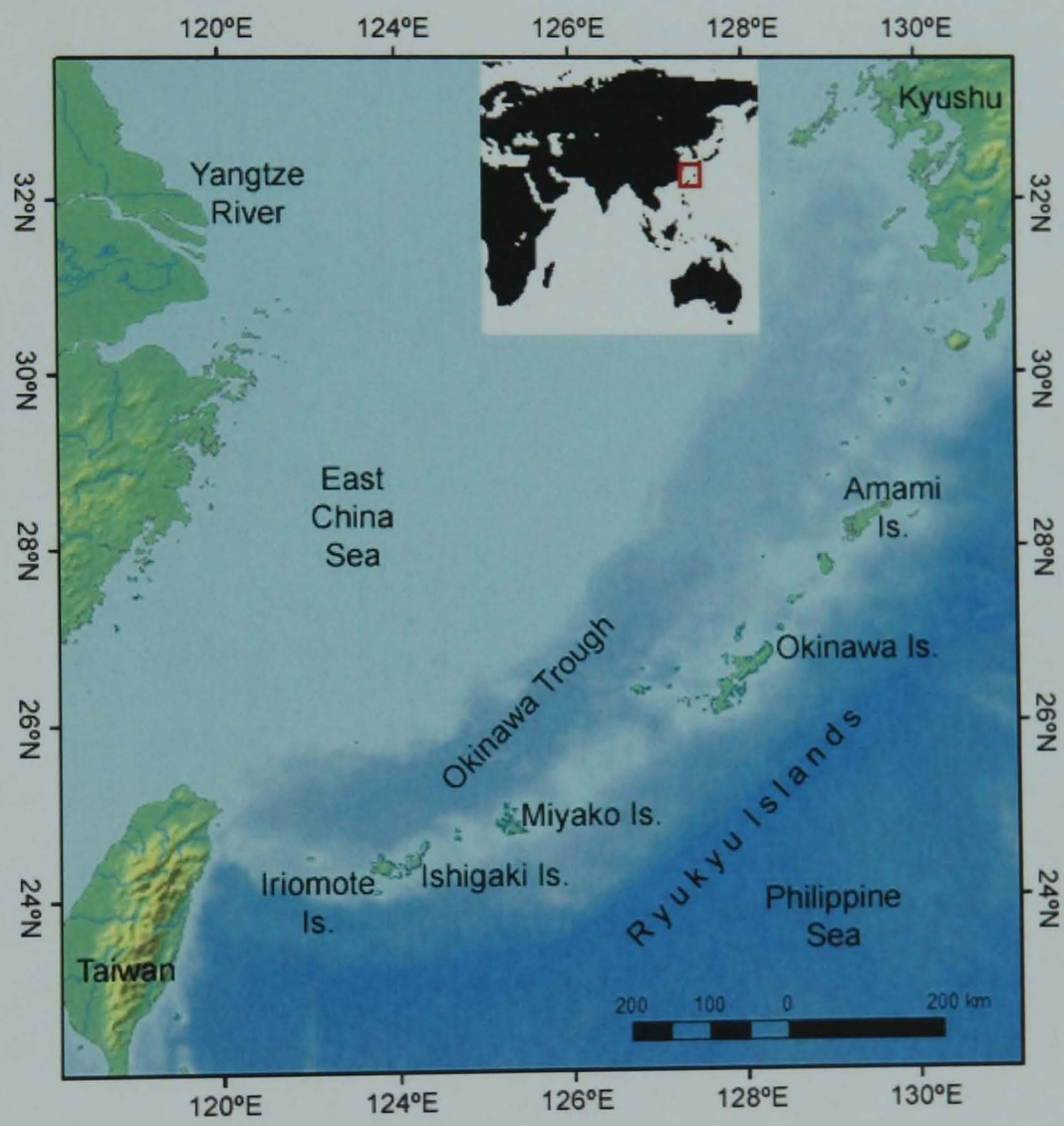

Fig. 1.3. Location of the Island of Okinawa and its surroundings.

The KC, one of the largest currents in the ocean (Gross, 1990), flows through the Okinawa Trough, which is a distinctive depression of 2000 m depth off the shelf. It provides a distinctive coastal environment around Okinawa within the East China Sea (ECS). Over the continental shelf in the ECS, ocean temperature is colder than off the shelf due to cold water inflow from the Yellow Sea, Chinese coastal water and the strong winter EAM (Mask and O'Brien, 1998). The continental shelf waters are also largely affected by the river discharges from the Chinese coast, particularly from the 3rd largest river in the world, the Yangtze River, and hence highly sediment and nutrient loaded compared to off the shelf. On the other hand, the KC provides a warm and oligotrophic environment, and the Okinawa Trough traps the sediment delivered from the continental shelf (Kao et al., 2003). Thus, waters in the off-shelf region are much less turbid.

These combined effects offer favourable conditions for coral reefs to develop – the water is warm and transparent enough, enabling photosynthetic activity to the shallow sea bottom around the Ryukyu Islands (Ujiie, 1991). The KC also brings the waters from Southeast Asia, the global centre of biodiversity of coral reefs, and hence there are abundant coral species around the Ryukyu Islands (Wilkinson, 2002). Okinawa enjoyed the combination of subtropical climate with abundant rainfall and a rich coral reef environment until the mid-20th century.

In the 1950s, Okinawa started to experience rapid development, leading to degradation of the land surface through significant introduction of pineapple fields which triggered serious soil erosion (Onaga et al., 1999). In the 1970s, a series of infrastructural developments occurred on the Island, such as dam construction, land reformation, tourism infrastructure constructions and agricultural land improvement. All were largely implemented without consideration of their impact on the delicate corals and subtropical vegetation of the Island. As a consequence, soil erosion and run-off were drastically enhanced, and coral reefs were observed to be degraded. Particularly, heavy soil run-offs have damaged the coastal coral ecosystem and impacted on the fishery and tourism industries. These problems have been recognised as leading to a most serious public nuisance, known as "red-soil run-off pollution" because of the reddish colour of the major soil "*Kunigami maji*" in the Island of Okinawa, locally termed "*Akathuchi*" (Omija, 1992). Since these problems came to light, extensive monitoring and research have been implemented around the coast of Okinawa to understand sediment delivery and deposition (e.g., Omija, 1992; Higa et al., 1995a; Nakasone et al., 1998). In 1985, an index to evaluate the sediment concentration was developed by Omija (1987). This measurement has been implemented since then as a locally standardised monitoring method to evaluate the status of the coastal environment. This monitoring technique has also been transferred to trainees from coral islands in developing countries through training courses organised by a Japanese governmental agency.

In order to mitigate soil run-off, the "Red-soil Ordinance" was legislated by the OPG in 1995 which regulates the sediment concentration in the discharge from the developing sites on land. Since the implementation of the Ordinance, sediment delivered to the coast of Okinawa has been reduced, due to reduced run-off from land development (Omija et al., 2002). However, this ordinance does not apply to agricultural fields. The run-off prevention method for agricultural fields has not been widely implemented due to the required additional cost and labour. To date, significant amounts of sediment are still delivered to the coast through run-off, stressing the coral reefs of Okinawa (Omija, 2004). Not only sediments but also nutrients are carried in this run-off. Omija et al. (2003) reported that the coastal zone with higher nutrient concentrations have smaller coral coverage, and suggested a negative impact of nutrient on coral.

Fig. 1.4 shows the coral coverage along the coast of Okinawa. These corals have been degraded by heavy soil run-off and sediment accumulation in the coastal zone, and the coral coverage has been declining[1]. In addition, impact from an extreme climate event has imposed considerable damage to these corals. Most regions experienced coral bleaching in 1998 due to the strong El Niño in 1997/98, and live corals were significantly reduced.

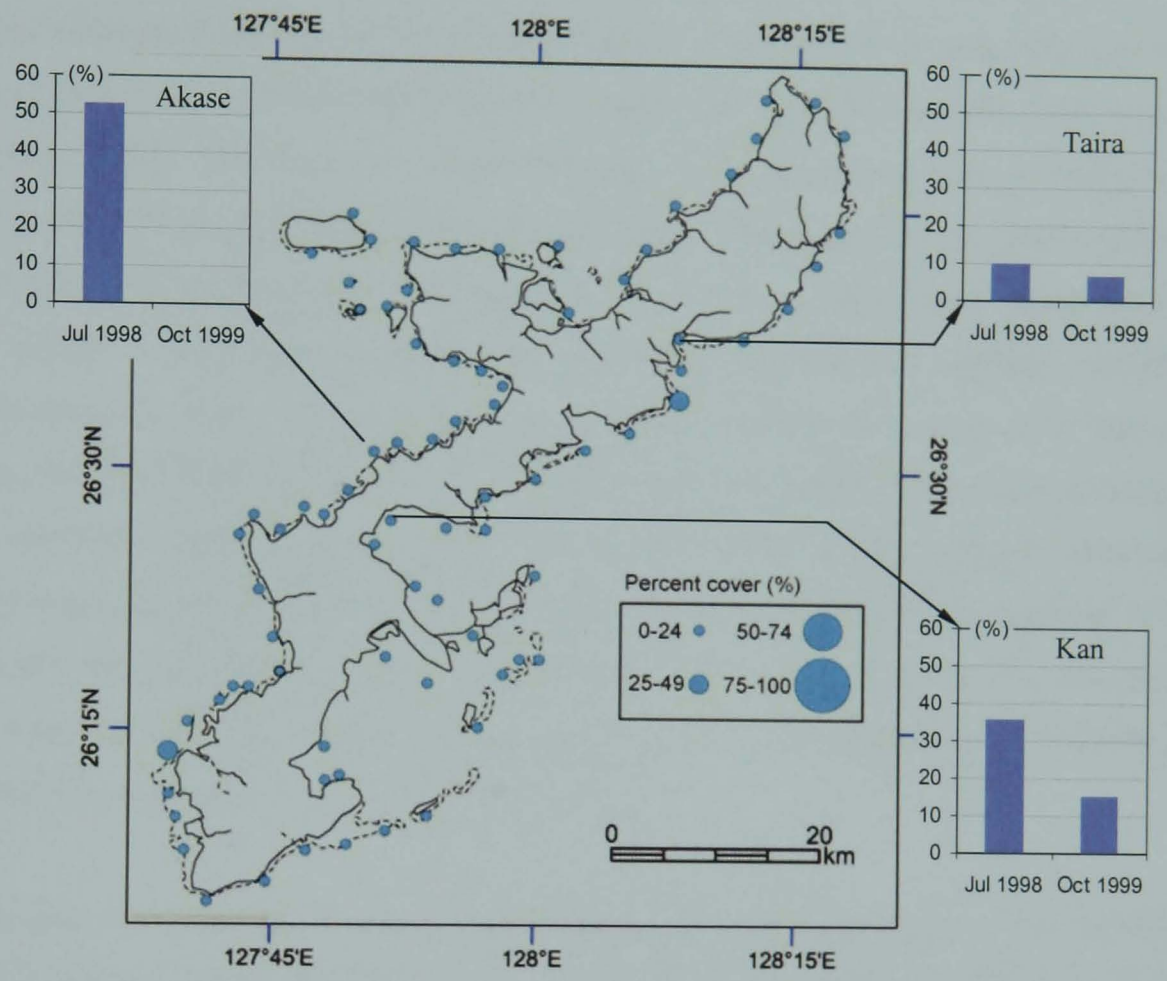

Fig. 1.4. Coverage of hermatypic corals in the coast around the Island of Okinawa in a survey. Coverage presented in circles are the survey carried out by the *OPG Environment Conservation Division* in 2003. (adapted from the Japanese Coral Reef Society and Ministry of Environment, 2004). Bar graph shows the difference in coverage (%) by Omija et al. (2000) before coral bleaching event (Jul 1998) and after (Oct 1999).

The bar graph in Fig. 1.4 shows the difference in coral coverage (Omija et al., 2000) in July 1998, before the event of the strong El Niño that caused anomalous high sea temperature around Okinawa, and in October 1999, after the significant coral bleaching event. In the western region, corals in Akase had about 50 % coverage before the bleaching event, but all of the corals died in the event. Under a global warming scenario, increasing sea temperature may trigger more frequent coral bleaching event, which would leads to a degradation of corals' resilience (Hughes et al., 2003).

[1] A survey of coral coverage around the Island was carried out in early 1990s. However, the monitoring method is different (e.g., measuring the coverage in a quadrat or averaging over transect), which makes it difficult to compare quantitatively here.

Typhoons are regular events during summer to autumn around the Ryukyu Islands. There are 7.7 typhoons per year which close to within 300 km of the Islands for 1982 – 2005, according to the *Japan Meteorological Agency* (JMA). JMA (2005) investigated typhoon occurrence for 1977 – 2004 whose wind intensity stronger than 33 m/s, and reported that the number of these typhoons ranges between 10 – 20 and no increasing or decreasing trend was seen. JMA (2005) also investigated the number of typhoons which maintained the same intensity (≥33 m/s) and proceeded northward beyond 30 °N, 35 °N and 40 °N. The number of such typhoons beyond 30 °N showed pronounced peak in 2004, however, apart from this, the numbers show no noticeable trend (JMA, 2005). The impact of these typhoons is significant, providing strong winds and heavy rainfall. The strong winds cause not only forest disturbance on the land surface but also physical damage to coral reef structure through impact from wind-induced waves. This effect of these winds is a natural process, providing long-term occasional and episodic control on coral structural development through pruning or substrate renewal; which in turn may aid coral reproduction (Highsmith, 1982). However, typhoons' heavy rainfall over a poorly managed land surface may also provide a combined climate and anthropogenic impact, enhancing both sediment and nutrient supply via increased run-off to the coast. Although typhoon winds are a driving force for sediment and nutrient transport that can remove sediment and nutrient from the coastal zone, Omija (1994) reported that sediment input is often greater than sediment dispersal at some location in Okinawa during typhoon events.

In this way, the climatic and terrestrial components of the hydrologic cycle interact to have major effects on coral reefs close to land. Given these processes i.e., climate and terrestrial processes, there will be a range of variabilities related to ocean properties which affect coral reefs e.g., temperature, sediment and nutrient concentrations, influenced by the EAM, typhoons, and sediment and nutrient input from the land of Okinawa. Being under the influence of the EAM and with the data relating to sediments around Okinawa available since the mid 1980s, the Island of Okinawa offers an ideal geographical setting to study the related effects of both climate and terrestrial controls on coastal environment status. Implications of this research for coral reefs of Okinawa will also be applicable throughout Southeast Asia and the western Pacific, where their invaluable coral reefs are under the influence of the EAM and typhoons, and significant human threats. Therefore, the coastal zone of the Island of Okinawa is selected as a study area of this thesis.

1.4 Research Aims and Objectives

To understand the terrestrial impact on coral reefs, soil run-off problems in the Ryukyu Islands, including Okinawa, have motivated many researchers to study geophysical processes on

land, e.g., soil erosion and run-off modelling (Onaga and Yoshinaga, 1983; Paringit and Nadaoka, 2003; Ohnuki and Shimizu, 2004; Sakai and Osawa, 2005), and coastal zone observation, e.g., sediment monitoring (Omija, 1987; Higa et al., 1995b; Nakasone et al., 1998; Omija et al., 2002). These studies are focused mostly on local scale. However, a large scale and long-term integrated study are rare. Okinawa Island is surrounded by a very active atmospheric/oceanic system, the EAM, one of the largest ocean currents, the Kuroshio Current, and the continental shelf that is largely influenced by the 3rd largest river in the world, the Yangtze River in China. Therefore, in identifying key climate and terrestrial controls on the coastal zone, an understanding of the spatial extents of key controls ranging from the ECS to the local scale of Okinawa is important. Although, variabilities related to ocean properties (e.g., the sea surface temperature, sediments and nutrients) have been studied at a fixed scale in the ECS (e.g., Milliman et al., 1985; Hama et al., 1997; Gong et al., 2003), influences at the regional scale of the ECS on the coastal zone around Okinawa have not yet been studied. At the local scale of Okinawa, Nadaoka et al. (2001a) investigated sea temperature variability in the coastal zone for a limited number (2) of months, and therefore hardly investigated the long term climate influence of the EAM. The suspended sediment survey carried out by the OPG provides useful data to monitor the terrestrial impact on the coast, but Omija et al. (2003) suggested an integrated approach is needed to evaluate the variability and impact of sediments which come from multiple scales.

In order to identify key controls on the coastal zone environment at large (e.g.,, the ECS) to small (e.g., Okinawa) scales, and for a long-term periods, large spatial coverage and consistent temporal observations, will be necessary. In this, satellite remote sensing is a useful (and perhaps the only) technique to observe important ocean properties for coral reefs; i.e. the sea surface temperature (SST) to estimate water temperature in coral environment; and the ocean colour to estimate sediment or nutrient loadings in the coral reef ocean through observed phytoplankton blooms. Therefore, key controls on the SST and ocean colour prevailing in space and time over the western Pacific around the Island of Okinawa can be substantiated using remote sensing data. Hence remote sensing data of the SST and ocean colour are major datasets used in this thesis. Remote sensing observations for the SST and ocean colour have been operated since the 1980s. Data for 10 – 20 years will be used in this study and the variability examined here will be confined to this period.

An important climate factor over the western Pacific, including the Island of Okinawa is the EAM. The winter EAM brings strong northerlies which cause cooling, upwelling and mixing in the ocean. The summer EAM brings the rainfall season which causes terrestrial run-offs, delivering sediments and nutrients to the ocean adjacent to the land. Over the continental shelf

in the ECS, the ocean colour variability near the Yangtze River estuary is significantly affected by the large discharge from the Yangtze River loaded with sediments and nutrients, which is modulated by the rainfall brought by the summer EAM (Milliman et al., 1985; Ichikawa and Beardsley, 2002; Gong et al., 2003). At the local scale of the coastal zone around Okinawa, West and van Woesik (2001) reported that the quantities of sediment and nutrient differ not only with the discharge volume but also with population and land-use in the catchments.

In this way, it is likely that the winter EAM modulates the regional SST and ocean colour, and the summer EAM affects the ocean colour through interaction with terrestrial components. However, the actual variability of the SST and ocean colour may exhibit different patterns and be dependent on different controls at scales ranging from the entire ECS to the small Island of Okinawa. Research challenges here are to identify the key climate and terrestrial controls, and to clarify the degree to which key controls affecting the coastal environment may evolve with scale. Provided with research questions associated with social importance, the overall objective and aims of this research are set down as follows:

Overall objective

To understand key controls on the coastal environment around the Island of Okinawa at both regional to local scale, and to understand their changes and impacts on coral reefs in the western Pacific.

Aim 1

To identify key climate controls on the SST and ocean colour in the western Pacific and the coastal zone around Okinawa.

Aim 2

To identify impacts of the terrestrial controls on the SST and ocean colour on the coastal zone around Okinawa.

Aim 3

To assess impacts of typhoons on the SST and ocean colour on the coastal zone around Okinawa.

Aim 4

To clarify relationships between key controls and the variability of sediment concentration in the coastal zone around Okinawa.

Aim 5

To clarify observed changes over time in key controls, and their impact on the coral reefs around Okinawa.

1.5 Thesis Structure

This thesis consists of 7 chapters including this introduction and their outlines are as follows.

Chapter 1: Introduction

Importance of coral reefs in coastal zone and need for understanding key controls are discussed in this chapter. A case study of the Island of Okinawa, research questions, aims and objectives are described.

Chapter 2: Key features of Climate, Ocean and the Island of Okinawa

Key climate and terrestrial controls on the SST and ocean colour are described in this chapter. It provides explanations of the EAM, ocean currents in the ECS and the characteristics of the Island of Okinawa.

Chapter 3: Data, Methodology and Preliminary Analysis

Description of data – satellite data, climate data, and geographic data of the Okinawa Island – are described in this chapter. The methodologies of the analyses on these data – objective analysis and empirical orthogonal function (EOF) – are also explained with results of pre-analysis (objective analysis) applied on the satellite data.

Chapter 4: Controls on the SST and Ocean Colour Variability in the East China Sea and around the Island of Okinawa: Interaction between Climate and Ocean

Results of key controls obtained from EOF analyses in three domains – (1) the ECS, (2) the KC and Okinawa, and (3) coastline of Okinawa – are presented in this chapter. Effects of episodic extreme event, e.g., typhoon and warm eddy are also discussed (aims 1 and 3).

Chapter 5: Controls on the SST and Ocean Colour Variability around the Island of Okinawa: Terrestrial influence and a link with the coastal environment

Results of terrestrial control around the coastal zone of Okinawa and effects of an extreme typhoon event are evaluated. Relationship between key controls and the variation in coastal sediment is also discussed (aims 1, 2 and 3).

Chapter 6: Spatial-Temporal Changes in Wind and Rainfall Patterns around Okinawa

Spatial-temporal changes in key controls (wind and rainfall) over Okinawa are discussed. Changes in typhoons are also examined. From the results obtained, the implications for the coral reefs of Okinawa are discussed (aims 3 and 4).

Chapter 7: Discussion and Implications

Discussion and implications of this research are described in this chapter. With the results of a case study in the Island of Okinawa, wider implications for coral islands in the western Pacific and future works are discussed.

Chapter 2 Key Features of Climate, the Ocean and the Island of Okinawa

2.1 Introduction

This chapter describes major features of climate and ocean systems in the East China Sea (ECS) and terrestrial features of the Island of Okinawa, which affect the variability of the SST and ocean colour. A summary of the relationship between climate, ocean and terrestrial controls is presented in Fig. 2.1. The East Asia Monsoon (EAM) is the governing climate system over the ECS; it provides cold and dry northerlies in winter and hot and wet southerlies in summer. There is also a typhoon season during summer and autumn. In the ocean, one of the largest currents in the world, the Kuroshio Current (KC), flows in the ECS; providing warm water. Other currents on the continental shelf, e.g., the Kuroshio Branch Current and the Yellow Sea Warm Current, exhibit various seasonal flow patterns. A tremendous terrestrial influence of the world's third largest river, the Yangtze River, also interacts with these currents, producing intricate variability of ocean colour over the continental shelf. In the coastal zone around the Island of Okinawa, coral reefs are well developed and exhibit high biodiversity. On Okinawa, a large amount of red soil run-off triggered by rapid development has led to coral mortality around Okinawa since the 1960s. Under the distinct climate system of (1) the EAM, (2) ocean currents including the KC and (3) the large river input from the Yangtze River, an important research question explored in this thesis is to understand how these climate, ocean and terrestrial processes control the variability of the SST and ocean colour in the ECS, and the coastal zone around Okinawa, and related impacts on the coral reefs around the Island. The following sections describe the characteristics of the EAM, ocean currents in the ECS and include a brief history of land development and how each of these have affected the coastal environment.

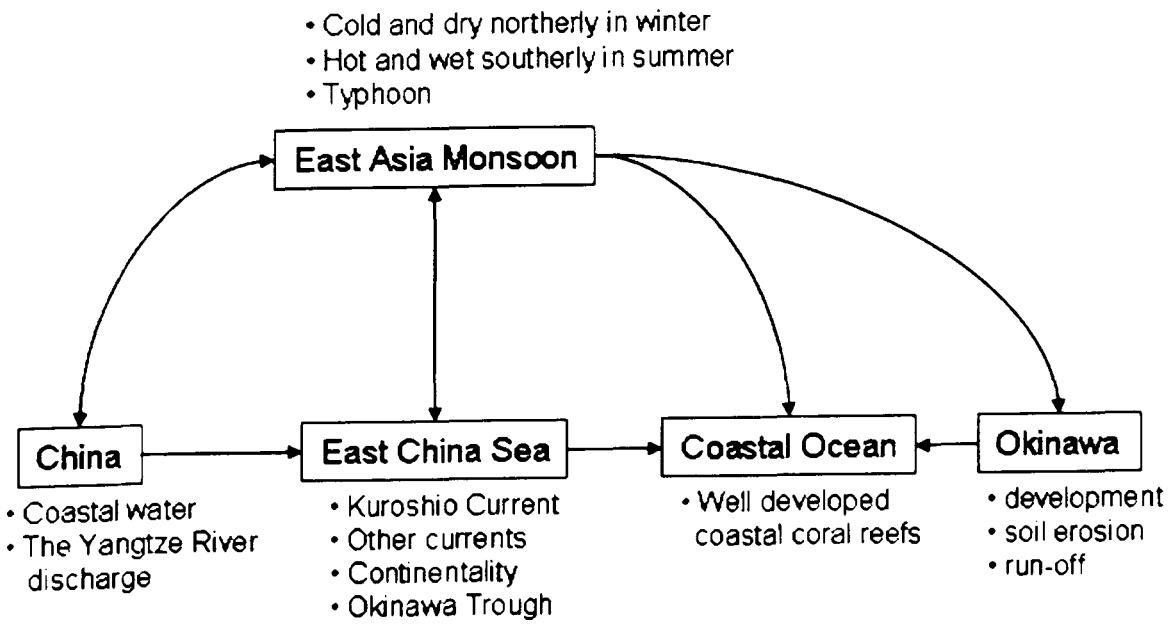

Fig. 2.1. Relationship between the climatic, oceanic and terrestrial processes in the ECS and around Okinawa.

2.2 Climate over the Western Pacific

2.2.1 General Mechanism of the East Asian Monsoon

The Monsoon is a seasonal wind, which reverses its direction. As the seasons change, the monsoon brings cold dry winds in winter and warm wet winds in summer. Ramage (1971) suggested the monsoon regions of West Africa, eastern and southern Asia and the maritime continent of northern Australia display both wind reversal and seasonal precipitation characteristics. The most famous observed monsoon is the Indian summer monsoon in the Asian monsoon system, with its wet phase accompanied by the sudden onset of heavy rain. In terms of the contrast between winter and summer, the East Asian Monsoon (EAM) exhibits the most distinct winter and summer component, which makes its character different from the Indian monsoon whose winter monsoon does not show a significant presence compared to the EAM (Lau and Li, 1984).

All monsoons share three basic physical mechanisms: (1) differential heating between the land and oceans, (2) Coriolis force and (3) the role of water which stores and releases latent heat as it changes its state. The combined effect of these mechanisms produces the monsoon's characteristic reversals of wind and precipitation (Webster, 1987a). The heat capacities of land and ocean under the annual cycle of radiative heating produce a pattern of atmospheric heating which is variable in space and time. In essence, it allows a pressure gradient force to exist between land and ocean. During winter, radiative cooling occurs. However, effective heat capacity is many orders of magnitude larger for the ocean than for land. Thus, in general, the ocean is warmer than the land during winter, and thus air flows from land to ocean at the surface to replace the uplifted air over the ocean. Therefore, during the winter monsoon air streams off the cold continent and heads towards the ocean. During summer, radiative heating of the surface takes place and the land surface heats rapidly. Land becomes warmer than the ocean, and then the air-flow is reversed: from warm ocean to warmer land (Webster, 1987a).

Fig. 2.2 shows analysis the monthly global surface wind observed by the SeaWinds sensor on the QuickSCAT satellite for, (a) January and (b) July in 2000 from the NASA ftp site (ftp://podaac.jpl.nasa.gov/pub/ocean_wind/quikscat/L3/data). Although these figures show wind patters over a limited time and possibly include some extreme events, they are useful to overview main monsoonal pattern. In the monsoon regions, the reversal of wind can be observed. In January, the Siberian High and the Tibetan Plateau are the source of winds over eastern Asia and India, respectively. The winds which flow from the Siberian High are very strong northwesterlies near western Japan (Fig. 2.2a). As it proceeds southward, it becomes northeasterly over Okinawa and Taiwan. This is in effect the winter EAM. The key driving force for the winter EAM is the available energy generated by the differential heating between

the Asian continent and the ocean near the equatorial western Pacific (which is the main heating source). When the northeasterly winds of the winter EAM reach South East Asia, they brings the rainy season to that region, producing a latent heat source over the "maritime continent" (the region of Southeast Asia which comprises many islands, peninsulas and shallow seas) of Indonesia and Borneo.

(a) January 2000

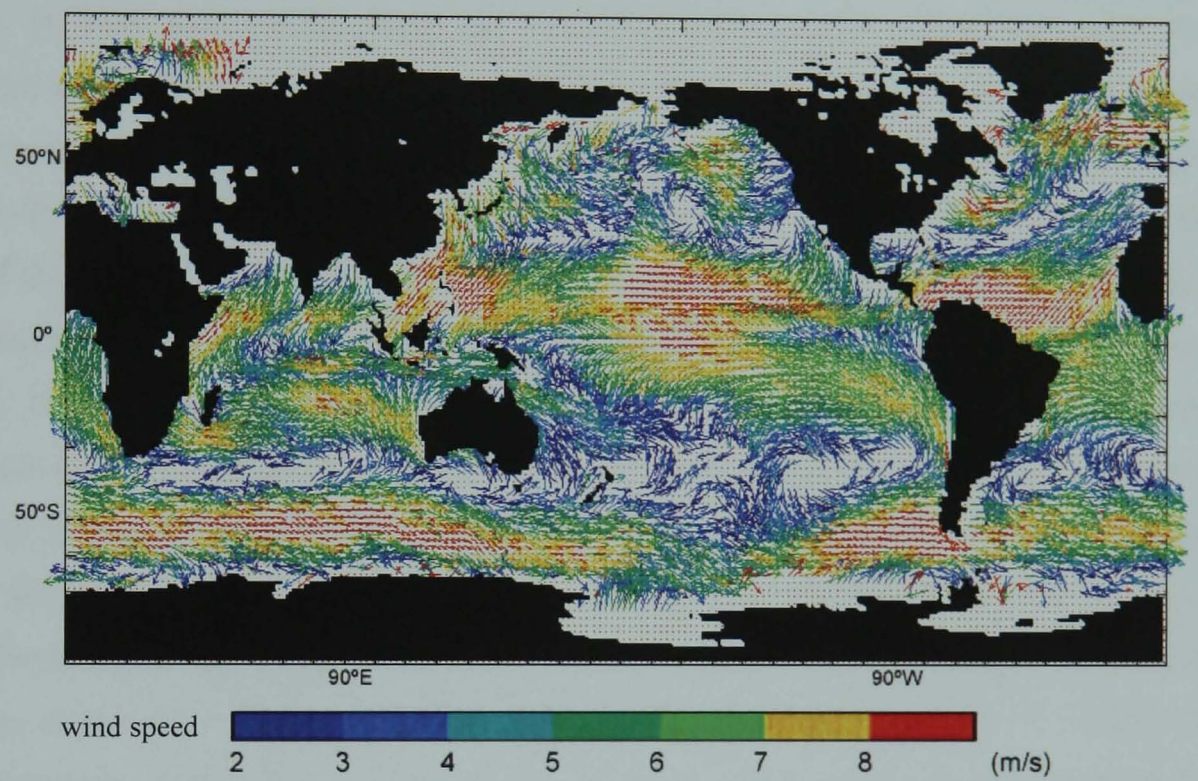

(b) July 2000

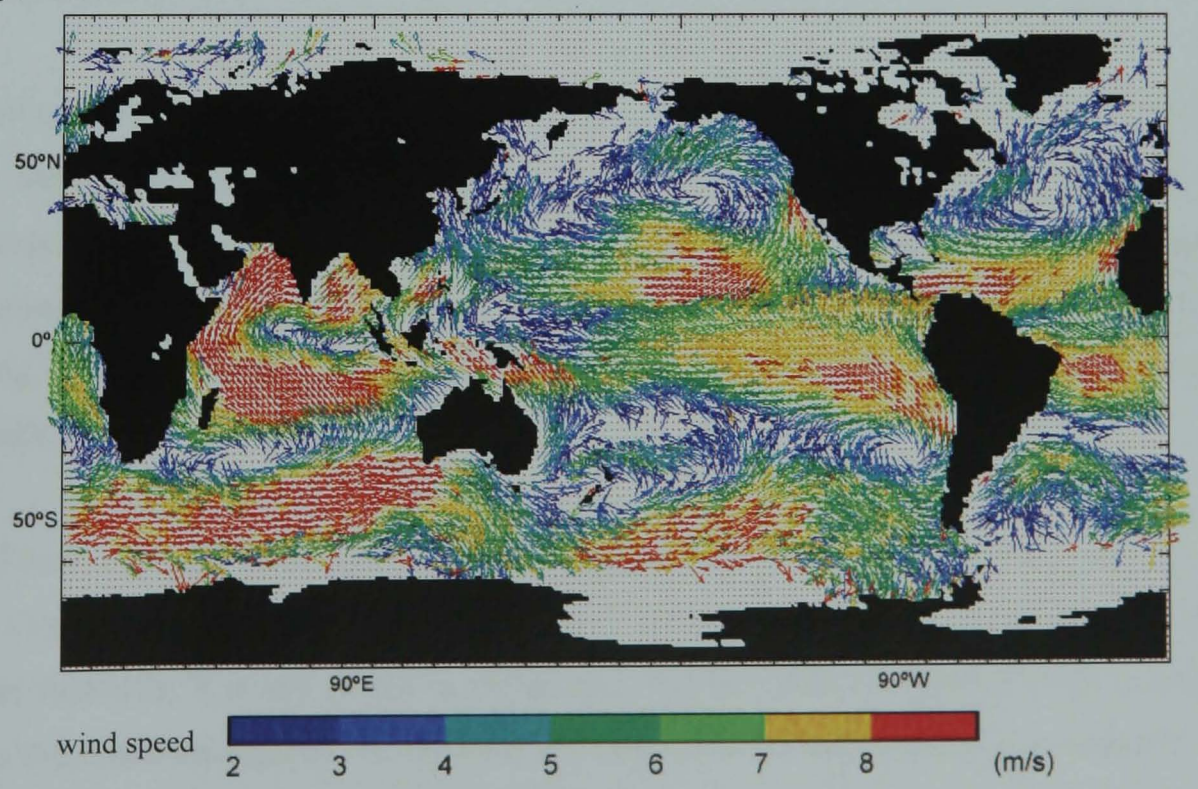

Fig. 2.2. The sea surface wind in (a) January 2000 and (b) July 2000. Processed here from the data acquired by the QuickSCAT Seawinds sensor, level 3 daily gridded ocean vectors.

The latent heat release associated with convective precipitation enhances the Hadley cell in the atmosphere. To the far north of the convective centre lies the strong Siberian High, covering the

entire East Asian continent. Existence of this very strong north-south thermal contrast between the heat source and the cold Asian continent leads to the winter EAM over a large part of Asia (Lau and Li, 1984).

In July (Fig. 2.2b), wind directions are opposite to those seen in January. The winds from the South Indian Ocean blow to the eastern coast of Africa, and proceed northeast to reach the western coast of India. This is the Indian summer monsoon, often accompanied by heavy rainfall. In East Asia, winds from the western Pacific Ocean which bear both north and northwest can be seen. This is the summer EAM, where transportation of moist air gained from the warm tropical ocean surface during summer occurs, providing rainfall over the bulk of East and South Asia. The heat source that drives the summer EAM is the huge and elevated land mass of the Tibetan Plateau. Sensible heat flux over the semi-arid western region of the plateau and latent heat release above the Himalayas contribute to a strong tropospheric heat source (Lau and Li, 1984). Southerly surface flow spreads from the maritime continent of Borneo and Indonesia towards East and South Asia. As the peak summer EAM period approaches, this southerly proceeds towards China and Japan, accompanied by the transportation of water vapour from the South China Sea and the western tropical Pacific region (Lau and Li, 1984). This advected moist air converges to form a quasi-stationary rain band called the *Mei-Yu* front in China, or the *Baiu* front in Japan (Chen and Chang, 1980; Matsumoto et al., 1970). After the *Baiu* season, the North Pacific High covers Japan and brings a hot and humid summer. It also affects the typhoon tracks in the western North Pacific (Ogura, 1999; Kataoka, 2003).

The Island of Okinawa lies the western Pacific Ocean and belongs to the EAM climate zone. During the winter, the northeasterlies over the surface of central and eastern Asia prevail, originating from the huge anticyclonic circulation over Siberia. This circulation brings a cold dry continental air mass to the eastern and southern region of China and the southern Japan, including Okinawa. During the summer, the southwesterlies influence the same region, with warm moist air from the Pacific Ocean which brings heavy rain.

The EAM is related to the global scale circulation that connects the monsoon regions and the Pacific Ocean. When surface pressure is anomalously high (low) in the monsoon regions of Asia and Australia, it is low (high) in the eastern Pacific Ocean. A transfer of mass takes place between the monsoon regions and the Pacific Ocean in the Walker circulation (Webster, 1987b). There have been studies that indicate a relationship between the summer EAM rainfall and the El Niño – Southern Oscillation (ENSO), suggesting that weak (strong) summer EAM rainfall is associated with the warm (cold) phase of ENSO (e.g., Webster and Yang 1992; Lau and Yang, 1996; Lau and Weng, 2001). However, such a relationship is not constant (Wang et al., 2000;

Lau and Wu, 2001). Because both monsoon and ENSO are highly complex and nonlinear natural phenomena, governed by the interaction of a large number of physical processes with various spatial and temporal scales, their relationship does not remain stationary (Lau and Wu, 2001), and there are studies indicating various types of the summer EAM rainfall – ENSO relationships. Wang and Shi (1992) found different impacts of two kinds of ENSO events on the summer rainfall in China, depending on whether the event first appeared in spring or autumn. They also indicated that not all severe floods/droughts over China were associated with El Niño/La Niña events. Shen and Lau (1995) showed that the summer EAM rainfall possessed a strong biennial cycle, particularly over the southeast China. They also showed that it was linked to the biennial oscillation of the sea surface temperature (SST) over the tropical Indian and Pacific Ocean, and that this link was more significant than with the ENSO. Lau and Wu (2001) found that for rainfall variability over the summer EAM region, about 30 % of the variability can be accounted for by ENSO-related basin-scale SST, and that regional processes can account for 20 %. In individual years and over sub-regions, these percentages can be much higher or lower.

The Third Assessment Report (TAR) of the Intergovernmental Panel on Climate Change (IPCC) reported that a warming environment will cause an increase in Asian summer monsoon precipitation variability (Houghton et al., 2001). Its Fourth Assessment Report (FAR) suggested that an increase in rainfall is projected at the end of the 21st century in the Asian monsoon along with an increase in interannual season-averaged precipitation variability; rainfall in the boreal winter is very likely to increase in East Asia (+10 %) and Southeast Asia (+6 %); rainfall in the summer is likely to increase in northern Asia (+9 %), East Asia (+9 %), South Asia (+ 11%) and most of Southeast Asia (+7 %); and extreme rainfall and winds associated with tropical cyclones are likely to increase in East Asia, Southeast Asia and South Asia (Solomon et al., 2007). Using the Global Precipitation Climatology Project (GPCP) monthly dataset from 1979 to 2005, Gu et al. (2007) found that the rain over the ocean, and the total (ocean plus land), had a significant increasing trend in the tropical region (25 °S – 25 °N). Changes in rainfall over the Island of Okinawa itself will be discussed in Chapter 6.

2.2.2 Effect of the East Asian Monsoon on the Ocean Surface

The effect of the EAM reaches not only the terrestrial sphere, including human society, but also the marine ecosystem. The strong winter EAM winds are influential in modifying the primary production in the western Pacific Ocean. The key mechanism is via wind-induced coastal upwelling, which supplies nutrients from the deeper ocean to the surface causing a phytoplankton bloom where there is enough sun light. Limsakul et al. (2001) indicated that

interannual changes in the intensity of the winter EAM had a significant impact on nutrient inputs into the euphotic zone which in turn leads to chlorophyll-a (Chl-a) blooms in the Northwestern Pacific Ocean. Liu et al. (2002) showed the effect of the EAM forcing on nutrient upwelling and phytoplankton growth in the South China Sea via satellite observation. Penaflor et al. (2007) found a dramatic increase of Chl-a concentration in the Luzon Strait between Taiwan and the Island of Luzon in the Philippines associated with the strong northeasterlies of the winter EAM. They also suggested that this monsoonal upwelling bloom was associated with interaction with the northward Luzon coastal current. Variability in sedimentary organic carbon content has been interpreted as evidence for changes in biological production, which has been linked to changes in the monsoon strength (Huang et al., 1997). Beaufort et al. (2003) found a pattern of intensified oceanic primary production during the winter EAM in the Sulu Sea, west of the Philippines over the last 380 kyr, from a piston core marine sediment record. While weaker than the winter EAM, the summer EAM wind still has an effect. Dippner et al. (2007) showed that coastal upwelling off the southwest coast of Vietnam was induced by the southerlies of the summer EAM.

Rainfall brought by the summer EAM is influential in the coastal environment through terrestrial run-off. Pinazo et al. (2001) showed that the nutrients carried in fresh water run-off have a significant effect in increasing the phytoplankton biomass. Under the influence of the summer EAM, the Yangtze River enhances its discharge during the rainy season, releasing a huge quantity of sediments and nutrients to the ECS. This results in increasing Chl-a around the Yangtze Estuary (Gong et al., 2003), which causes another Chl-a bloom season in addition to the winter EAM-induced bloom season. Although the scale of the land-mass and river length are smaller than the Chinese coasts and the Yangtze River, it is likely that the coastal zone around the Island of Okinawa may have a similar effect from both the winter and summer EAM. The effect of the EAM in the western Pacific including the Island of Okinawa will be analysed in Chapter 4 and 5. Changes in the winter and summer EAM will be discussed in Chapter 6.

2.2.3 Typhoons in the western Pacific

There are several terms for typhoons or cyclones depending on the location of their occurrence. A cyclone formed over the tropical ocean is called a tropical low pressure. A tropical low pressure that stays in the North Western Pacific (north of the equator and west of 180 °E) or in the South China Sea, and which possesses a maximum wind speed (10 minutes averaged) of over 33 m/s is called a "typhoon". Around the Island of Okinawa, therefore, "typhoon" is the word for storms and will be used in this study. These events are called a "hurricane" in the North Atlantic Ocean, the Northeast Pacific Ocean east of the dateline, or the

South Pacific Ocean east of 160° E. There are also termed a "tropical cyclone" in the Indian Ocean region.

Fig. 2.3 shows the tracks of tropical storms during 1979 – 1988 (image from the Ministry of Education, Culture, Sports, Science and Technology, 2006). Cyclogenesis occurs in the North Pacific, the western South Pacific, the north and south Indian Ocean, and the North Atlantic Ocean where the SSTs are high. Generally, tropical cyclones occur over warm SST regions where the temperature is above 26 – 27 °C (Gray, 1968; Lighthill et al, 1994; Ogura, 1999). This is a reason why relatively few are observed in the eastern Pacific Ocean or in the Southern Hemisphere where the annual SST is below 26 °C (Fig. 2.4).

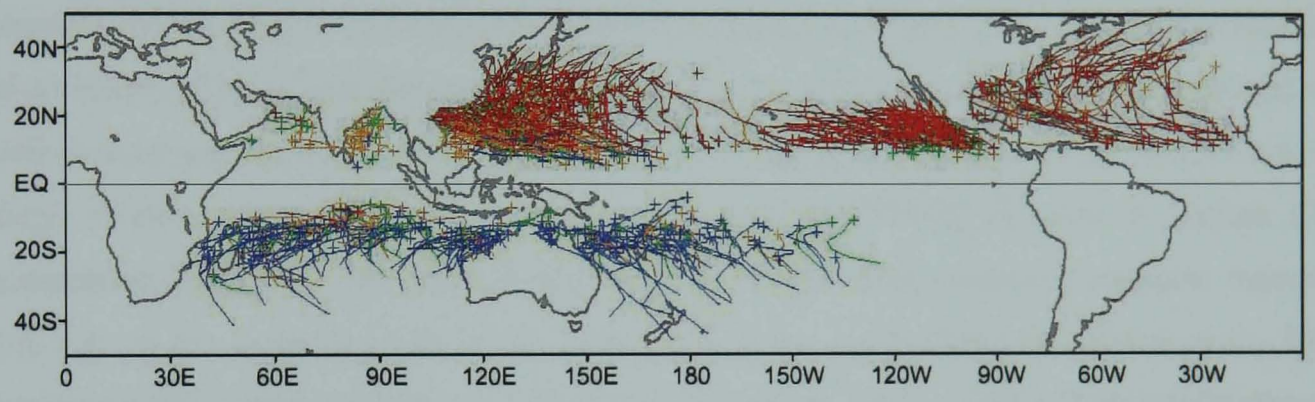

Fig. 2.3. Tracks of tropical storms during 1979 – 1988. Image from the Ministry of Education, Culture, Sports, Science and Technology (2006), Fig. 1-5. The time of tropical cyclone occurrence is classified by the colour: blue – JFM, green – AMJ, red – JAS, and orange – OND.

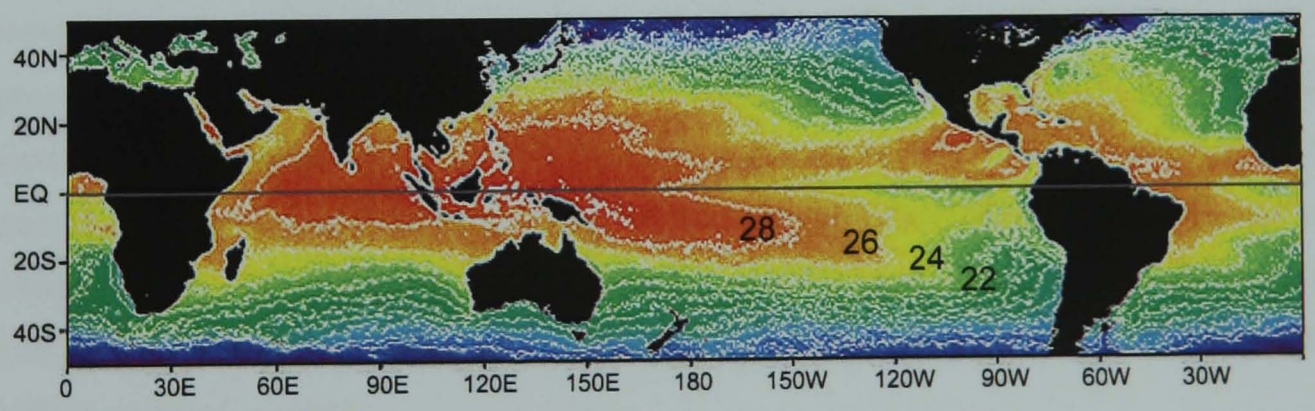

Fig. 2.4. Annual global SST in 2005. Temperature contour in the white line. Values of 22 – 28 °C are labelled in the South Pacific. Processed from the Advanced Very High Resolution Radiometer (AVHRR) version 5 level 3.

The western North Pacific region including the Island of Okinawa is one of the most active places for typhoon occurrence (Fig. 2.3). When a typhoon begins to form in the low latitudes of the western North Pacific, it moves westward influenced by the easterlies. In addition, the Coriolis effect forces it to veer northward. As it proceeds to the mid latitudes, it is accelerated eastward by stronger westerlies. Eventually it turns into an extra-tropical cyclone (Ogura, 1999).

Strong winds associated with typhoons also have a significant cooling effect on the ocean surface. They cause water mixing, upwelling of colder water to the surface, and hence an observed SST decrease. Lin et al. (2003a) analysed the cold SST regions formed in the trail of two typhoon events in 2000 off southern Taiwan. They observed anomalously cold SST of up to 6 °C below the surrounding warm tropical ocean. Nadaoka et al. (2001b) also surveyed the SST response during a typhoon passage in 1998 over the shallow reef of Ishigaki Island, southwestern Okinawa, and indicated that the atmospheric cooling of the reef water was mainly due to enhanced evaporation on the ocean surface.

Water mixing by wind forcing can also affect the surface Chl-a concentration. Mixing and upwelling event brings nutrient-rich water from a deeper and colder layer to the light-replete euphotic zone, leading to enhancement of photosynthetic activities, and hence a phytoplankton (Chl-a) bloom (Eppley and Renger, 1988; Marra et al., 1990). Lin et al. (2003b) affirmed such an effect accompanied by the SST decrease caused by a typhoon in 2000 in the South China Sea through satellite observation. They estimated an average 30-fold increase in surface Chl-a concentration during the typhoon's 3-day stay. There are many studies of typhoon impact on Chl-a, e.g., in the Japan Sea (Son et al., 2006), and in the South China Sea (Shiah et al., 2000). Other research has been carried out in the hurricane region, e.g., in Gulf of Mexico (Walker and Leben, 2005), in Bermuda (Acker et al., 2004), in the Sargasso Sea in the North Atlantic (Babin et al., 2004), and off Honduras (Andréfouët et al., 2002). The effects of typhoons on Chl-a blooms comes not only from strong winds but also from heavy rainfall. Zheng and Tang (2007) observed near-shore Chl-a increases around Hainan Island in the South China Sea, and suggested that its increase resulted from rainwater discharge and seaward advection by a typhoon-induced current. The effects of typhoons on the coastal zone around Okinawa will be discussed in Chapter 4, and the effect of associated winds and rainfall will be further discussed in Chapter 5 in order to investigate the impact of typhoons on the variability in observed SST and ocean colour. Changes in typhoon occurrence and rainfall intensity around Okinawa will be also discussed in Chapter 6.

2.3 Ocean Currents in the East China Sea

2.3.1 Location and Surroundings

The East China Sea (ECS) is the largest marginal sea in the western Pacific, connected to the Japan Sea in the northeast through the Tsushima Strait, the Yellow Sea in the north, the South China Sea in the south through the Taiwan Strait, and is adjacent to the Philippine Sea in the east (Fig. 2.5). The ECS is bounded by the Kyushu and Ryukyu Islands of Japan in the east,

Taiwan in the south, and the Chinese coast to the west. The continental shelf occupies more than 70 % of the area of the ECS. To the east of the shelf edge, there is a depression, called the Okinawa Trough, and east of the trough lies the Ryukyu Arc.

As mentioned above, along the Chinese coast, there are many rivers carrying a huge quantity of fresh water into the ECS with dissolved and suspended matter. Among these rivers, the Yangtze River is the largest, constituting about 85 % of the total discharge of all rivers into the ECS (Ning et al., 1998). Its mean discharge is about 928 km^3/year (Zhang et al., 1990). By comparison, discharge from Minjiang (58.4 km^3/year) and Qiantangjiang (35.3 km^3/year) is at least one order of magnitude smaller (Lee and Chao, 2003).

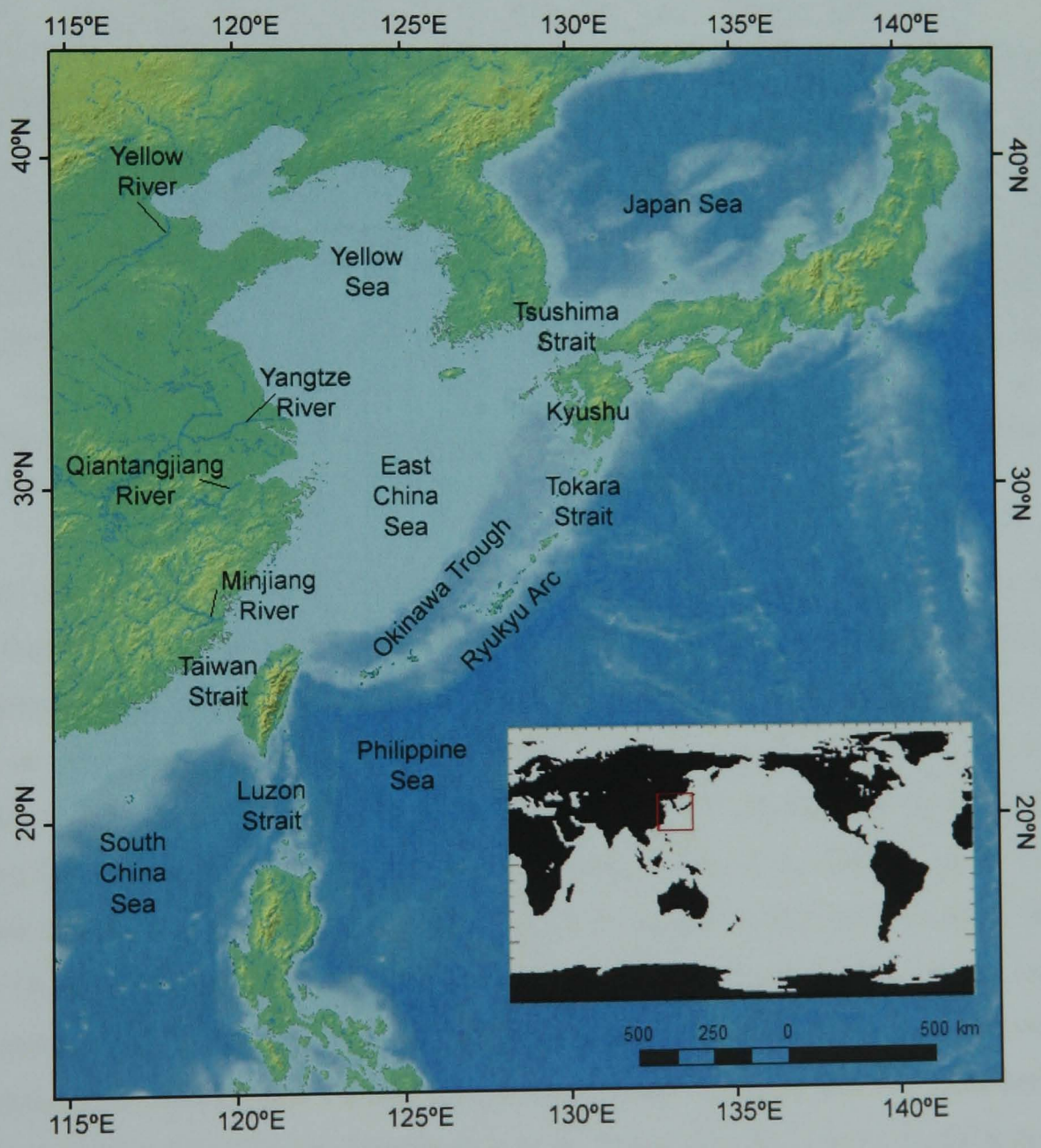

Fig. 2.5. The ECS and its surrounding in the western North Pacific.

2.3.2 Ocean Currents

Fig. 2.6 shows the global surface ocean currents. In the North Pacific, the North Equatorial Current flows westward due to the influence of the easterlies (trade wind: Fig. 2.2) in the tropics.

It becomes the Kuroshio Current as it proceeds northward in the ECS. In the mid-latitudes, some part of the Kuroshio extension streams eastward, affected by westerlies, and becomes the California Current which flows southward along the west coast of the North American continent, forming a large circulation in the North Pacific. It is known that the volume transport of the southern KC (about 137 °E) is linked to the wind stress over the central North Pacific that drives a subtropical gyre (Hanawa and Kamada, 2001).

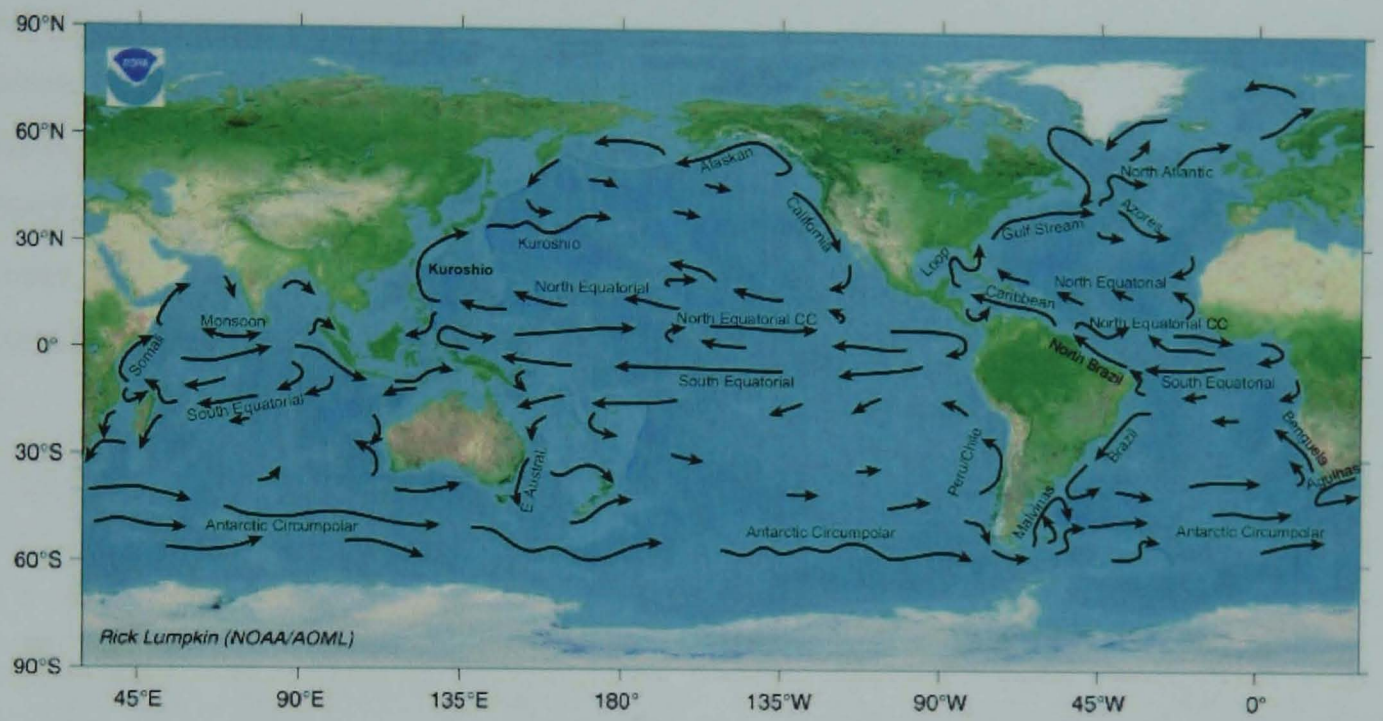

Fig. 2.6. The global surface ocean current. Adapted from National Oceanic and Atmospheric Administration (NOAA) Office of Climate Observation (http://www.adp.noaa.gov/currents.jpg).

Ocean circulation in the ECS is generally influenced by a counter-clockwise circulation system that consists of the Kuroshio Current (KC), Tsushima Warm Current (TSWC), Yellow Sea Warm Current (YSWC) on the eastern side of the sea, and the Chinese Coastal Water (CCW) on the west side (Fig. 2.7). The former comes from the tropical ocean with high temperature and salinity, bringing oligotrophic water with low chlorophyll concentrations. The latter has low-salinity but high-nutrient concentrations (Ning et al., 1998). The KC exerts an important thermal and biological effect on the ECS. It enters the ECS east of Taiwan and flows into the Okinawa Trough. Over the shelf break (about 200 m deep), the KC mostly follows the curved isobaths of the Trough. The KC carries the warm and saline water of the subtropical mode water in the western Pacific and appears as a warm tongue in the SST field between the continental shelf and the Ryukyu Islands (Xie et al., 2002). The KC leaves the ECS through the Tokara Strait. The main stream of the KC flows south of Japan and then east of Japan. However, the KC bifurcates, and some of the current proceeds northward to the Japan Sea and forms the TSWC, and another flows northwestward becoming the YSWC. The KC is also vertically dynamic. There are considerable upwellings northeast of Taiwan and southwest of Kyushu.

Both are associated with meanders of the KC and its response to bathymetric forcing (Lee and Chao, 2003).

The circulation patterns in the ECS are not stationary. There exhibit some variability under the influence of the huge freshwater discharge from the continent, and regional atmospheric forcing, e.g., the EAM. Fishing activity in the ECS is very high, hampering long-term moored current measurements to derive a clear circulation pattern. However, during the 1990s, new technologies for measuring the currents (e.g., Acoustic Doppler Current Profiler and satellite remote sensing) and high resolution three-dimensional numerical model experiments have allowed an advance in understanding of the current system in the ECS. Ichikawa and Beardsley (2002) presented the current pattern in the ECS, indicating winter and summer variability. In winter (Fig. 2.7a), the TSWC has a single source, the KC which transports a mixture of Kuroshio water, and the Yangtze River Water (YRW) northward to form the YSWC.

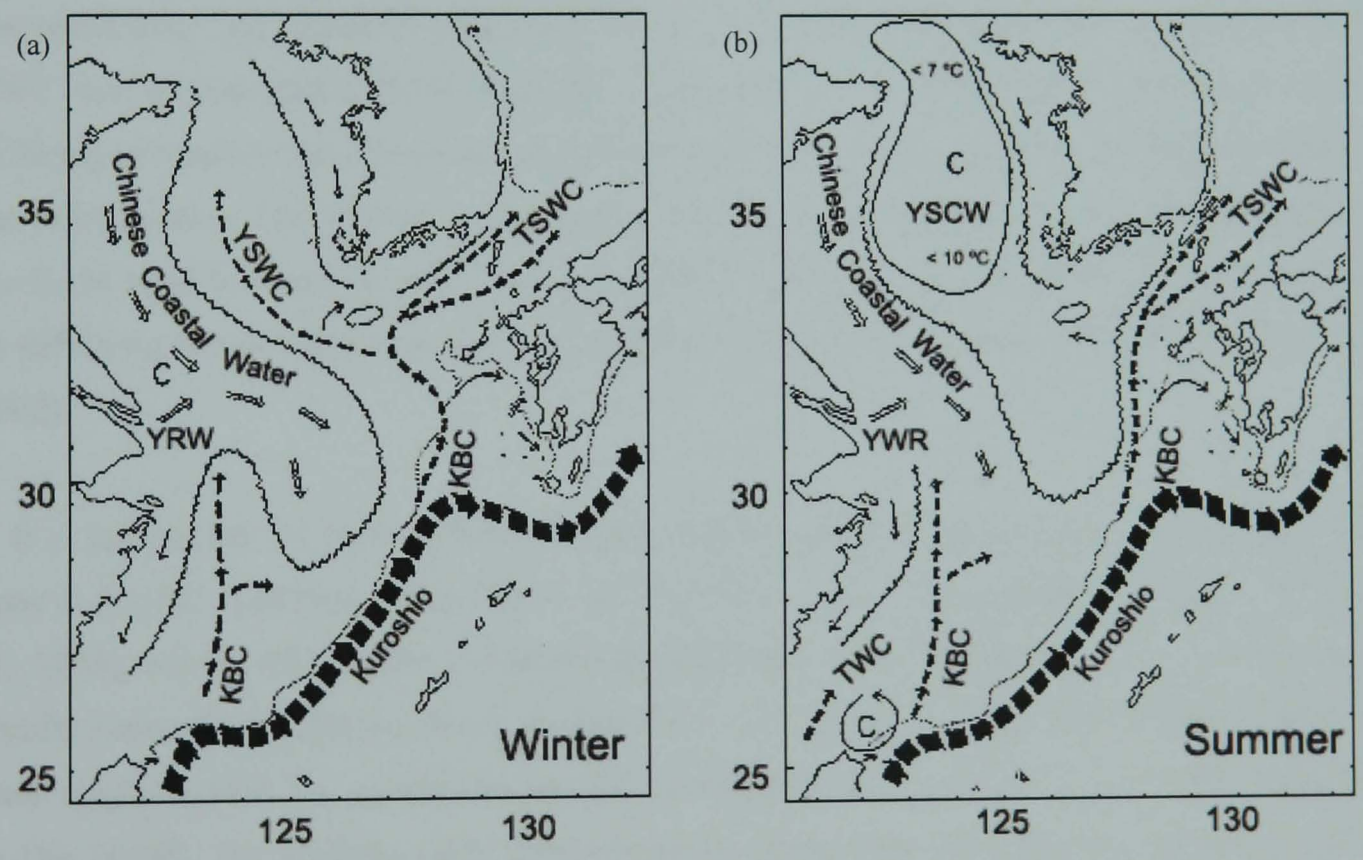

Fig. 2.7. The surface current pattern in the ECS in (a) winter and (b) summer. Adapted from Ichikawa and Beardsley (2002).

In summer (Fig. 2.7b), the TSWC has multiple sources, i.e., the Taiwan Warm Current (TWC) north of Taiwan, and Kuroshio branch currents (KBC) to the west of Kyushu. The summer surface circulation in the ECS has interannual changes corresponding to the interannual variations of the YRW (Ichikawa and Beardsley, 2002). The YRW dispersal and associated suspended sediments entering the ECS (Beardsley et al., 1985), and the YRW often form a narrow band of cold water off-shore of the 50 m isobath (Pan et al., 1991).

The YSWC is a main feature of the circulation in the Yellow Sea in the northern ECS. The Yellow Sea is a shallow basin of less than 50 m depth, carrying highly turbid water (Milliman et al., 1985). In winter, Yellow Sea Cold Water (YSCW) is formed owing to strong mixing under the influence of the prevailing winter EAM (Mask and O'Brien, 1998). In summer, the YSCW flows southward under the thermocline. It becomes the Yellow Sea mixed water with warmer temperatures (Gong et al., 1996) and interacts with the KC to form fronts, eddies, meanders, and cold/warm core rings (Zheng and Klemas, 1982; Yuxiang, 1996).

In the south of the ECS, across the continental shelf northeast of Taiwan, intrusion of the KC has been observed, and it is known that this intrusion also has a seasonal variability (e.g., Lin et al., 1992; Tang and Yang, 1993). The KC apparently extends its front onto the shelf in winter and retreats to the shelf edge in summer and autumn. Chuang and Liang (1994) observed two types of intrusion; one is seasonally correlated with the arrival of winter high pressure and low temperature, and the other is due to typhoon passage in summer. In the Taiwan Strait, the TWC has seasonality, too. There is often a northward current on the east side, the main current of the TWC, and a southward current on the west side in the strait. The eastern current has sources differing in season: one is from the South China Sea in summer and others are from the KBC in the other seasons. The western current carries the colder CCW. Both currents are modulated by the EAM wind forcing (Jan et al., 2002). Generally, the ECS loses much heat to the atmosphere as the strong winter EAM brings in cold and dry air from the continent during winter (Xie et al., 2002).

It is known that the western North Pacific has two eddy-rich zones; one is the northern eddy zone in the KC extension region (30 ° – 40 °N, 140 °E – 180 °W) southeast of Japan (Yasuda et al., 1992), and the other is the southern eddy zone (Qiu, 1999; Hwang et al., 2004) in the North Pacific Subtropical Counter-current region (18 ° – 25 °N, 122 ° – 160 °E). Northern eddy rich zone originate from KC extensions and the western boundary currents (Qiu, 1999). According to Qiu (1999), the southern eddy zone eddies originate from the baroclinic instability of the weak flow between the westward North Equatorial Current and the eastward Subtropical Countercurrent. In particular, the belt along 22°N is where eddies most frequently occur (Hwang et al., 2004). Higher SST in the warm eddies has an effect on atmospheric pressure development. Lin et al. (2005) reported that Super Typhoon Maemi's intensity rapidly increased when it encountered a warm eddy in the western Pacific in September 2003. Warm eddies that reached Okinawa have been recently observed in the summer 2001 and 2003. They affected the local sea temperature and caused anomalous tidal levels due to the expanded mass of the warm water (Fukushima and Yamazaki, 2001; Japan Meteorological Agency, 2005).

One of the largest currents, the KC flows to the west of Okinawa, bringing warm/saline water and affecting circulation in the ECS. Warm eddies are actively formed southwest of Okinawa. Their warmer SSTs have the potential to enhance a typhoon's intensity. Fukushima and Yamazaki (2001) reported that warm eddy observed off east of Okinawa in July 2001 have the temperature of 21 °C at 200 m depth. Warm eddies' anticyclonic current may affect the surface current when they interact with the Island. The Island of Okinawa is indeed surrounded by a highly dynamic atmospheric and oceanic environment.

2.3.3 Temperature and Chlorophyll Variations

In the ECS, bathymetry plays an important role in ocean temperature variability in combination with atmospheric forcing. Under intense surface cooling by the winter EAM, water is well mixed from up to 100 m depth (Ichikawa and Beardsley, 2002). Thus, the thermal inertia of the water column is proportional to the bottom depth (Xie et al. 2002). Therefore, the SST variability associated with surface winds appears greater over the shallow shelf.

The warm water of the KC plays another important role, effectively rendering the environment of Okinawa subtropical. Without the presence of the KC, Okinawa and Japan would experience a much colder climate. Previous studies revealed that during the Last Glacial Maximum (LGM), the KC was not able to enter the Okinawa Trough because of the appearance of a land bridge connecting Taiwan and the central and southern Ryukyu Arc (Ujiie et al., 1991; Ahagon et al., 1993). Instead, its current turned to the east at the southern end of the arc (Fig. 2.8), resulting in climatic cooling in East Asia, including the Japanese Islands and the northwestern Pacific region (Ujiie and Ujiie, 1999). Several studies estimated that SST in the Okinawa Trough region was 5 °C colder in the LGM from sediment analysis (Thunell et al., 1994; Martinez et al., 1997; Zhao et al., 2005). With the warm water brought by the KC into the Okinawa Trough, the influence of the winter EAM over the KC region may be different from that on the shallow continental shelf. This will be discussed in Chapter 4.

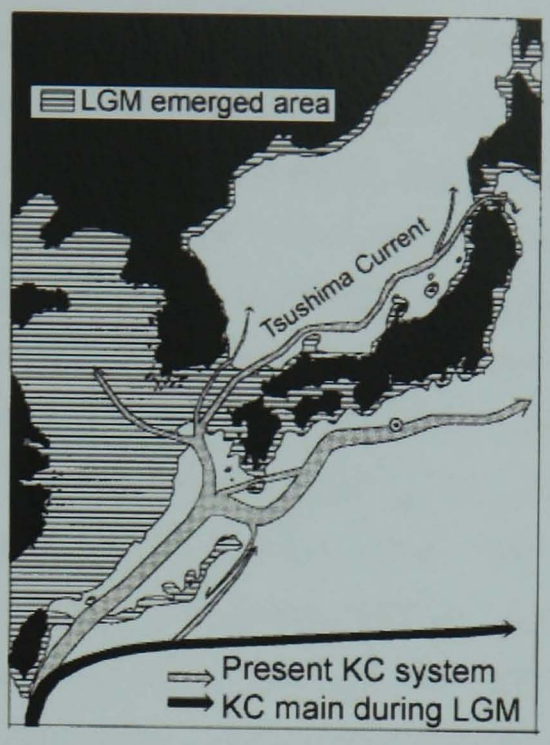

Fig. 2.8. The KC in the present and in the LGM. Adapted from Ujiie and Ujiie (1999).

The ECS receives a tremendous quantity of nutrients (0.8 Mt N/y; Huang et al., 1983) and suspended sediment (1.5 Gt/y; Milliman et al., 1985) from the Yangtze River. This highly turbid water, however, does not seem to reach Okinawa because of the presence of the Okinawa Trough. The Okinawa Trough has been noted as an important depositional site for the sediment from the shelf (Kao et al., 2003). Particularly, its southern region receives 10 times higher sedimentation rates (0.10 – 0.95 cm/y; Chung and Chang, 1995) than the northern and central trough (< 0.01 – 0.08 cm/y; Ikehara, 1995). This is also an important factor that keeps the turbid water condition away from Okinawa, offering the clean environment required by corals in addition to the KC supplied warm water (Ujiie, 1991). Due to the presence of the Okinawa Trough, there is a distinct difference in the ocean productivity between on and off shelf regions. Hama et al. (1997) measured the primary production in the ECS and found that productivity was 2.7 times higher in the shelf region than off the shelf over the KC region. They also found that high Chl-a throughout the euphotic zone was observed over the shelf rather than in the off-shelf region, and suggested that this was due to higher nutrient availability on the shelf.

Highly variable nutrient supply and productivity from the influences of the rivers, the currents and the EAM is a feature of the environment of the ECS. In an extensive cruise survey, Gong et al. (2003) investigated the seasonal variability of Chl-a concentration and primary production over the ECS during 1997/98. In the northwest of the ECS, especially off the Yangtze River mouth, nutrient concentrations were high all year-round, but primary production showed high seasonal variability. In winter and early spring, primary production decreased to 10 % of the summer value due to low temperature and low sun-light availability. In the southeast of the ECS, nutrient concentrations also showed seasonal variability: intermediate values during winter and early spring under the influence of the prevailing northerly EAM, and

almost depleted values in summer and autumn. As for Chl-a, higher concentrations were observed near the Yangtze River mouth in the northwest of the ECS in summer and autumn, and in the southeast of the ECS in winter and spring. In early spring, a patch of high Chl-a was observed over the middle shelf. Higher Chl-a concentration over the shelf than the off-shelf region was also recognised by satellite observation (Kiyomoto et al., 2001). However, it should be noted that satellite images tend to overestimate Chl-a concentration due to contamination by resuspended sediment raised by the strong winter northerly over the ECS (Kiyomoto et al., 2001; Gong et al., 2003). In this thesis, surface chlorophyll-a concentration data were derived from satellite observation, using the Sea-viewing Wide Field-of-view Sensor (SeaWiFS). Because of the overestimating tendency for turbid water by satellite remote sensing, the term "ocean colour" is used to represent the concentration of chlorophyll-a, other pigments and particles that affect ocean surface colour. Since the algorithm called Ocean Chlorophyll version 4 is used to determine the concentration of chlorophyll-a, the term "OC4" will be referred to the ocean colour derived from satellite observation (see Chapter 3, §3.2.3 for further details).

Yanagi et al. (1996) studied sediment transport variability in the northern Okinawa Trough through both observation and numerical experiment. They found that sediment was transported from the shelf edge to the inner shelf in summer and in the opposite direction in autumn and winter. This transport is induced by the southerly summer EAM and the northerly winter EAM respectively. In the southern Okinawa Trough, the intrusion of the KC modulates Chl-a concentration. Gong et al. (1997) observed that the intrusion of the KC suppressed the subsurface nutrient supply, and thereby reduced Chl-a in the KC upwelling region to the north of Taiwan. In the shelf region, northwest of Taiwan, a high Chl-a level was supported by the nutrient-rich upwelled KC subsurface water which intrudes northwestward.

In summary, as described in this section, the ECS has high variability in current pattern and productivity, because of the seasonal variability of the currents, river discharges, and the EAM. These processes enhance the variability of ocean colour over the continental shelf, and the existence of the Okinawa Trough and the KC is likely to prevent coastal effects from influencing the coastal zone around the Island of Okinawa. Quantification of the variability of sea surface temperature and ocean colour at large ECS and local Okinawa scale will be discussed in Chapter 4, in order to see the difference in the variabilities and influences from the ECS to Okinawa.

2.4 The Island of Okinawa

2.4.1 Climate

Because of the KC, the Island of Okinawa is rendered as subtropical. In monthly average data produced by the Japan Meteorological Agency (JMA), average air temperature stays above 20 °C from April to November, reaches to 28 °C in June and drops to about 16 °C at the coldest in January to February at the Naha weather station southwest of Okinawa (Fig. 2.9a). Under the influence of the summer EAM, the warm and humid southerlies blow from April until September. The rainy season visits from May to June (Fig. 2.9a). In addition, the typhoon season from July to September (Fig. 2.10a) brings abundant rainfall, leading to totals of over 2000 mm per year (annual mean of 1952- 2006 at Naha). During the winter EAM, the cold and dry northeasterlies start to prevail in October and last until March. The strong winds mostly occur during November to February (Fig. 2.9b). In July and August, the wind speed increases due to the influence from the tropical low pressure and typhoons during summer.

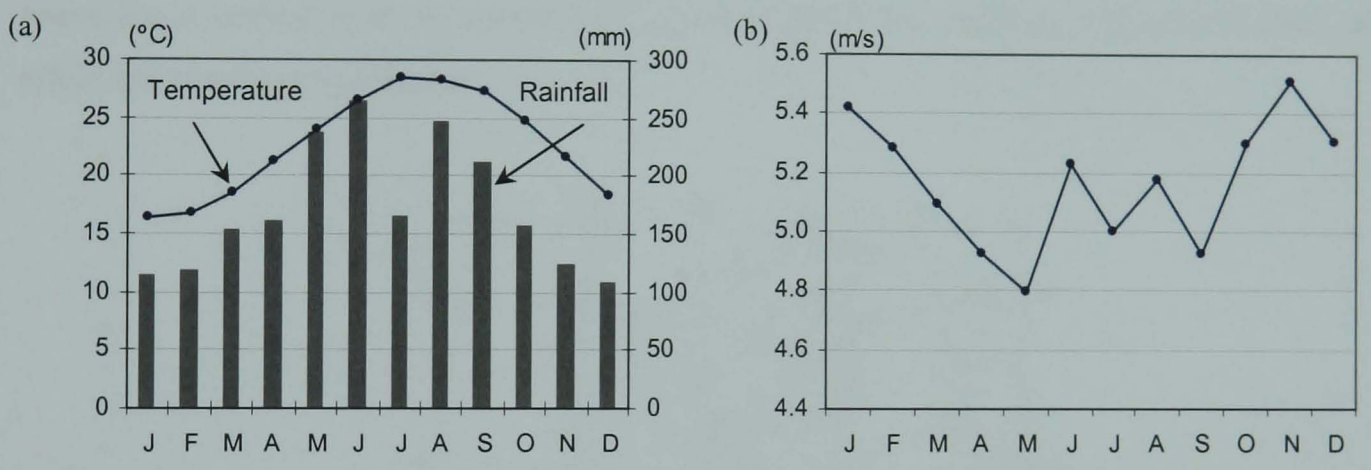

Fig. 2.9. Weather data recorded at the Naha weather station (1952 – 2006). (a) Monthly air temperature and rainfall: annual total rainfall – 2068 mm, annual mean temperature – 22.7 °C and (b) Monthly wind speed.

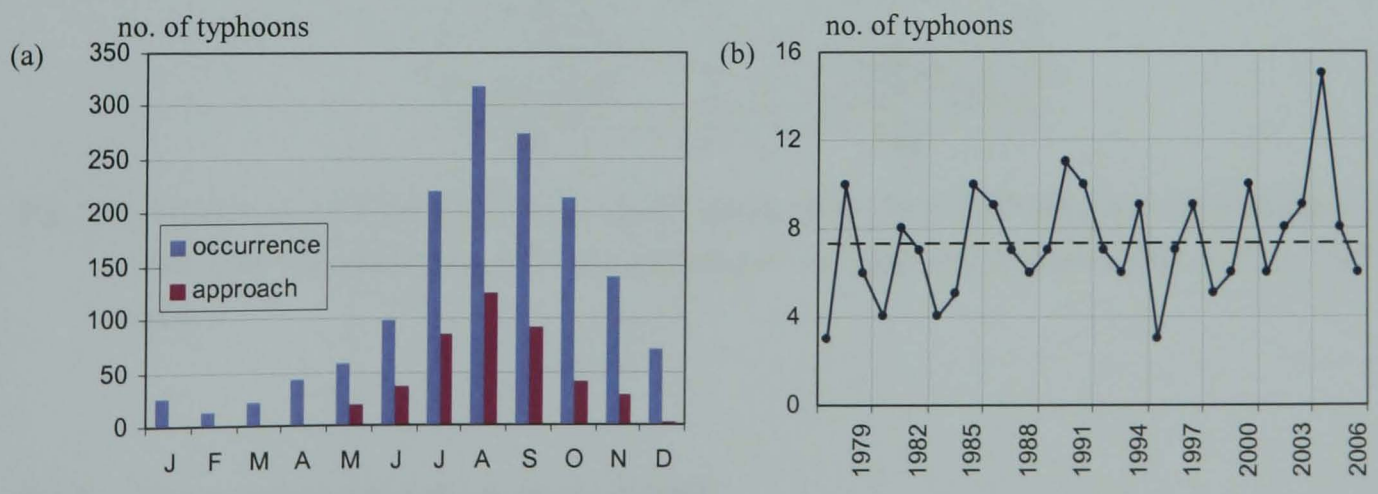

Fig. 2.10. (a) Number of typhoon occurrence and approaching the Ryukyu Islands (1977 – 2006): "Typhoon approach" is defined by the distance from the typhoon centre to the Ryukyu Islands which falls within 300 km. (b) Annual variation of typhoons approaching Okinawa. Mean value (7.4) is indicated by the dashed line.

The total number of monthly typhoon occurrences in the northwestern Pacific and number of approaching Okinawa is given in Fig. 2.10a. It shows that Okinawa experiences a typhoon season during JAS. Of 27 typhoon occurrences per year on average in the northwestern Pacific, there are 7.4 typhoons approaching the Ryukyu Islands (Fig. 2.10b), including Okinawa, during 1951 – 2006 (JMA, http://www.data.jma.go.jp/fcd/yoho/typhoon/statistics/accession/okinawa.html).

Fig. 2.11 shows typical typhoon tracks in the western North Pacific. The recurvature points occur around 20° – 30° N from July to September. This characteristic means Okinawa is frequently visited by typhoons (see Fig. 2.3 also). Compared to their intensity near mainland Japan, typhoons around Okinawa usually maintain stronger winds due to the energy supply from the warmer water. The speed of typhoon movement is slower before it is affected by the westerlies in higher latitudes, thus, Okinawa is often impacted by associated strong winds and heavy rainfall. Although typhoons are episodic events, this extreme process may have an important contribution to the variability of the sea surface temperature and nutrient input, which affect the coastal environment.

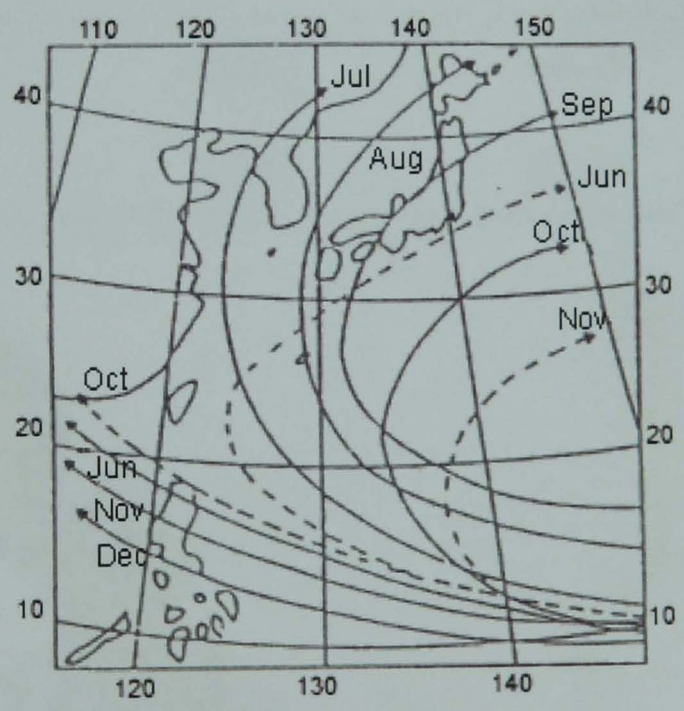

Fig. 2.11. Typhoon tracks in the North Western Pacific during 1940 – 1970 (from Japan Weather Association, 1973). The solid line represents major tracks according to the month and the dashed lines indicate quasi-major tracks.

2.4.2 Geographical Features of the Island

The topography of the Island of Okinawa is shown in Fig. 2.12. The map is based on the survey in 1972 by the Okinawa Prefecture Government (OPG) *Land Management Section*. There are other small islands around the main Island of Okinawa connected by bridges, except the Island of Ie, Minna, Tsuken and Kudaka.

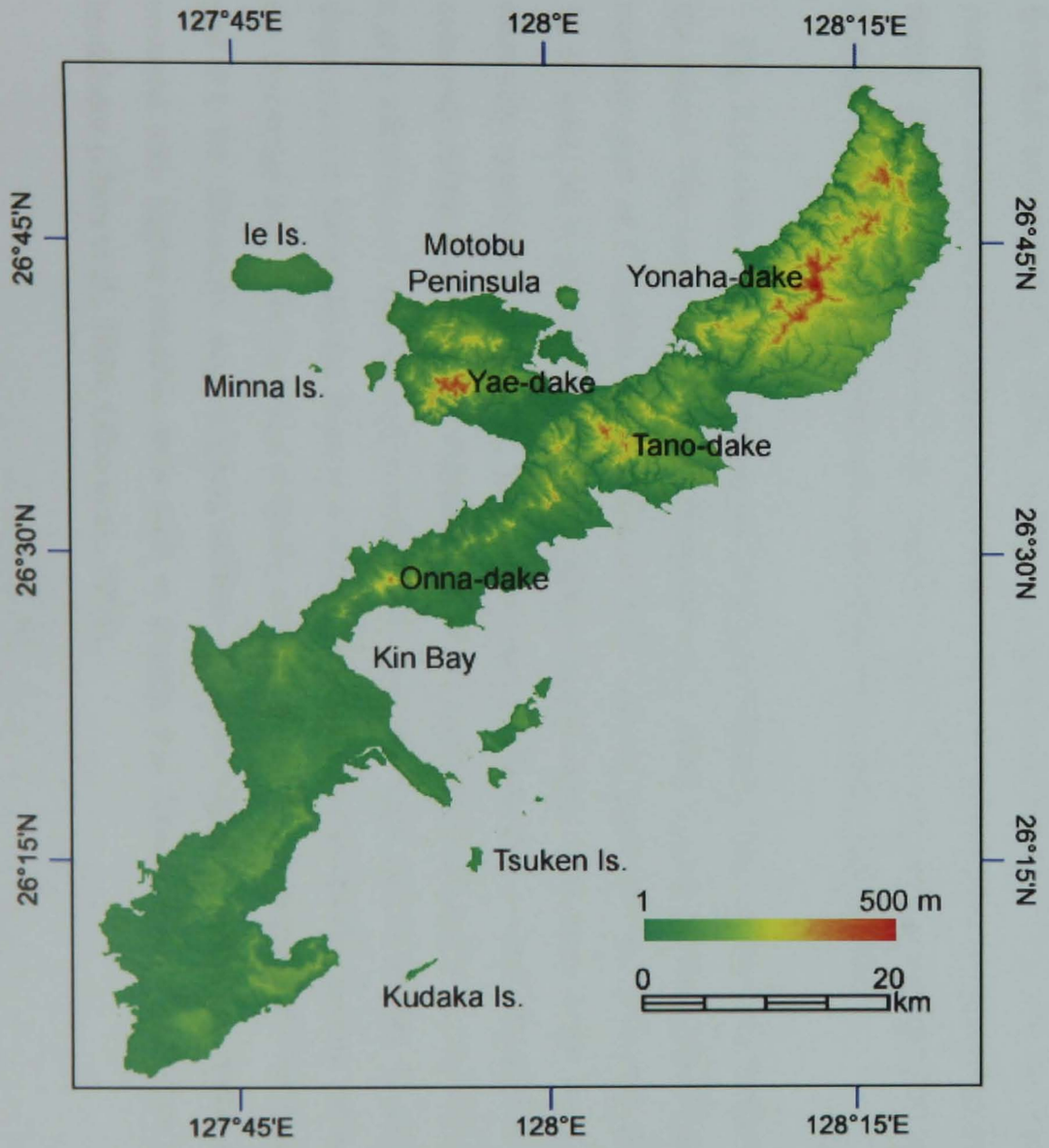

Fig. 2.12. Topography of Okinawa. Data were produced by the *OPG Land management section* (1972).

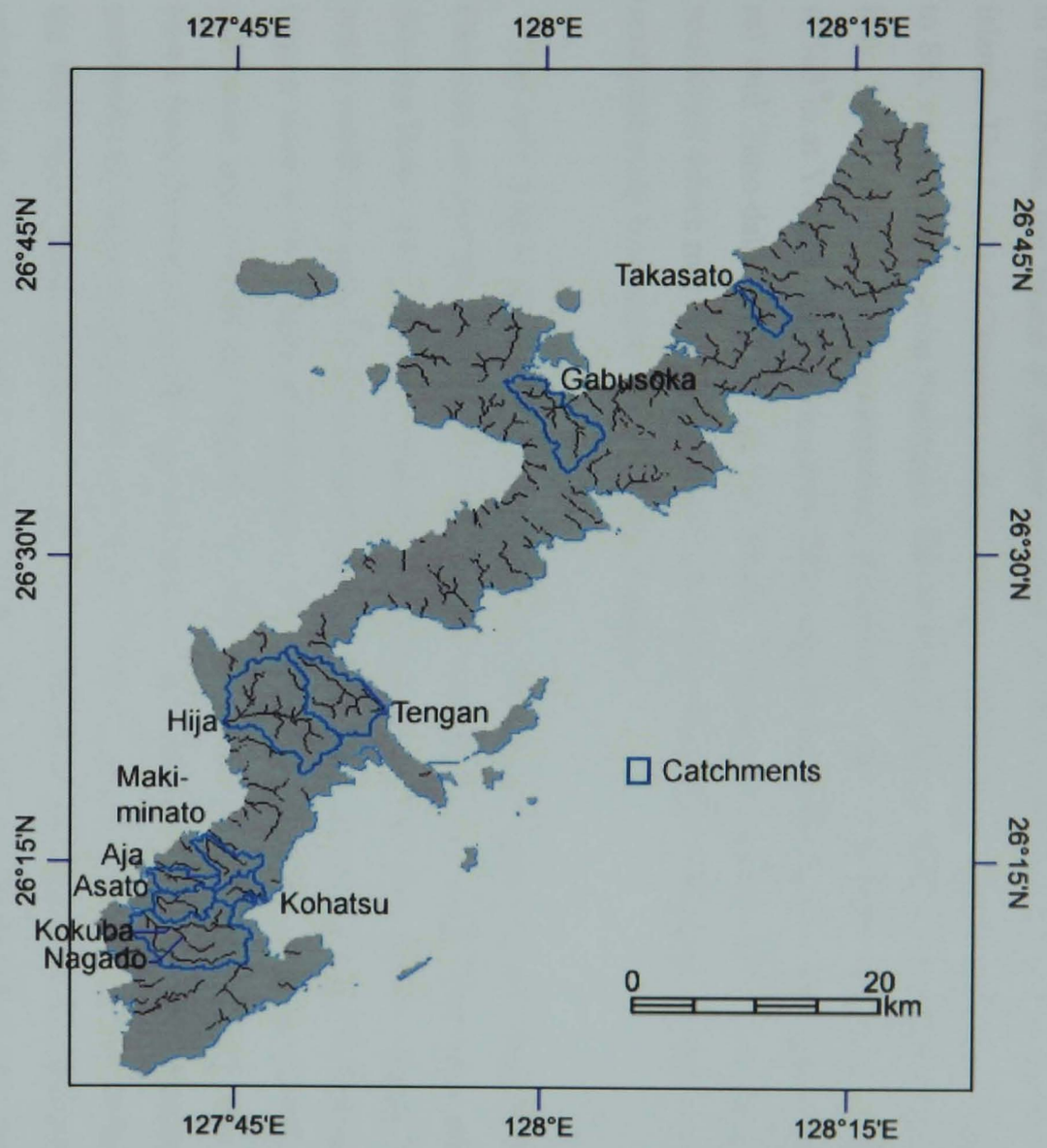

Fig. 2.13. The rivers in Okinawa. Discharge of 10 rivers is measured by the *OPG River Section*: 8 rivers on the west side and 2 on the east side. The Nagado River is a branch current of the Kokuba River hence it stays in the same catchment as the Kokuba River.

In this thesis, the Island of Okinawa means the main Island of Okinawa and excludes these islands. The Island of Okinawa is about 120 km long NE to SW and about 10 – 20 km wide NW to SE, except the Motobu Peninsula. The narrowest part is about 4 km in the middle near Kin Bay. The northern part is mountainous; the altitude ranges from 100 – 500 m. The highest point is 503 m at Yonaha-dake in the north. Other highlands are also seen in the north, Yae-dake (454 m) and Tano-dake (396 m). In the middle, the highest point is 363 m at Onna-dake. The southwest where main cities are located, including the capital Naha city, is relatively flat but the southeast parts have some steeply sloped regions.

The river map is shown in Fig. 2.13. Since Okinawa is a narrow island, most of the rivers in Okinawa are less than 10 km in length, and the catchments are small. They are torrent streams, flowing down steep slopes, particularly in the north of Okinawa (Kochi, 2003). Due to the heavy rainfall brought by the summer EAM and typhoons, the streams are highly variable. The largest river in the Island of Okinawa is the Hija River. Its total length is 14 500 m and the catchment area is 49.66 km^2 (Okinawa Construction Technology Center, 2003). The Hija River flows from Okinawa City, the second largest city in Okinawa. In the most urbanised area, the southwest of Okinawa where the capital city, Naha, is located, there are several rivers flowing to the west coast. These rivers are subject to discharge of wastewater as an inevitable result of urbanisation. The main sources of pollutant in these rivers are wastewaters from domestic and livestock industry (OPG, 2004), which are transported from the rivers to the estuary. Such riverine transport can be regarded as a pathway for input of nutrients to the coastal environment. Since 1992 the OPG selected the southern cities for the priority regions for waste water management, and has put effort to facilitate filtering systems (OPG, 2004).

Fig. 2.14 shows the soil types on the Island of Okinawa. There are mainly 3 types of soil on the Island. The major soil is called *Kunigami maji*, which is predominantly distributed over the northern part of Okinawa. This soil is an acid soil and generally red coloured, composed of 58 % sand, 30 % silt and 12 % clay. It occurs in the steep slope areas in the north, which are relatively susceptible to erosion. The second major soil type is a weak alkaline soil, dark red coloured, called *Shimajiri maji*, composed of 70 % sand, 21 % silt and 9 % clay. Another type is a grey alkaline soil, called *Jagaru*, with 43 % sand, 46 % silt and 11 % clay. It occurs in steep slope areas in the southeast. Higa et al. (1998) estimated the erodibility factors of these soils for the Universal Soil Loss Equation (USLE), and suggested 0.4 for *Jagaru*, 0.3 for *Kunigami maji* and 0.1 for *Shimajiri maji* (higher number indicates higher erodibility). Steep slope areas covered with higher erodible soils such as *Jagaru* and *Kunigami maji* are often affected by landslides (Zhou et al., 1996; Gibo et al., 1998).

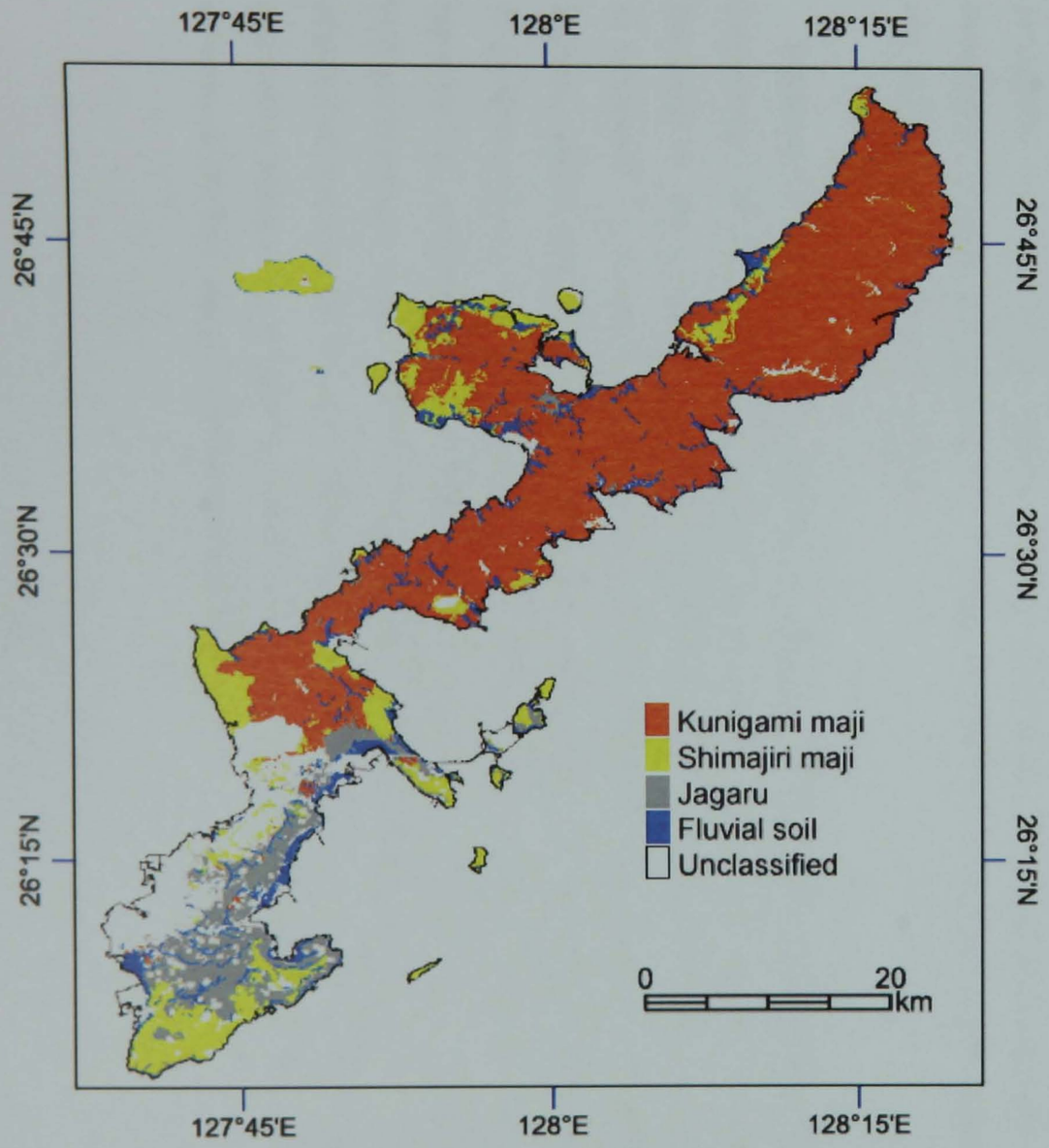

Fig. 2.14. Soil type in Okinawa (1992). Data from the *OPG Land Management Section*.

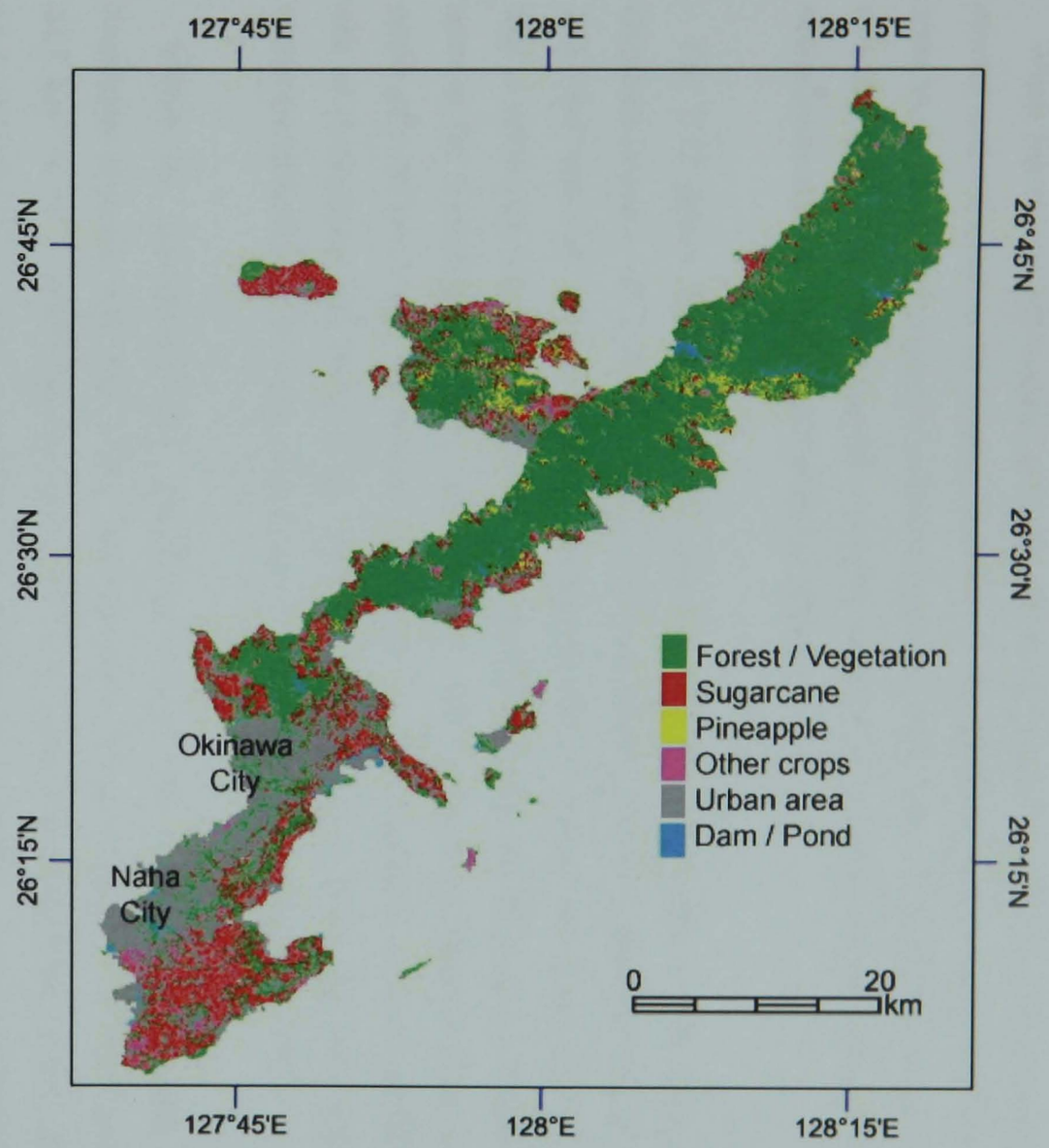

Fig. 2.15. Land use of Okinawa (1998). Data from the *OPG Land Management Section*.

When heavy rainfall occurs, soils on the steep slopes and less vegetated areas are easily eroded and delivered to the coastal zone through the short rivers. Such soil run-off to the coastal zone has been an environmental problem since the 1970s. Due to the reddish colour of the major soil, *Kunigami maji*, such run-off is known as red-soil run-off pollution, leading to abnormal sedimentation in the coastal zone (Omija, 1992).

Fig. 2.15 shows the land-use map produced in 1998. According to this map, the area of Okinawa Island is 1272.6 km^2. The area of forest, agricultural field and urban use are 667.5 km^2, 255.5 km^2 and 295.1 km^2 respectively. Generally, the northern part is covered by forest, and the mid to south part is urbanised. The agricultural fields (sugarcane, pineapple and other fields) are seen in the southeast, mid-east, mid west and north of Motobu Peninsula. The mountainous north part enriched with the forest is called the Yanbaru region. It is dominated by evergreen oak or chinquapin. The forest in the northwest is a secondary forest. The natural forest in the northeast harbours many endemic and endangered birds and mammals (Ito, 1997).

Within the agricultural zone, sugarcane occupies 149.6 km^2, and pineapple 22.4 km^2. Pineapple coverage was only 0.9 km^2 in 1954, but it was dramatically increased, and peaked at 44.5 km^2 in 1975 (OPG Agriculture, Forestry and Fisheries Department, 2007). Because the acid soil *Kunigami maji* is suitable for cultivating pineapple, rapid land development for pineapples occurred in the northern part of the Island. This rapid development, where the topography is steep and reddish soil is dominant, has been considered as one of the causes of red soil run-off (Onaga et al., 1999).

Sugarcane is a key agricultural product in Okinawa (OPG Agriculture, Forestry and Fisheries Department, 2007). It is widely cultivated in the Island except on the soil of *Kunigami maji*. In the south lies the capital city of Naha where the population is 312,393, out of the total 1,230,346 in the Island. The second largest city is Okinawa City with a population of 126 400 (Statistics Bureau, 2005). Rivers that flow in populated urban areas tend to be polluted by wastewaters from domestic sources and the livestock industry (OPG, 2004). West and Woesik (2001) reported that a strong positive relationship existed between the population densities and both biological oxygen demand (BOD) and suspended particle matter in the rivers of Okinawa. As population has been growing in Okinawa, urbanised land-use has also increased (Table 2. 1), suggesting associated increase in waster water. The coastal zone response to the river discharge in terms of the SST and OC4 is discussed in Chapter 5.

Table 2.1 Population and residential area in Okinawa (OPG Statistic Section, 1999, 2001, 2005)

Year	population	residential area (m^2)
1999	1,308,010	124,652,918
2001	1,326,367	126,594,179
2005	1,360,830	128,717,488

Heavy rainfall on uncontrolled bare lands and inappropriately managed agricultural fields with highly erodible red-soils, particularly in the north, often trigger severe soil erosion and soil run-off through the rivers. Sediments deposited in the coastal waters adversely impact the coastal environment including coral reefs. Fig. 2.16 shows satellite images of the Island of Okinawa, scanned by the earth observation satellite Landsat on (a) 17 December 1996 and (b) 26 November 2000. In Fig. 2.16 (a), soil run-off can be seen along the mid west coast, drifting southward the surface in Kin Bay. From a comparison with Fig. 2.16 (b), it is clear that this part is not a shallow reef but run-off. This event was captured about 10:30 am local time, and the preceding rainfall event occurred between 22:00 pm 16th – 2:00 am 17th, providing 40 mm of rainfall near Kin Bay.

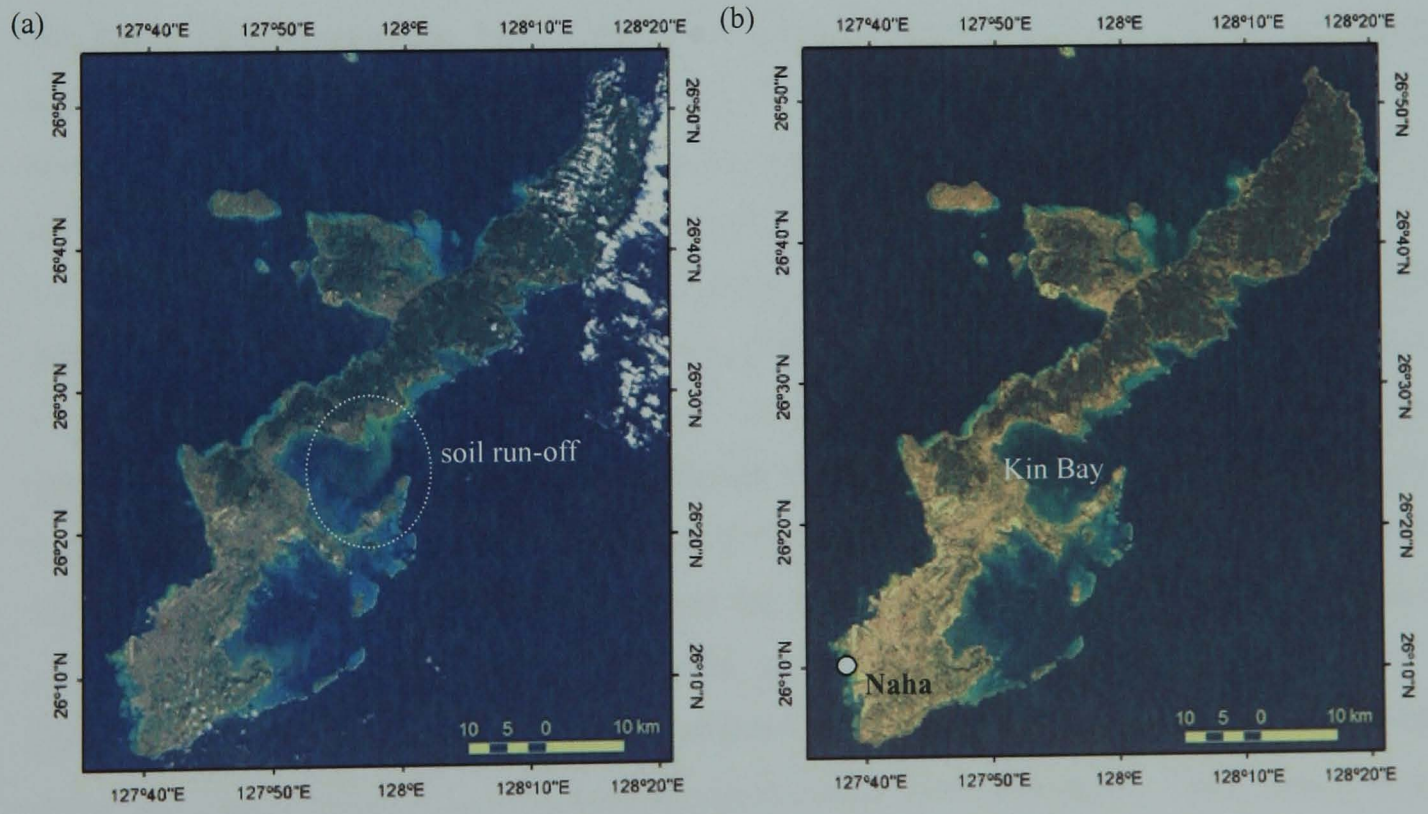

Fig. 2.16. Landsat images of the Island of Okinawa (a) 17 December 1996 and (b) 26 November 2000.

2.4.3 Land Development and Coastal Environmental History

In the history of agriculture in Okinawa, the most dramatic change was an introduction of pineapple farming and its rapid development in the northern, acid red soil region, in the late 1950s. The area of pineapple farming on Okinawa in 1954 was 89 ha. It was increased by a

factor of 20 by 1957 and by a factor of 60 in 1967, with a total area of 5,380 ha. This drastic development subsequently caused extreme soil erosion (Onaga et al., 1999). In addition, the rapid construction of US military facilities was started around 1960. In the post-World War II period, Okinawa was under the control of the U.S. until 1972. At the reversion of Okinawa to Japanese control in 1972, excessive re-development on the Island started, including dam construction, flood control works, and land reformation. These combined actions escalated the soil erosion, not only endangering agricultural soil conservation, but also affecting the coastal environment through soil runoff. According to a 1993/94 survey (Higa et al., 1995a), a total of 320,000 tons of top-soil was washed in that year from the land of Okinawa into the rivers and sea, with land development being the major source (57 %), followed by agriculture (33 %) and U.S. military activities (9 %).

Since the initiation of enhanced soil run-off and its associated threat to the coastal environment, which damages the coral reefs, this issue has become one of the most serious environmental problems, recognised as red-soil run-off pollution, locally termed *Akastuchi* (Omija, 1992). A typical red-soil is generally composed of the red coloured soil, *Kunigami maji*, which is predominantly distributed over the northern part of Okinawa. Red-soil run-off to the coast can be easily seen after heavy rainfall through the contrast in the colour of the sea. As red-soil has a clay composition, both sedimentation and resuspension have at least three adverse effects on corals: (1) unconsolidated sediment with no hard bottom is an unstable substrate for new coral settlement or reef formation, (2) acute stress can result from the smothering effects of rapid sediment deposition by terrestrial run-off and resuspension, and (3) chronic stress can result from an enhanced suspended load which reduces water clarity and light levels, hampering photosynthetic activities (Sakai and Nishihira, 1991; McLaughlin et al., 2003). The heavy soil run-off of Okinawa displays a typical example of terrestrial impact on coral reefs which reduces the resilience of corals. As a result, the landscape will deteriorate and the abundance of reef fish and the richness of species will be degraded (Bellwood et al., 2004). Furthermore, recent global warming significantly impacted corals around the world (Wilkinson, 1998), including Okinawa. After the strongest El Niño event in 1997/98, almost all the corals along mid-west coast of Okinawa experienced bleaching due to anomalous sea temperature. Combined with the chronic terrestrial impact through red-soil run-off, most corals died (Yamazato, 1999; Omija et al., 2000; Nakano, 2004).

In 1994 the OPG established the *Okinawa Prefecture Red-soil Erosion Prevention Ordinance* (the Red-soil Ordinance) which has been enforced since October 1995. This Ordinance requires land developers whose project site is greater than 1,000 m^2 to suppress the suspended sediment in the discharge from their development site to less than 200 mg/l. As a result of the implementation of the ordinance, estimates from water sampling surveys conducted by the

prefectural institute reported that the yearly amount of measured soil run-off was reduced by 30 % between 1996 and 1997 estimated by the use of USLE (Nakasone et al., 1998). To monitor sediments in coastal waters, measurement of the content of suspended particles in sea sediment (SPSS [1]) was developed by the Okinawa Prefectural Institute of Health and Environment to monitor soil pollution in 1985 (Omija, 1987, see Chapter 3, §3.2.5.3 for its measurement). The SPSS concentration corresponds well with the benthic properties of the sea which provides an index of the sea environment (Table 2.2). Thus this method has been used to monitor the sediment in the sea since 1983.

In the survey by Omija et al. (2002), it is reported that the mean value of SPSS over all Okinawa regions was improved from 45.5 kg/m^3 to 36.3 kg/m^3 after the implementation of the Red-soil Ordinance, showing a decrease of 20 %. Fig. 2.17 shows this comparison and indicates an improvement around most of the island including northern Okinawa. This effect can be attributed to the enforcing of the ordinance (Omija et al., 2002), however, in order to evaluate the SPSS increase and decrease, not only the terrestrial effect but also interaction with the climate system on a larger scale should be considered.

Table 2.2. Relationship between the SPSS values and the status of coastal bottom (Omija, 1987).

SPSS (kg/m^3)			Status of sediment in the bottom and other characteristics
Rank	Lower bound	Upper bound	
1	-	< 0.4	Not measurable. Fine particles are not suspended even when bottom is stirred. White sand dominates the area but few organisms observed.
2	0.4	< 1	Fine particles are not easily suspended even when bottom is stirred. White sand dominates the area but few organisms observed.
3	1	< 5	Fine particles are resuspended when bottom is stirred. A lively coral reef can be observed. Water transparency is high.
4	5	< 10	Water becomes slightly turbid when bottom is stirred, although it will not occur in calm conditions. A lively coral reef can be observed.
5a	10	< 30	Fine particles are observed on the bottom surface by careful observation. Limit of a lively coral reef.
5b	30	< 50	Dust-like fine particles cover the bottom surface. Water transparency and coral coverage decline.
6	50	< 200	Red-soil sedimentation is clear at a glance. Its resuspension is apparent when bottom is stirred. Above this rank, it can be empirically estimated that the red soil run-off and pollution are caused by human activities.
7	200	< 400	Foot steps can remain clearly on the surface. Remarkable sedimentation of red soil, but some sand can be still observed. Large colonies of branching type coral are not observed, more massive type corals appear instead.
8	400	-	Foot steps get bogged in mud. Sand can rarely be observed, but dotted with massive type corals.

[1] Although the word "suspended" is used in this term, actual measurement is carried out from the bottom sediment, therefore it does not measure "suspended" particles at site. However, in determining the concentration at lab, turbidity in a cylinder caused by suspended particles is used (§ 3.2.5.3). Thus "SPSS" will be used to describe bottom sediment in this thesis as it was originally coined by Omija (1987).

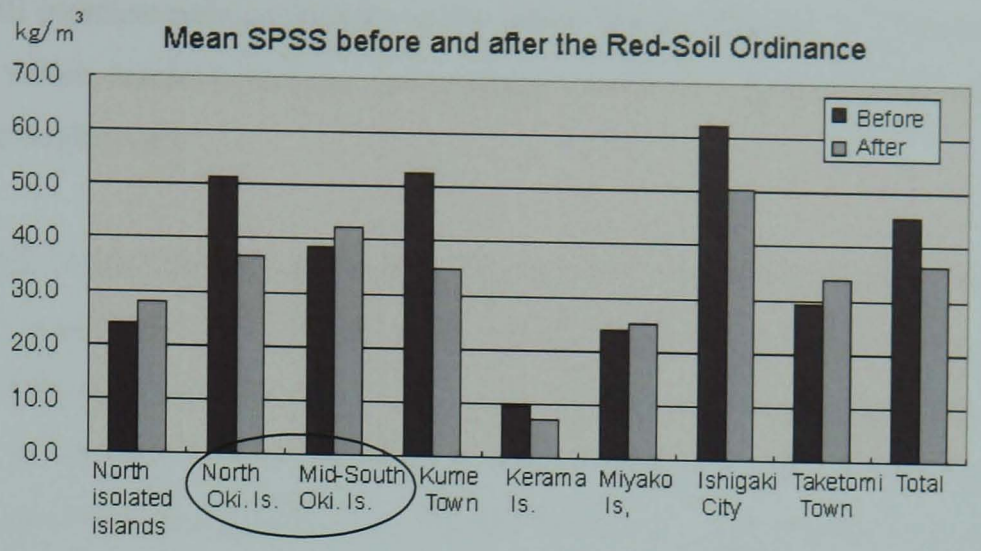

Fig. 2.17. Mean SPSS before and after the Red-soil Ordinance enforcement in 1995. The circle indicates the region of the Island of Okinawa, north and mid-and-south regions. For the location of other islands, see Fig. 1.3 in Chapter 1. (Adapted from the Okinawa Institute for Health and Environment website: http://www.eikanken-okinawa.jp/suiaka/akatuti/umi/umi.htm).

2.4.4 Summary: Climate and Terrestrial Influences on the Coastal Zone

Under the influence of the EAM, the Island of Okinawa experiences strong/dry northerlies in winter and weak/wet southerlies in summer. Wind strengths above 10 m/s occur mostly in winter. Other seasons that bring stronger winds are only the typhoon seasons during summer and autumn. Therefore, the effect of wind on the coast differs between the west and east side of the Island due to the wind direction. Waves induced by winds become strong along the west coast in winter, but occasionally affect the east coast in typhoons (Mesaki, 1985), which will make a difference in the SPSS distribution between the west and east coast.

Considering topography (Fig. 2.12), soil type (Fig. 2.14), land-use (Fig. 2.15) and the dramatic development of pineapple field (§2.4.3), it can be speculated that pineapple fields which occur on fragile soil in steep slopes are the most sensitive areas to soil erosion. Such areas are seen over northeast of Okinawa. The acid soil *Kunigami-maji* is suitable for cultivating pineapple, these fields often occur in hilly northern region. These conditions of high erodibility of *Kunigami-maji* and steep topography tend to be conducive to soil erosion. Actually noticeable erosion and gullies in pineapple fields are often reported which contribute to sediment delivery to adjacent coastal zone (Omija, 1992; Nakasone et al., 2000; Omija et al., 2002). Not only pineapple fields, other agricultural fields on fragile soil in steep topography can be the vulnerable areas for erosion according to their crop stages when the vegetation cover decreases. In addition, under the climate change scenarios with increasing rainfall as IPCC FAR provided (Solomon et al., 2007), enhanced rainfall will also accelerate erosion. Moreover, natural hazard such as land slide may be more often triggered over steep slope areas with increasing rainfall (see Chapter 6, §6.6). Increase of population will lead to extending of urban

areas, which will increase nutrient supply in the waste water. Without an appropriate treatment of urban waste water, nutrient loadings, particularly southwest region, will increase in adjacent coastal zones through rivers.

In general, soil run-off occurs in the rainy season, thus, the SPSS reaches a maximum after the rainy season in summer. The rainfall in Okinawa is often squally, with a large drop size and high erosivity. Rainfall rates heavier than 3 mm/10 min, which are generally regarded as "erosive" rains, often occur in Okinawa (Onaga and Yoshinaga, 1983). Being affected by strong northerlies during winter, sediments in the coastal waters are dispersed by waves and the SPSS decreases (Omija, 2002). This pattern is particularly observed on the west coast, thus, the SPSS shows a seasonal variability on the west side of the Island. On the east side, on the other hand, the effect of northeasterlies seems small and shows little seasonal variability compared to the west coast (Nakasone et al., 2000). There are factors affecting run-off and SPSS concentrations, e.g., geographical shape of the coast, bathymetry, geology, adjacent land-use and ground waters (Nakasone et al., 2000; Omija et al., 2002). Among them, climate appears to be a major control on SPSS variability. However, little quantitative analysis has been carried out about sediment variability in relation to the larger scale EAM.

Along with soils and sediments, nutrients are another terrestrial input to the ocean through the rivers. These inputs affect the ocean Chl-a, as shown in the previous section about the Yangtze River discharge to the ECS. On the Island of Okinawa, Higa et al. (2001) surveyed the concentrations of the total nitrogen (TN), total phosphorus (TP) and suspended sediments (SS) in the 98 river mouths around the Island, and reported that both TN and TP concentrations are higher in the southern rivers than in the north, probably due to the differences in land-use and waste water efflux. In rainfall events, TN and TP tend to increase, correlating with SS increase. West and van Woesik (2001) analysed BOD and SS in the 7 river mouths in Okinawa, and found a significant positive relationship between human population densities within river catchment areas and both BOD and SS. These studies suggest that higher nutrients are discharged from the rivers in urbanised southern Okinawa, and enhanced by rainfall.

Nutrient input may be even more enhanced by extreme events such as typhoons which affect not only the ocean surface but the land surface. Typhoons are considered to be an important form of natural disturbance for the native forest. A direct typhoon hit on the land can cause extensive tree felling and uprooting that produces gaps in the forest (Bellingham et al., 1996). It increases the uncovered surface, exposing top soil for possible erosion. In addition, increased salt stress induced by the strong wind imposes further damage on trees, leading to extensive defoliation (Xu et al, 2004). Both impacts cause a reduction in vegetation cover, and hence

increase of erosion and soil run-off. Therefore, typhoons have another role in enhancing nutrient supply in addition to the gap producing function. Another link between typhoons and increasing nutrient input is as follows. In general, forest production and nutrient cycling are strongly correlated to litterfall (Bray and Gorham, 1964). Xu et al. (2004) measured nutrients in leaf litter of northern Okinawa from 1996 to 2001, and found that the highest concentrations of nitrogen and phosphorus were recorded in the typhoon season. This means the highest nutrient input to soil occurs during typhoons. Run-off containing such soil will certainly increase nutrient delivery to the ocean along with suspended sediment.

As mentioned earlier, wind-driven upwelling is an important mechanism to supply nutrient to the ocean surface, which modulates both the sea surface temperature and Chl-a concentration. The typhoon influence leads to additional nutrient inputs to the ocean. Although the size of the Island is small, signals of coastal zone response to typhoons may be significant due to the combined effect of typhoons and terrestrial input.

Chapter 3 Data, Methodology and Preliminary Analysis

3.1 Introduction

This chapter describes the data used in this study. Fig. 3.1 shows the data and their temporal coverage. Methodology and the result of preliminary analysis are also discussed. The outline is as follows:

(1) Data used (Fig. 3.1)

- Remote sensing data: the SST, ocean colour, and the ocean wind.
- Climate data recorded at the weather stations in Okinawa.
- Terrestrial data: river discharge and sea sediments in the coast around Okinawa.

(2) Methodology

- Objective analysis by optimum interpolation of the remote sensing data.
- Empirical orthogonal function (EOF) analysis for variability study.

(3) Result of preliminary analysis

- Result of the objective analysis of the remote sensing data.

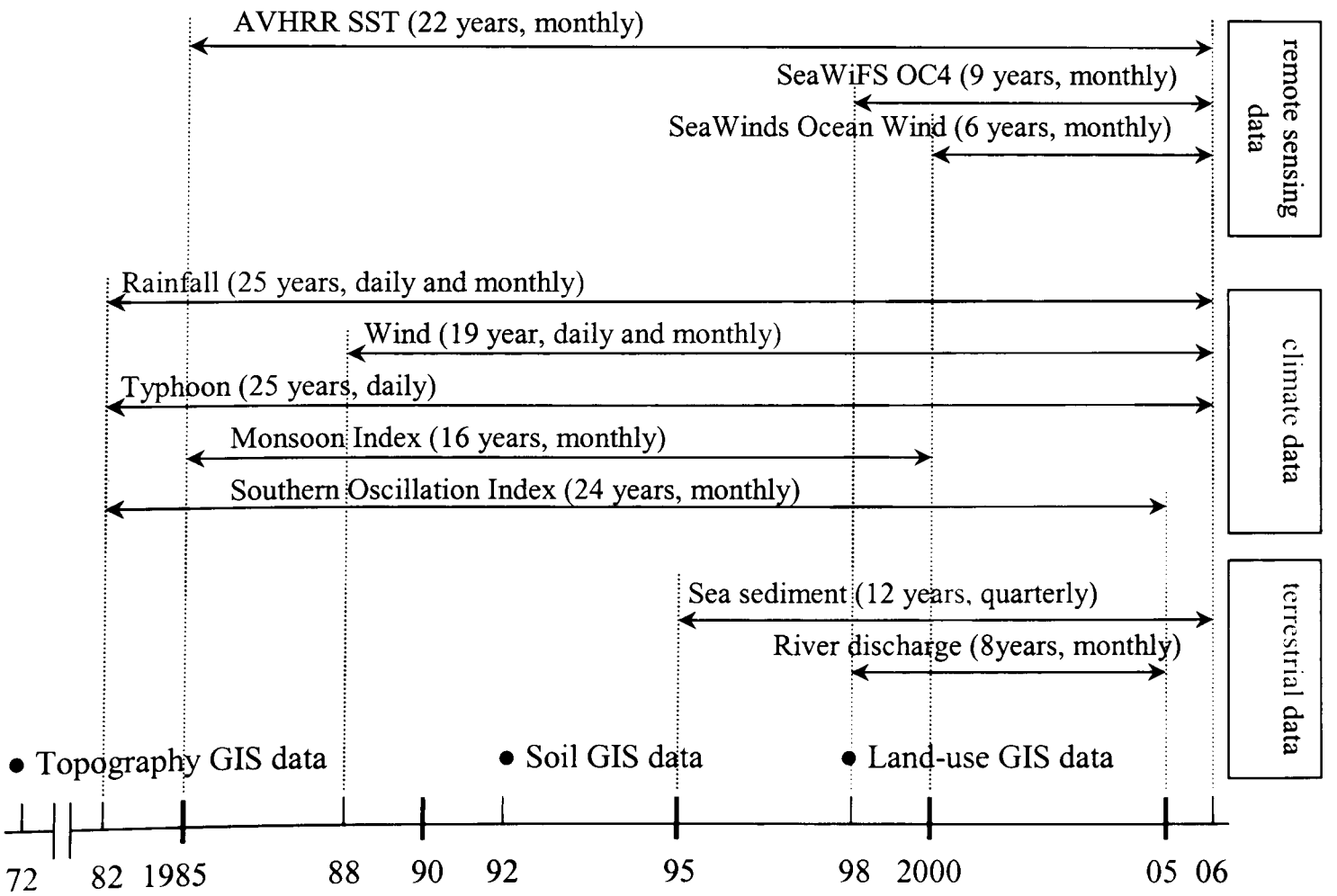

Fig. 3.1. Data used in this thesis: remote sensing, climate, terrestrial and GIS data.

3.2 Data

3.2.1 Sea Surface Temperature

Observing the sea surface temperature (SST) by remote sensing is a useful method to analyse its spatial and temporal variation over the East China Sea, e.g. the warm water of the Kuroshio Current (KC), or the influence of the East Asian Monsoon (EAM). Satellite data acquired by the Advanced Very High Resolution Radiometer (AVHRR) sensor loaded on the NOAA satellite series are used to observe the SST. In order to observe the SST at close time to ocean colour observation by SeaWiFS, daytime daily and monthly SST data whose observation time falls around 2 pm local time (approximately 2 hours later than the time of SeaWiFS observation of ocean colour – see next section) are collected. Characteristics of the AVHRR are given in Table 3.1.

Table 3.1. Characteristics of NOAA 6 to 15 (adapted from Lillesand, 1999).

Parameter	NOAA 6, 8, 10, 12 and 15	NOAA 7, 9, 11 and 14
Launch	27/6/79, 28/3/83, 17/9/86, 14/5/91, 13/5/98	23/6/81, 12/12/84, 24/9/88, 30/12/94
Altitude (km)	833	870
Period of orbit (min)	101	102
Orbit inclination	98.7 °	98.9 °
Orbits per day	14.2	14.1
Distance between orbits	25.6 °	25.6 °
Day-to-day orbital shift	5.5 °E	3.0 °E
Orbit repeat period (days)	4-5	8-9
Scan angle from nadir	±55.4 °	±55.4 °
Swath width (km)	2400	2400
Coverage	Every 12 hr	Every 12 hr
Northbound equatorial crossing	7:30 p.m.	1:30-2:30 p.m.
Southbound equatorial crossing	7:30 a.m.	1:30-2:30 a.m.
Spatial resolution (km)	1.09 km	1.09 km
AVHRR spectral channels (μm)		
1	0.58-0.68	0.58-0.68
2	0.72-1.10	0.72-1.10
3	3.55-3.93[*1]	3.55-3.93
4	10.5-11.50	10.5-11.50
5	Channel 4 repeat[*2]	11.5-12.50

*1 NOAA 15 includes two separate channels: 3A (1.58-1.64 μm) and 3b (3.55-3.93 μm).

*2 NOAA 12 and 15 include a separate channel 5.

The daily and monthly SST data (1985 – 2006: 22 years) were collected from the NASA ftp site (ftp://podaac.jpl.nasa.gov/pub/sea_surface_temperature/avhrr/pathfinder/data_v5/). The global SST level 3 product Pathfinder Version 5.0 developed by the NOAA/NASA Oceans Pathfinder Program which has been built with 4 km resolution over the globe were used. The Pathfinder algorithm combines the multiple observations by the NOAA satellites as long as they have a compatible data quality.

AVHRR measures the radiation at wavelengths of 3.7 μm and/or near 10 μm. The method of measuring the temperature is based on the theory that all objects radiate energy according to their blackbody temperature. A blackbody is a hypothetical object that absorbs all incoming thermal energy, but with none of that energy reflected or transmitted. Since no object can ideally absorb 100 percent of incident energy, a blackbody serves as a comparative measure of thermal emission. As the temperature of an object increases, the total amount of the emitted energy also increases, and the wavelength of that energy becomes shorter, as Wien's law describes (Fig. 3.2). According to the Stefan-Boltzman law, objects with a higher temperature give off more thermal energy per unit area than objects with a lower temperature. Remote sensing in the thermal infrared spectral region (approximately 7 μm to 14 μm) involves measuring the radiance of objects. More specifically, thermal remote sensing measures the differences in the ability of objects to absorb shortwave energy and emit it back as long wave energy.

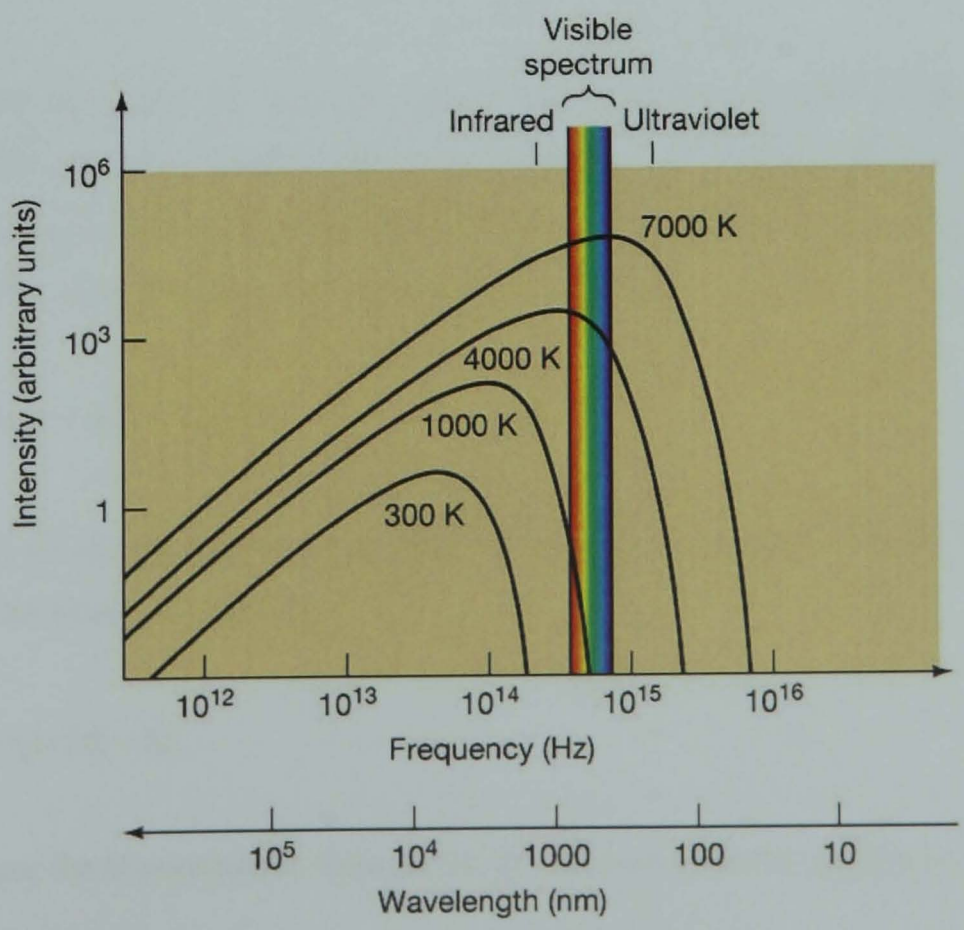

Fig. 3.2. Wien's law: The wavelength corresponding to the peak emission in various black body spectra as a function of temperature (http://physics.uoregon.edu/~jimbrau/BrauImNew/Chap03/FG03_11.jpg).

The radiation interacts little with air molecules at around 10 μm (atmospheric window, Fig. 3.3). For a surface at a brightness temperature around 300 K, the spectral radiance peaks at a wavelength around 10 μm. For this reason, most satellite sensors for measurement of the earth surface temperature have a band detecting infrared radiation around 10 μm (channel 4 and 5 for AVHRR, see Table 3.1). The sea surface temperature of the earth ranges from 271 to 312 K, and the emission from the sea surface has an energy peak around 9 – 11 μm. In this range, sea surface emissivity is close to 1 (0.98 – 0.99) which can be regarded as black body emission. Therefore, measuring the radiation energy derives the temperature.

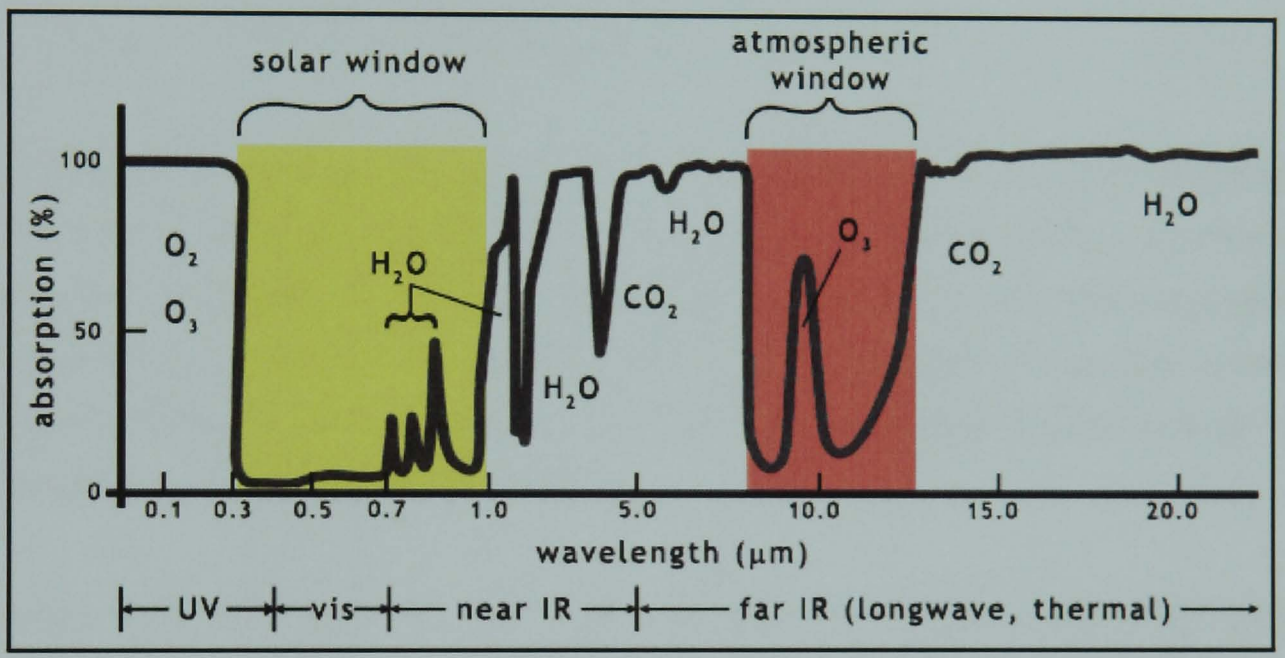

Fig 3.3. Atmospheric radiation absorption in respect to wavelength (http://www.helpsavetheclimate.com/climate.html).

Algorithms for deriving SST were developed using brightness temperatures and radiances as inputs. This early work was based on the theoretical work of McMillin (1975), who showed that a simple linear combination of the radiances measured at two wavelengths gave a good estimate of the radiance leaving the surface and hence the SST values:

$$\mathrm{SST} = aT_i + \gamma(T_i - T_j) + c \qquad \text{(Eq. 3.1)}$$

where T_i and T_j are the brightness temperature measured in channels i and j respectively, and c is a constant. The γ term is defined as

$$\gamma = (1 - \tau_i) / (\tau_i - \tau_j) \qquad \text{(Eq. 3.2)}$$

where τ_i and τ_j are the transmittance through the atmosphere from the surface to the satellite.

All AVHRR algorithms share the general equation described above with various modifications developed over the years to improve performance. This multi-channel SST (MCSST) algorithm was based on linear differences in brightness temperatures among AVHRR channels and assumed a constant γ (McClain et al., 1985). Other improvements in the atmospheric correction involved non-linear formulations in which the γ was proportional to the brightness temperatures described by Walton (1988) and Walton et al. (1990). The AVHRR Oceans Pathfinder SST algorithm is based on the non-linear SST (NLSST) algorithm (Walton et al., 1998) in which γ is assumed to be proportional to a first guess SST value, and is given by

$$\mathrm{SST}_{\mathrm{sat}} = a + bT_4 + c(T_4 - T_5)\mathrm{SST}_{\mathrm{guess}} + d(T_4 - T_5)[\sec(\theta) - 1] \qquad \text{(Eq. 3.3)}$$

where $\mathrm{SST}_{\mathrm{sat}}$ is the satellite-derived SST estimate, and T_4 and T_5 are brightness temperatures in the 10.8 and 11.4 μm bands of AVHRR channel 4 and 5 respectively. $\mathrm{SST}_{\mathrm{guess}}$ is a first guess value, and θ is the satellite zenith angle. Coefficients a, b, c, and d are estimated from regression analyses with in-situ and satellite measurements. A global measurement accuracy of MCSST algorithm is claimed to be 0.7 K (Barton, 1995). For NLSST algorithm, it improves to be 0.59 K for the highest quality (Kilpatrick et al., 2001).

Along with the SST values in the data acquired, information on quality level is also produced for each pixel according to the quality condition tests which examine cloud obstacles, the uniformity of the values in the neighbouring pixels, zenith angle, influence of glint, and so on. These tests classify the quality into eight possible overall levels from 0 to 7 to which a pixel may be assigned. A level 0 indicates the lowest quality of SST data, while level 7 means the highest. Naturally the available coverage of SST decreases with the increase quality. End users can make their own decisions on the geographic coverage and accuracy used on the basis of quality level. For instance, if quantitative analyses are to be performed on the SST values, one will only require the best quality SST estimate. On the other hand, if monitoring the patterns is of interest, one may be willing to accept lower quality levels in trading off SST quality to gain more coverage (Kilpatrick et al., 2001). In this study, as the interest lies in finding the spatial and temporal pattern, quality level 4 which is the minimum quality that at least passed the cloud test were used. The procedure to convert AVHRR/SST global coverage level 3 (note the processing level, not the quality level) data value x, which has a single layer of 8-bit (0-255) resolution, to the SST (degree Celsius) is given by the formula: $0.075x - 3$. For a comparison between the AVHRR SST and in-situ data off the coast of Okinawa, see Appendix A.1.

3.2.2 Ocean Colour (chlorophyll-a)

In order to estimate sediment or nutrient distribution in the coastal zone that impact coral reef environment, ocean colour data acquired by satellite remote sensing are used. Photosynthetic organisms, as phytoplankton, absorb light at blue and red wavelengths and transmit in the green, and hence affect the colour of the ocean. Chlorophyll-a (Chl-a) is the pigment that participates directly in the reactions of photosynthesis. All phytoplankton in water bodies contain the photosynthetically active pigment Chl-a. The growth of phytoplankton depends on the availability of nutrients and sun-light. The controls are in turn regulated by the solar cycle, physical processes of ocean circulation (Nicol et al., 2000; Thomas et al., 2001), mixed-layer dynamics (Campbell and Aarup, 1992; Michaels et al., 1994; Nakamoto et al., 2001), upwelling (Strass, 1992; Morales et al., 1996; Thomas, 1999; Chen et al., 2003), or atmospheric dust deposition (Erickson et al, 2003; Meskhidze et al., 2003; Jickells et al., 2005). Nutrient supply through river run-off containing sediments including nitrogen, phosphorus and iron is a significant terrestrial effect on the Chl-a bloom. Therefore, terrestrial influence can be observed by the changes in Chl-a concentration around river estuaries and adjacent coastal zones (Hama et al., 1997; Gong et al., 2003).

In order to observe, monitor and understand Chl-a distribution within the study area, a space-borne remote sensing technique is used. The influence of phytoplankton on the ocean colour has been well studied (Gordon et al., 1980; Gitelson, 1992; Mitchell, 1994). Satellite sensors determine ocean colour by measuring the radiance in a number of wavebands which correspond to absorption by Chl-a. It is well understood that Chl-a absorbs relatively more blue and red light than green, and the spectrum of backscattered sunlight (wavelengths of 400 – 700 nm) varies with the concentration of Chl-a and other plant pigments present in the water, i.e., the more phytoplankton present, the greater the concentration of Chl-a and the greener the water (Fig. 3.4, Clarke et al., 1970; Gordon et al., 1988; Han 1997). As seen in Fig. 3.4, algae-laden water reflects from the green band (around 550 nm) and absorbs the red and blue bands. In this study, the level 3 global mapped data, with a spatial resolution of 9 km, acquired by the Sea-viewing Wide Field-of-view Sensor (SeaWiFS) was used. The daily and monthly data of SeaWiFS Ocean Reprocessing 5.1 version from 1998 to 2006 (9 years) were collected from the Ocean Color Web ftp site operated by NASA at ftp://oceans.gsfc.nasa.gov/SeaWiFS/Mapped/. SeaWiFS (Table 3.2) was loaded on the SeaStar satellite, launched in 1 August 1997, and raised to a 705 km circular, sun-synchronous orbit. The time of observation at the equator is approximately local noon+20 minutes (approximately 2 hours before the AVHRR/SST observation time) in descending orbit (passes from north to south) (Barnes et al., 1994). The observed data have been processed since September 1997. The satellite was still operating as of June 2008.

Table 3.2. Characteristics of SeaWiFS (adapted from http://oceancolor.gsfc.nasa.gov/SeaWiFS/SEASTAR/SPACECRAFT.html).

Parameter	Characteristics
Launch	1/8/97
Altitude (km)	705
Period of orbit (min)	99
Revisit time (day)	1
Scan angle from nadir	58.3 ° for LAC*1 ; 45 ° for GAC*2
Swath width (km)	2801 km for LAC; 1502 km for GAC
Equator crossing	Noon ± 20 min, descending
Spatial resolution (km)	1.1 km for LAC; 4.5 km for GAC
Spectral channels (nm)	
1	402-422
2	433-453
3	480-500
4	500-520
5	545-565
6	660-680
7	745-785
8	845-885

*1 Local Area Coverage

*2 Global Area Coverage

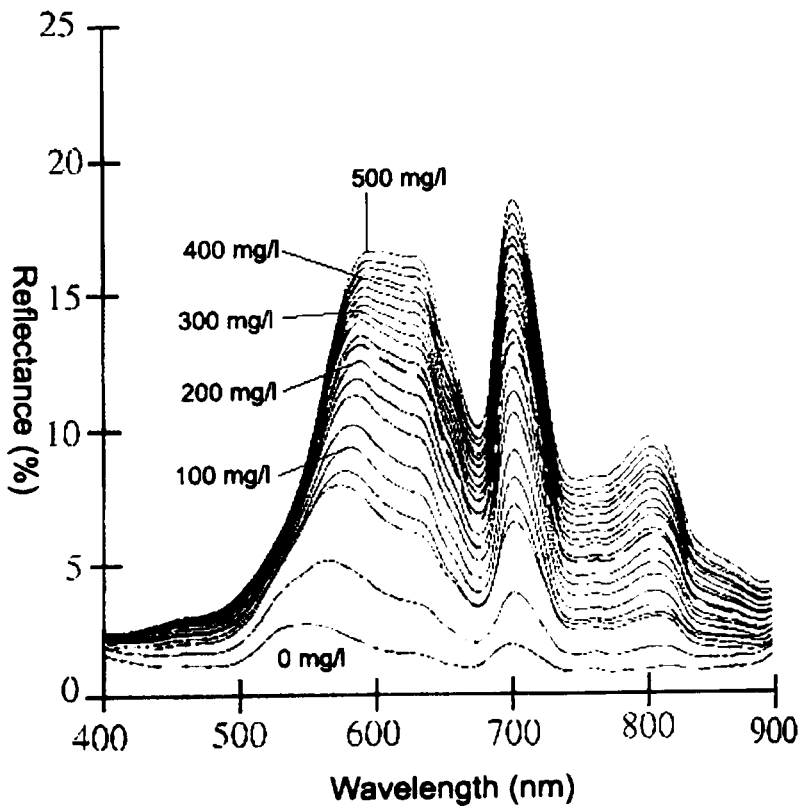

Fig. 3.4. Reflectance of algae-laden water with various suspended sediment concentrations (adapted from Jensen, 2000).

The algorithm, applied on the SeaWiFS level 3 data, which determines the Chl-a concentration uses an empirically derived ocean colour algorithm called "ocean chlorophyll 4" (OC4) consisting of a formulation involving four bands: 443, 490, 510, and 555 nm The power equation has been widely used to relate radiance ratios to Chl-a since the OC1 (Clark, 1981: Mitchell and Holm-Hansen, 1991; O'Reilly et al., 1998). Since OC2, a multi cubic power equation has been used whose form is given,

$$\text{Chl-a} = 10^{\wedge} (a0+a1*R+a2*R^2+a3*R^3) + a4 \qquad \text{(Eq. 3.4)}$$

where R = log((Rrs443 > Rrs490 > Rrs510)/Rrs555), Rrs(x) = reflectance in band x. In OC4, the coefficients are provided as

$$a0 = 0.4708,\ a1 = -3.8469,\ a2 = 4.5338,\ a3 = -2.4434, \text{ and } a4 = -0.0414. \qquad \text{(Eq. 3.5)}$$

With these coefficients used in OC4 algorithm, RMS error is claimed to be 0.156 (O'Reilly et al., 1998). The level 3 mapped data contain a single layer of 8-bit (0-255) resolution. Conversion of this 8-bit value to the Chl-a concentration (mg/m^3) can be carried out by using the formula: $10^{(0.015x-2)}$ (as of SeaWiFS Ocean Reprocessing 5.1, http://oceancolor.gsfc.nasa.gov/REPROCESSING/SeaWiFS/R5.1/).

In estimation of Chl-a concentration by remote sensing, it has to be mentioned that Chl-a concentration is likely overestimated in the coastal zone because of elevated concentrations of terrestrial particulate matter, coloured dissolved organic matter (CDOM) and inorganic particulates including terrestrial particulate matter transported by the rivers or resuspended sediments (International Ocean Color Coordinating Group 2000). As seen in Fig. 3.4, when both suspended sediment and Chl-a are present in water at the same time, spectral response differs dramatically. The peak reflectance of algae-laden water in the visible wavelength shifted from 547 nm at 0 mg/l to 596 nm at 500 mg/l. Studies in Korean waters by Ahn et al. (2001) reported that the wavelength 625 nm is optimal wavelength for evaluation of suspended sediments (SS) concentration, and the spectral channel 5 of SeaWiFS (545 – 565 nm) can be an alternative. Ahn et al. (2001) also found that the presence of sediment in coastal zones lead to overestimation of Chl-a concentration greater than 20 – 500 %. Tan et al. (2006) also found the 545 – 565 nm band of SeaWiFS to be particularly good at detecting the reflectance of SS in the Malacca Straits. Tan et al. (2006) speculated that Chl-a bloom during rainy season is more severely influenced by SS which are flushed into the sea, and that strong northerlies of the Asian monsoon during winter contribute to Chl-a bloom. Similarly, off the coast of China especially around the Yangtze River estuary will show an enhanced signal of OC4 due to a large amount

of discharge with high sediment load (Huanting et al., 1998) during rainy season (i.e., the summer EAM). Since the Chinese coastal zones contains highly turbid waters, remotely sensed Chl-a indicates a higher value than the in-situ measurement even during dry winter (Kiyomoto et al., 2001). This thesis' objective is to observe the variability of sediments and nutrients impact on the coastal zone that can be interpreted through changes in Chl-a, not to quantitatively determine Chl-a. Therefore, to describe the ocean colour affected by ocean Chl-a estimated by SeaWiFS algorithm Ocean Colour version 4, the term "OC4" is defined as an ocean colour index in this thesis, without modification in Chl-a algorithm.

3.2.3 Ocean Winds

In addition to the wind data recorded at the weather stations in Okinawa, satellite ocean wind data were used to observe this variable's spatial distribution (data collected from ftp://podaac.jpl.nasa.gov/pub/ocean_wind/quikscat/L3/data). The level 3 data acquired by the SeaWinds sensor on the QuickSCAT satellite from 2000 to 2006 were collected (Perry, 2000). The sensor is a scatterometer which transmits microwave pulses to the ocean surface and measures the backscattered power received at the instrument. Wind stress over the ocean generates ripples and small waves, which roughen the sea surface. These waves modify the radar cross-section (sigma-0) of the ocean surface and hence the magnitude of backscattered power. In order to determine wind velocity from these measurements, one must understand the relationship between sigma-0 and near-surface wind velocity (e.g. Tsai et al., 1999; Naderi et al., 1991; Dunbar et al., 2001). This relationship is known as the geophysical model function. The QSCAT-1 model function was used to derive winds from the SeaWinds on QuickSCAT data (Lungu, 2006). The accuracy of QuickSCAT data is 2 m/s for wind speed and 20 degree for direction in the range of 3 – 20 m/s (NASA JPL, http://winds.jpl.nasa.gov/missions/quikscat/index.cfm).

The level 3 data are provided at daily temporal resolution and consists of gridded values of scalar wind speed, meridional and zonal components of wind velocity, squared wind speed and time given in fractions of a day. The spatial resolution is provided on an approximately 0.25 × 0.25 degree global grid. Rain flagging is included as an indicator of wind values which may have degraded accuracy due to the presence of rain. If the rain flag occurs, Huddleston and Stiles (2007) recommended that the wind vector cell not be used. Therefore, the data were filtered to eliminate rain contamination.

3.2.4 Climate Data

The climate data of the Island of Okinawa were collected from weather stations (WS) operated by the *Japan Meteorological Agency* (JMA) (Fig. 3.5). In addition to these, rainfall data recorded by the *Okinawa General Bureau* (OGB) and the *Okinawa Prefecture Government* (OPG) were used. Their grid coordinates and measuring items are listed in Table 3.3.

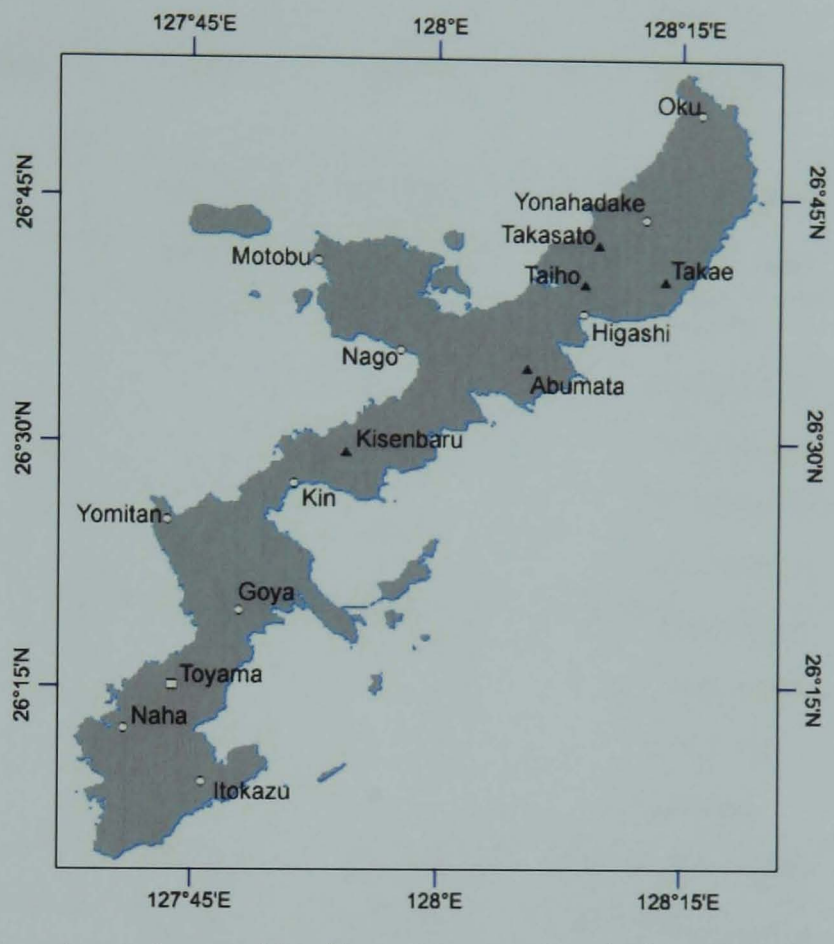

Fig. 3.5. Location of the weather stations used for this study, operated by the Japan Meteorological Agency (○: JMA), the Okinawa General Bureau (▲: OGB) and the Okinawa Prefecture Government (□: OPG).

Data relating to typhoon track, centre pressure and strength are obtained from the Digital Typhoon website (http://agora.ex.nii.ac.jp/digital-typhoon/) operated by the *National Institute of Informatics*. Wind data from the WS in Okinawa can be used to quantify the influence of the EAM and typhoons. To describe the intensity of the winter EAM on a larger scale, the Monsoon Index (MOI) is used. The Monsoon Index (MOI) that is determined by the sea level pressure difference (SLP) in hPa between Nemuro, Japan, and Irkutsk, Russia is used (1985 – 2000). Distance between these locations is approximately 5800 km. SLP at Irkutsk is available until 2000, thus the MOI used here ceases in 2000. SLP data in Nemuro are collected from the WS of the JMA, and SLP data in Irkutsk are collected from the climate and historical weather records website of *El Tiempo* at http://www.tutiempo.net/en/ Climate/Irkutsk/307100.htm. To investigate effects of the El Niño – Southern Oscillation (ENSO), the Southern Oscillation index (SOI) was obtained from the SOI data archive site operated by the *Bureau of Meteorology*, Australia (http://www.bom.gov.au/climate/current/soi2. shtml).

Table 3.3. Information of the weather stations (WS) in Okinawa.

Operated by	Weather Station (WS)	Latitude	Longitude	Altitude (m)	Measuring data	Operation period
JMA	Oku	26.833	128.272	232	Precipitation, Temperature, Wind, Sun duration	1/1/1976 ~
	Yonahadake	26.727	128.215	375	Precipitation	1/1/1976 ~ 20/12/2005
	Motobu	26.683	127.880	25	Precipitation	1/1/1976 ~
	Higashi	26.630	128.152	24	Precipitation	1/1/1976 ~
	Nago	26.593	127.965	6.1	Pressure, Precipitation, Temperature, Humidity, Wind, Sun duration	1/4/1973 ~
	Kin	26.4567	127.857	8	Precipitation, Temperature, Wind, Sun duration	1/1/1976 ~
	Yomitan	26.4183	127.728	99	Precipitation	1/1/1976 ~
	Goya	26.3267	127.802	86	Precipitation	1/1/1976 ~
	Naha	26.2067	127.685	28.1	Pressure, Precipitation, Temperature, Humidity, Wind, Sun duration	1/1/1891 ~
	Itokazu	26.153	127.763	186	Precipitation, Temperature, Wind, Sun duration	1/1/1976 ~
OGB	Takasato	26.701	128.167	146*	Precipitation	13/7/1976 ~
	Takae	26.665	128.235	179*	Precipitation	2/6/1974 ~
	Taiho	26.661	128.153	162*	Precipitation	10/4/1973 ~
	Abumata	26.575	128.094	162*	Precipitation	16/4/1973 ~
	Kisenbaru	26.489	127.910	53*	Precipitation	12/3/1973 ~
OPG	Toyama	26.252	127.734	50	Precipitation	21/3/1976 ~

* Altitude measured from GIS DEM data produced by the Okinawa Prefecture Government Land Management Section in 1975 according to their grid coordinates.

3.2.5 Terrestrial Data

3.2.5.1 River Discharge

Daily discharge data of the rivers on the west side of the Island of Okinawa were used to examine the relationship between the terrestrial input to the coastal zone and the response of SST/OC4. Fig. 3.6 shows the catchments and the measuring points of the rivers. The length of the rivers is given in Table 3.4. The *OPG River Section* measures the stages of 10 rivers in Okinawa and calculates their discharges.

In estimating the discharge, the discharge rating curves were derived from the river stages, flow speed and cross section areas of the rivers, measured by the *OPG River Section*. The river stage is automatically measured once every 10 minutes. The flow speed measurement is carried out once a month. The *OPG River Section* releases hourly and daily data. Monthly data averaged from daily data from 1998 to 2005 were used. In this study, the discharge data of 8 rivers which flow to the west of Okinawa are used to investigate the terrestrial influence through the rivers on the SST and OC4 in the coastal zone.

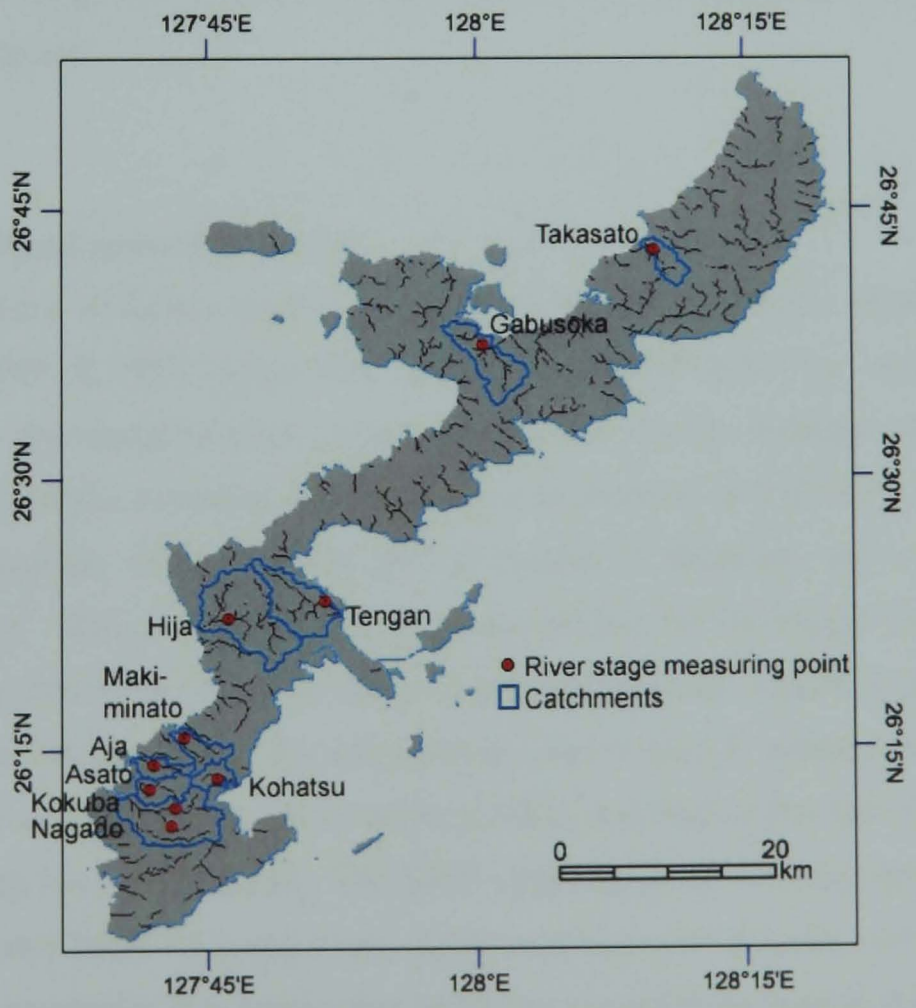

Fig. 3.6. River stage measuring points. Discharges are calculated from the rating curves by the *OPG River Section*.

Table 3.4. River length and the grid coordinates of the measuring point.

Name of the rivers	Total length (km)	Latitude (degree)	Longitude (degree)	Altitude (m)	Distance from the river mouth to the measuring point (km)
Takasato	4.9	26.712	128.165	3	1.77
Gabusoka	3.7	26.623	128.007	6	2.22
Tengan	11.9	26.386	127.860	12	2.07
Hija	14.5	26.369	127.770	5	3.90
Makiminato	3.3	26.260	127.728	3	1.02
Aja	5.2	26.236	127.701	2	1.69
Kohatsu	4.0	26.223	127.759	10	1.63
Asato	7.3	26.215	127.697	5	2.15
Kokuba	9.1	26.196	127.720	10	5.00
Nagado	2.3	26.180	127.715	3	5.86

3.2.5.2 GIS Data

GIS data provided by the OPG Land Management Section were used to overview the characteristics of topography (1972), soil distribution (1992) and land-use (1998). See Chapter 2 §2.4.2 for there figures.

3.2.5.3 Sea Sediment around Okinawa

The OPG Institute of Health and Environment has been surveying the deposited soil around Okinawa since 1983. In 1987, Omija (1987) developed a quick method to measure the sediment concentration on the coastal bottom floor which can be used to estimate bottom status (see Table 2.1). This method estimates the sediment concentration derived from the transparency measured in a cylinder filled with the diluted sample of sediment, and it is calculated in kilogram per 1 m^3. Measured value is called concentration of the Suspended Particle in Sea Sediment (SPSS). The SPSS survey has been carried out quarterly. Usually it is sampled once in the spring months (MAM) before the rainy season (June), once in summer months (JASO) or after the typhoon season, once in fall to winter (OND), and once at the end of the winter EAM when the northerly has calmed (JFM). The SPSS sampling points and their grid coordinates are given in Fig. 3.7 and Table 3.5 respectively. Each sampling point actually consists of two points sampled in close proximity. It is known that SPSS has a logarithmic normal distribution (Omija, 1987), thus the geometric average of these two points was used to represent the SPSS value for the sampling point.

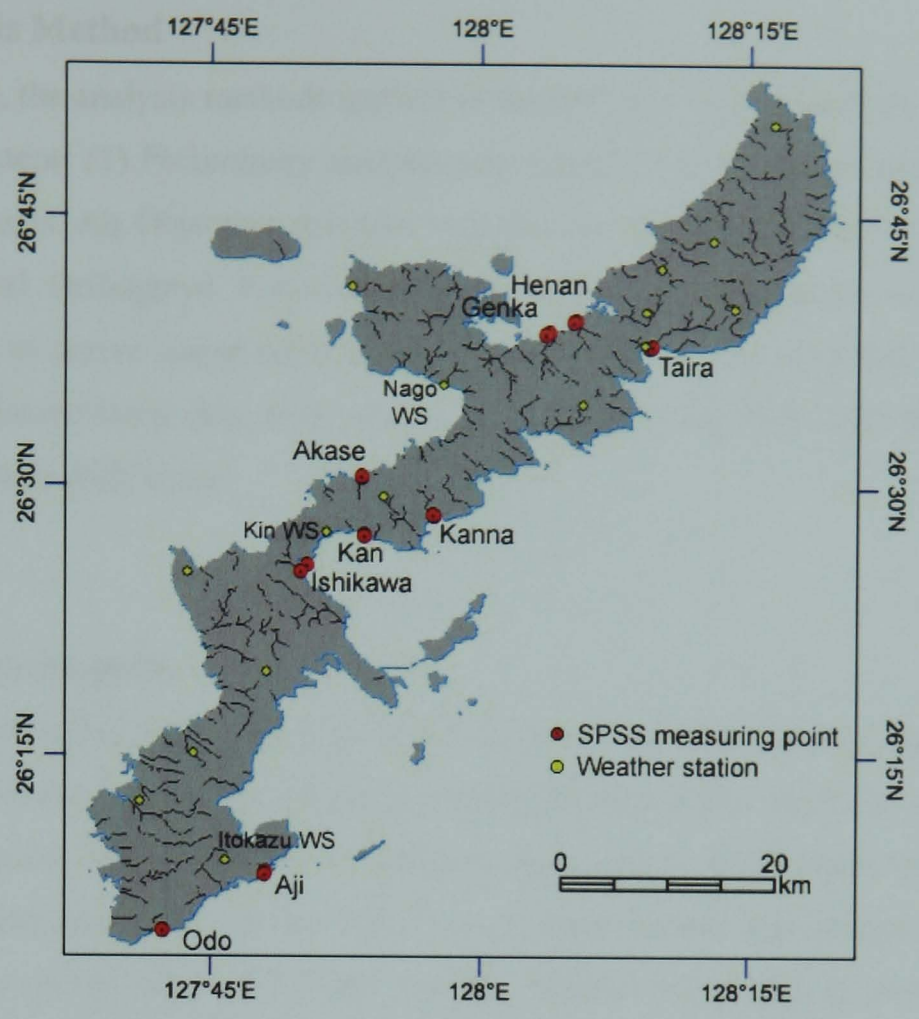

Fig. 3.7. The Suspended Particle in Sea Sediment (SPSS) sampling points around Okinawa.

Table 3.5. SPSS sampling grid coordinate.

		code	latitude (degree)	longitude (degree)
East	Henan	no. 2	26.648	128.088
		no. 3	26.649	128.091
	Genka	no. 1	26.636	128.063
		no. 3	26.638	128.066
	Akase	no. 2	26.504	127.892
		no. 3	26.503	127.892
West	Taira	no. 2	26.624	128.159
		no. 3	26.625	128.160
	Kanna	no. 1	26.469	127.957
		no. 3	26.467	127.959
	Kan	no. 2	26.449	127.894
		no. 3	26.449	127.894
	Ishikawa	no. 2	26.416	127.836
		no. 3	26.422	127.841
South	Aji	no. 2	26.138	127.803
		no. 3	26.136	127.802
	Odo	no. 1	26.085	127.708
		no. 3	26.085	127.710

3.3 Analysis Method

In this section, the analysis methods applied to the SST and OC4 dataset are described. There are mainly two steps: (1) Preliminary analysis was required to interpolate the missing points in the satellite datasets. An Objective Analysis was thus undertaken for both SST and OC4 data. (2) An Empirical Orthogonal Function (EOF) analysis was performed on the objectively analysed dataset to derive major controls on the variability of SST and OC4 in three different sized domains. Interpolated data were also used to examine the SST and OC4 response to a typhoon and a warm eddy event.

3.3.1 Objective Analysis

The sea surface is frequently obscured by cloud cover, sun-glint and high levels of aerosol in the atmosphere. In most cases, the coverage of satellite data is not complete due to such issues affecting the quality. Higher temporal resolution data tend to have much less coverage (e.g. daily or 8-day mean data) than the monthly or yearly data because the chances to compensate or to take an average of the obstructed points are less. Monthly mean data to gain a greater spatial coverage were used. The monthly mean data, however, still have missing points, meaning the EOF analysis may not perform well.

In order to estimate the values of the missing data, an Objective Analysis was applied by the use of the Optimum Interpolation (OI) technique (Carter, 1983; Carter and Robinson, 1987; Steele et al., 2001). The principle of the OI lies in minimising the errors between the true values in observed data and the estimated values in the missing points. The theory is described in the following statistical model. To process OI on the satellite data, the programme was written in IDL 6.0 with functions provided by ENVI 4.0.

It is presumed that the observed value P_i at the point i consists of the true value θ_i, and the error associated in the measurement, ϵ_i. The estimated value for the missing point to be interpolated, P', is assumed to have contributions from points nearby with certain weightings α_i added to the first guess value Fg. Thus,

Observed value: $$P_i = \theta_i + \varepsilon_i \qquad \text{(Eq. 3.6)}$$

Estimated value: $$P' = Fg + \sum \alpha_i (P_i - Fg_i)$$

$$= Fg + \sum \alpha_i (\theta_i + \varepsilon_i - Fg_i) \qquad \text{(Eq. 3.7)}$$

It is also presumed that the error is uncorrelated with the error at other measurement points and also with the true field, i.e.

$$E(\varepsilon_i \varepsilon_j) = \sigma_e^2 \delta_{ij} \qquad \text{(Eq. 3.8)}$$

$$E(\varepsilon_i P_j) = E(\varepsilon_i F g_j) = 0 \qquad \text{(Eq. 3.9)}$$

where δ_{ij} is Kronecker delta (1 if $i = j$, 0 other wise), E is the expectation value operator (which calculates the sum of the probability of each possible event multiplied by the value of the event), and σ_e^2 is the error variance. The aim of OI is to minimise the errors between the virtually presumed true value θ and the estimated value at the missing point. Advantage of this method compared to a simpler method based on distance-weighted averaging is that the OI minimises the error contained in the surrounding pixels. Its disadvantage is that this requires much longer computing time than a simpler distance-weighted averaging. The OI assumes errors are totally random error. Therefore this method cannot work in minimising a bias noise, such as OC4 overestimation for SS contaminated water, for example.

$$P' - \theta \rightarrow 0 \qquad \text{(Eq. 3.10)}$$

If the variance of this error $(P' - \theta)$ is taken, it can be written

$$\text{var}(P' - \theta) = E(P' - \theta)^2 \qquad \text{(Eq. 3.11)}$$

The derivative with respect to all the weightings of this variance is required to be zero in order to achieve the minimum error. Therefore, the differential can be laid out as

$$\frac{\partial}{\partial \alpha_j} \text{var}(P' - \theta) = 0 \qquad \text{(Eq. 3.12)}$$

Thus,

$$\frac{\partial}{\partial \alpha_j} E(P' - \theta)^2 = 0 \qquad \text{(Eq. 3.13)}$$

Inserting Eq. 3.7 into Eq. 3.13 gives,

$$\frac{\partial}{\partial \alpha_j} E\left\{\sum \alpha_i(\theta_i + \varepsilon_i - Fg_i) + Fg - \theta\right\}^2 = 0 \qquad \text{(Eq. 3.14)}$$

Differentiating Eq. 3.9 with respect to the weighting α_j gives

$$2E\left\{\sum \alpha_i(\theta_i + \varepsilon_i - Fg_i) + Fg - \theta\right\}(\theta_j + \varepsilon_j - Fg_j) = 0 \qquad \text{(Eq. 3.15)}$$

Expanding the parenthesis and using Eq. 3.3 gives:

$$E\left\{\sum \alpha_i(\theta_i\theta_j - \theta_i Fg_j - \theta_j Fg_i + Fg_i Fg_j + \sigma_e^2) - \theta\theta_j + \theta Fg_j + \theta_j Fg - FgFg_j\right\} = 0$$

(Eq. 3.16)

Rearranging Eq. 3.16 gives:

$$E\left[\sum \alpha_i\left\{(\theta_i - Fg_i)(\theta_j - Fg_j) + \sigma_e^2\right\} - (\theta - Fg)(\theta_j - Fg_j)\right] = 0 \qquad \text{(Eq. 3.17)}$$

If the variable θ' is written as

$$\theta' = \theta - Fg \qquad \text{(Eq. 3.18)}$$

Eq. 3.17 can be rewritten in the form,

$$E\left\{\sum \alpha_i(\theta'_i\,\theta'_j + \sigma_e^{\,2})\right\} = E(\theta'\theta'_j) \qquad \text{(Eq. 3.19)}$$

In a matrix form, Eq. 3.19 can be rewritten

$$\left[\begin{bmatrix} E(\theta'_1\theta'_1) & E(\theta'_1\theta'_2) & \cdots & E(\theta'_1\theta'_j) \\ E(\theta'_2\theta'_1) & E(\theta'_2\theta'_2) & \cdots & E(\theta'_2\theta'_j) \\ \vdots & \vdots & \ddots & \vdots \\ E(\theta'_i\theta'_1) & E(\theta'_i\theta'_2) & \cdots & E(\theta'_i\theta'_j) \end{bmatrix} + \begin{bmatrix} \sigma_{e11}^2 & 0 & 0 & 0 \\ 0 & \sigma_{e22}^2 & 0 & 0 \\ 0 & 0 & \ddots & 0 \\ 0 & 0 & 0 & \sigma_{ejj}^2 \end{bmatrix}\right]\begin{bmatrix} \alpha_1 \\ \alpha_2 \\ \vdots \\ \alpha_j \end{bmatrix} = \begin{bmatrix} E(\theta'\theta'_1) \\ E(\theta'\theta'_2) \\ \vdots \\ E(\theta'\theta'_j) \end{bmatrix}$$

(Eq. 3.20)

The premise of the estimated value as expressed in Eq. 3.7 without the term of the first guess is:

$$P' = \sum \alpha_i (P_i) = \sum \alpha_i (\theta_i + \varepsilon_i) . \qquad \text{(Eq. 3.21)}$$

With the presumptions of Eq. 3.8 and 3.9, and differentiating the Eq. 3.21 with respect to the weightings, α_i, and proceeding through the same steps of Eq. 3.16 and 3.17, it yields the same form as Eq. 3.19.

$$E\left\{\sum \alpha_i (\theta_i \theta_j + \sigma_e{}^2)\right\} = E(\theta \theta_j) \qquad \text{(Eq. 3.22)}$$

Given α_i as the standard deviation of θ_i, and assuming that the standard deviation of all observations stays constant ($\sigma_i = \sigma_j = \sigma$), the correlation can be derived as

$$\frac{E\left\{(\theta_i - \overline{\theta_i})(\theta_j - \overline{\theta_j})\right\}}{\sigma_i \sigma_j} = \frac{\mathrm{cov}(\theta_i, \theta_j)}{\sigma^2} = correlation(\theta_i, \theta_j) \qquad \text{(Eq. 3.23)}$$

A typical application of this correlation to geophysics is to use a function that is dependent only upon the distance between two points θ_i and θ_j. Such a correlation function is traditionally chosen to be a Gaussian form. Therefore,

$$\frac{E\left\{(\theta_i - \overline{\theta_i})(\theta_j - \overline{\theta_j})\right\}}{\sigma^2} = \exp(-\frac{d_{ij}^2}{c^2}) \qquad \text{(Eq. 3.24)}$$

$$\frac{E\left\{(\theta - \overline{\theta})(\theta_j - \overline{\theta_j})\right\}}{\sigma^2} = \exp(-\frac{d_j^2}{c^2}) \qquad \text{(Eq. 3.25)}$$

where d_{ij} is the distance between θ_i and θ_j, and c is the correlation length. Since the left hand terms of Eq. 3.24 and 3.25 are expressed as a function of distance, it can be denoted

$$R = \frac{E(\theta_i \theta_j)}{\sigma^2} = \exp(-\frac{d_{ij}^2}{c^2}) \qquad \text{(Eq. 3.26)}$$

$$S = \frac{E(\theta \theta_j)}{\sigma^2} = \exp(-\frac{d_j^2}{c^2}) \qquad \text{(Eq. 3.27)}$$

This relation between θ and the correlation function is the same whether θ or θ' is used. It means that the weightings from the adjacent points do not depend on the first guess. If the weightings is written as $\alpha_i = W$, Eq. 3.20 can be rewritten with the identity matrix I.

$$\left[R + \frac{\sigma_e^2}{\sigma^2} I\right] W = S \qquad \text{(Eq. 3.28)}$$

The weightings W can be derived by applying the inverse matrix

$$W = \left[R + \frac{\sigma_e^2}{\sigma^2} I\right]^{-1} S \qquad \text{(Eq. 3.29)}$$

Once the weightings are derived, the estimated interpolation will be achieved by substituting the weighting values into Eq. 3.7.

Thus, in order to calculate an interpolated value, one must provide a dataset of the observation value and location, an error variance, the first guess and a correlation length. In practice, it is difficult to obtain the error variance of the observation. Instead, the root mean square (RMS) values in the algorithms to calculate SST (Kilpatrick et al., 2001) and OC4 (O'Reilly et al., 1998) are used. The climatology of each month from January to December was prepared for the first guess. The OI was iterated 5 times, however, there were still points left to be interpolated. The climatology was inserted into these points. Such points were only found along the coastline of China so that this insertion will not affect the further analysis around the Island of Okinawa. The correlation function can be made non-isotropic by expanding the spatial dependence c in the X and Y direction, and additionally, to the temporal dimension t. Therefore, the correlation function Eq. 3.21 and 3.22 can be noted as

$$\exp(-\frac{d}{c^2}) = \exp\{-(\frac{X^2}{c_x^2} + \frac{Y^2}{c_y^2} + \frac{t^2}{c_t^2})\} \qquad \text{(Eq. 3.30)}$$

The spatial dependence c_x, c_y, and temporal dependence c_t will be determined by the correlation lengths in space and time (see §3.4).

3.3.2 Empirical Orthogonal Function (EOF) analysis

Empirical Orthogonal Function (EOF) analysis, which uses the same mathematical theory as Principal Component Analysis, is commonly used in oceanography and meteorology for decomposing space-time distributed observations into a smaller number of independent spatial patterns explaining significant variance in the data (Smith et al., 1996; Otero and Siegel, 2004;

Hannachi et al., 2007). In other words, given a space-time field, EOF analysis decomposes a set of orthogonal spatial patterns along with a set of associated uncorrelated time series (equivalent to principal components), which may be related with atmospheric or oceanographic dynamics.

Suppose that a dataset Z is composed of $m \times n$ elements where m denotes the number of observation points (grid or pixel) and n is the number of times observed (day, month, etc.). If a variable in the m-th position in the n-th timeline are written as x_{mn}, Z can be written in a matrix form

$$Z(m,n) = \begin{bmatrix} x_{11} & x_{21} & \cdots & x_{m1} \\ x_{12} & x_{22} & \cdots & x_{m2} \\ \vdots & \vdots & \ddots & \vdots \\ x_{1n} & x_{2n} & \cdots & x_{mn} \end{bmatrix} \qquad \text{(Eq. 3.31)}$$

EOF analysis decomposes Z using a set of spatial functions $s_k(m)$ and temporal functions $t_k(n)$.

$$Z(m,n) \Rightarrow \sum_{k=1}^{m} s_k(m) t_k(n) \qquad \text{(Eq. 3.32)}$$

where m is the number of modes contained in the field. The spatial function $s_k(m)$ is called the EOF in the k-th mode. The temporal functions $t_k(n)$ are equivalent to principal components. The aim of EOF analysis is to find uncorrelated linear combinations of the different variables which explain the maximum variance of the field. Thus, the temporal functions in different modes are required to be orthogonal, thus uncorrelated:

$$t_{k1} t_{k2}^{T} = \begin{cases} \lambda_{k1}, & (k_1 = k_2) \\ 0, & (k_1 \neq k_2) \end{cases} \quad (\lambda_k : \text{eigenvalue, } T\text{: rotation operator}) \qquad \text{(Eq. 3.33)}$$

Eigenvalue explains the variance of the temporal function, and hence the temporal function (principal component) which has the maximum eigenvalue indicates the most significant temporal variance. In EOF it is represented as the first mode (k = 1). The second maximum variance is referred to as the second mode, and k-th maximum, the k-th mode respectively. In practice, only the first few modes are calculated to find the major components of the variance rather than deriving all the modes.

The EOF analysis derivation is as follows: The dataset Z (Eq. 3.31) can be presented as series of data $(X_1 - X_n)$ consisting of n times observations at the point of the m-th pixel. Note that X_m is

not an array of a geographical image but an array of time series data at the point of the *m*-th pixel.

$$X_1 = \begin{bmatrix} x_{11} \\ x_{12} \\ \vdots \\ x_{1n} \end{bmatrix}, \quad X_2 = \begin{bmatrix} x_{21} \\ x_{22} \\ \vdots \\ x_{2n} \end{bmatrix}, \quad \cdots, \quad X_m = \begin{bmatrix} x_{m1} \\ x_{m2} \\ \vdots \\ x_{mn} \end{bmatrix} \qquad \text{(Eq. 3.34)}$$

Since there are *m* matrices (as many as the number of pixels in a data), the *m*-square spatial covariance matrix can therefore be written in a symmetric form as

$$A = \begin{bmatrix} a_{11} & a_{21} & \cdots & a_{m1} \\ a_{12} & a_{22} & \cdots & a_{m2} \\ \vdots & \vdots & \ddots & \vdots \\ a_{1m} & a_{2m} & \cdots & a_{mm} \end{bmatrix} \qquad \text{(Eq. 3.35)}$$

where

$$a_{11} = \text{cov}(X_1, X_1), \quad a_{12} = \text{cov}(X_1, X_2), \quad \cdots, \quad a_{mm} = \text{cov}(X_m, X_m) \qquad \text{(Eq. 3.36)}$$

The *k*-th EOF is simply given by the *k*-th "eigenvector" (equivalent to component loadings in Principal Component Analysis, indicating the loadings of the *k*-th principal component) $e_k = (e_{k1}, e_{k2}, \ldots, e_{km})^T$ of *A* which is obtained as the solution to the eigenvalue (λ_k) problem given,

$$Ae_k = \lambda_k e_k \qquad \text{(Eq. 3.37)}$$

The projection of the dataset ($X_1 \sim X_n$) i.e., *Z*, onto the *k*-th EOF $e_k = (e_{k1}, e_{k2}, \ldots, e_{km})^T$ is the *k*-th temporal function,

$$c_k = Ze_k = \begin{bmatrix} x_{11} & x_{21} & \cdots & x_{m1} \\ x_{12} & x_{22} & \cdots & x_{m2} \\ \vdots & \vdots & \ddots & \vdots \\ x_{1n} & x_{2n} & \cdots & x_{mn} \end{bmatrix} \begin{bmatrix} e_{k1} \\ e_{k2} \\ \vdots \\ e_{km} \end{bmatrix} \qquad \text{(Eq. 3.38)}$$

Temporal function (principal component) → EOF (eigenvector)

Dataset (satellite images: *m* pixels, *n* times observations)

whose elements c_{ik} (i=1,2,…,n) are given by

$$c_{ik} = \sum_{j=1}^{m} x_{ij} e_{kj} \qquad \text{(Eq. 3.39)}$$

Thus the set of the temporal functions from 1 to k will be obtained,

$$\begin{bmatrix} c_{11} & c_{21} & \cdots & c_{k1} \\ c_{12} & c_{22} & \cdots & c_{k2} \\ \vdots & \vdots & \ddots & \vdots \\ c_{1m} & c_{2m} & \cdots & c_{km} \end{bmatrix} \qquad \text{(Eq. 3.40)}$$

Elements where k =1 ($c_{11} - c_{1n}$) are the coefficients of the temporal function in the first mode representing the temporally-varying amplitude which has the maximum variance in the field. Elements in the second mode ($c_{21} - c_{2n}$) explain the second largest amount of variance and the k-th ($c_{k1} - c_{km}$) explains the k-th most variance respectively. Theoretically, k ranges from 1 to m since covariance matrix A is a m-square matrix that possesses up to k eigenvalues. However, as mentioned earlier, to achieve effective data reduction, k will be a small number to describe only the major variances.

The EOFs are also known as the PC loadings. The spatial distribution of EOF in the k-th mode can be displayed by applying the value of the eigenvectors e_k on each position x_j (j = 1, 2, …, m). In general the variance accounted for in percentage terms is given by

$$\frac{\lambda_k}{\sum_{k=1}^{m} \lambda_k} \times 100(\%) \qquad \text{(Eq. 3.41)}$$

3.4 Preliminary Analysis Result

3.4.1 Preliminary Measurement for Objective Analysis

To carry out the Objective Analysis, it is necessary to define the correlation lengths ("c" shown in Eq. 3.30) for the SST and OC4 dataset. To determine the spatial correlation, four sampling regions were used in both AVHRR SST and SeaWiFS OC4 data that are averages of all data (Fig. 3.8).

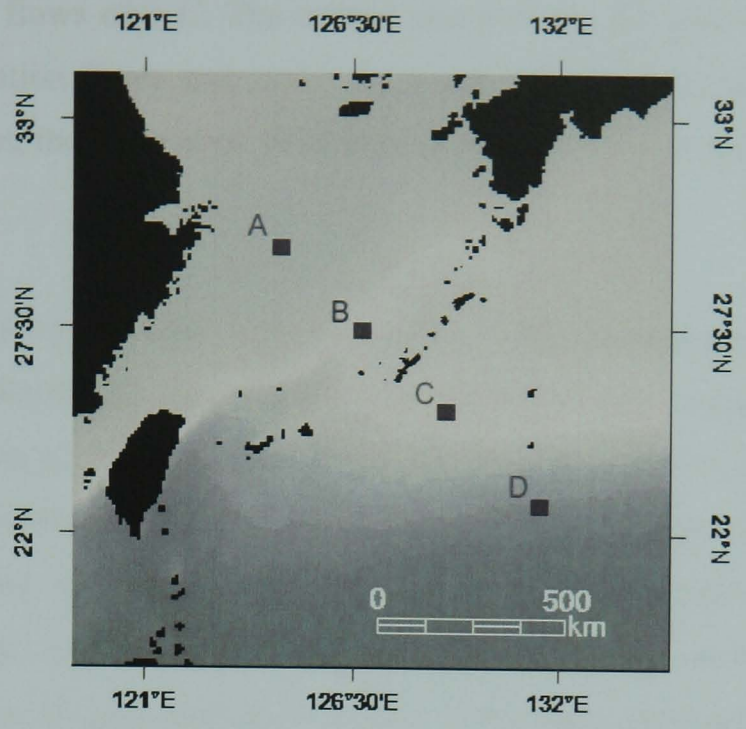

Fig. 3.8. Sampling regions (A – D) on a SST image.

The correlations were obtained for each sampling regions. The temporal correlation was determined by calculating the cross correlation between the values in the whole image of each month's climatology. The size of sampling region, the distance range and the temporal lag are indicated in Table 3.6.

Table 3.6. Sampling specification to estimate spatial and temporal correlations.

		AVHRR SST	SeaWiFS OC4
Spatial Correlation	Size of sampling region	40 × 40 km (10 × 10 pixels)	54 × 54 km (6 × 6 pixels)
	Distance range	16 km (4 pixels)	36 km (4 pixels)
Temporal Correlation	Size of sampling region	Whole image (360 × 360 pixels)	Whole image (190 × 190 pixels)
	Lag	1 - 12 months	1 - 12 months

3.4.1.1 Correlation Length: SST

Fig. 3.9 shows the correlation fields (distribution of correlation coefficients obtained from calculating the correlation between the sampling region and the proximity regions defined in Table 3.4) for SST. In all regions, the correlation above 0.7 provides a closed boundary in an ellipsoid shape. Such fields are seen in an ellipsoid shape, wider in the west-east (X) direction than the north-south (Y) direction in each field except C. On the basis of this ellipsoid shape and the length in the Y direction given by the field above 0.7 reaching to nearly 4 km, the spatial correlation length is set to be 4km (1 pixel resolution) in the Y direction and 8 km in the X direction (c_y and c_x in Eq. 3.30 respectively). The KC flows over the sampling region B and D,

and its branch current flows over C. The current speed of the KC and the variation of its axis may affect the correlation fields and make them smaller. Over the continental shelf where several currents interact, the correlation field from sampling region A may also be under similar condition.

Fig. 3.10 shows the temporal cross correlation of the SST climatology over 12 months. From January to June and October to December, the correlation varies similarly; well correlated in spring (MAMJ), autumn (ON), and winter (DJF) and less correlated in summer (JAS). For the low correlation period (JAS) the correlation shows a distinct spike and drops drastically in the preceding and following months. A possible reason for this behaviour is that because these months are during the typhoon season in the western Pacific, and storms cause strong disturbance to the ocean surface leading to surface temperature modulation in various regions, this will result in less correlation between adjacent months. Although the correlation levels score over 0.9 through all the months, in order to set the threshold, the minimum correlation was set to 0.95. Thus 1 month is taken as the temporal correlation length (c_t in Eq. 3.30).

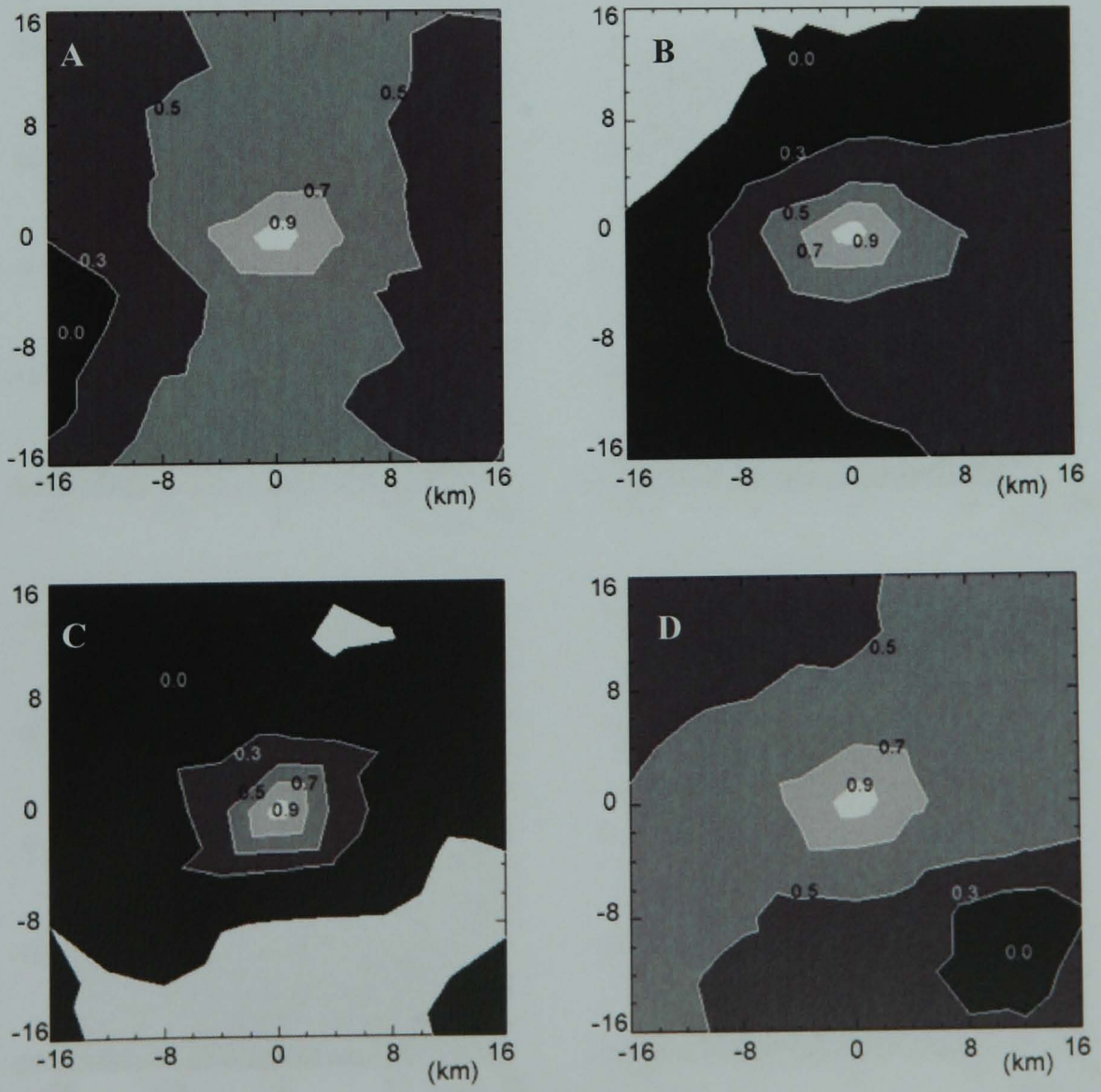

Fig. 3.9. Correlation Field in AVHRR SST over the four regions A – D in Fig. 3.7.

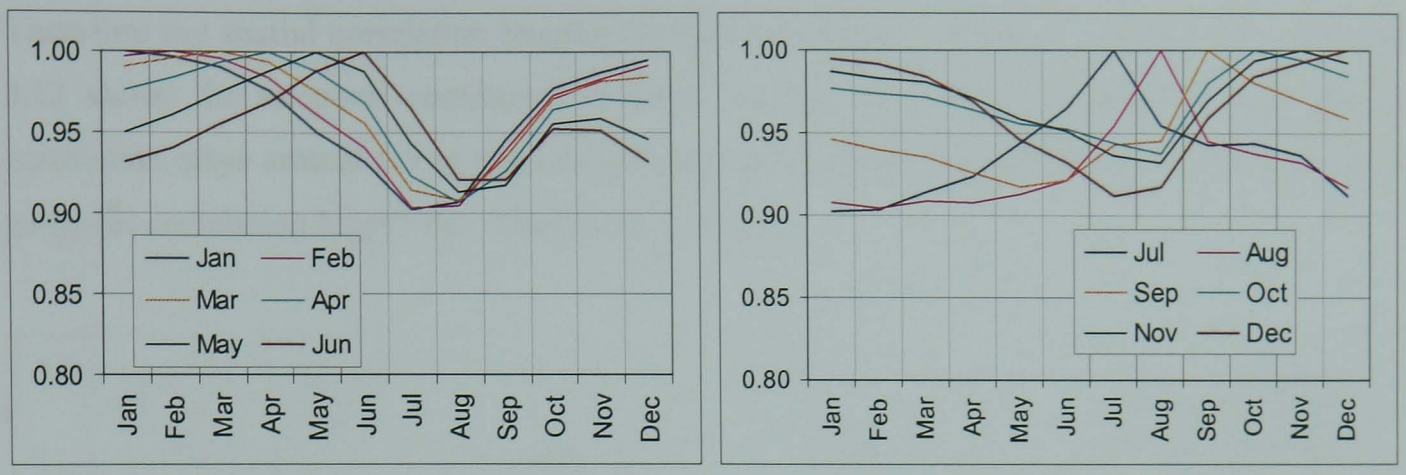

Fig. 3.10. Temporal Cross Correlation of the SST climatology (left: Jan – Jun, right: Jul – Dec).

3.4.1.2 Correlation Length: OC4

Fig. 3.11 shows the correlation field of OC4. In region A, the correlation field over 0.7 is observed over more than half the northeast region. In the rest of regions B – D, such fields above 0.7 are seen in about 9 km (1 pixel resolution) spread in the *X* and *Y* directions.

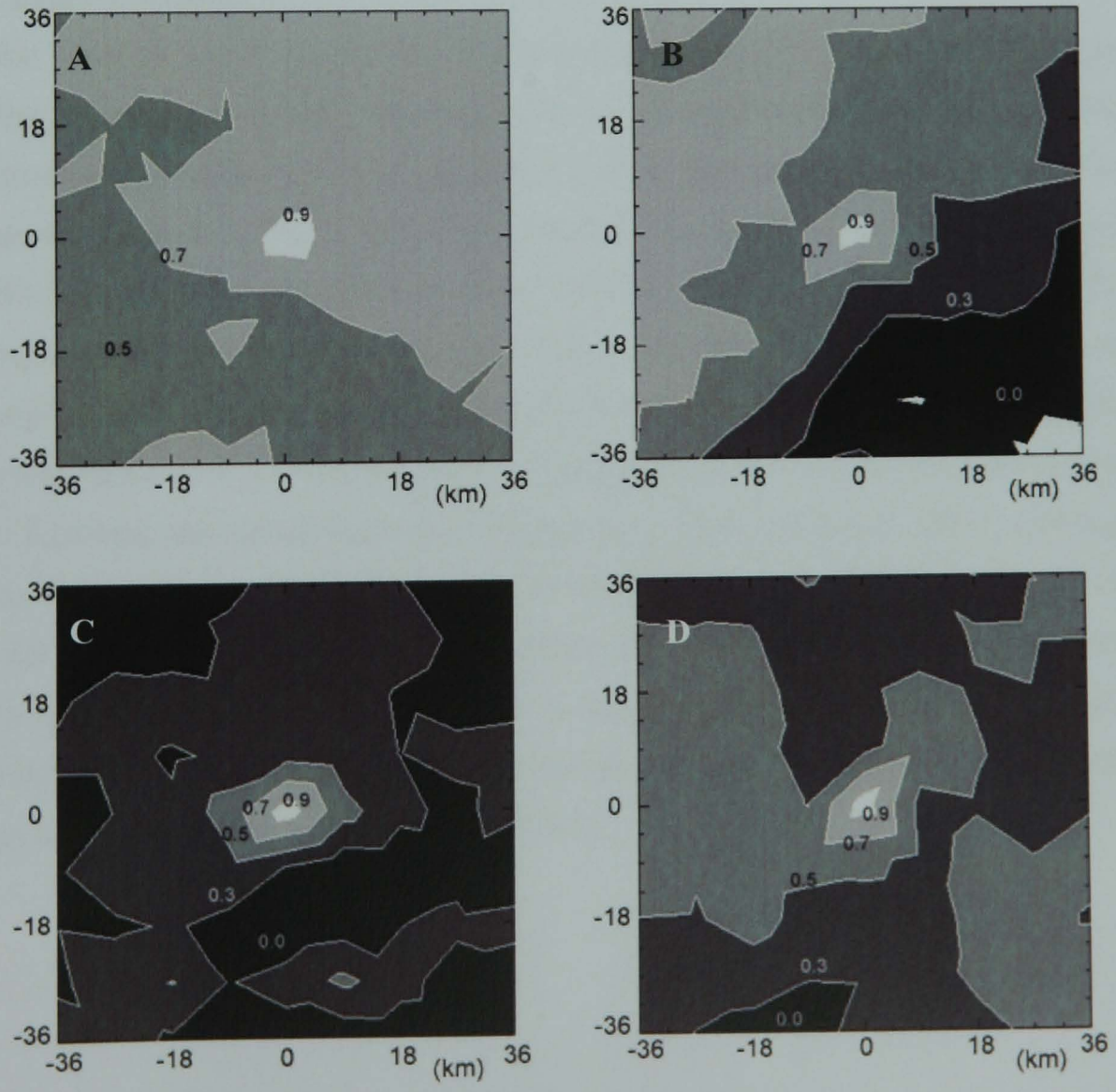

Fig. 3.11. Correlation Field in SeaWiFS OC4 over the four regions A – D in Fig. 3.7.

Therefore the spatial correlation lengths for both the X and Y directions were set to 9 km. Fig. 3.12 shows the temporal correlation of OC4. For all the months, the peak is clear and the correlation stays around 0.9 in adjacent preceding and following months for all the lags. So the temporal correlation length was taken to be 1 month.

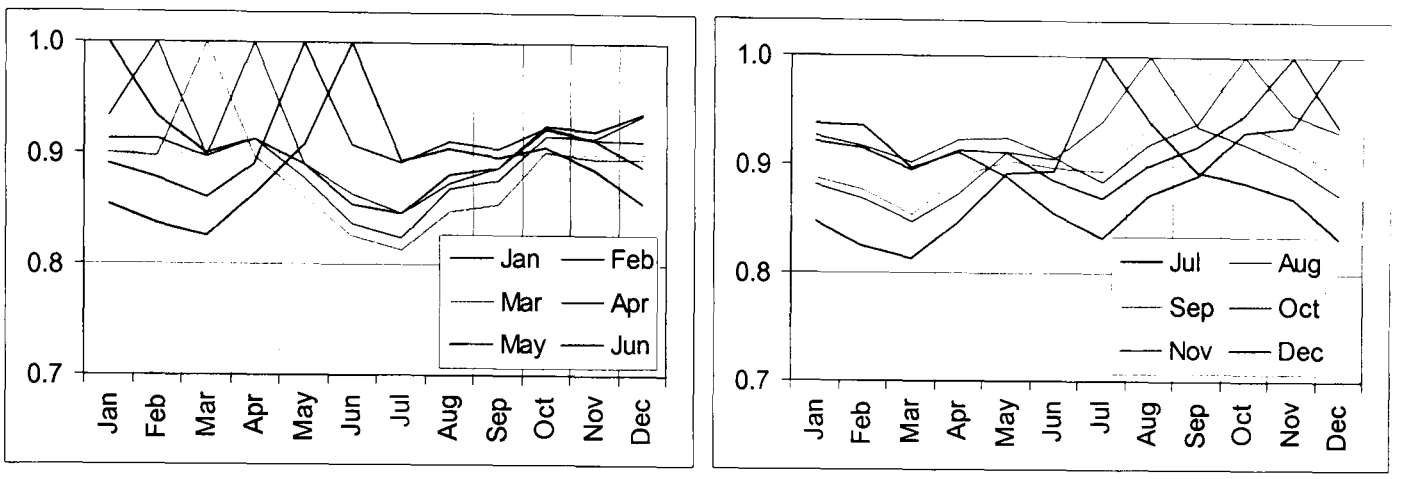

Fig. 3.12. Temporal Correlation: SeaWiFS OC4 (left: Jan – Jun, right: Jul – Dec).

3.4.1.3 Error Variance

Another variable to be determined is the error variance. This value will be obtained by measuring the true value and the error that occurred in observation. In practice, however, it can be substituted by another value (e.g., RMS) rather than carrying out an exhaustive field measurement out in the ocean. RMS values which were obtained in modelling the algorithm to derive SST (Kelpatrick et al., 2001) and OC4 (O'Reilly et al., 1998) are used. For the first guess the climatology of each month is allocated. Since the correlation lengths are just one or two pixel lengths, a single calculation does not fill all the missing data in the image. Hence the process was repeated five times for both SST and OC4. If there were still missing points after the five iterations, the climatology was inserted (e.g., Bigg and Inoue, 1992). Although a few iterations were actually sufficient to interpolate the missing data in the ocean, five iterations still did not fill some areas along the Chinese coastline. These areas were the last interpolated pixels, and they will little affect the EOF analysis in the ocean around the Island of Okinawa. The specifications for objective analysis, correlation lengths for space and time, error variance and the value of the first guess, as shown in Table 3.7.

Table 3.7. Specifications for objective analysis of the SST and OC4.

	AVHRR SST	SeaWiFS OC4
Correlation Length (in space)	X – 8 km (2 pixels) Y – 4 km (1 pixel)	X, Y – 9 km (1 pixel)
Correlation Length (in time)	1 month	1 month
Error Variance	0.76 (RMS of Pathfinder ver. 4 algorithm)	0.156 (RMS of OC4 algorithm)
First Guess	Climatology of each month (1985 – 2006)	Climatology of each month (1998 – 2006)
Process Iteration	5	5

3.4.2 Result of Objective Analysis

The interpolation was successfully implemented to provide a full coverage. Examples are given in Fig. 3.13 and 3.14, which show (a) the raw data and (b) the result of objectively analysed AVHRR SST and SeaWiFS OC4 respectively both in March 1998. The interpolated SST for this month shows a wide range of temperature from 6 to 29 °C. The KC can be recognised by its higher temperature as it flows from off the east coast of Taiwan to the west side of Okinawa. Cold water is observed in the Yellow Sea and to the north along Chinese coast. In the OC4 image, a high concentration area is distributed along the Chinese coast. It spreads from the Yangtze Estuary to offshore.

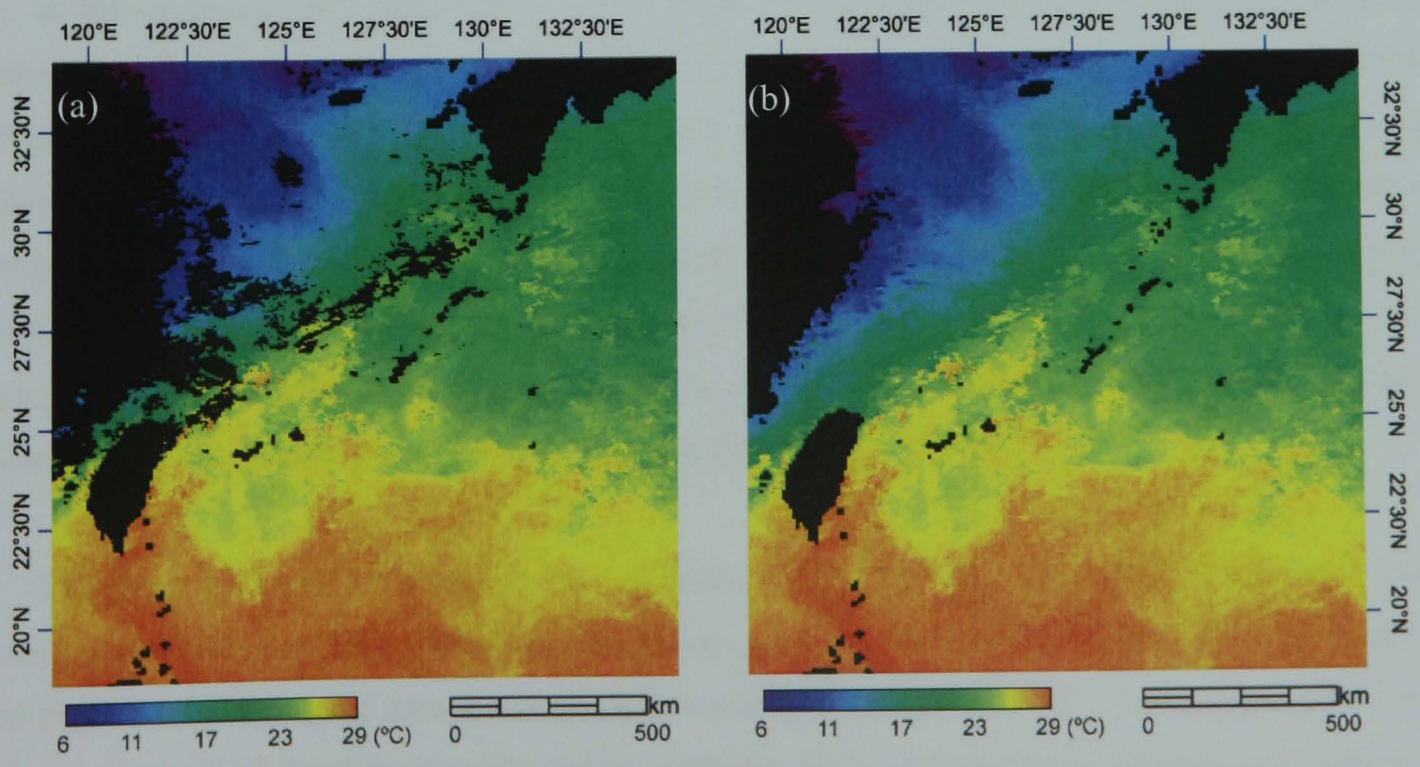

Fig. 3.13. AVHRR SST image in March 1998: (a) raw data, (b) result of objectively analysis.

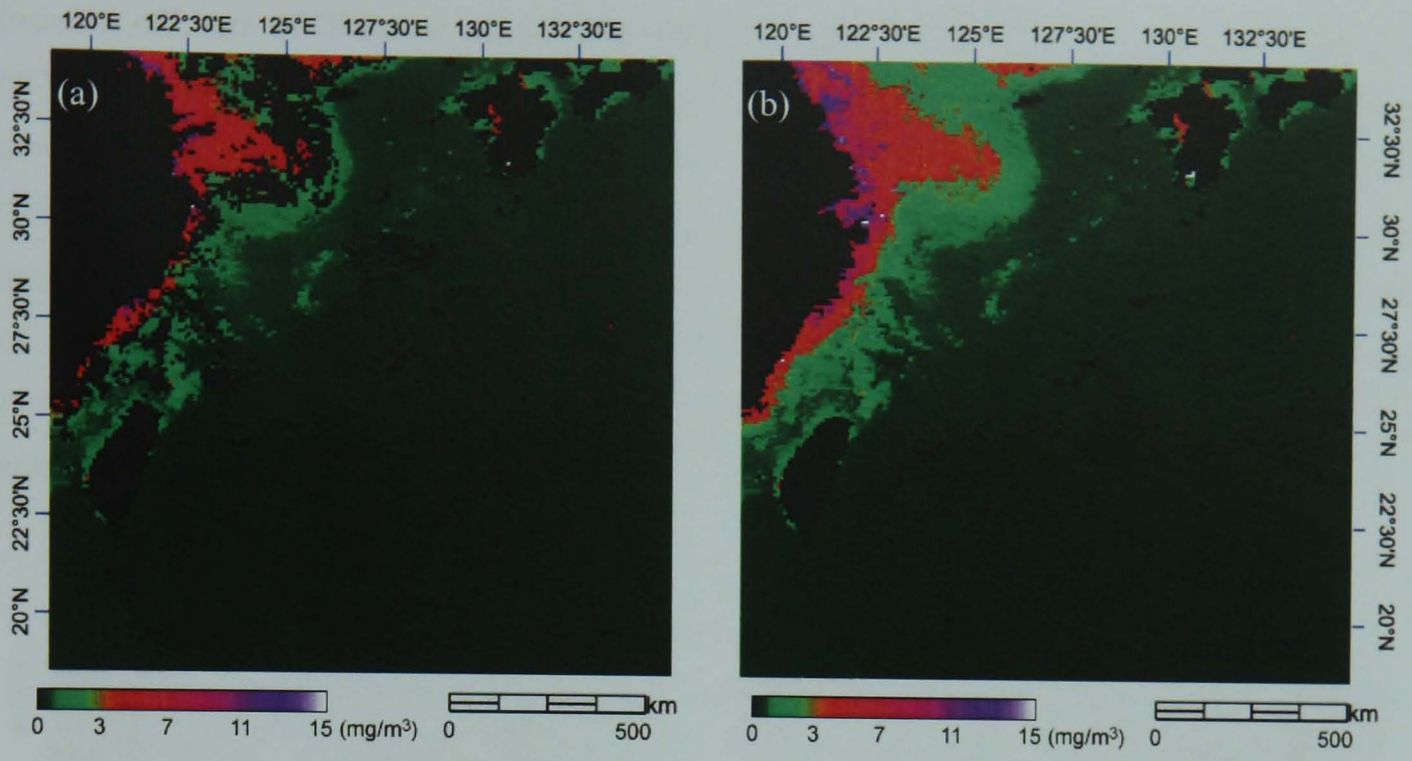

Fig. 3.14. SeaWiFS OC4 image in March 1998: (a) raw data, (b) result of objectively analysis.

In the temporally averaged images of both SST and OC4 (both for 1998 – 2006) with the bathymetry overlaid (Fig. 3.15), the KC can be clearly seen in the SST, and there is a characteristic spatial distribution of both SST and OC4 over the continental shelf.

In the averaged SST image (Fig. 3.15a), the KC is illustrated by the warmer temperature (> 24°C) as it brings warm water from the south. On the continental shelf region (< 200m deep), SST is lower than in the Kuroshio. The lowest temperature (~ 12 °C) is seen in the shallow region less than 50 m deep, and in the Yellow Sea.

In the averaged OC4 image (Fig. 3.15b), High OC4 concentration distributes over the shelf and around the Islands of Taiwan and Japan. It remains less than 1 mg/m^3 in the rest of the region. On the shelf region, Chl-a distribution is mostly parallel to isobath of 50 m, 100 m and 200 m. The 50 m isobath appears to be the front of cold water and high OC4. The highest OC4 regions are along the shallow Chinese coast less than 10 m deep. There are many rivers along the coast supplying huge quantity of fresh water containing dissolved and suspended matter. In particular, the world's third largest river, the Yangtze River, discharges about 85 % of the total discharge from all rivers into the East China Sea (Fairbridge, 1980).

The mean SST and OC4 values on a transect drawn from the East China Sea towards the southeast offshore of Okinawa across the KC are compared in Fig. 3.16. The grey shaded zone in Fig. 3.16 indicates the area where the KC is crossing the transect. T1 – T90 are the points on the transect which head from northwest to southeast. Both SST and OC4 values around T43 are masked by the presence of the Island of Okinawa. From T1, the SST increases and reaches a peak in the KC. It then decreases as it comes close to Okinawa. It shows a small but rapid

increase offshore of Okinawa around T48 then continues rising gradually as it goes south. The OC4 on the transect decreases linearly until it reaches to the edge of the shelf. Off the shelf OC4 concentration is relatively low and stable (0.16 – 0.18 mg/m^3). A little increase due to the island mass effect (Doty and Oguri, 1956) can be seen around Okinawa on T43. This effect is attributed to the disturbance of flow caused by the presence of an island leading to enrichment of nutrients at the surface from the sea bottom. Out in the deep region far offshore to the southeast of Okinawa, Chl-a concentration is lower than 0.1 mg/m^3 indicating an oligotrophic environment.

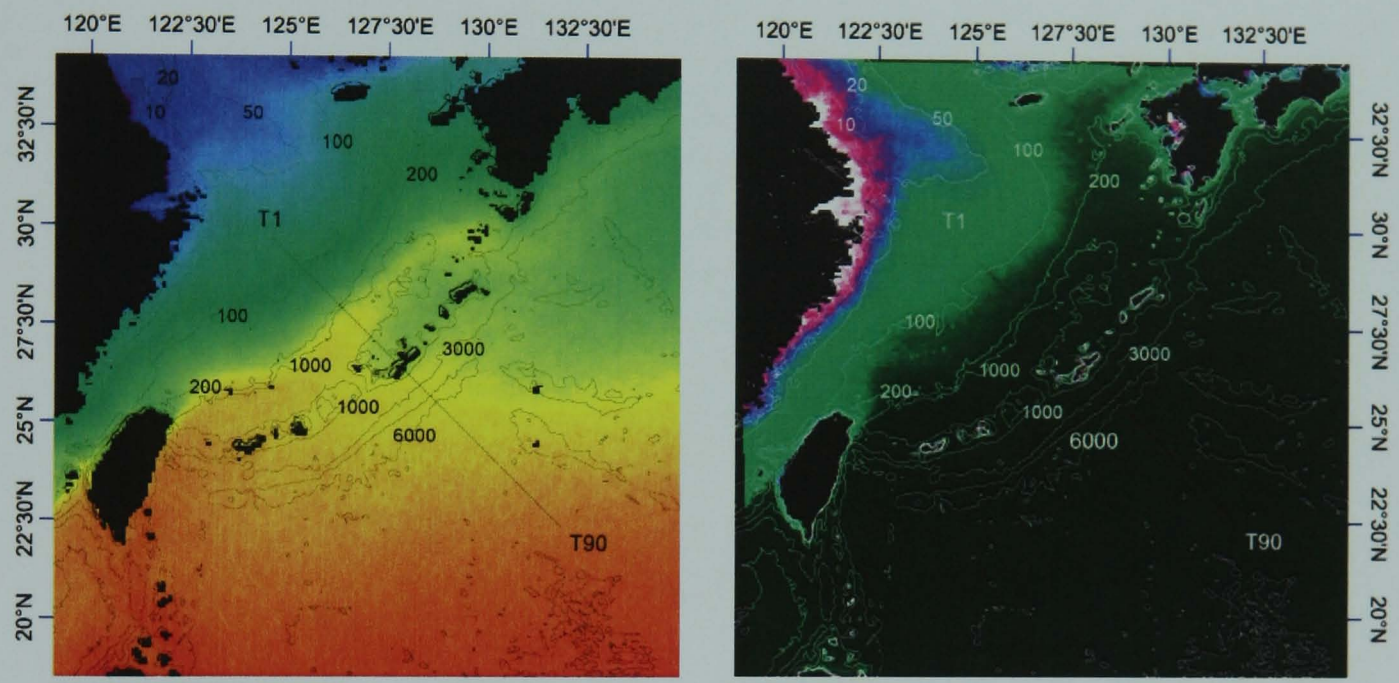

Fig. 3.15. Averaged image (1998 - 2006) of SST (left) and OC4 (right). T1 – T90 are the transect on which the value of SST and OC4 are plotted in Fig. 3.14. Bathymetry is indicated in black (white) in the SST (OC4).

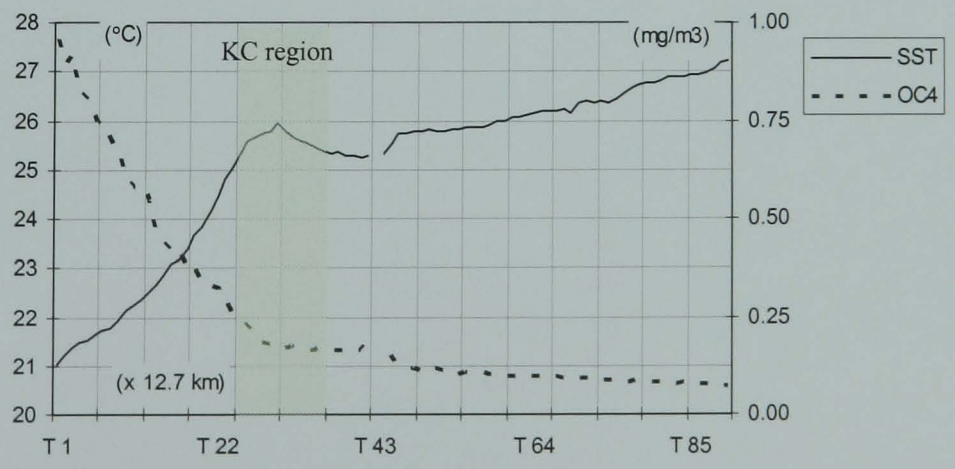

Fig. 3.16. SST and OC4on the Transect in Fig. 3.15. T values indicate the locations on the transect drawn in Fig. 3.15. The length of the transect is about 1145.5 km. Around T43 is the location of the Island of Okinawa. Shaded zone indicates the KC region.

Overall, the lower SST and the higher OC4 occur over the continental shelf compared to the off shelf region. On the shelf region there appears to be a bathymetric effect on the distribution

of both SST and OC4. The cold water on the shelf does not reach the Island of Okinawa due to the KC. The high OC4 over the shelf seems not to be influential around Okinawa, apparently due to the deep Okinawa Trough (Chung et al., 2000; Iseki et al., 2003; Kao et al., 2003). The variability of both SST and OC4 under these conditions will be discussed in the next chapter.

Chapter 4 Controls on the SST and Ocean Colour Variability in the East China Sea and around the Island of Okinawa: Interaction between Climate and Ocean

4.1 Introduction

This chapter describes key controls on the sea surface temperature (SST) and ocean colour determined by the SeaWiFS algorithm Ocean Colour version 4 (OC4) at different scales ranging from the regional scale of the East China Sea (ECS) to the local scale of the Island of Okinawa by applying empirical orthogonal functions (EOF) to objectively analysed satellite data. The period here for the SST and OC4 is 1985 – 2006 (22 years) and 1998 – 2006 (9 years), respectively. The Island of Okinawa is surrounded by a distinct system, the East Asian Monsoon (EAM), one of the largest ocean currents, the Kuroshio Current (KC), and the continental shelf that is largely influenced by the world's third largest river, the Yangtze River in China. Variabilities of the SST and OC4 may exhibit different patterns and key controls and their interactions may also differ between scales. The EOF analyses were applied at three different scales:

Domain 1 (D1) - a region covering the East China Sea and the Philippine Sea.
Domain 2 (D2) - a sub region of D1 - around Okinawa, including the Kuroshio Current.
Domain 3 (D3) - a sub region of D2 - near the coastline of the Island of Okinawa.

It was found that there is a greater variability of both SST and OC4 over the continental shelf compared to other regions due to the shelf's shallow depth and proximity to land. The SST over the shelf region has smaller thermal inertia compared to the deeper off-shelf region, and hence greater variability under the influence of solar heating and the EAM (§4.5). The solar radiation is a dominant control on the SST variability in all the domains; it was represented by the 1st mode of the SST EOF at all scales. For the OC4 variability, the huge input of the Yangtze River discharge and the shallower bathymetric features produce a greater variability compared to the off-shelf region (§4.6). The surface of the Okinawa Trough appears to be deficient in nutrients, therefore the OC4 is lower in D2 and D3 than D1. The strong northerly brought by the winter EAM appears to be an important control on the OC4 variability in all the domains, but its impact becomes greater in the smaller domains as the effect of the Yangtze River discharge becomes less influential. This suggests that the climate control, the EAM, is an important factor for the coastal environment around Okinawa. In D1, the terrestrial input of the Yangtze River run-off appeared to be influential over the continental shelf. In D3 (around Okinawa), terrestrial control may have a much smaller effect compared to the impact from the Yangtze River, and hence the EAM control prevails. This impact of typhoons was also observed through reduction

of the SST and increase of the OC4 off the coast of Okinawa (§4.7.1). Effects of warm eddies that approach Okinawa are also discussed (§4.7.2).

Data used in this chapter, and their temporal coverage, are given in Fig. 4.1. The main dataset here are objectively analysed satellite data, except ocean wind. In-situ wind means wind data recorded at the weather stations in the Island, operated by the *Japan Meteorological Agency* (JMA). The monsoon index (MOI) is determined by the sea level pressure difference between Nemuro, Japan, and Irkutsk, Russia. The sea level pressure at Irkutsk is available until 2000, thus the MOI used here is stays in 2000. In addition, typhoon events during July – August in 2000 and 2005, and the sea surface height anomaly in July 2001 and August 2004 were used in a case study.

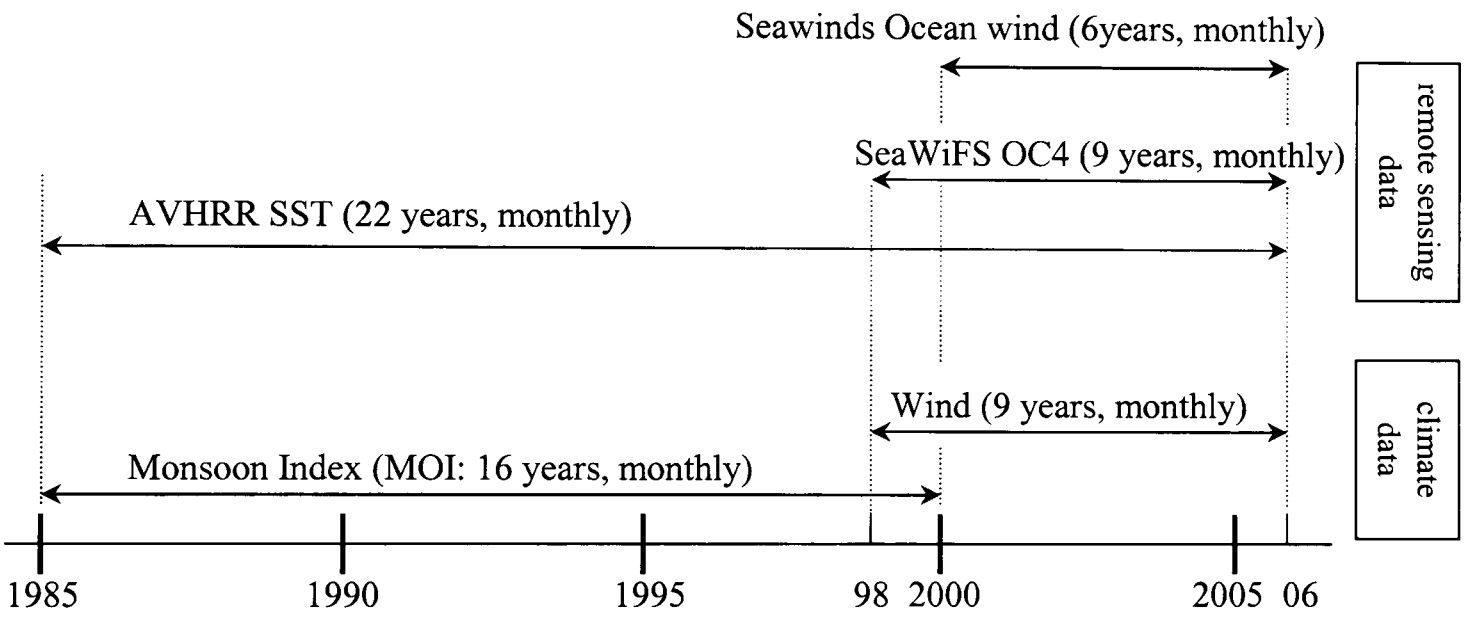

Fig. 4.1. Date used in this chapter and their temporal coverage. Typhoon data in July – September 2000 and 2005, and the sea surface height anomaly in July 2001 and August 2003 were used in a case study.

4.2 Geographical Settings: The Study Area

The study area is shown in Fig. 4.2. To the east of the Island of Okinawa lies the Ryukyu Trench with the depth reaching to about 7000 m in the deep open ocean of the Philippine Sea. To the west lies a depression called the Okinawa Trough in the ECS. Its deepest point is down to 2000 m in its southwest extensions; it becomes shallower in the northeast but has 1000 m depth to the west of Okinawa. The continental shelf spreads to the west of the Okinawa Trough, occupying more than 70 % of the ECS. The bathymetry of the shelf tilts from the northwest of the Chinese coast with a depth of less than 50 m, to the southwest with a depth more than 200 m at the shelf margin. In front of the Yangtze River estuary, there is a shallow region less than 50 m deep. This is an ancient Yangtze delta known as Changjiang Hillock. See Chapter 2, §2.3.2 for ocean currents description.

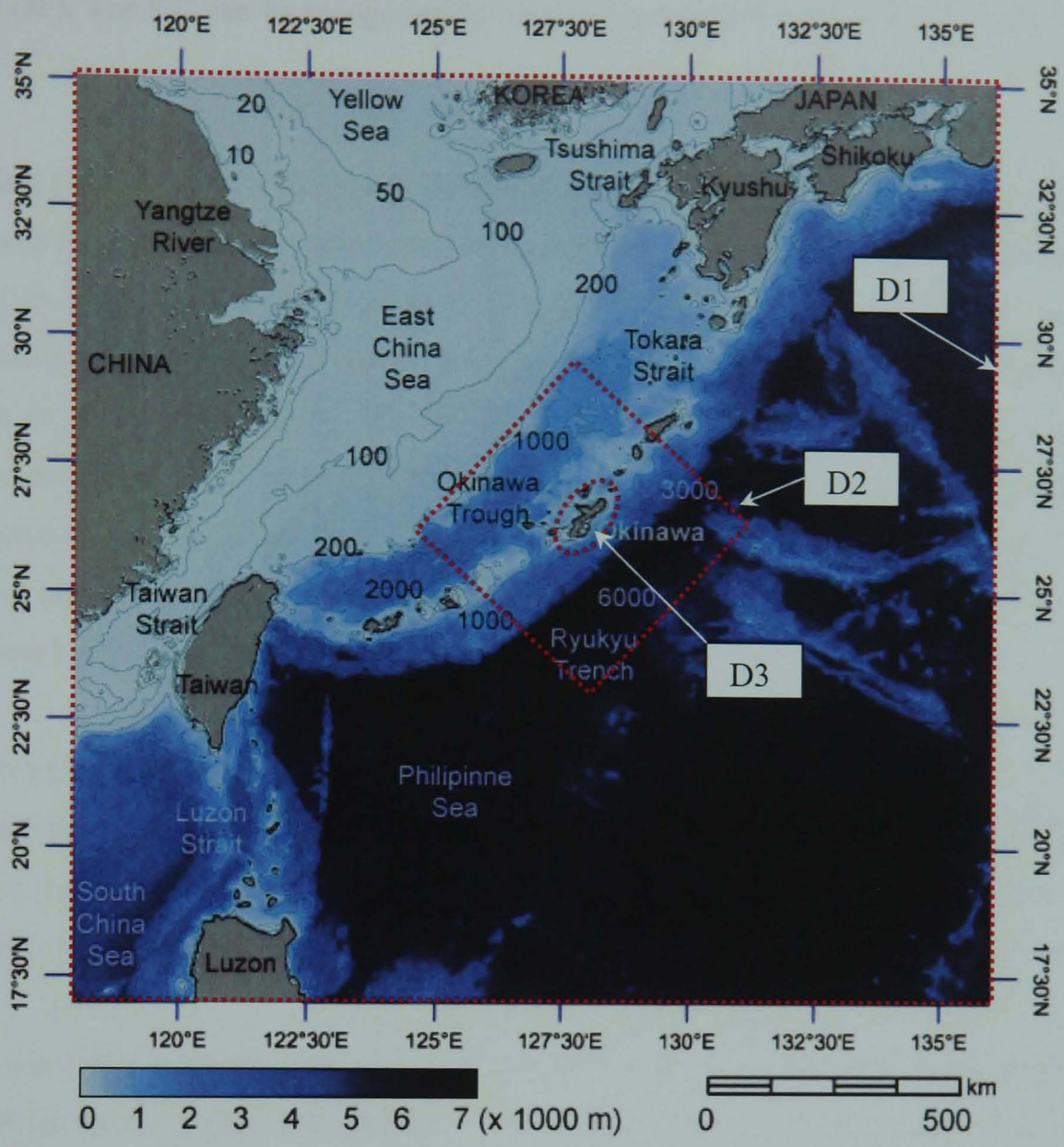

Fig. 4.2. Study Area: Land area is coloured in grey. Bathymetric feature is represented in blue colour and isobath in black line. The Island of Okinawa is located in the centre of the map. Regions surrounded by red dots indicate D1 – D3.

4.3 Climatological Atmospheric and Oceanic Features

Using the objectively analysed satellite data, the monthly climatologies for both the SST and OC4 were created. In addition, the climatological ocean wind was processed from the SeaWinds data without applying an objective analysis.

4.3.1 SST

The Monthly climatology of the SST was produced using the AVHRR data from 1985 to 2006 (Fig. 4.3). In winter (DJF), cold water begins to spread from the north coast of China to the offshore region of 100 m depth under the influence of strong northerlies brought by the winter EAM. The warm water front (> 26 °C), on the other hand, starts to decline from 21 °N to 19 °30'N. A tongue of 5 °C water can be seen along the 50 m isobath (JF). The coldest water

mass (< 5 °C) occurs over an even shallower region less than 20 m deep, along the north coast of China (JF). The KC can be recognised by its warmer water along the flank of the continental shelf.

In spring (MAM), cold water forms the greatest mass in March on the shelf less than 100 m deep. But at the same time the warm water front starts to move from the south. Cold water starts to retreat in April. The coldest SST in May is around 10 °C and is seen in the south of the Yellow Sea region. In May, the warm water front reaches northern Taiwan. The temperature in the south increases up to nearly 30 °C. The KC becomes more clearly distinguished by its warmer temperature. The flow of the KC through the Tokara Strait can also be traced. The branch current of the KC in the Taiwan Strait, the Taiwan Warm Current, is also recognisable in May. It is also notable that the warm water starts to intrude into the shelf region from the Taiwan Strait (Chuang 1985, 1986; Wang and Chern, 1988).

In summer (JJA), the warm water front keeps moving north. Its intrusion into the shelf region can be seen not only from the Taiwan Strait but also from the southern Okinawa Trough in June. The warm water front reaches to 32 °N in July, and the SST distribution eventually becomes rather uniform, except in the south Yellow Sea, in August (Ning et al., 1998; Gong et al., 2003).

In autumn (SON), the warm water front starts to retreat to the south from the north Chinese coast and the south Yellow Sea region. Cooled water starts to spread on the shelf region in October, and the cold water mass (~ 10 °C) appears off the north Chinese coast in November. The branch current of the KC shows its flow to the Tsushima Strait by its warm SST (OJ).

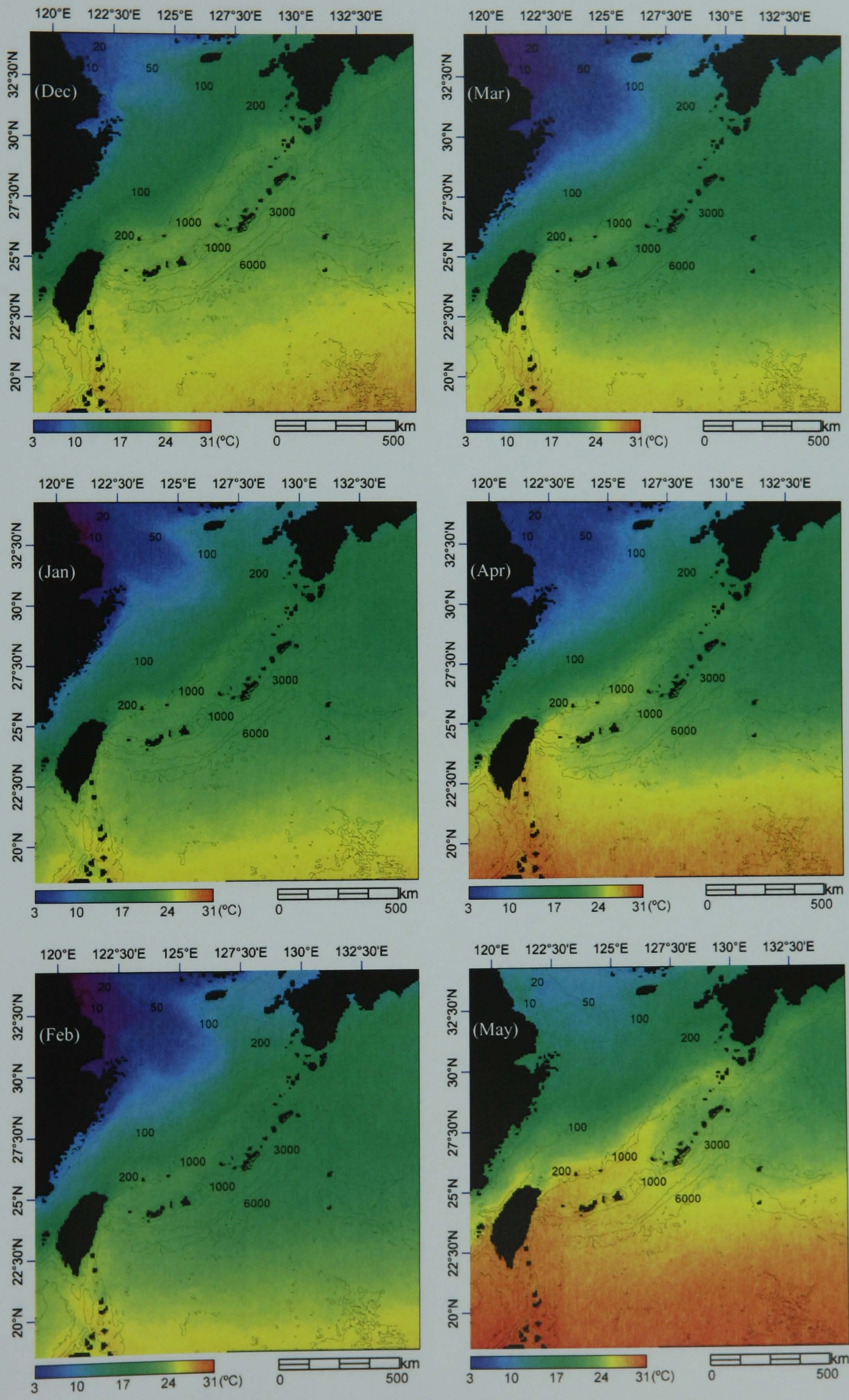

Fig. 4.3. Monthly climatology (1985 – 2006) of SST (Dec – May). Bathymetry is drawn in the black line.

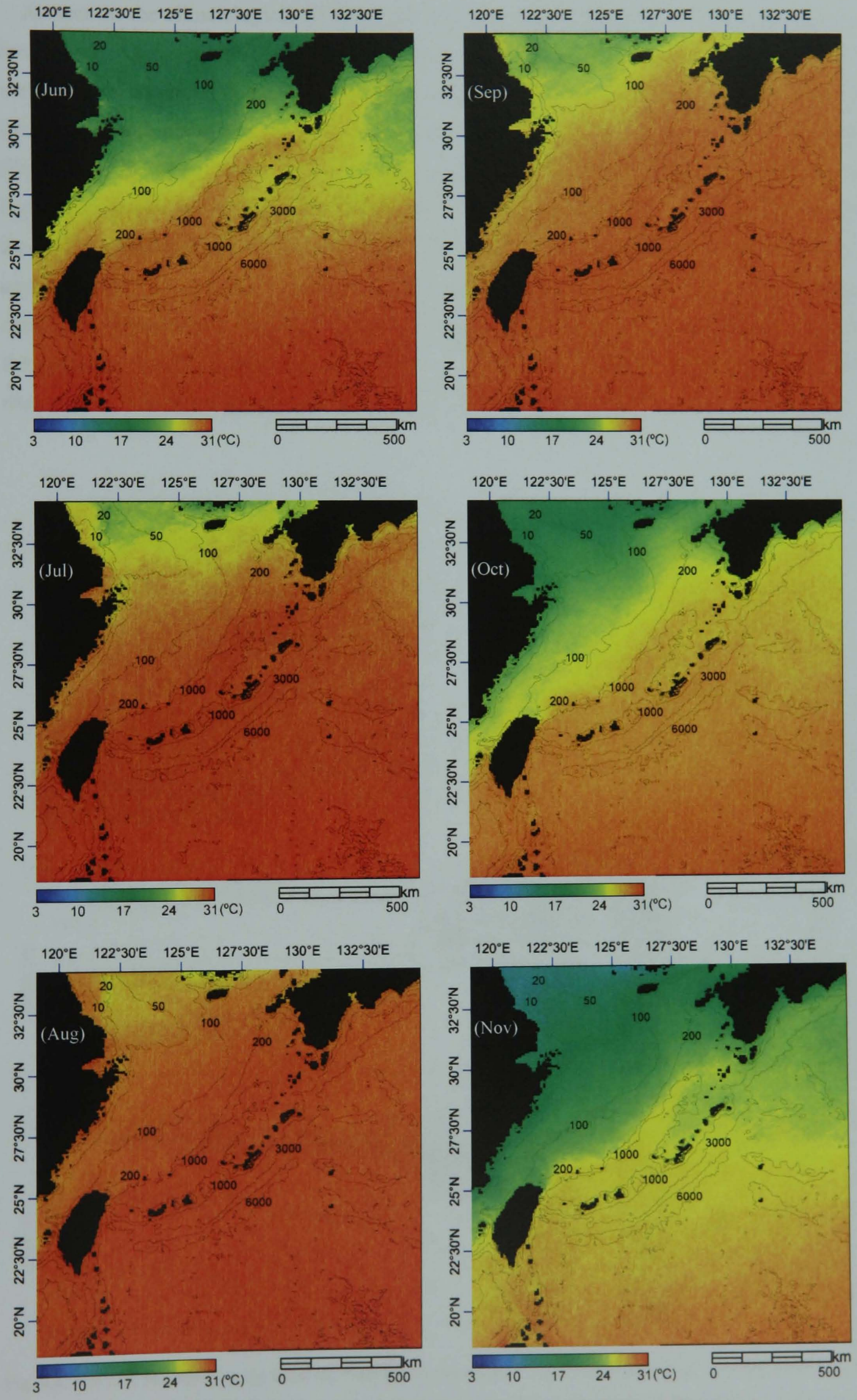

Fig. 4.3 (continued). Monthly climatology (1985 – 2006) of SST (Jun – Nov). Bathymetry is drawn in the black line.

As seen in the climatological SST through the year, the continental shelf region appears to have a wider range of SST variation than the rest of the region. Fig. 4.4 presents the SST variability on a transect in the ECS. The transect extends from the Yangtze Estuary, eastward to the 50 m isobath point, and southeastward to the Ryukyu Trench across the Island of Okinawa (Fig. 4.4a). Fig. 4.4 (b) shows the climatological monthly SST and the depth on the transect, and Fig. 4.4 (c) shows the standard deviation of the SST on the transect with depth. They show that the SST variability becomes greater in the shallower region within the continental shelf of approximately less than 200 m deep, and is relatively low and flat off the shelf region (> 200 m depth). The highest SST occurs in August, forming the least gradient. The lowest occurs in February and it is the period when the SST in the shelf region decreases greater than in the off-shelf region, suggesting the greater winter EAM influence on this region.

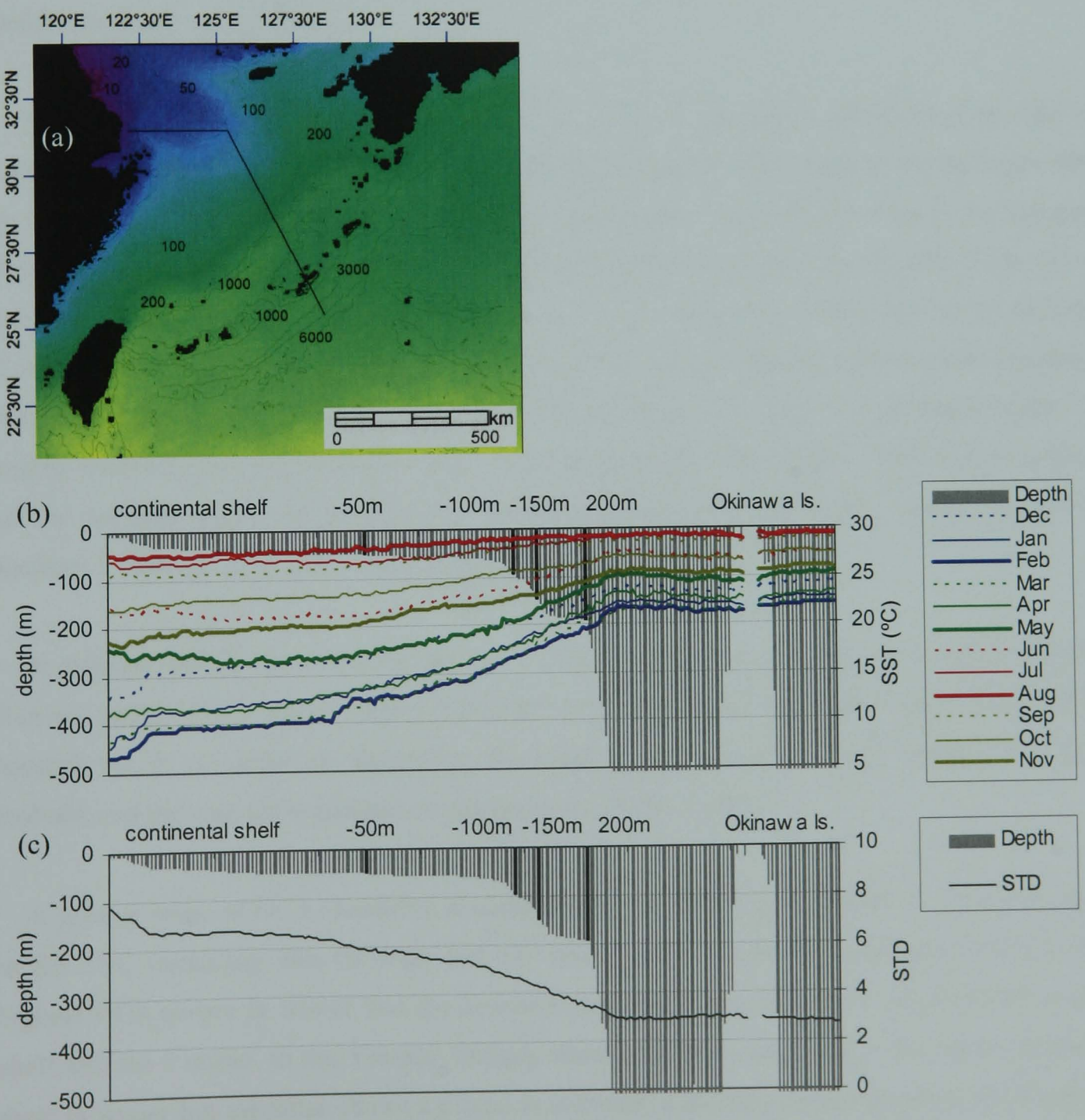

Fig. 4.4. The SST variability in the ECS. (a) Transect for the observation, (b) the climatological monthly SST and the depth on the transect, and (c) the standard deviation of the SST and the depth on the transect. Black bars in the depth indicate the depth of 50 m, 100 m, 150 m and 200 m, respectively.

4.3.2 OC4

The monthly climatology of OC4 was produced using the SeaWiFS data (1998 – 2006: Fig. 4.5). High OC4 concentration occurs over the continental shelf through the year compared to the other regions. In winter (DJF), high OC4 (> 3 mg/m^3) is seen on the shelf region of less than 100 m depth, including the Taiwan Strait. Higher OC4 (> 7 mg/m^3) occurs over shallower regions of the shelf. The 7 mg/m^3 front and the 11 mg/m^3 front are almost parallel to the isobaths of 50 m and 20 m respectively. Both fronts reach their maximum spread in February.

In spring (MAM), high OC4 continues to spread over the shelf until April. The 3 mg/m^3 front crosses the 100 m isobath, but the tongue of the 7 mg/m^3 front starts to fade in April. In May, the 3 mg/m^3 front also starts to shrink within the 100 m isobath and in the Taiwan Strait. On the other hand, higher OC4, greater than 7 mg/m^3, starts to spread from the Yangtze Estuary to the south Chinese coast in May.

In summer (JJA), the region of the OC4 over 3 mg/m^3 appears to retreat from the 100 m isobath, however, offshore of the Yangtze Estuary the 3 mg/m^3 front starts to extend to the 100 m isobath in July. Higher OC4 regions, greater than 7 mg/m^3, show a protrusion in the Yangtze Estuary in June. This is likely to be due to the increased discharge from the Yangtze River in the rainy season which begins from May (Hama et al., 1997; Gong et al., 2003). This higher OC4 (> 7 mg/m^3) also remains along the south Chinese coast, which suggests influences of increased water discharged from the rivers along the coast, flowing south. In July, the tongue of the 11 mg/m^3 front off the Yangtze Estuary turns towards the north. This is due to the combined effect of the Yangtze plume during the rainy season and the prevailing Taiwan Warm Current in summer (Yuan and Xia, 1987; Zhao, 1991; Ning et al., 1998).

In autumn (SON), the 3 mg/m^3 and the 7 mg/m^3 fronts start to grow on the shelf and the Taiwan Strait. The 7 mg/m^3 region develops along the northern Chinese coast and extends towards the 50 m isobath. In November, the 3 mg/m^3 region also extend its front to the 100 m isobath, and the high OC4 distribution returns to its winter pattern.

A greater range of OC4 variability is observed on the shelf region, similar to what was seen in the SST variability. But the high and low peaks occur in opposite seasons. Generally the highest OC4 occurs in winter and the lowest in summer. However, the 3 mg/m^3 front on the shelf and the 7 mg/m^3 in the Yangtze Estuary show a different seasonality: the former extends most in winter but the latter shows a plume in summer, indicating influences from the Yangtze discharge which increases in the rainy season.

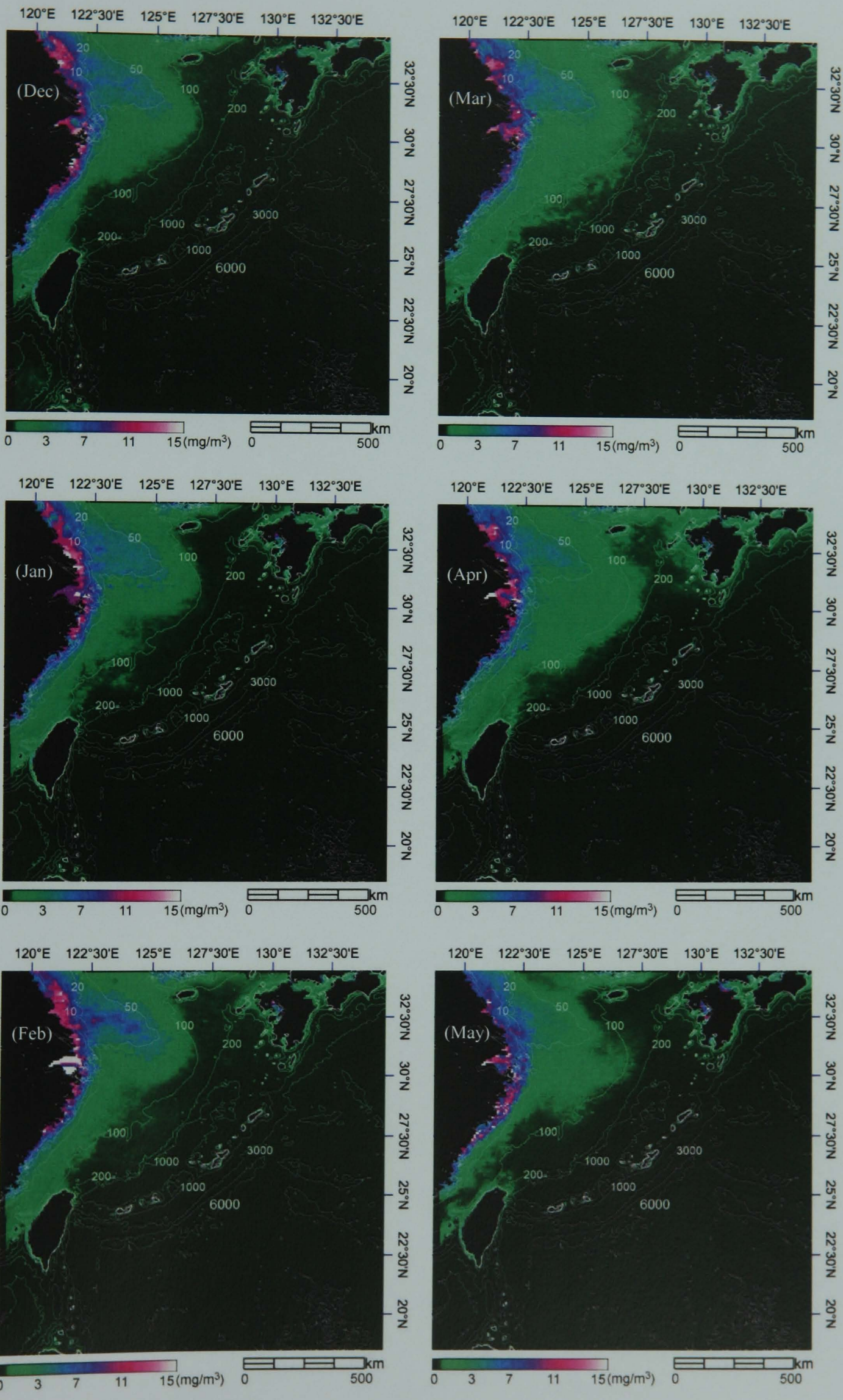

Fig. 4.5. Monthly climatology (1998 – 2006) of OC4 (Dec – May). Bathymetry is drawn in the white line.

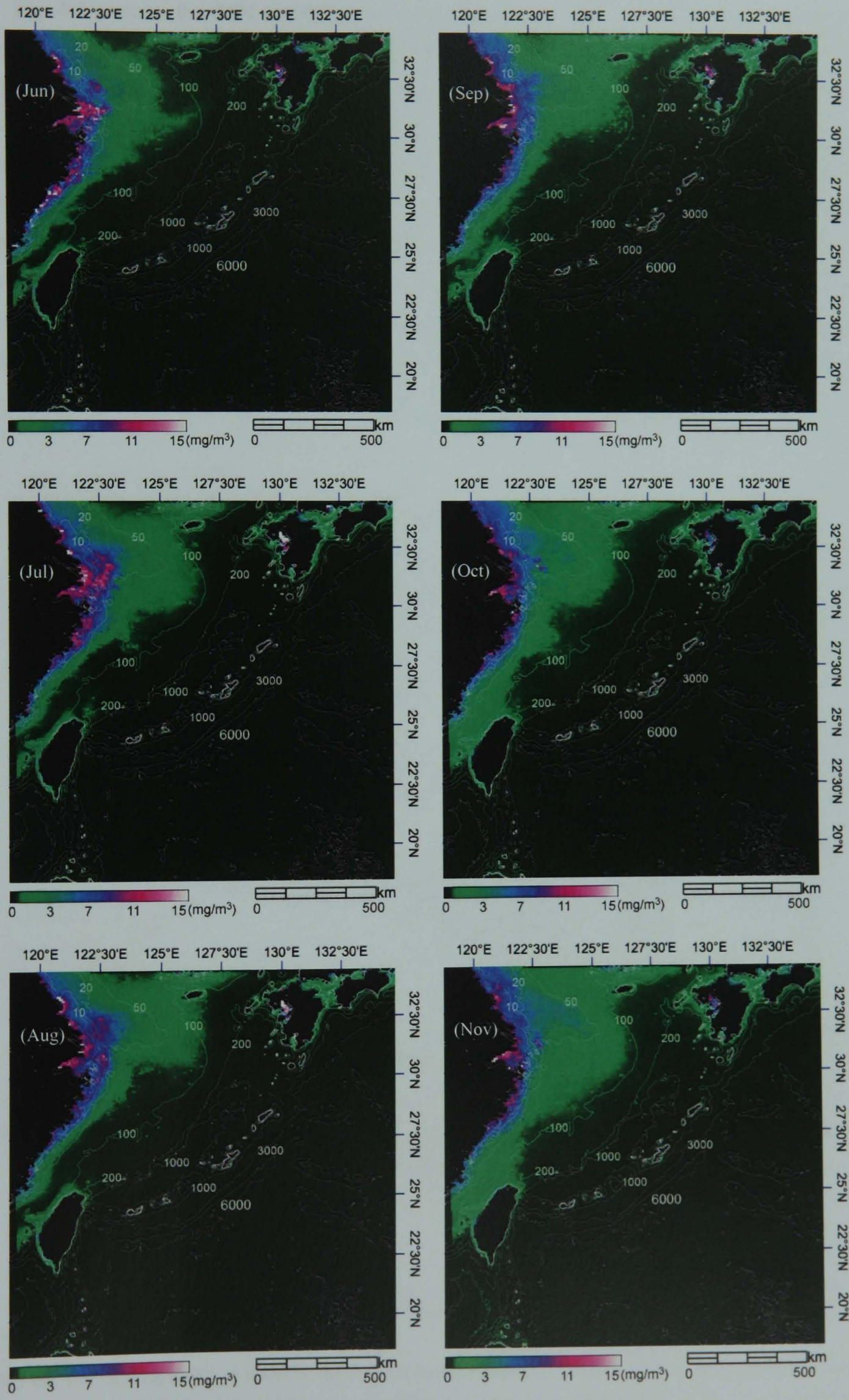

Fig. 4.5 (continued). Monthly climatology (1998 – 2006) of OC4 (Jun – Nov). Bathymetry is drawn in the white line.

Fig. 4.6 presents the OC4 variability on a transect in the ECS (Fig. 4.6a), the same transect used in Fig. 4.4 (a). The climatological monthly OC4 (1998 – 2006: Fig. 4.6b) and its standard deviation on the transect (Fig. 4.6c) show high OC4 variability particularly over the shallow regions of less than 50 m deep. The highest variability occurs off the coast at about 20 m deep. It becomes low and flat off the shelf regions deeper than 200 m. Around the 50 m depth regions, the highest OC4 occurs in February (thick blue) and the lowest in July (dotted red). Around the 20 m depth regions, the highest OC4 occurs in July and August (thin and thick red lines) and the lowest around October and November. These different patterns suggest multiple controls exist affecting the OC4 variation both in space and time over the ECS. It should be noted that several extreme peaks, noted by the arrows in Fig. 4.6. (b), occur due to the short time series (9 years) compared to the SST data (22 years).

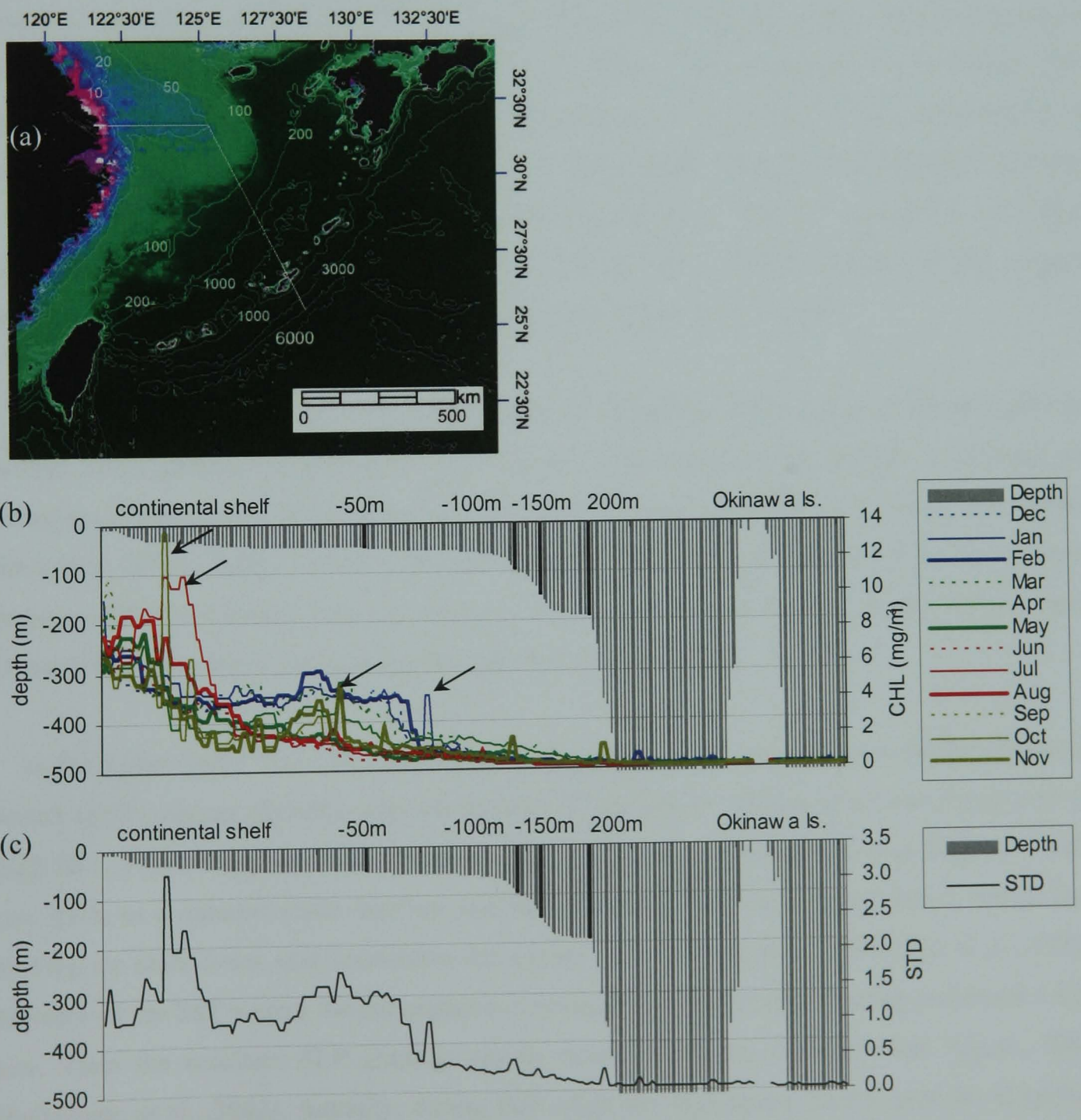

Fig. 4.6. The OC4 variability in the ECS. (a) Transect for the observation, (b) the climatological monthly OC4 and the depth on the transect, and (c) the standard deviation of the OC4 and the depth on the transect. Black bars in the depth indicate the depth of 50 m, 100 m, 150 m and 200 m, respectively.

4.3.3 Ocean Surface Winds

The monthly climatology of ocean wind was produced using the SeaWinds data from 2000 to 2006. Fig. 4.7 shows the vector mean and Fig. 4.8 shows the scalar mean.

In Fig. 4.7, the wind direction shows its alternation between summer and winter, indicating that the study area is under the EAM climate: the southwest winds accompanied by heavy rain in summer and the strong northeast wind in winter originating from a huge anticyclone over Siberia (Lau and Li, 1984).

As seen in winter (DJF), a strong northeasterly prevails from the Chinese continent. The direction veers to the west as it proceeds southward. In March, the wind direction maintains the same pattern as in winter, but with decreased velocity. In April, northeasterlies are still observed over the continental shelf region, but an easterly starts to blow in the south Philippine Sea. From May, the southeast wind starts to prevail and it brings the rainy season until June. This southeasterly continues until August. The wind system in this season is the summer EAM. It usually begins in early to mid-May with a convective rainfall front that extends from southern China to Japan (Johnson et al., 1993). This period is called the "*Mei-Yu*" (plum rain) in China, or "*Baiu*" in Japan (Chen and Chang, 1980). In this season, the southern region of the Yangtze River experiences continuous rainfall, yielding a great quantity of run-off.

In September, the wind turns to become northerly, it increases its velocity in October, and the winter EAM pattern is established in November. There are several indices to indicate the intensity of the winter EAM (Jhun and Lee, 2004; Zhu et al., 2005; Hui, 2007). For further discussion in this study, a simple Monsoon Index (MOI) which is determined by the sea level pressure (SLP) difference between Nemuro, Japan, and Irkutsk, Russia, in hPa will be used. Distance between these two locations is approximately 5800 km.

In the scalar mean field (Fig. 4.8), high wind speed is observed in the Kuroshio region in winter (DJF), spring (MAM), and late autumn (ON), which appears to be associated with its high SST. This atmospheric effect from the SST variability can be explained as follows. A SST rise leads to a reduced static stability and hence stronger vertical mixing, which brings fast-moving air aloft down, and accelerates the surface wind (Hayes et al., 1989; Xie et al., 1998). Increase of the SST warms the atmospheric boundary layer by sensible heating and forms a SLP low. Then the resultant SLP gradient causes wind adjustment (Lindzen and Nigam, 1987; Hashizume et al., 2002). Actually, during DJF when the high speed occurs over the Kuroshio, the DJF SST difference between the Kuroshio region and the Yellow Sea region is high (see Fig. 4.3 DJF and Fig. 4.4b) .

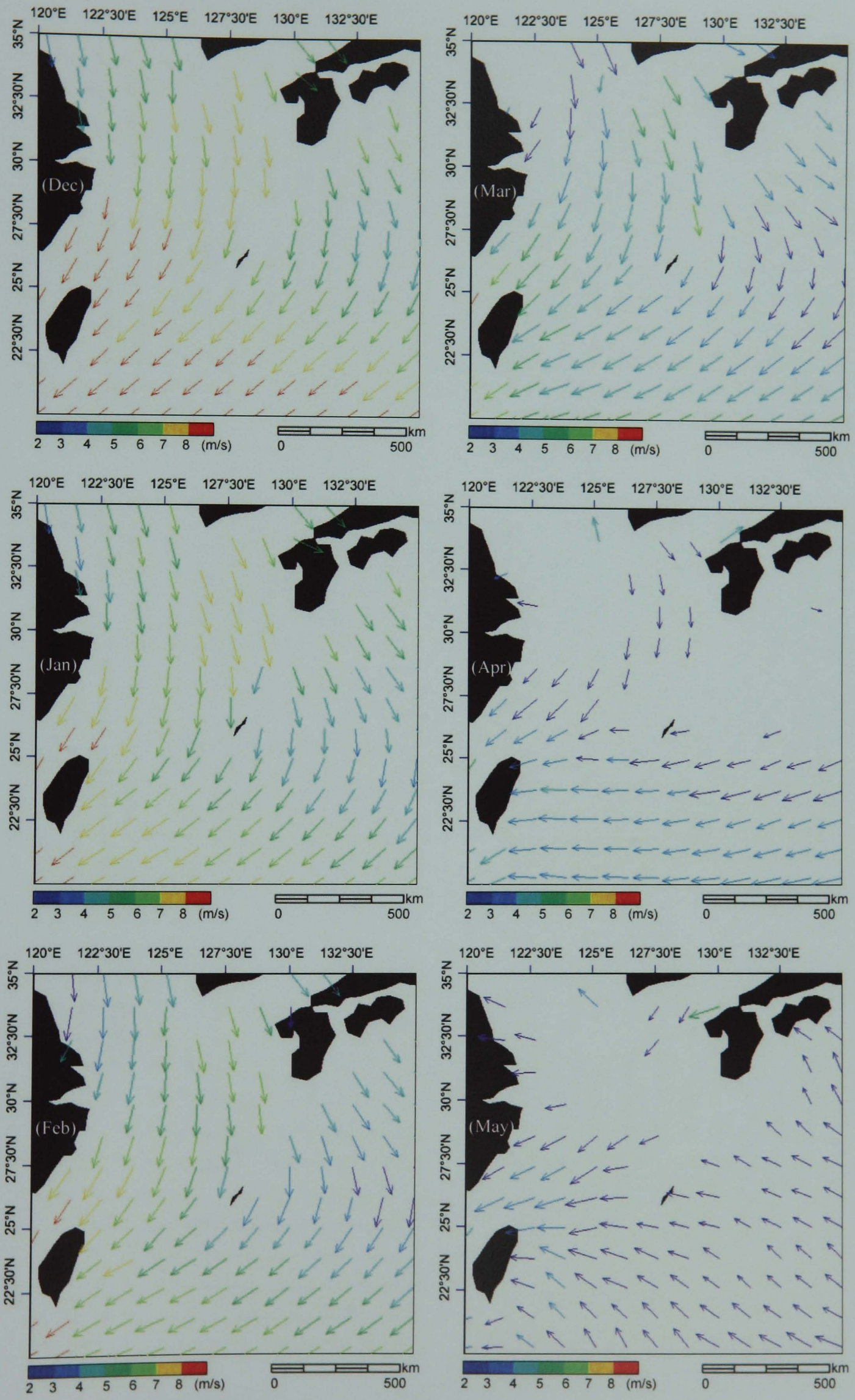

Fig. 4.7. Monthly climatology (2000 – 2006) of ocean wind (Dec – May). Grid resolution was sub-sampled from 0.25° to about 3 °. Blank area without a vector has a lower value (< 2 m/s) than the scale.

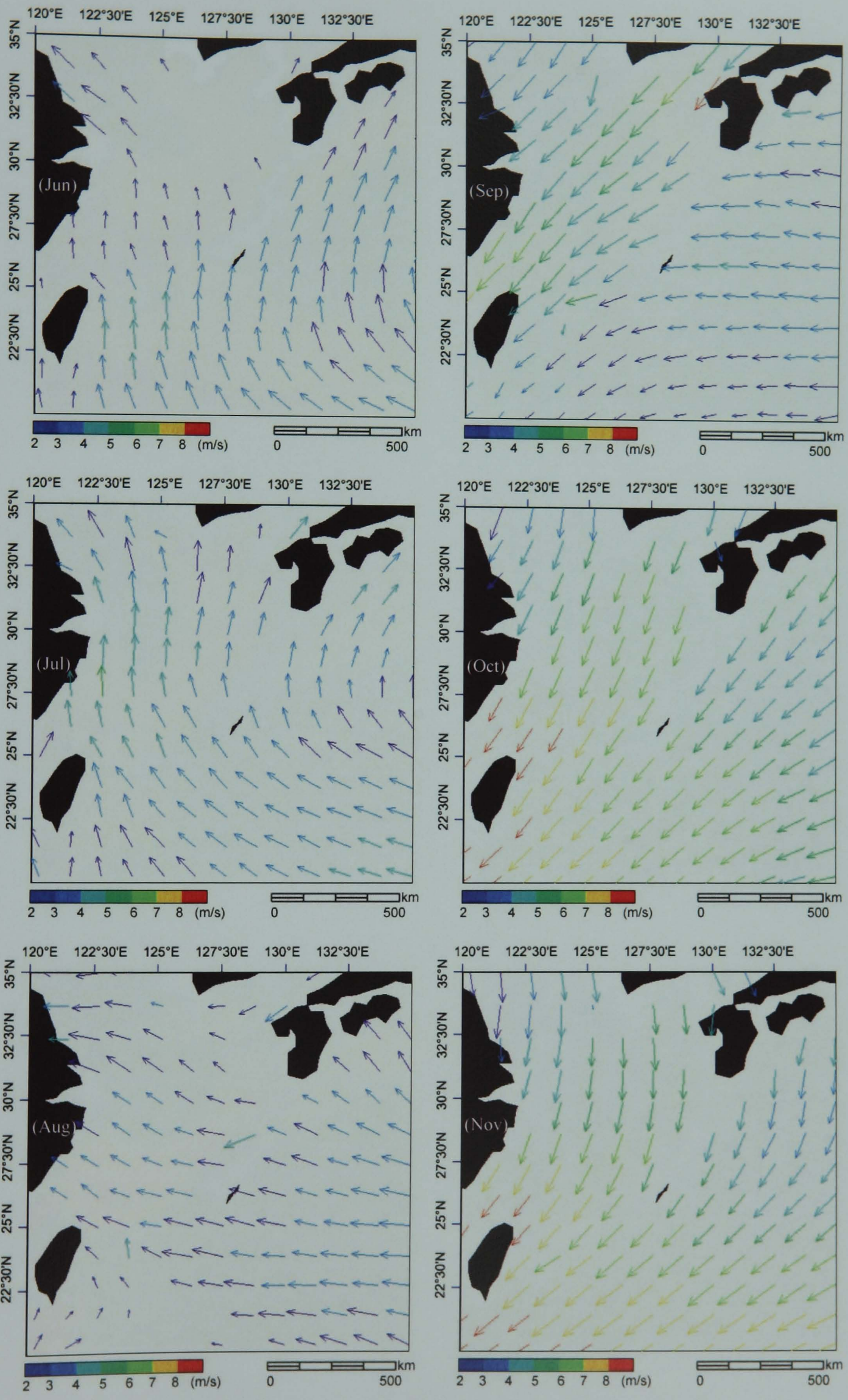

Fig. 4.7 (continued). Monthly climatology (2000 – 2006) of ocean wind (Jun – Nov). Grid resolution was sub-sampled from 0.25° to about 3 °. Blank area without a vector has a lower value (< 2 m/s) than the scale.

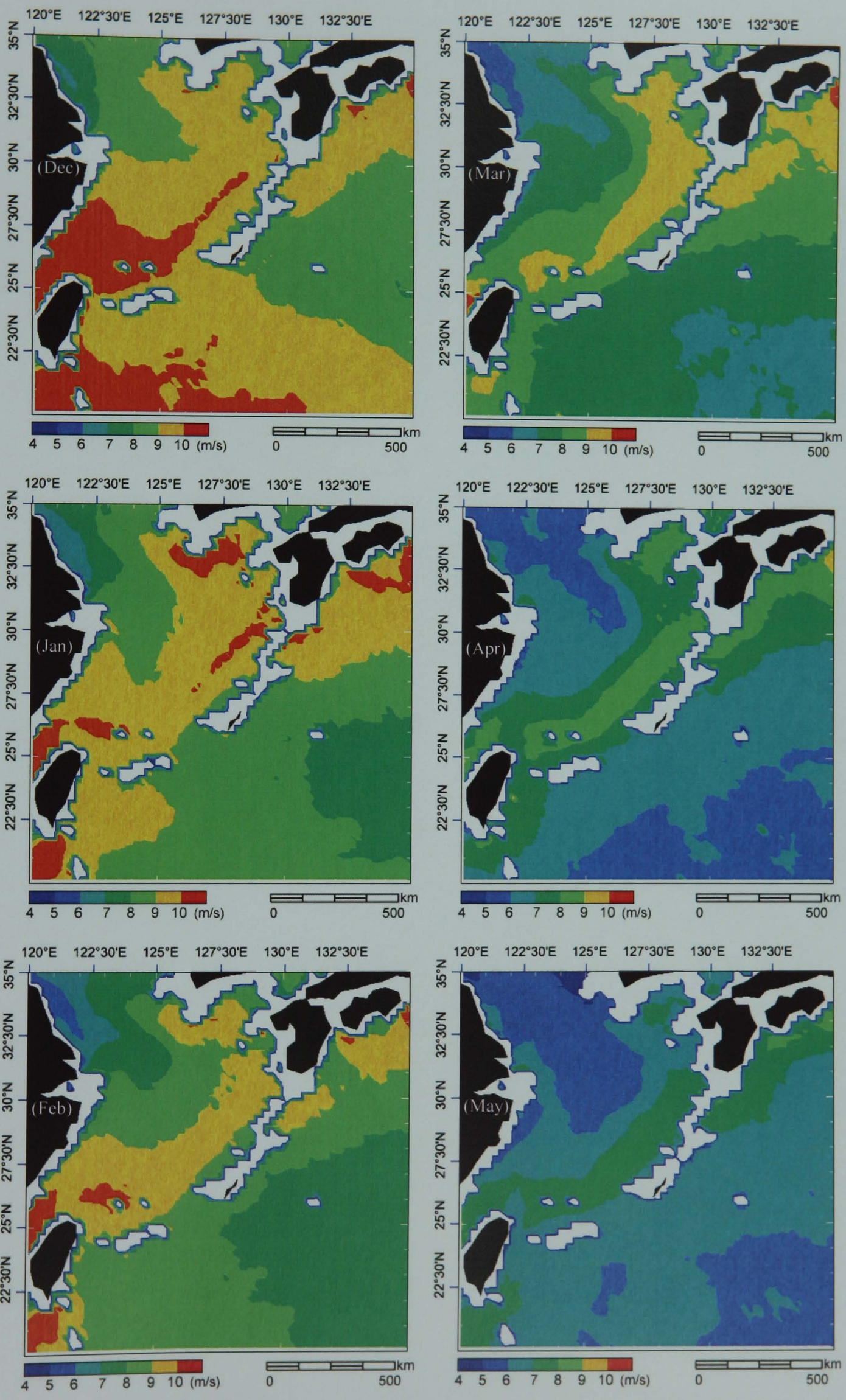

Fig. 4.8. Monthly climatology (2000 – 2006) of scalar ocean wind (Dec – May). Scales are adjusted from the vector map to enhance the distinction. Lower values (4 < m/s) than the scale appears as blank area.

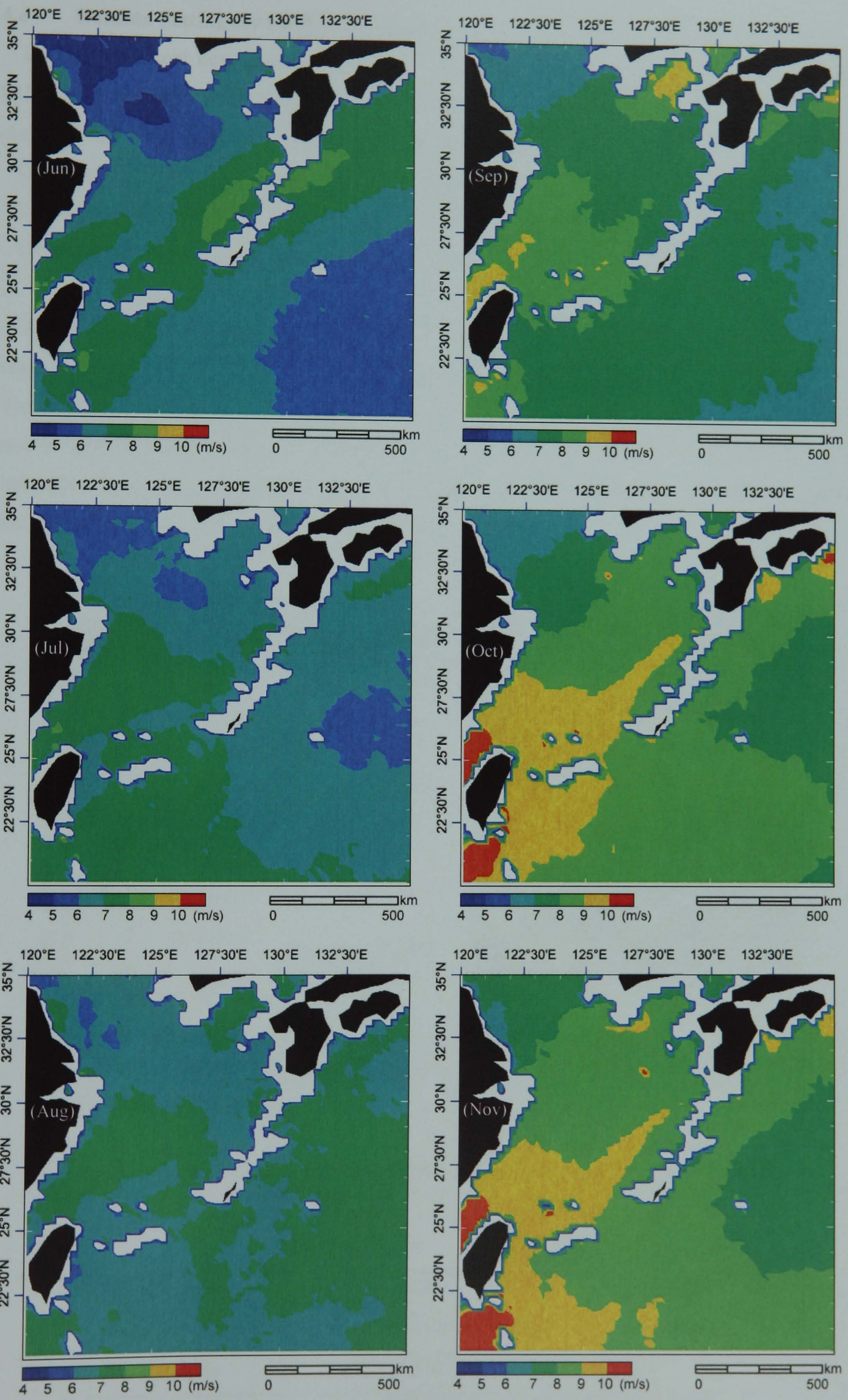

Fig. 4.8. (continued). Monthly climatology (2000 – 2006) of scalar ocean wind (Jun – Nov). Scales are adjusted from the vector map to enhance the distinction. Lower values (4 < m/s) than the scale appears as blank area.

4.4 Domain Setting for the EOF Analysis

In order to detect key controls on the SST and OC4 variability at different scales over the ECS, three domains were defined (Fig. 4.9) for the EOF anlyses. The size of the domains changes from large ocean scale to the small island scale.

Domain 1 (D1): the ECS (including Chinese coast and Okinawa) and the Philippine Sea

Domain 2 (D2): a sub region of D1 - around Okinawa, including the KC.

Domain 3 (D3): a sub region of D2 - near the coastline of Okinawa itself.

For computing convenience, the satellite data of D1 (SST and OC4) and D2 (SST) were resampled at a lower resolution. The number of pixels used in the analysis is given in Table 4.1. The pixels in D3 were carefully chosen with high resolution imagery overlaid (e.g., LANDSAT) not to include Okinawa and the neighbouring small islands. Due to the difference in the instrument resolutions, 4 pixels of the AVHRR data (4-km resolution) are averaged to represent the same 1 pixel of the SeaWiFS (9-km resolution).

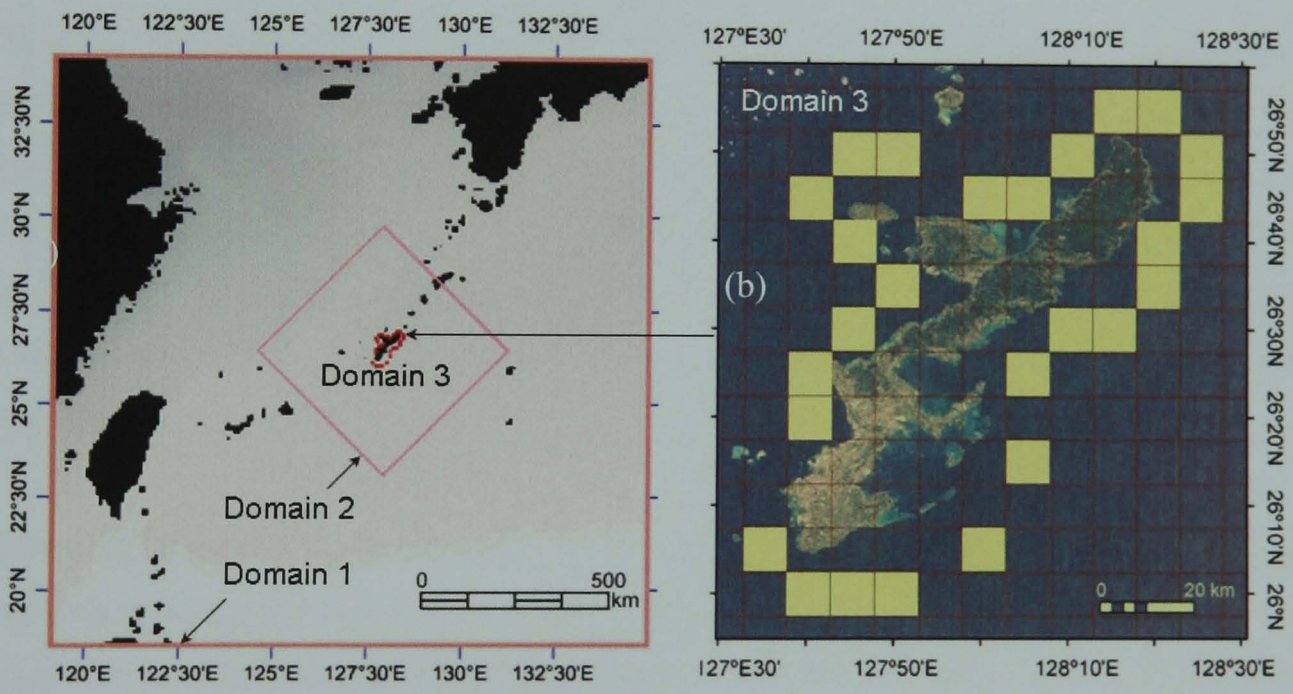

Fig. 4.9. Three Domains defined for the EOF analyses: (a) Domain 1 and Domain 2 are indicated in red square. Domain 3 is marked by red dots. (b) Enhanced image of Domain 3. 26 pixels (white coloured) are selected along the coast of Okinawa.

Table 4.1. Number of spatial and temporal variables in the three domains for the EOF analyses.

		Domain 1 (374,463 km^2)	Domain 2 (29,520 km^2)	Domain 3 (234 km^2)
SST	No. of pixels	4226	2456	26 (26 × 4× 1/ 4)
	No. of months	264 (January 1985 – December 2006)		
OC4	No. of pixels	4334	3211	26
	No. of months	108 (January 1998 – December 2006)		

4.5 SST EOF

4.5.1 Result in Domain 1: SST

Fig. 4.10 shows the eigenvalues of the modes derived from the EOF analysis of the SST in D1. The 1st mode is dominant and accounts for 91.6 % of the total variance. The 2nd mode explains 2.6 %, and the rest of the modes explain less than 1 % of the total variance each.

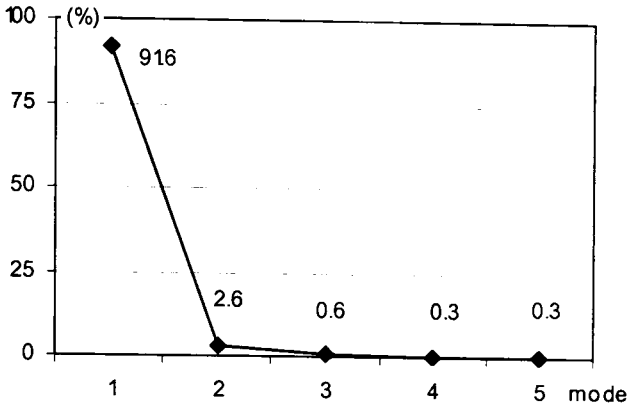

Fig. 4.10. Eigenvalues of the SST EOF in D1.

Fig. 4.11 shows the eigenvectors of the SST EOF in D1 with bathymetry. The yellow dots show the axis of the KC estimated by the *Japanese Coast Guard* during 1 August 2006 – 2 February 2007 (http://www1.kaiho.mlit.go.jp/KANKYO/KAIYO/qboc/index.html). Fig. 4.12 shows (a) the temporal functions and (b) the spectra of each mode. The temporal variation of the 1st mode has a clear and smooth annual cycle (Fig. 4.11.M1a and 4.11.M1b) – high values in summer and low values in winter. It fits the cycle of the solar radiation intensity in the Northern Hemisphere.

All the eigenvectors in the 1st mode have positive values (Fig. 4.11.M1). High eigenvector values (>2) were observed mainly over the continental shelf including the Yellow Sea. Those isolines over the shelf are mostly parallel to the isobaths. Off the shelf region, the eigenvector values are low in the Okinawa Trough and the Philippine Sea. Given the annual solar heating cycle of the 1st mode, this characteristic eigenvector distribution over the shallow shelf can be explained by the thermal attributes of water. The thermal inertia of a water column on the shelf is linearly proportional to the bottom depth, which determines the cooling/warming rate of the water column. In other words, shallow water is more susceptible to the cooling/warming forcing than the deep water. This bathymetric-control mechanism suggests a strong association between the eigenvectors of the 1st mode and bathymetry (Xie et al., 2002). Because of the intense cooling by the winter EAM, the ECS are well mixed in the upper 100 m (Chen et al., 1994; Ichikawa and Beardsley, 2002). Thus, shallow water cools much more quickly than deep water. Therefore, the SST variability on the shelf region displays higher variability than the off shelf region modulated by the solar radiation, as seen in Fig 4.4.

(M1)

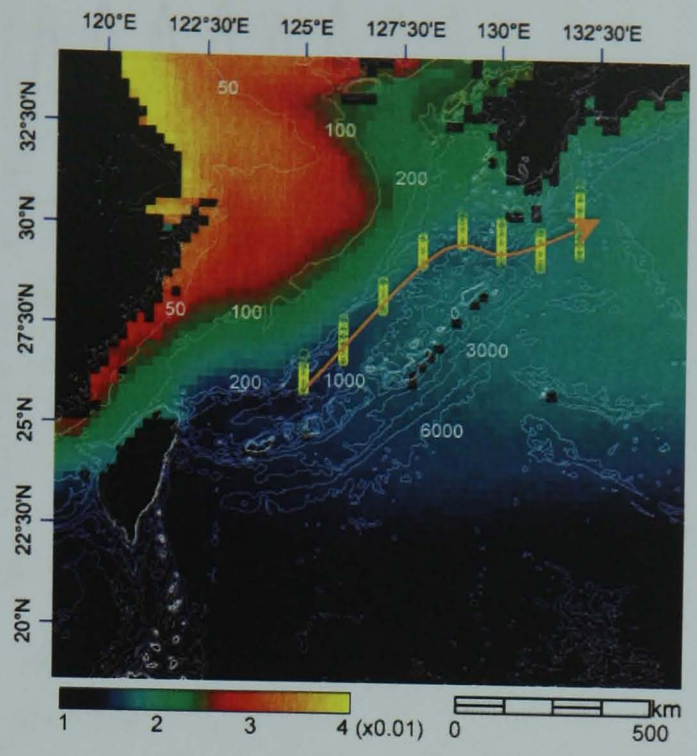

Fig. 4.11. Eigenvectors of the SST EOF in D1: (M1) the 1st mode, (M2) the 2nd mode and (M3) the 3rd mode. The white lines indicate isobath. The yellow circles are the axis of the KC estimated by the *Japanese Coast Guard* based on their observation from 1/8/2006 to 2/2/2007. The arrow shows the direction of the KC.

Eigenvalue = 91.6 %

(M2)

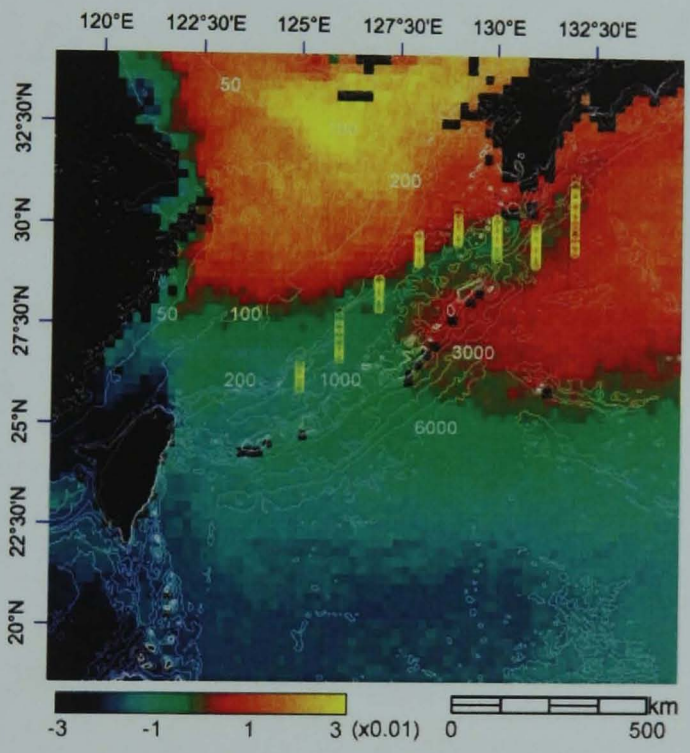

Eigenvalue = 2.6 %

(M3)

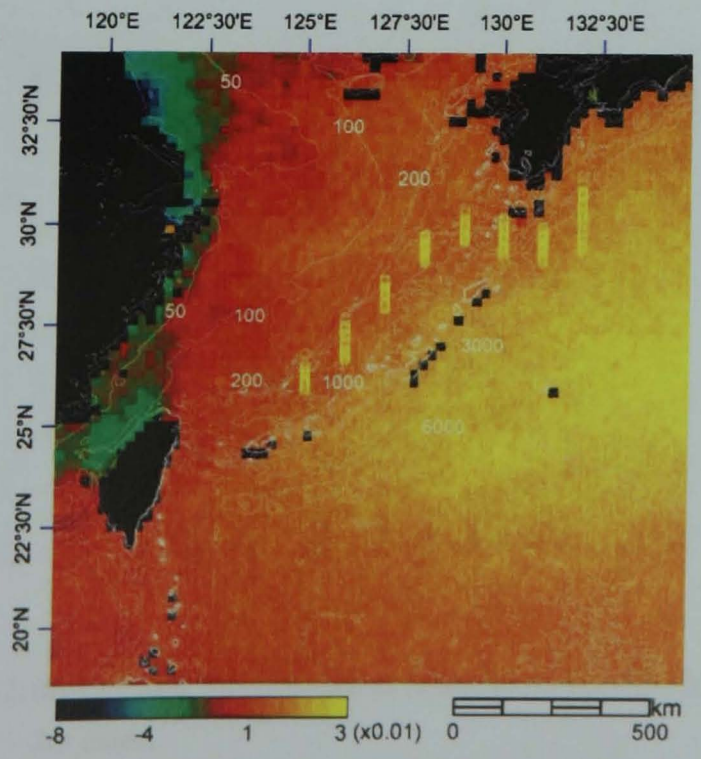

Eigenvalue = 0.6 %

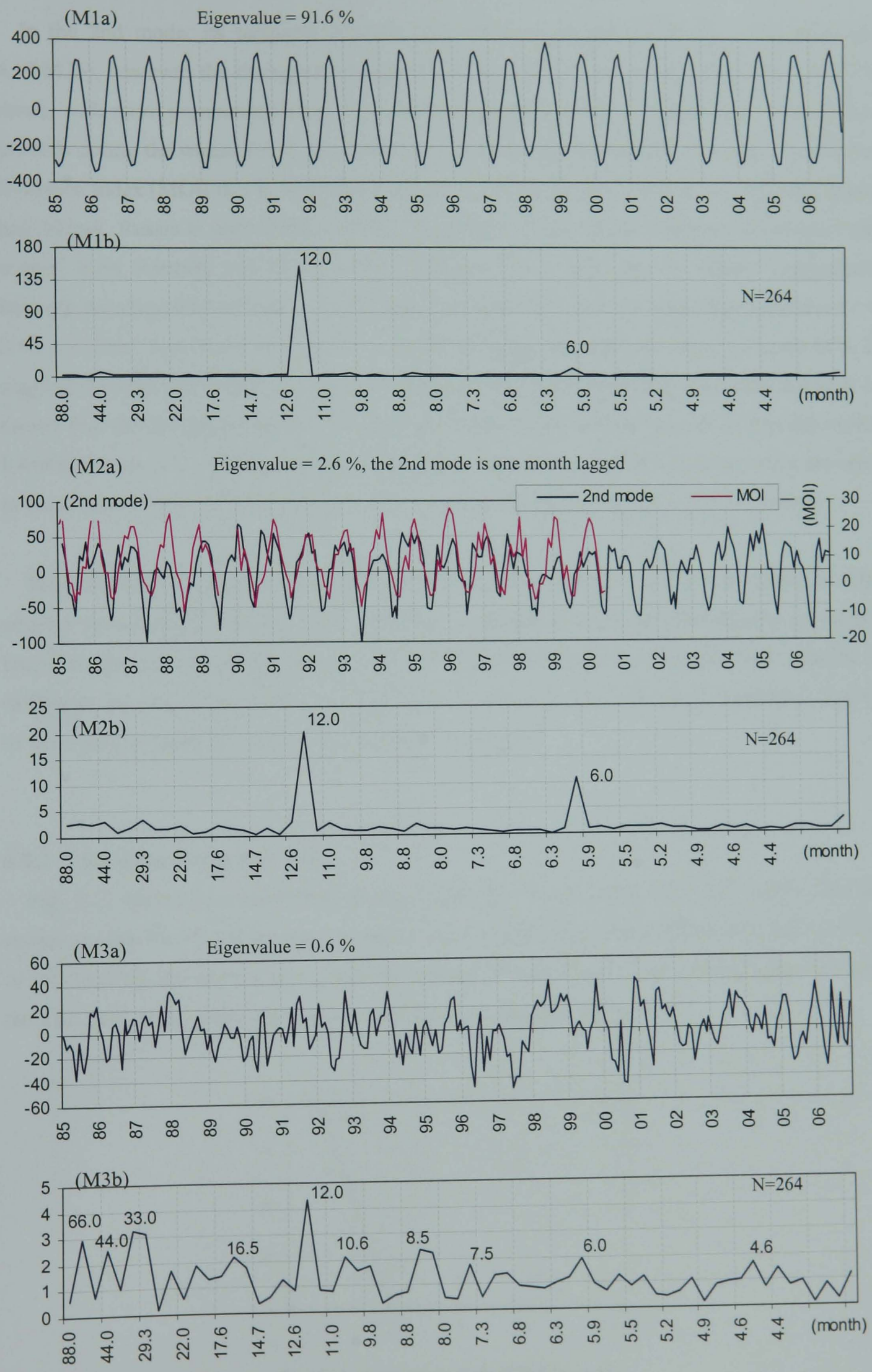

Fig. 4.12. (a) Temporal functions and (b) spectrum of the SST EOF in D1: (M1) 1st mode, (M2) 2nd mode and (M3) 3rd mode.

In the 2nd mode, its temporal function also shows an annual cycle (Fig. 4.12.M2a and 4.12.M2b), however, the timing of the high and low values in the season is opposite to the 1st mode, with more pronounced short term peaks, suggesting a link to the strong northerly that prevails during the winter EAM. In order to examine the relationship with the winter EAM, the Monsoon Index (MOI) that is determined by the SLP difference in hPa between Nemuro, Japan, and Irkutsk, Russia is used (1985 – 2000). The MOI is a convenient indicator to represent the overall wind intensity and hence cooling character in a wide area in winter. Comparison between the temporal function in the 2nd mode and the MOI shows a significant correlation $r = 0.67$, $p < 0.001$ with a month's lag of the 2nd mode. High values appear on the northern ECS. It suggests that the 2nd mode is a control on cooling the SST represented by the winter EAM. It is known that the cooling during the winter in the western North Pacific is controlled by the winter EAM (Hanawa et al., 1988; Bingham, 1992; Suga and Hanawa, 1995). Negative values are seen in the southern ECS and the Philippine Sea, along the Chinese coast and in the KC region.

The variance explained by the 3rd mode is very low at 0.6 % of the total variance. The positive values spread over the ocean water east of the Ryukyu Arc, and the negative values are found along the Chinese coast line and in the Taiwan Strait. This mode may indicate a difference between ocean water and coastal water. However, this will not be considered further as the signal is weak and likely to be dominated by noise.

4.5.2 Result in Domain 2: SST

Fig. 4.13 shows the eigenvalues of the modes derived from the SST EOF in D2. The 1st mode explains 94.6 % of the total variance, which is higher than that explained by the 1st mode of D1 (91.6 %). All other modes explain less than 1 % each. Fig. 4.14 shows the eigenvectors of the SST EOF in D2. Their temporal variabilities are indicated in Fig. 4.15.

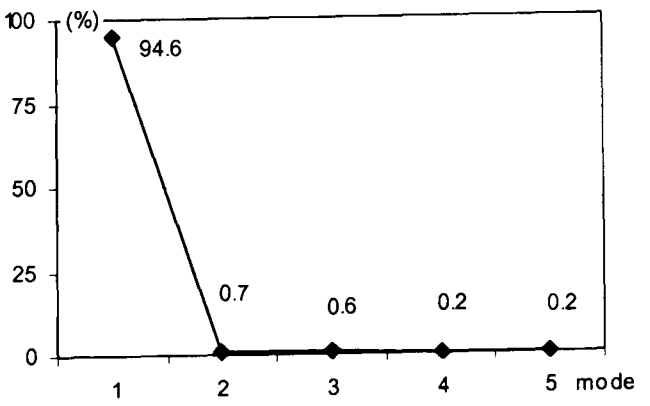

Fig. 4.13. Eigenvalues of the SST EOF in D2.

In the eigenvector of the 1st mode (Fig. 4.14.M1), all the values indicate positive values, and the highest values (> 0.024) are seen at the edge of the continental shelf indicating high variability in this region, as seen in the 1st mode eigenvector in D1. A tongue of low values (< 0.02) can be found along the KC in the Okinawa Trough. Bathymetric features otherwise have little contribution to the distribution. Instead, the north part tends to have higher values than the south of D2. The temporal function of the 1st mode (Fig. 4.15.M1a and 4.15.M1b) indicates an annual cycle as seen in the 1st mode in D1, suggesting the primary control on the SST variability in D2 is also solar radiation.

The 2nd and the 3rd modes account for less than 1 % of the variance and their eigenvector patterns are strongly linked to the shape of the region. It is therefore thought that they are mostly noise (Richman, 1986); hence they will be neglected.

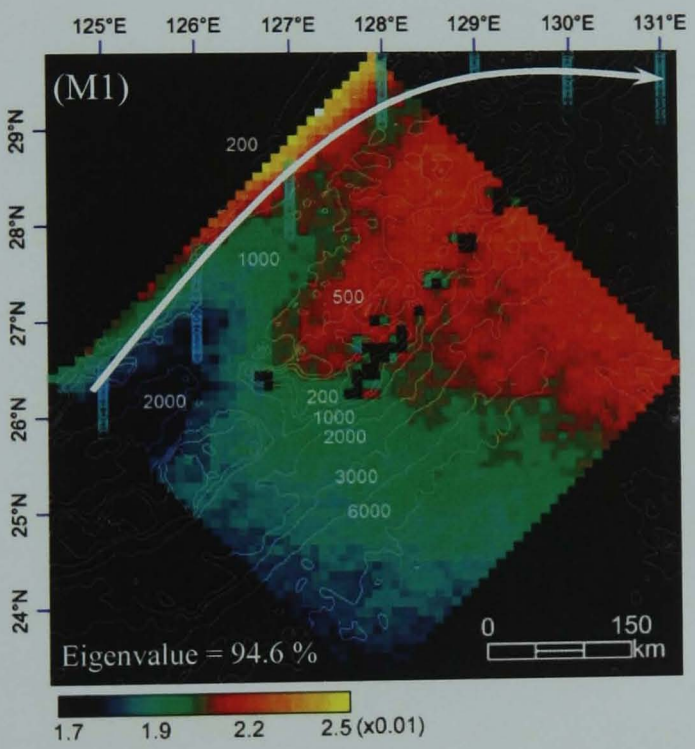

Fig. 4.14. Eigenvectors of the SST EOF in D2: (M1) the 1st mode, (M2) the 2nd mode and (M3) the 3rd mode. The thin white lines indicate isobath. The blue circles are the axis of the KC estimated by the *Japanese Coast Guard* based on their observation from 1/8/2006 to 2/2/2007. The thick white arrow shows the direction of the KC.

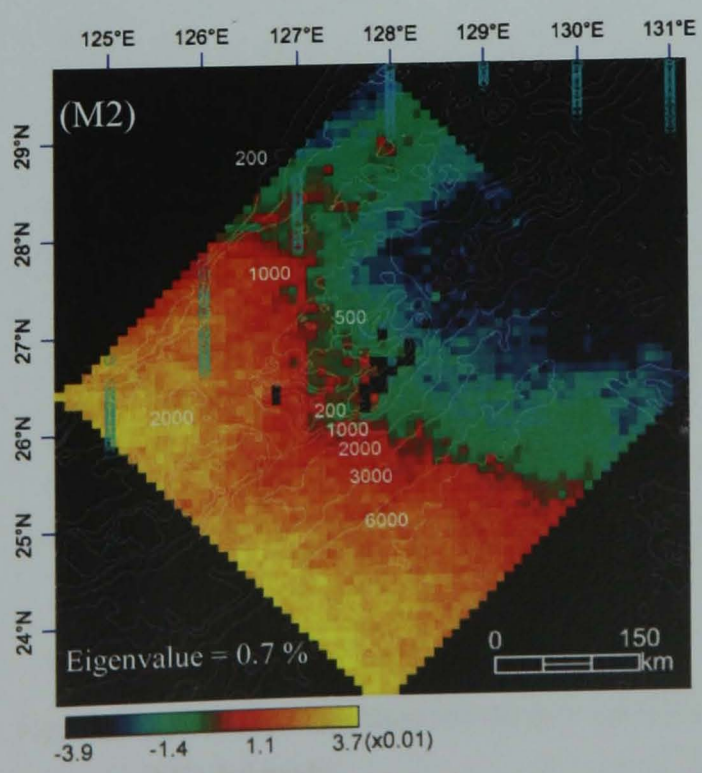

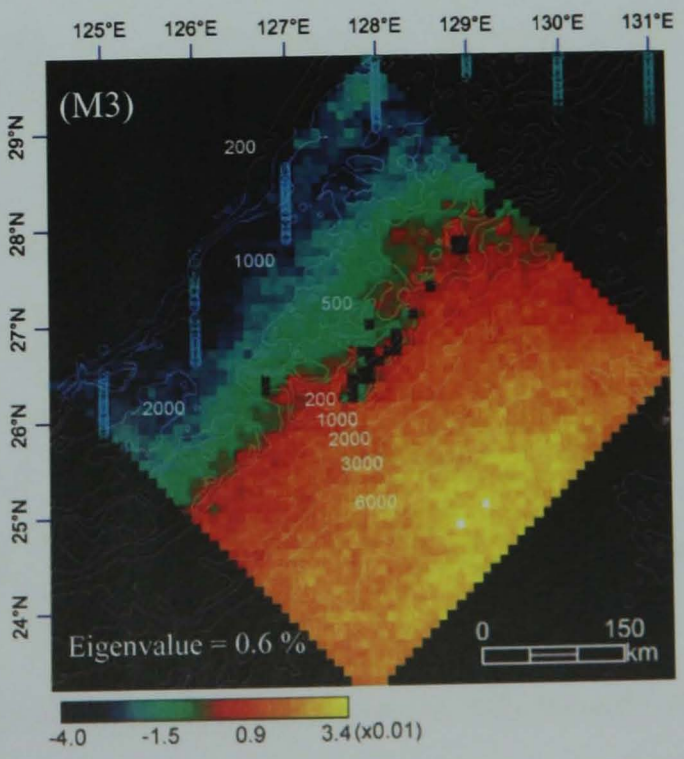

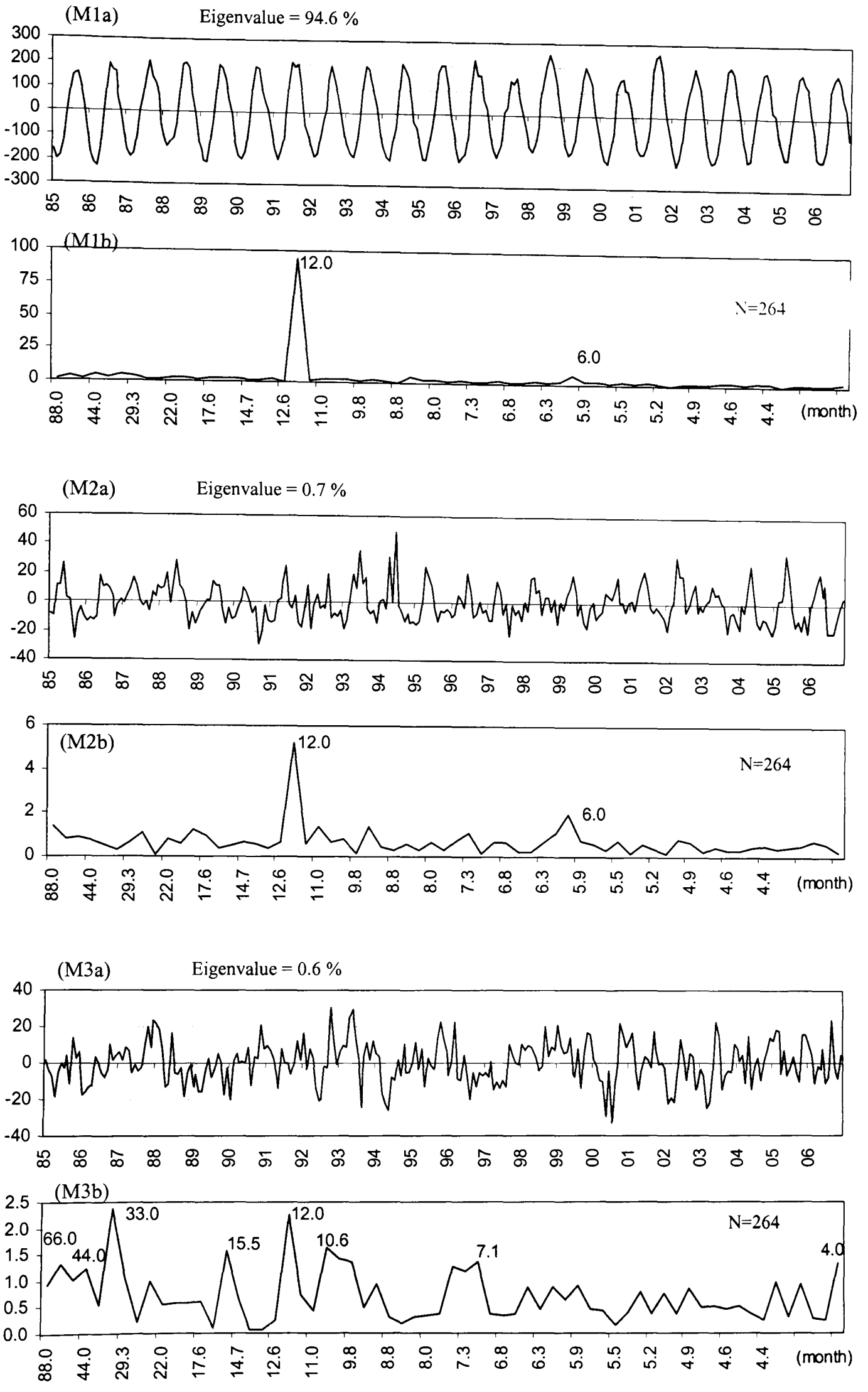

Fig. 4.15. (a) Temporal functions and (b) their spectrum of the SST EOF in D2: (M1) 1st mode, (M2) 2nd mode and (M3) 3rd mode.

4.5.3 Result in Domain 3: SST

Fig. 4.16 shows the eigenvalues of the modes derived from the SST EOF in D3. The 1st mode is a dominant control, accounting for 97.6 % of the total variance. As the domain focuses more locally, the 1st mode contributes to greater extent (D1 → D2 → D3; 90.6 → 94.6 → 97.6 %). The rest of the modes account for less than 1 % of the total variance each.

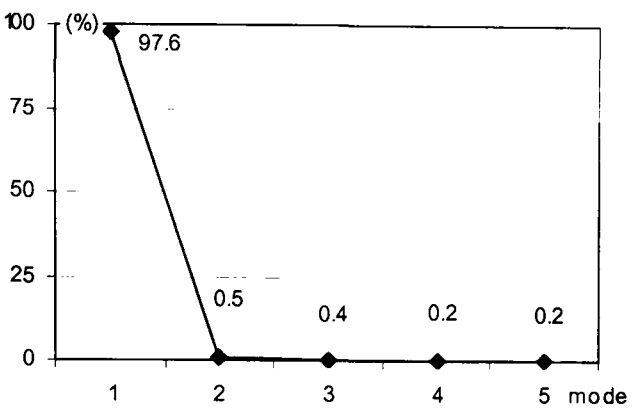

Fig. 4.16. Eigenvalues of the SST EOF in D3.

Fig. 4.17 shows the eigenvectors of the SST EOF in D3. Their temporal functions and the latter's spectra are indicated in Fig. 4.18 (a) and (b) respectively. The temporal function of the 1st mode displays the same annual cycle (Fig. 4.18.M1a and 4.18.M1b) as seen in D1 and D2, which suggests a relation to the solar radiation cycle. Although its amplitude is an order of magnitude less than those for D1 and D2, meaning less variability, the eigenvector still explains 97.6 % of the total variance. Given the annual cycle obtained from the 1st modes in the three domains, solar radiation is a primary and dominant control which accounts for more than 90 % of the total variance in all the domains.

The eigenvector of the 1st mode (Fig. 4.17.M1) shows a tendency for higher values in the north of Okinawa compared to the south. This tendency – high values in the north and low values in the south – is also seen in the 1st mode eigenvectors in the off-shelf region of D1 and D2.

The 2nd and the 3rd modes explain 0.5 % and 0.4 % of the total variance, respectively. These two modes have variable spectra (Fig. 4.18.M2b and 4.18.M3b), thus they are showing noise rather than a signal representing a significant control.

(M1)

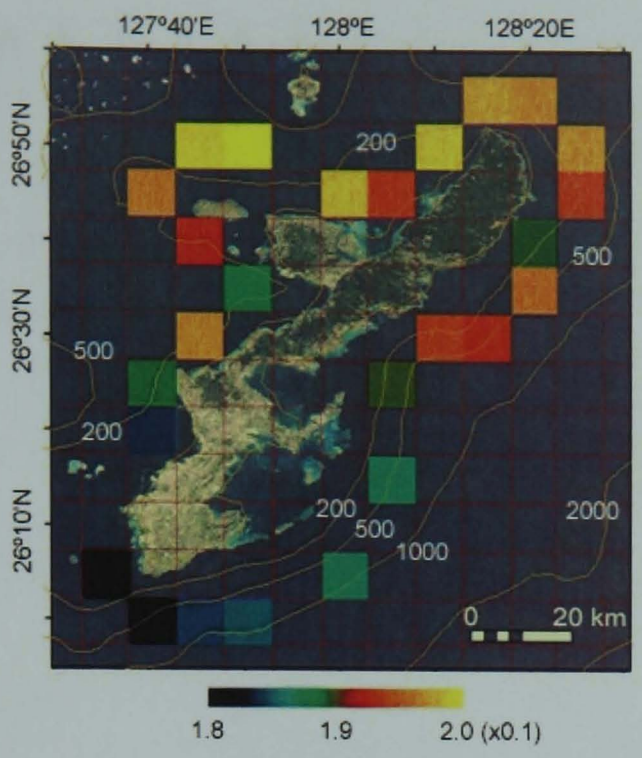

Fig. 4.17. Eigenvectors of the SST EOF in D3: (M1) the 1st mode, (M2) the 2nd mode and (M3) the 3rd mode. The isobaths are shown by the light brown lines.

Eigenvalue = 97.6 %

(M2)

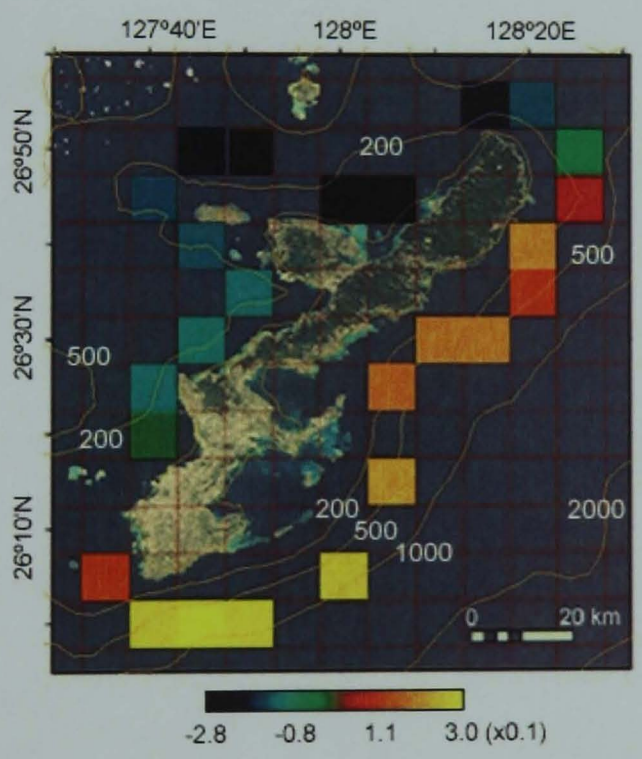

Eigenvalue = 0.5 %

(M3)

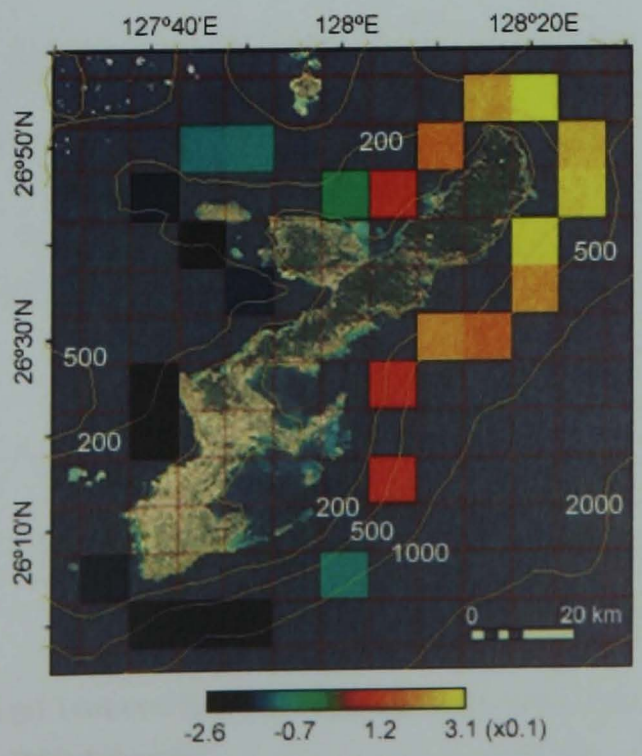

Eigenvalue = 0.4 %

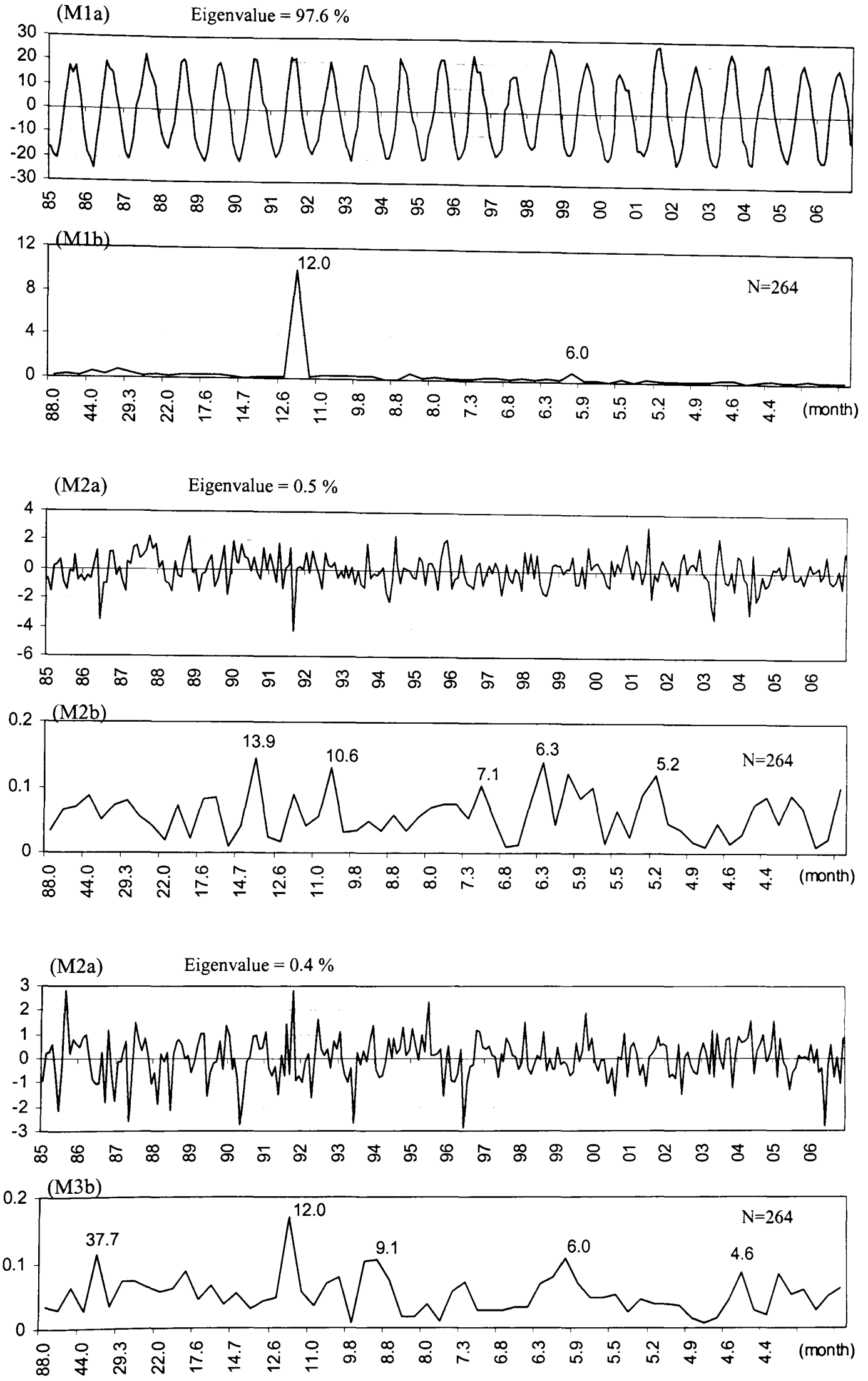

Fig. 4.18. (a) Temporal functions and (b) their spectrum of the SST EOF in D3: (M1) 1st mode, (M2) 2nd mode and (M3) 3rd mode.

4.6 OC4 EOF

4.6.1 Result in Domain 1: OC4

Fig. 4.19 shows the eigenvalues of the modes derived from the EOF analysis of the OC4 in D1. The 1st mode accounts for 13.8 % of the total variance. The rest of the modes slowly decrease their accountability for the variance. The modes greater than 5 % are discussed here i.e. the 1st, 2nd, 3rd and 4th mode.

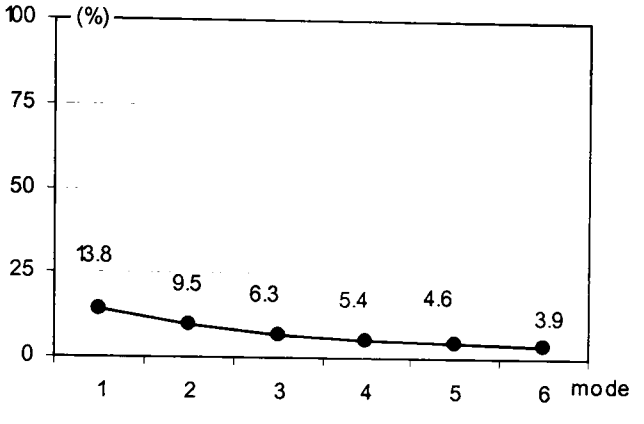

Fig. 4.19. Eigenvalues of the OC4 EOF in D1.

Fig. 4.20 shows the eigenvectors of the OC4 EOF in D1. Their temporal functions and spectra are indicated in Fig. 4.21. The temporal function of the 1st mode shows a periodic annual cycle, but with a few pronounced short term peaks (Fig. 4.21.M1a): high peak values in March associated with the spring bloom and low values in June. In a comparison with the MOI (Jan 1998 – Jul 2000), it shows a statistically significant correlation with a month's lag ($r = 0.81$, $p < 0.001$). Although the comparison between the temporal function and the MOI is limited due to the data availability at Irkutsk, considering their annual periodicity, the correlation suggests that the winter EAM is a control on the OC4 variability in D1.

In the eigenvector of the 1st mode (Fig. 4.20.M1), positive values appear over the continental shelf, especially over the Yellow Sea whose turbid water extends offshore to the 100 m isobath (Chen et al., 1994; Gong et al., 1996). The ECS receives large amount of nutrients from the Yangtze River which can greatly enhance OC4 on the shelf compared to off the shelf and over the Okinawa Trough (Gong et al., 1996; Kiyomoto et al., 2001). Due to this high concentration of nutrients on the shelf, and the water mixing induced by the winter EAM, the OC4 becomes abundant in spring as seen in the temporal function (Fig. 4.21.M1a), hence high seasonal variability of the OC4 is seen over the shelf region compared to other regions (Yanagi et al., 1996; Hama et al., 1997). The distribution of high eigenvectors indicates such variability over the shelf and the Yellow Sea. The negative eigenvectors around the Yangtze Estuary on the other hand suggests an effect of the large plume which occurs during the rainy season in summer. Off the shelf, the eigenvector variation is low because of less nutrient availability. In

the KC region the eigenvectors range from 0.03 to 0.05, and to the west of Okinawa it is around 0.01 – 0.03. The 1st mode is therefore dominantly driven by nutrient flux variability. This is pronounced on the continental shelf and strongly climatically controlled.

(M1)

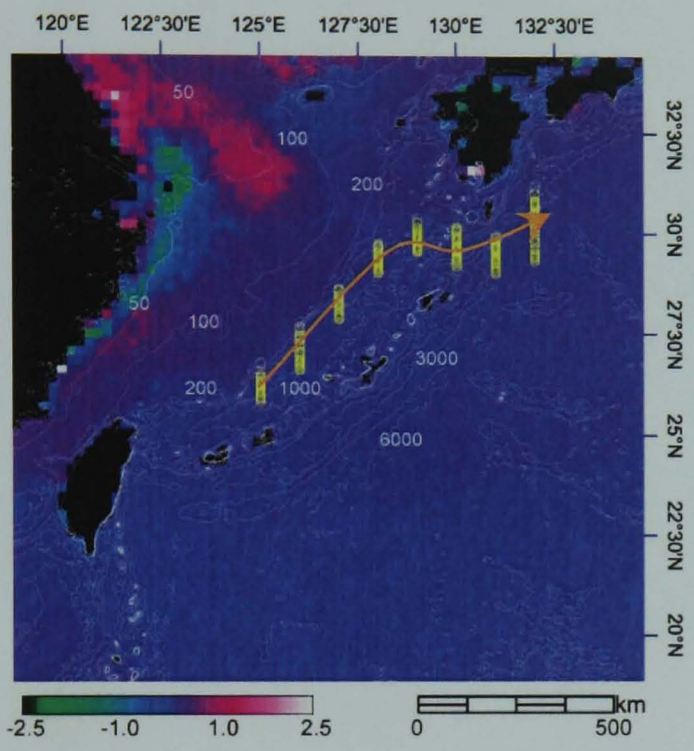

Eigenvalue = 13.8 %

(M2)

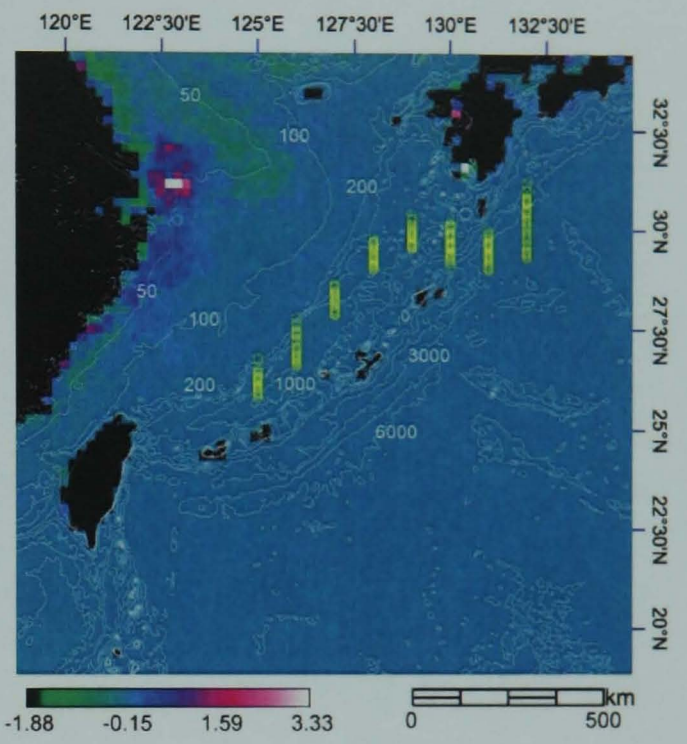

Eigenvalue = 9.5 %

(M3)

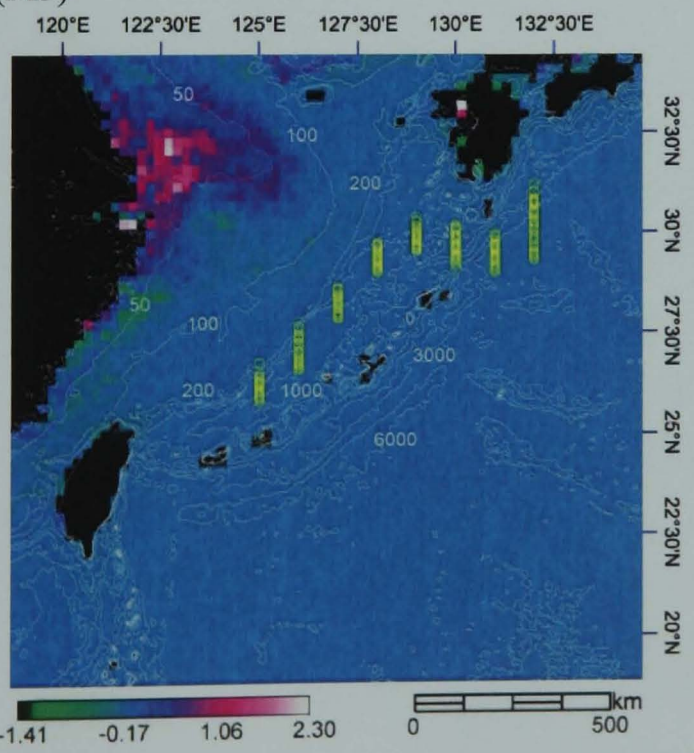

Eigenvalue = 6.3 %

(M4)

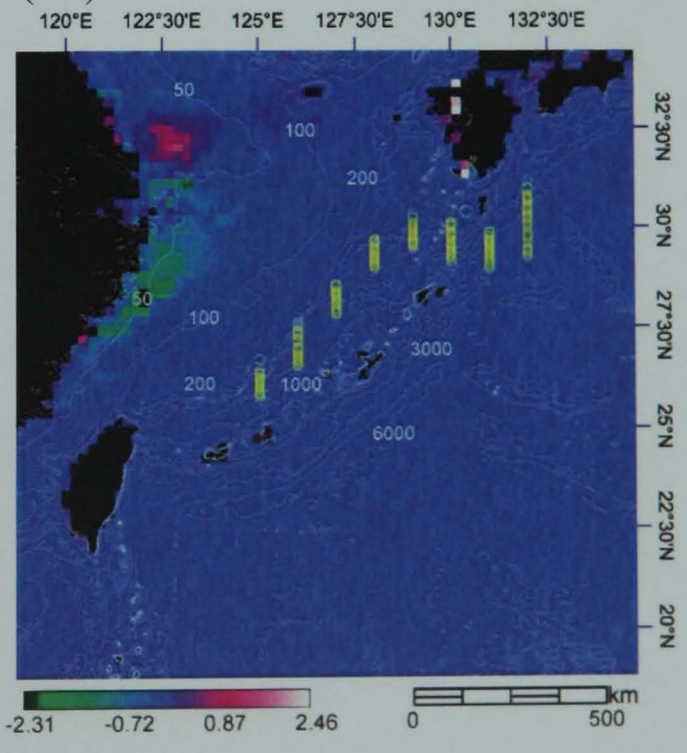

Eigenvalue = 5.4 %

Fig. 4.20. Eigenvectors of the OC4 EOF in D1: (M1) the 1st mode, (M2) the 2nd mode, (M3) the 3rd mode and (M4) the 4th mode. The white lines indicate isobath. The yellow circles are the axis of the KC estimated by the *Japanese Coast Guard* based on their observation from 1/8/2006 to 2/2/2007. The arrow in (M1) shows the direction of the KC.

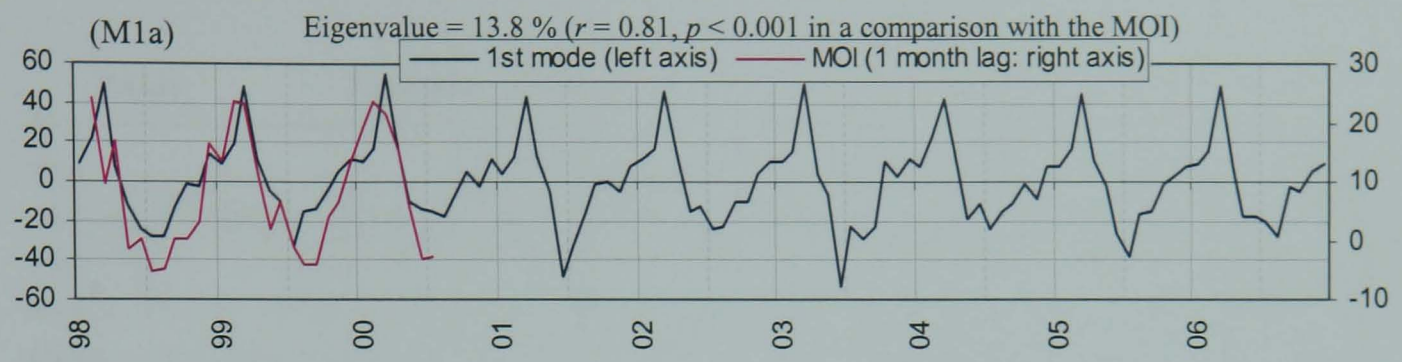

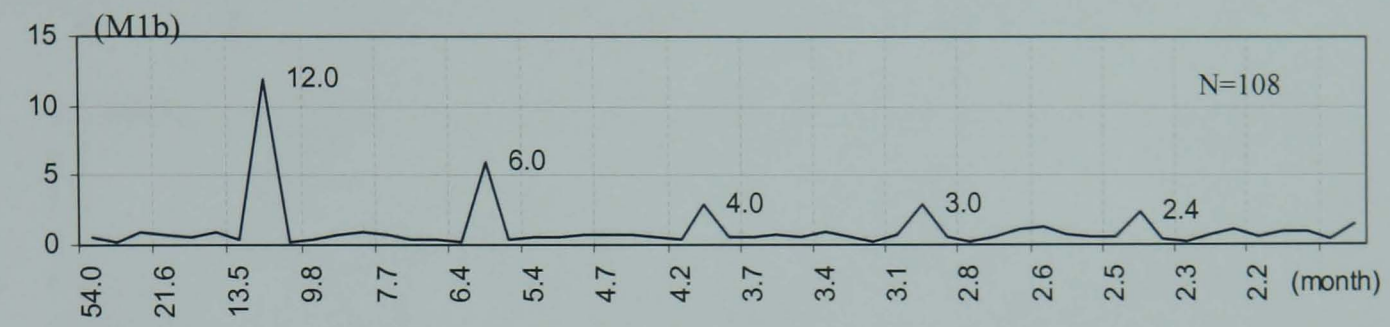

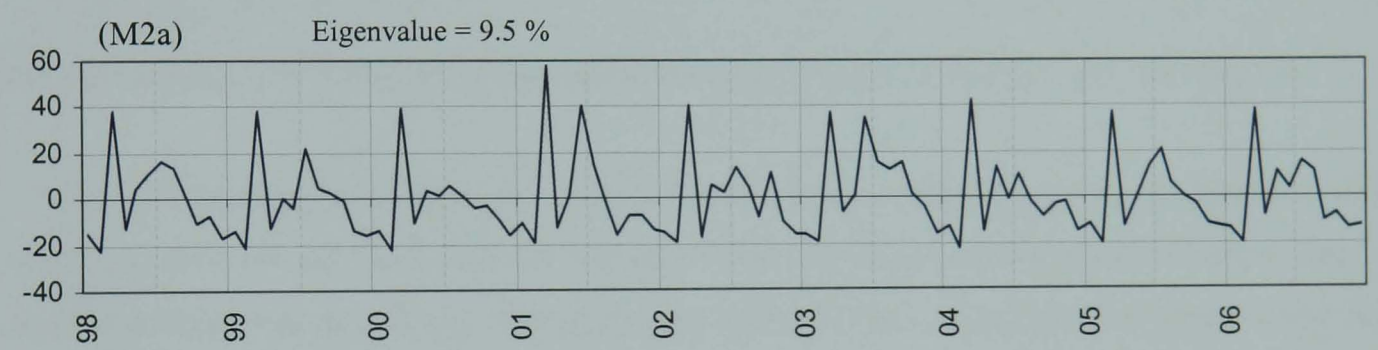

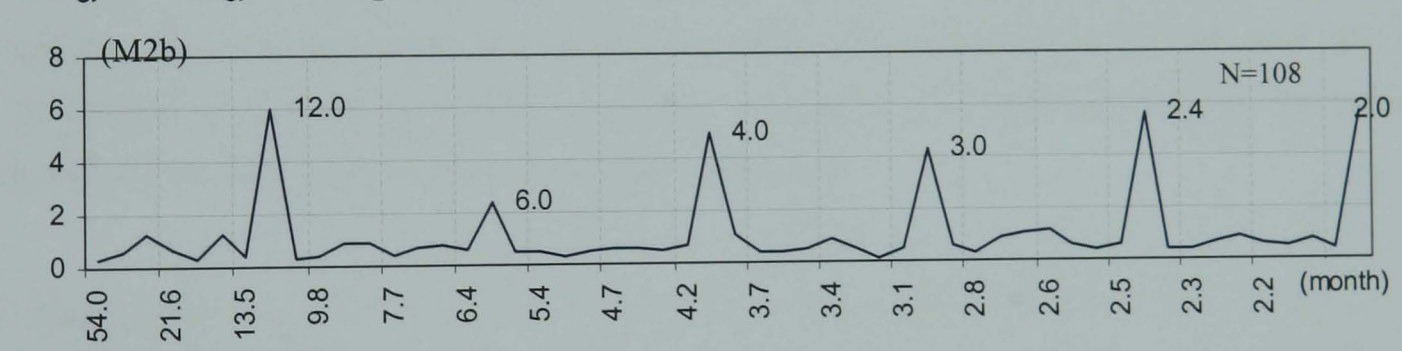

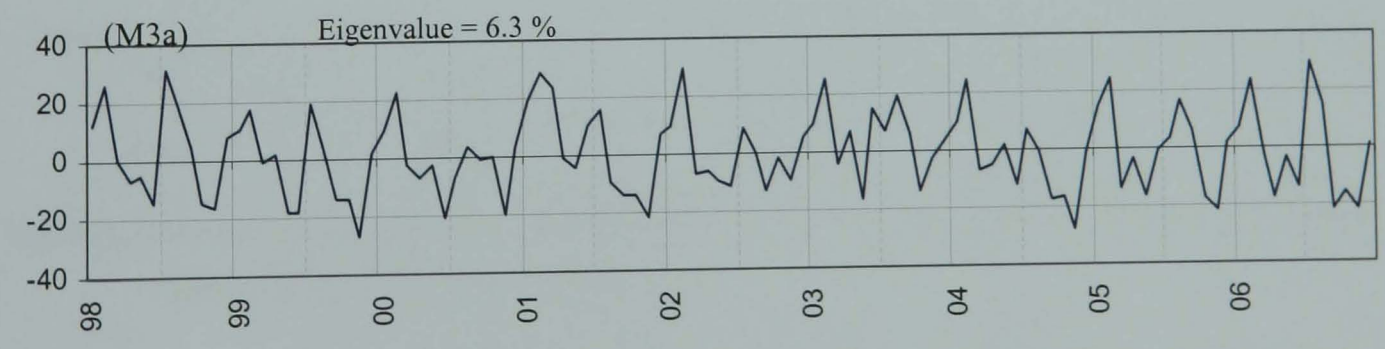

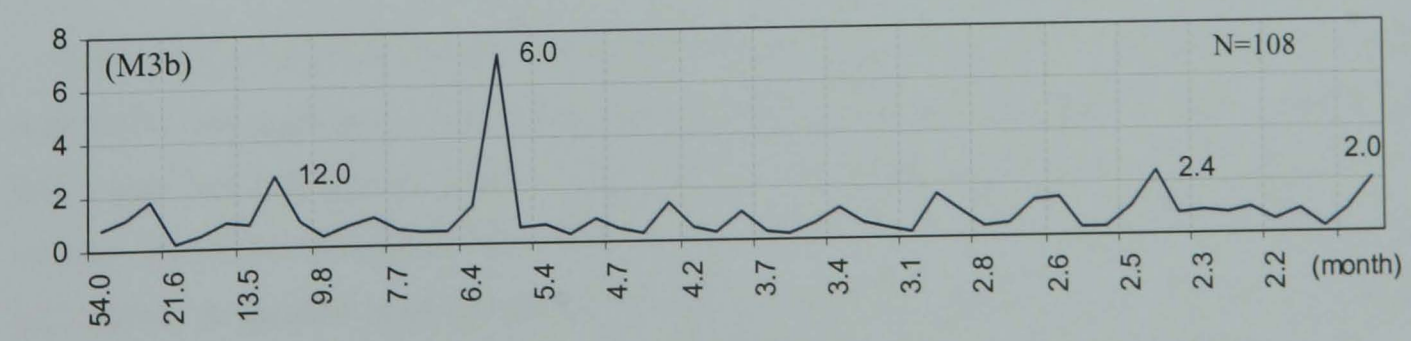

Fig. 4.21. (a) Temporal functions and (b) their spectrum of the OC4 EOF in D1: (M1) 1st mode, (M2) 2nd mode and (M3) 3rd mode.

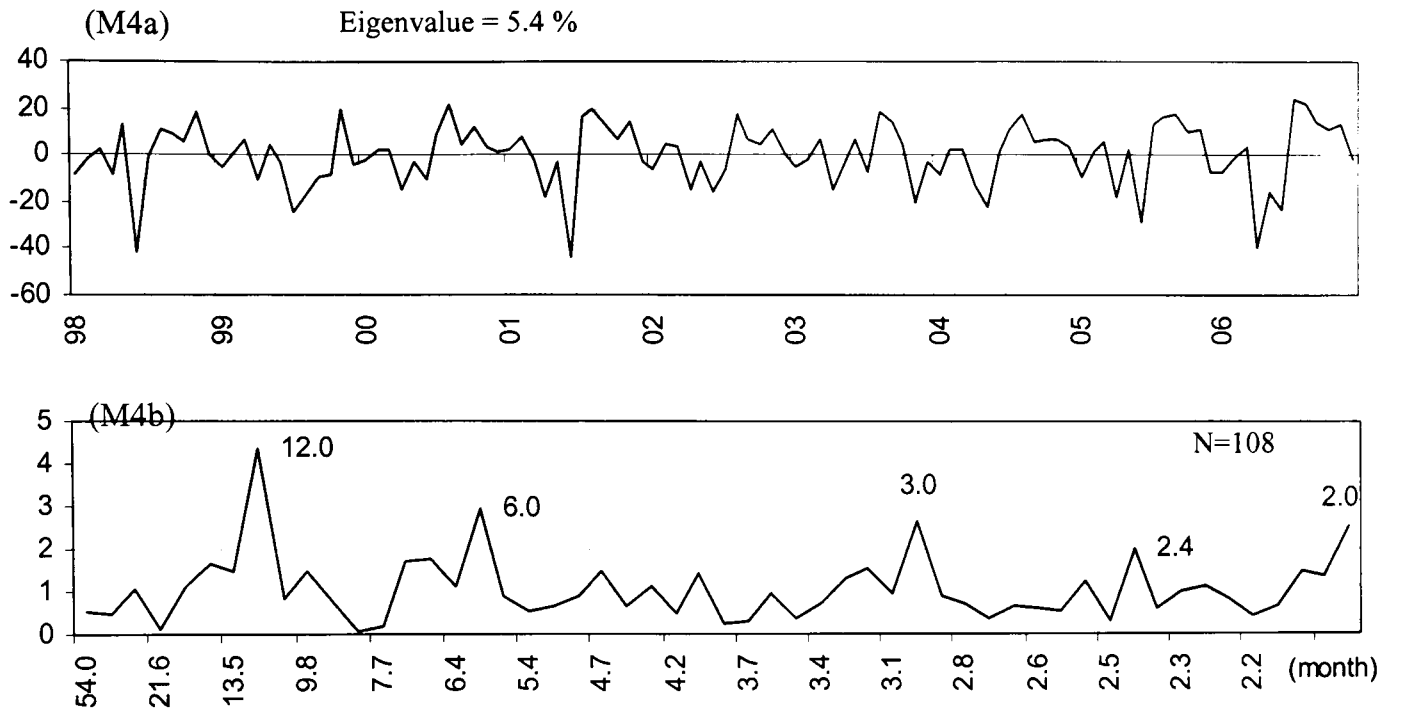

Fig. 4.21 (continued). (a) Temporal functions and (b) their spectrum of the OC4 EOF in D1: (M4) 4th mode.

The 2nd mode in D1 explains 9.5 % of the total variance. High positive eigenvectors (>1) are seen in a spot off the estuary of the Yangtze River. It suggests a dominant influence from the discharge of the Yangtze River. The discharge record of the Yangtze River is given in Fig. 4.22, showing the peaks in summer during the rainy season. The two peaks in the 2nd mode, one in March and another during summer, are likely associated with blooms caused by the winter EAM and the later Yangtze River discharge respectively.

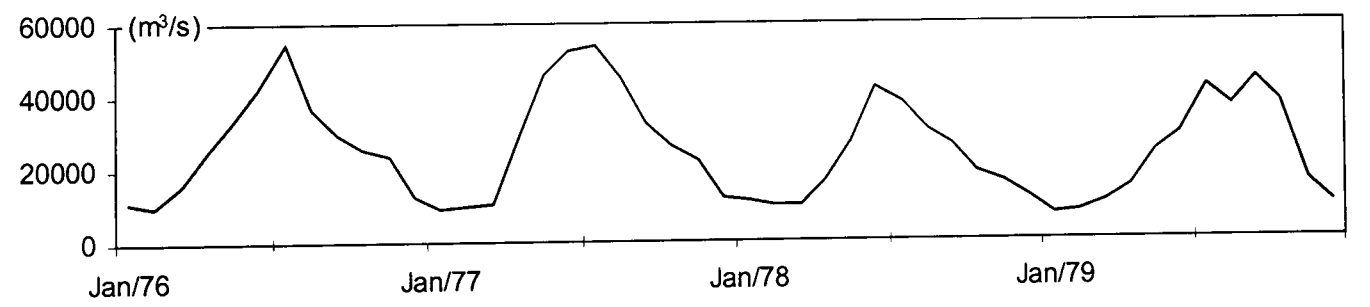

Fig. 4.22. Discharge of the Yangtze River from 1976 to 1979: the data are collected from SAGE River Discharge Database at http://www.sage.wisc.edu/riverdata.

The eigenvector of the 3rd mode (accounting for 6.4 % of the total variance) is shown in Fig. 4.20 (M3). The high positive values (> 1.00) are seen in the Yangtze River estuary as seen in the 2nd mode but they spread wider to include the water from the Yellow Sea along the 50 m isobath. Its temporal function shows the peaks in January and June with short term peaks (Fig. 4.21.M3a). A spectral analysis shows 6 months seasonality with a weak 12 and 2.4 months frequency (Fig. 4.21.M3b). This mode is fundamentally driven by the same factor as the 2nd mode, but over a less confined area, suggesting an interaction with the water from the Yellow Sea.

The eigenvector of the 4th mode (accounting for 5.4 %: Fig. 4.20.M4) shows high values around the west of Kyushu, Japan. Thus this mode is related to the OC4 variability to the west of Kyushu, and its variation is represented by the temporal function (Fig. 4.21.M4a) with an annual cycle (Fig. 4.21.M4b), having low values in January – June and high values in July – December. Other high value areas occurs to the north of the Yangtze River estuary, but low values occur to the south of the estuary, indicating the different variability of this mode which is likely caused by the different water masses of the Chinese Coastal Water from the north and the Yangtze River Water flowing southward along the coast.

4.6.2 Result in Domain 2: OC4

For the OC4 EOFs in D2, the 1st mode emerges as a clearer major control in D2 compared to the 1st mode in D1, explaining 58.1 % of the total variance (Fig. 4.23).

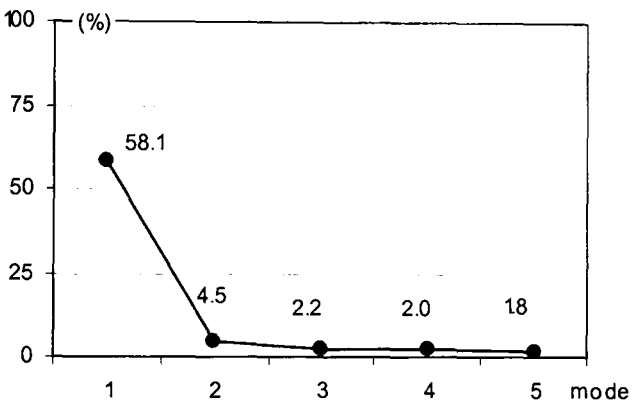

Fig. 4.23. Eigenvalues of the OC4 EOF in D2.

Fig. 4.24 shows the eigenvectors of the OC4 EOF in D2. Their temporal functions and spectra are indicated in Fig. 4.25 (a) and (b) respectively. The temporal function shows an annual cycle: high values in winter and spring, and low values in summer (Fig. 4.25.M1a), which is also seen in the 1st mode in D1. The spectral analysis shows a clear signal of the frequency at 12 months (Fig. 4.25.M1b), showing a significant correlation with the MOI (Jan 1998 – Jul 2000) with a month's lag ($r = 0.92$, $p < 0.001$). Although this comparison is not for a long time series, the annual cycles of the 1st mode and the MOI suggests a closely related link. An influence from the winter EAM on the OC4 variability becomes greater in D2 than D1. All the values of the 1st mode eigenvector are positive (Fig. 4.24.M1). The high values (> 0.03) are mostly seen at the edge of the shelf. Other high values (0.02 – 0.03) are found in northwest of Okinawa where the bathymetry is shallower (< 500 m) than the Okinawa Trough region (> 1000 m). The values are low to the east of the Ryukyu Arc, over the deep Philippine Sea.

The Yangtze River supplies considerable nutrients with its discharge to the continental shelf, resulting in high OC4 variability over the shelf region. Fig. 4.24 (M1) shows that such influence does not extend beyond the shelf region. It has been reported that the sediment from the shelf is deposited into the deep depression of the Okinawa Trough (Chung et al., 2000; Iseki et al., 2003; Kao et al., 2003), therefore the OC4 variability appears much lower on the surface of the Trough. This is why the deep region of the Okinawa Trough in Fig. 4.24 (M1) shows low values indicating less variability. For the eigenvectors of the 2nd (Fig. 4.24.M2) and 3rd mode (Fig. 4.24.M3), the OC4 variation at the points of the extreme high values noted by the arrow show a pronounced peak that coincides with the peak of the temporal function of the 2nd and 3rd mode in March 2001 (Fig. 4.25.M2a) and in Feb 2004 (Fig. 4.25.M3a), respectively. It suggests a strong influence of these high value pixels on the 2nd and 3rd mode, but they account for relatively little, 4.5 % and 2.2 % respectively, of the total variance, suggesting merely noise.

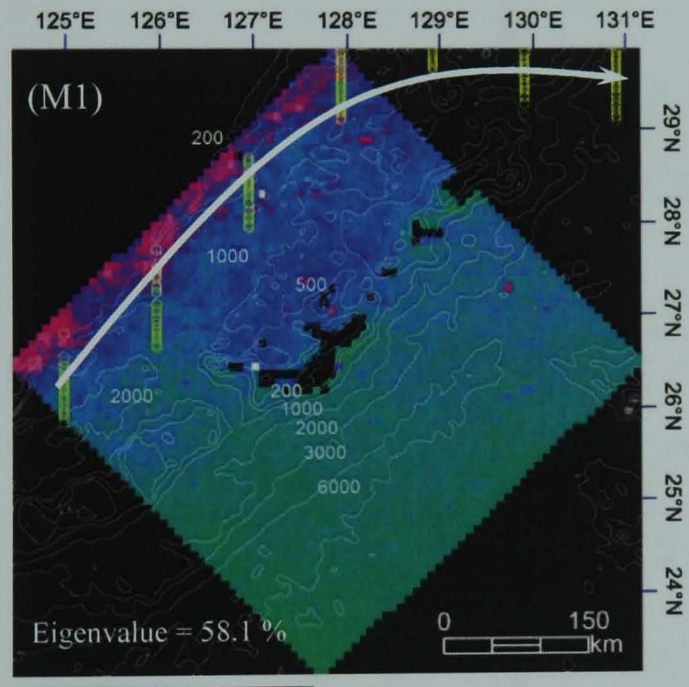

Fig. 4.24. Eigenvectors of the OC4 EOF in D2: (M1) the 1st mode, (M2) the 2nd mode and (M3) the 3rd mode. The thin white lines indicate isobath. The yellow circles are the axis of the KC estimated by the *Japanese Coast Guard* based on their observation from 1/8/2006 to 2/2/2007. The arrow shows the direction of the KC.

The thin arrows in (M2) and (M3) indicate the pixels whose OC4 patterns are strongly influential to their temporal function of the EOF.

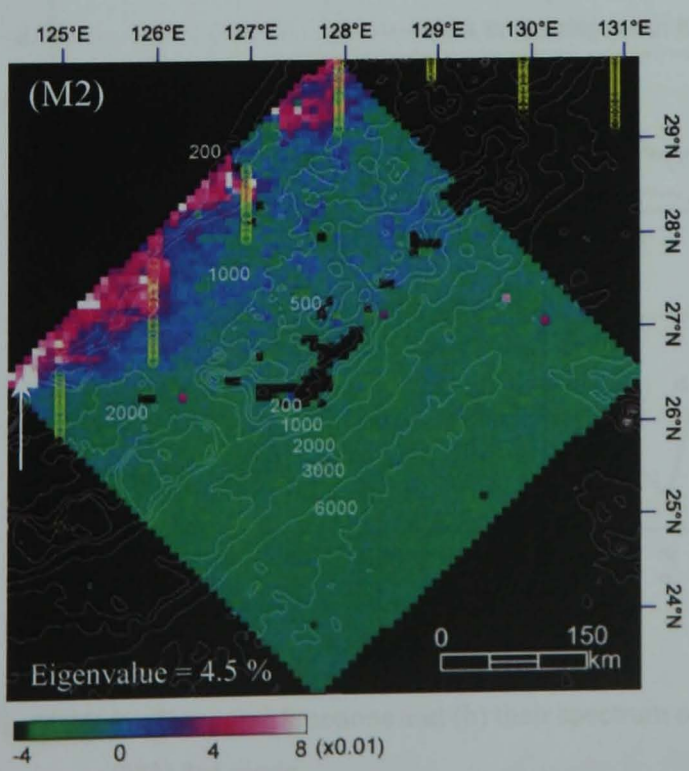

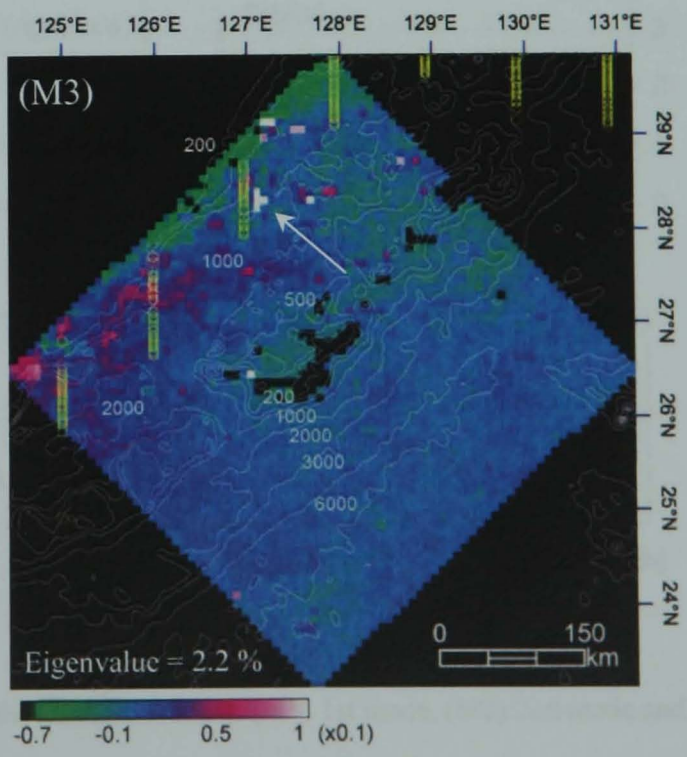

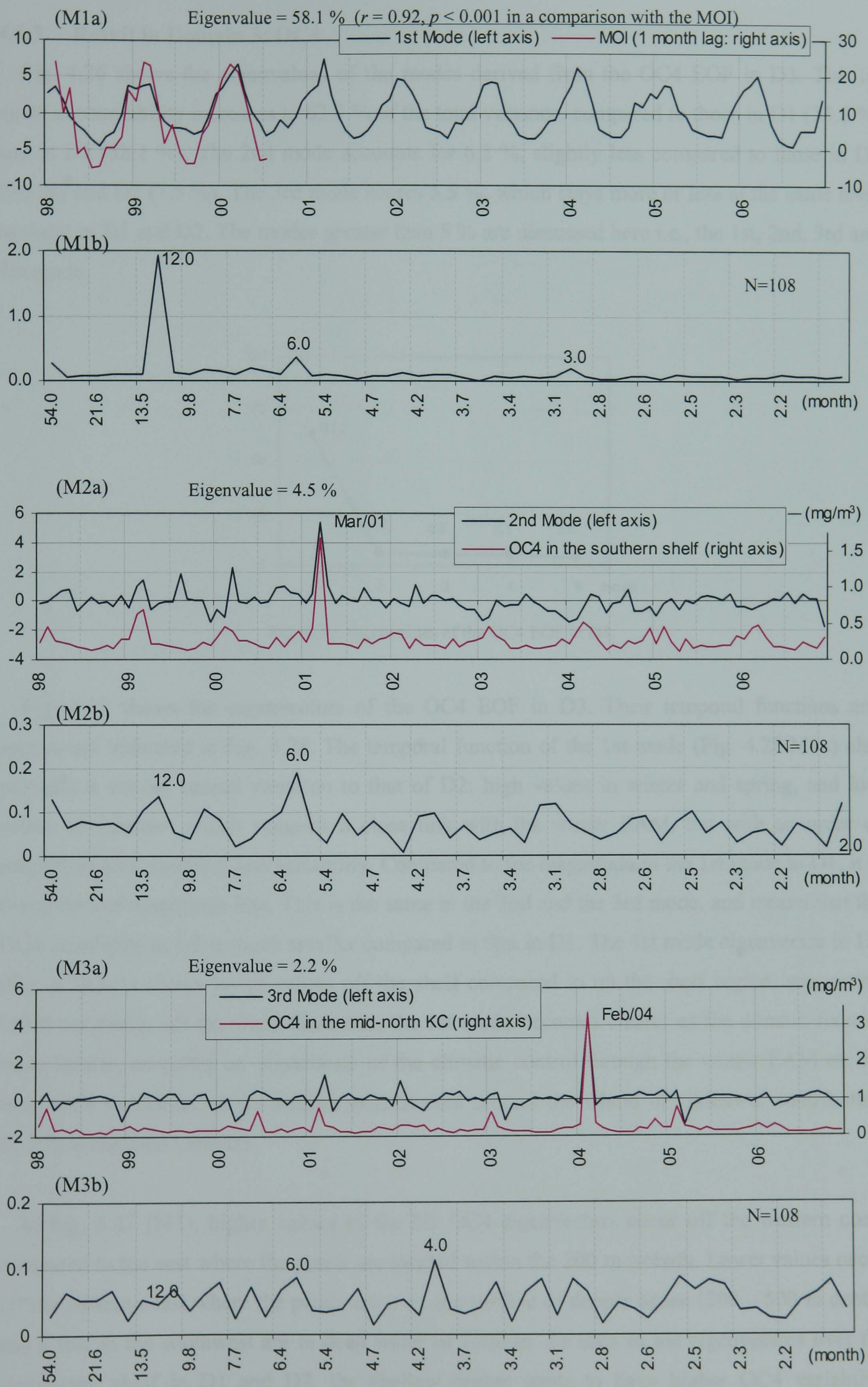

Fig. 4.25. (a) Temporal functions and (b) their spectrum of the OC4 EOF in D2: (M1) 1st mode, (M2) 2nd mode and (M3) 3rd mode.

4.6.3 Result in Domain 3: OC4

Fig. 4.26 shows the eigenvalues of the modes derived from the OC4 EOF in D3. The 1st mode accountability increases to 62.7 % of the total variance, compared to those in D1 (13.8 %) and in D2 (58.1 %). The 2nd mode accounts for 6.2 %, slightly less compared to those in D1 (9.5 %) and D2 (7.5 %). The 3rd mode scores 5.5 %, which stays more or less at the same level as those in D1 and D2. The modes greater than 5 % are discussed here i.e., the 1st, 2nd, 3rd and 4th mode.

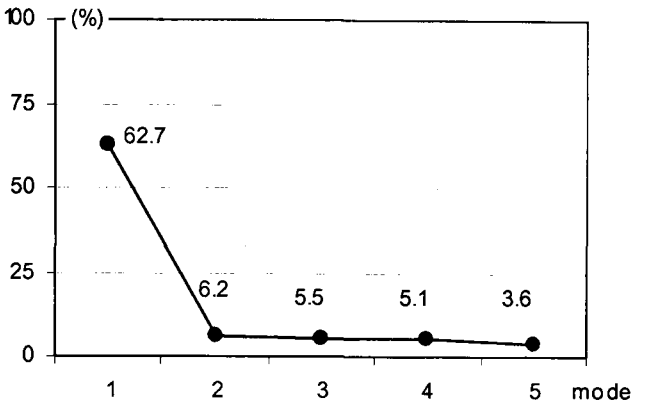

Fig. 4.26. Eigenvalues of the OC4 EOF in D3.

Fig. 4.27 shows the eigenvectors of the OC4 EOF in D3. Their temporal functions and spectra are indicated in Fig. 4.28. The temporal function of the 1st mode (Fig. 4.28.M1a) also provides a similar annual variation to that of D2: high values in winter and spring, and low values in summer, which suggests a close link with the winter EAM, but with an order of magnitude less, meaning less variability. Compared to the magnitude in the 1st mode in D1, it is two orders of magnitude less. This is the same in the 2nd and the 3rd mode, and means that the OC4 variability in D3 is much smaller compared to that in D1. The 1st mode eigenvector in D1 (Fig. 4.20.M1) shows lower values off the shelf compared to on the shelf region, suggesting lower variability off the shelf. However, the 1st mode becomes clearer as the domain focuses more locally, revealing an importance of the climatic control through the winter EAM on the local OC4 variability in the coastal environment around the Island of Okinawa, contributing 62.7 % to the total variance.

In Fig. 4.27 (M1), higher values of the D3 OC4 eigenvectors occur off the western coast compared to the east where the pixels are located within the 200 m isobath. Lower values occur off the eastern coast where the pixels are over the surface of deeper ocean (200 – 500 m depth) and a few in the southwest are in deep water of 1000 m. As seen in the eigenvectors over the continental shelf in D1 and D2, the shallow region tends to have higher OC4 variability compared to the deep region in D3. It suggests that the winter EAM, which causes upwelling

and nutrient supply to the surface, has a greater influence over the shallower region, resulting in higher variability.

(M1)

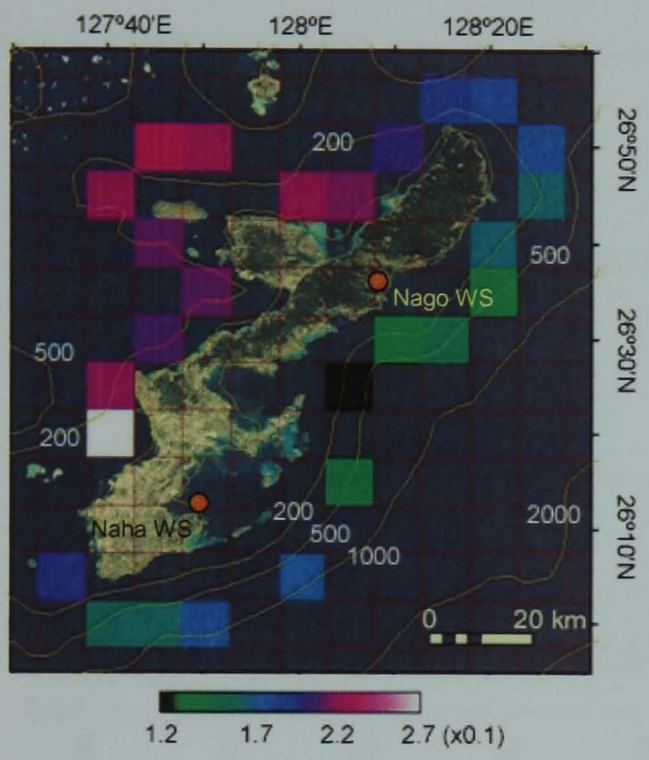

Eigenvalue = 62.7 %

(M2)

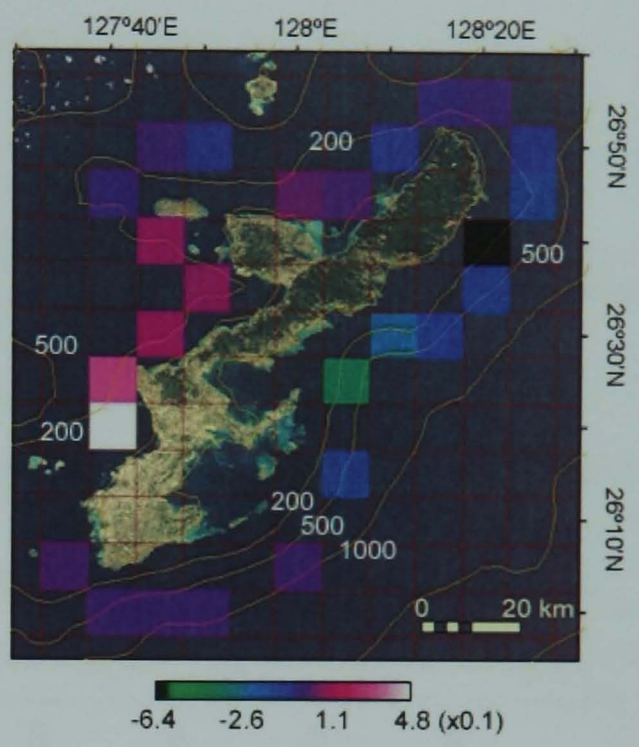

Eigenvalue = 6.2 %

(M3)

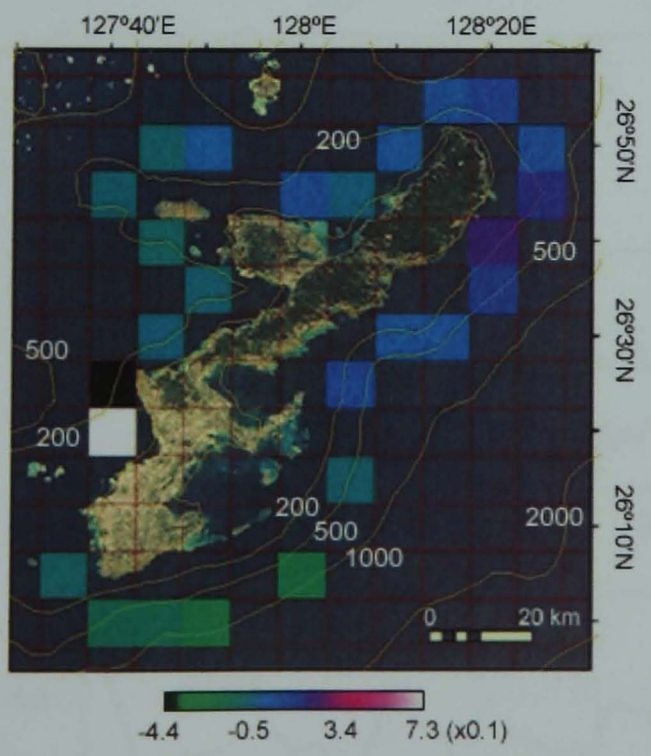

Eigenvalue = 5.5 %

(M4)

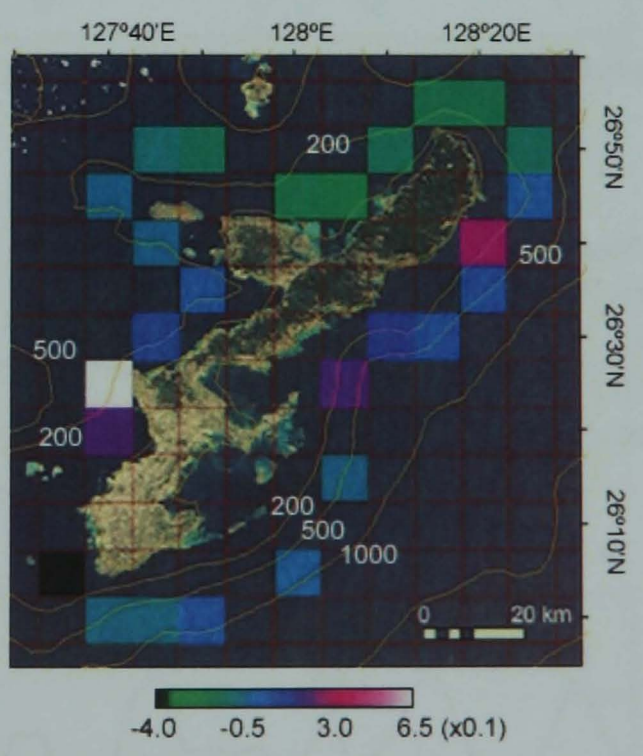

Eigenvalue = 5.1 %

Fig. 4.27. Eigenvectors of the OC4 EOF in D3 overlaid with isobaths: (M1) the 1st mode, (M2) the 2nd mode, (M3) the 3rd mode and (M4) the 4th mode. The isobaths are shown by the light brown lines.

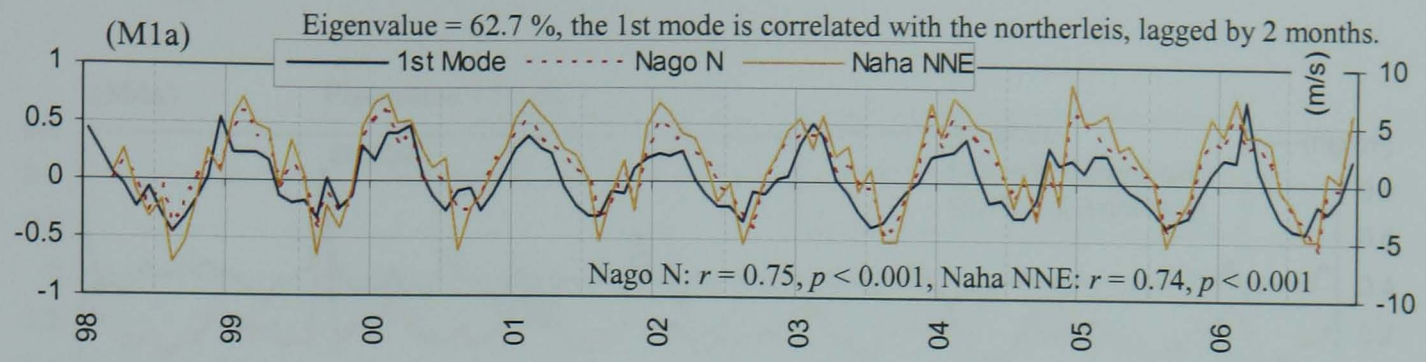

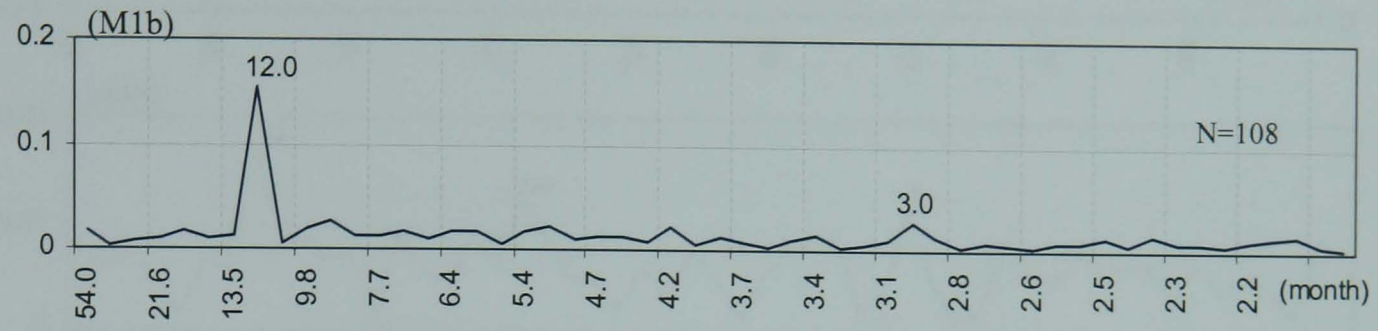

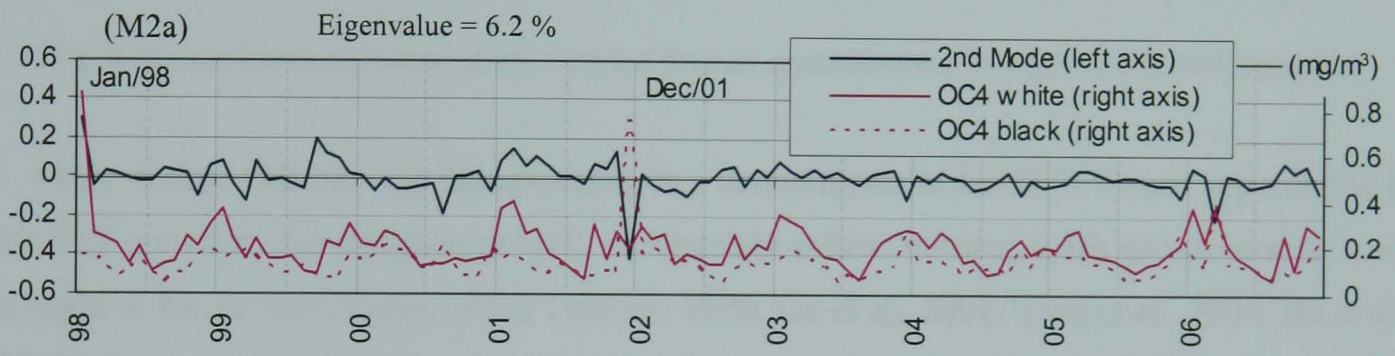

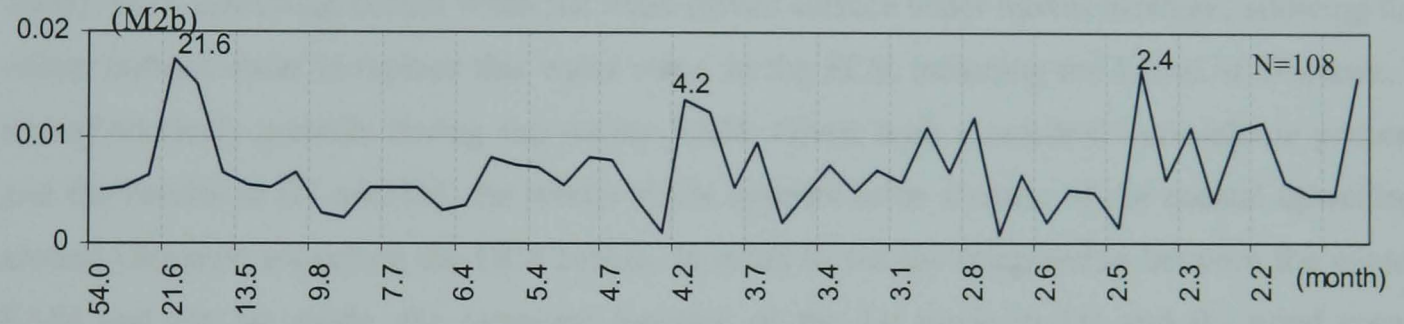

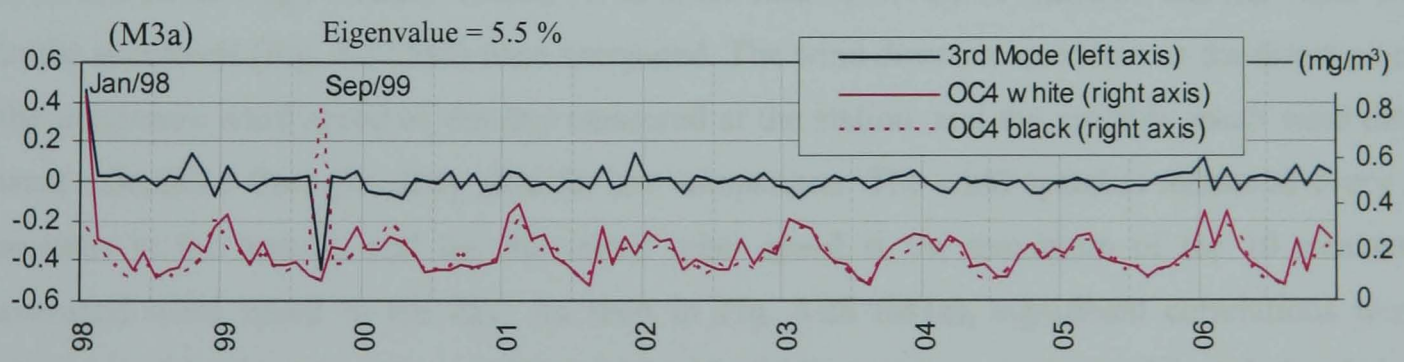

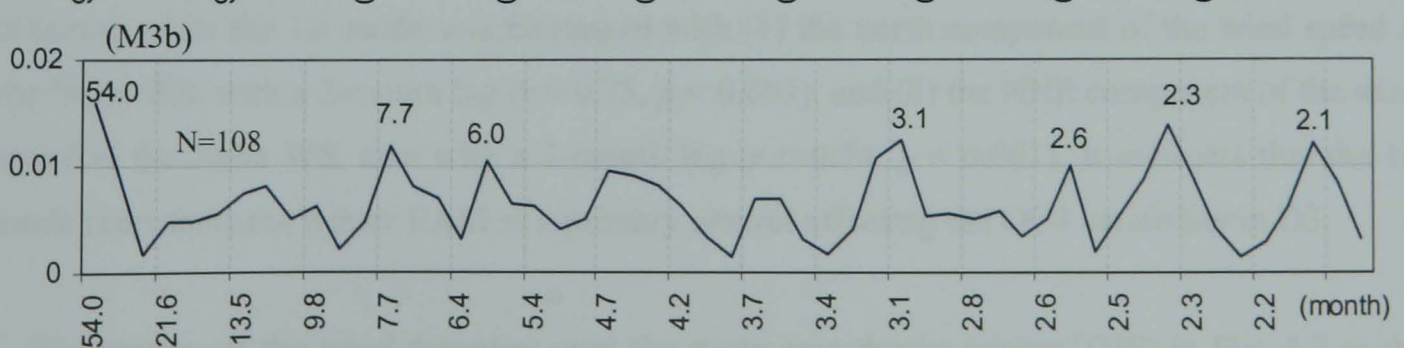

Fig. 4.28. (a) Temporal functions and (b) their spectrum of the OC4 EOF in D3: (M1) 1st mode, (M2) 2nd mode and (M3) 3rd mode.

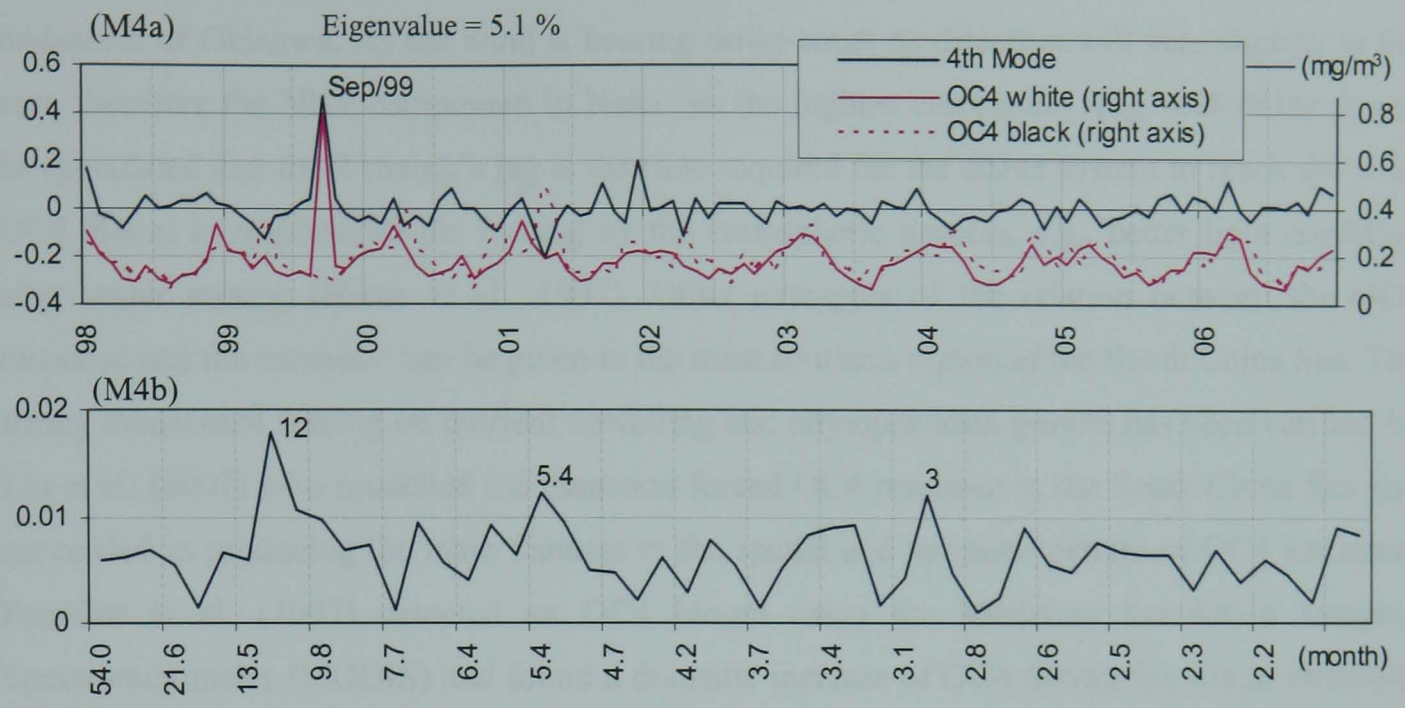

Fig. 4.28 (continued). (a) Temporal functions and (b) their spectrum of the OC4 EOF in D3: (M4) 4th mode.

Many studies indicate that the upwelling is a strong driver of the OC4 bloom, represented in the SST record by the decrease in SST, as relatively colder, nutrient-laden and deep waters are brought to the surface (Strass, 1992; Thomas, 1999; Liu et al., 2002; Tang et al., 2004; Ho et al., 2004). Such upwelling occurs when the wind-driven surface water moves offshore, allowing the colder bottom water to replace this water mass. In the ECS, including the Island of Okinawa, a strong northerly prevails during the winter EAM. Given such a seasonal atmospheric process and the results in D1 and D2, the winter EAM appears to be a cause of the coastal upwelling around Okinawa triggering the OC4 bloom. In order to see the relationship between the winter EAM and the 1st mode, the temporal function of the 1st mode in D3 and the wind speed recorded at the Nago weather station (WS) in the mid northwest of Okinawa and the Naha WS in the southwest (Fig. 4.27.M1) were compared. The wind direction used here is the direction of the maximum wind speed of the day measured at the station, and the monthly mean wind data were calculated from the daily data for the comparison. The wind speed is measured every 2 seconds at the station, and the maximum wind speed is the maximum of the 10 minutes-averaged wind speed in the day. As seen in Fig. 4.28 (M1a), significant correlations were obtained when the 1st mode was compared with (1) the north component of the wind speed at the Nago WS, with a 2-month lag ($r = 0.75$, $p < 0.001$), and (2) the NNE component of the wind speed at the Naha WS, also with a 2-month lag ($r = 0.74$, $p < 0.001$). It indicates that the 1st mode represents the winter EAM as a primary control affecting the OC4 variability in D3.

The pattern of the wind direction over the study area during winter (DJF) in Fig. 4.7 in the previous section (§4.2.3) shows that the wind direction is diverted from northwesterly to northeasterly as it proceeds south. Such a wind distribution may explain the difference in the components of the wind direction that is correlated with the temporal function of the 1st mode

in Okinawa. The highest correlation was obtained with the N component wind in Nago in the mid-north of Okinawa. As the wind is bearing down south its direction will veer slightly to the east, therefore the NNE component in Naha has the highest correlation (Fig. 4.28.M1a). It can be speculated that the 2 month's lag is the time required for the ocean system to reach the peak OC4 bloom in response to the forcing by the atmospheric process, e.g., better light condition after water mixing (Hama et al., 1997). Other examples of the relation between the OC4 response and the monsoon can be given in the most southern region of the South China Sea. The strong monsoonal forcing on nutrient upwelling and phytoplankton growth has been verified by Liu et al. (2002) who modelled the monsoon-forced OC4 response in the South China Sea and succeeded in producing the main features in the spatial and temporal pattern of OC4 variation. Penaflor et al. (2007) detected an OC4 bloom using the Moderate Resolution Imaging Spectroradiometer (MODIS) and found a dramatic increase of OC4 during the winter monsoon in the Luzon Strait.

In the 2nd mode eigenvector (Fig. 4.27.M2), the highest value occurs to the southwest of the Island (in the white pixel), and the lowest in the northeast (in the black pixel). Its temporal function is strongly affected by the OC4 variations in these locations (Fig. 4.28.M2a), as its highest peak coincides with the peak of the OC4 of the white pixel in Jan 1998 and its lowest peak is inversely influenced by the OC4 of the black pixel in December 2001. In the eigenvector of the 3rd mode (Fig. 4.27.M2), the highest value occurs in the same location as the 2nd mode, the southwest of the Island (in the white pixel), and the lowest in the north (in the black pixel). The temporal function is again strongly influenced by the OC4 at these locations (Fig. 4.28.M3a), as its highest peak coincides with the peak of the OC4 of the white pixel in January 1998 and its lowest peak is inversely influenced by the OC4 of the black pixel in September 1999. The highest value of the 4th mode eigenvector occurs in the pixel to the north of the pixel which has the highest value in other modes (Fig. 4.27.M4). Similar to the 2nd and 3rd mode, the temporal function is strongly influence by the OC4 pattern of the pixel with the highest value (Fig. 4.28.M4a), showing a coincident peak in September 1999.

The 2nd, 3rd and 4th mode suggest a local influence of the highest value pixels on the OC4 variability. In particular, the highest value of the 2nd and the 3rd mode eigenvectors appears in the same pixel, which is near the largest river in the Island, the Hija River, inferring an influence from the river. In D1, high values of the 2nd and the 3rd mode eigenvectors occurred around the Yangtze estuary, suggesting influences from its discharge. As the domain scale becomes more locally focused to Okinawa, similar influence from the rivers in the Island, particularly during the rainy season or the typhoon season, may be expected. Such terrestrial and typhoon influences will be discussed in the next chapter.

4.7 Effect of Extreme Events

The winter EAM has been found to be an important control on the variability of the SST and OC4, however, other factors may also have a contribution. One of these in Okinawa may be typhoons. There are approximately 7.4 typhoon visits around the Ryukyu Islands per year, according to the JMA (http://www.data.jma.go.jp/fcd/yoho/typhoon/statistics/accession/okinawa.html). The strong winds produced by typhoons can cause disturbance to the sea surface, and water mixing that will decrease SST and supply nutrients to the surface OC4. This may give a signal of decreased SST or increased OC4 during the passage of a typhoon during summer, at a time when the OC4 concentration is usually low around Okinawa (less than 0.15 mg/m^3). Examples are given in the ocean south of Taiwan by Lin et al. (2003b) when Typhoon Kai-Tak passed over the South China Sea in July 2000, and in the Gulf of Mexico after Hurricane Ivan's passage in September 2004 (Walker et al., 2005). Combining remote sensing data with in-situ measurements in the Japan Sea, Son et al. (2006) found 2 – 4 °C decrease of SST and 70 % increase of OC4 after passage of Typhoon Meigi in August 2004.

Secondly, the effect of mesoscale eddies may be worth investigating. Many mesoscale eddies consisting of a warm water mass at the surface have been observed propagating from the Kuroshio Recirculation region in the western North Pacific subtropical gyre to the east of the Ryukyu Islands, located in the latitude range of 24 – 31 °N (Aoki et al., 1995; Ebuchi and Hanawa, 2001; Kobashi and Kawamura, 2001). The warmer water mass in an eddy has a raised sea surface, and when it approaches the coast it produces anomalies in the height of the tide. The water in a warm eddy flows anticyclonically. Such movement, in contrast to the case of mixing by typhoon winds, may remove the available nutrients away from the surface through downwelling. Therefore, OC4 depletion may be anticipated.

For these two type of events, the SST and OC4 signals were examined around Okinawa (D3 region) in the objectively analysed monthly data to see if they show either increase or decrease during typhoon visits and warm eddy approaches, respectively.

4.7.1 Case Study: Typhoons

To examine the effect of typhoons, the OC4 responses in D3 from July to September in 2000 and 2005 were compared. Fig. 4.29 displays the typhoon paths in these periods. In 2000 there were 4 typhoons that approached Okinawa from July to September: Bolevan, Jelawat, Bopha and Saomai. Two of them directly hit the Island (Jelawat and Saomai). The paths of their centres show that they approached from the east, crossed over the Island and moved away towards west. One did not come close to Okinawa but passed 330 km to the southwest

(Prapiroon). In contrast, there is no typhoon that directly hit Okinawa during the same months in 2005, therefore less impact of typhoons would be expected on the coastal zone around of Okinawa than during the same period in 2000.

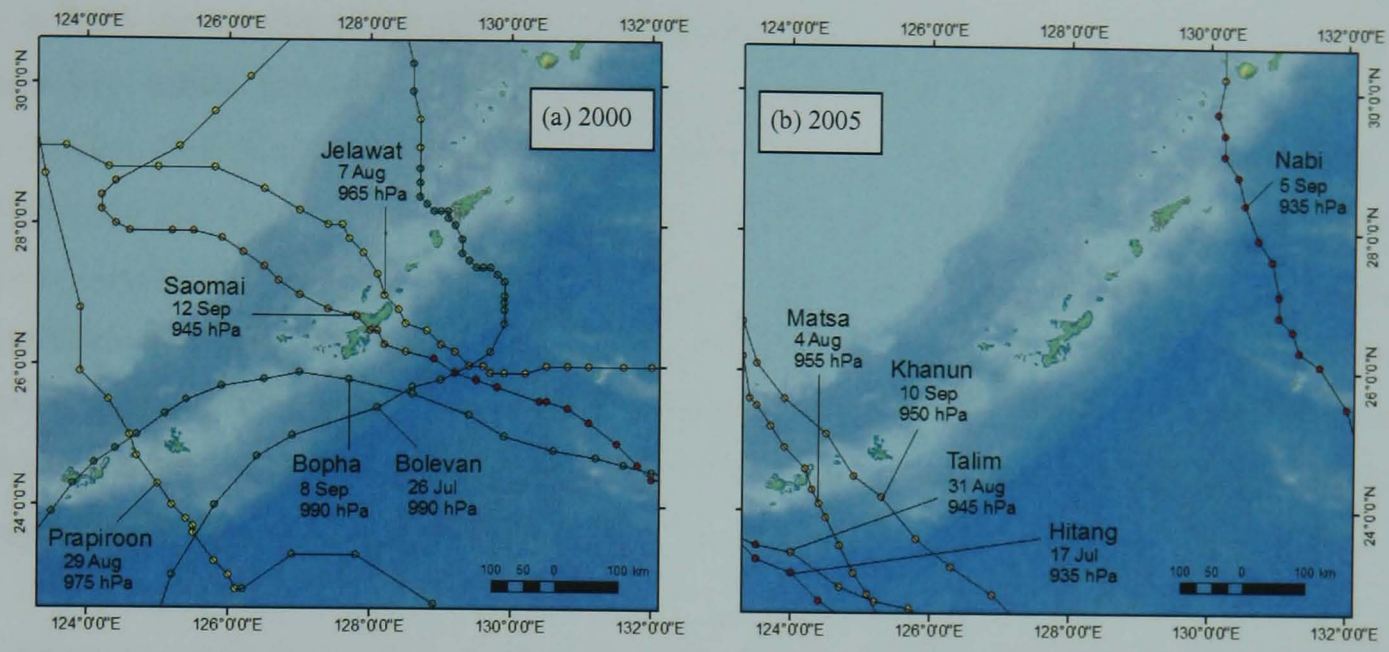

●:< 940, ●: 940 – 960, ●: 960 – 980, 980 < ●: (hPa)

Fig. 4.29. Typhoon Path from July to September in (a) 2000 and (b) 2005.

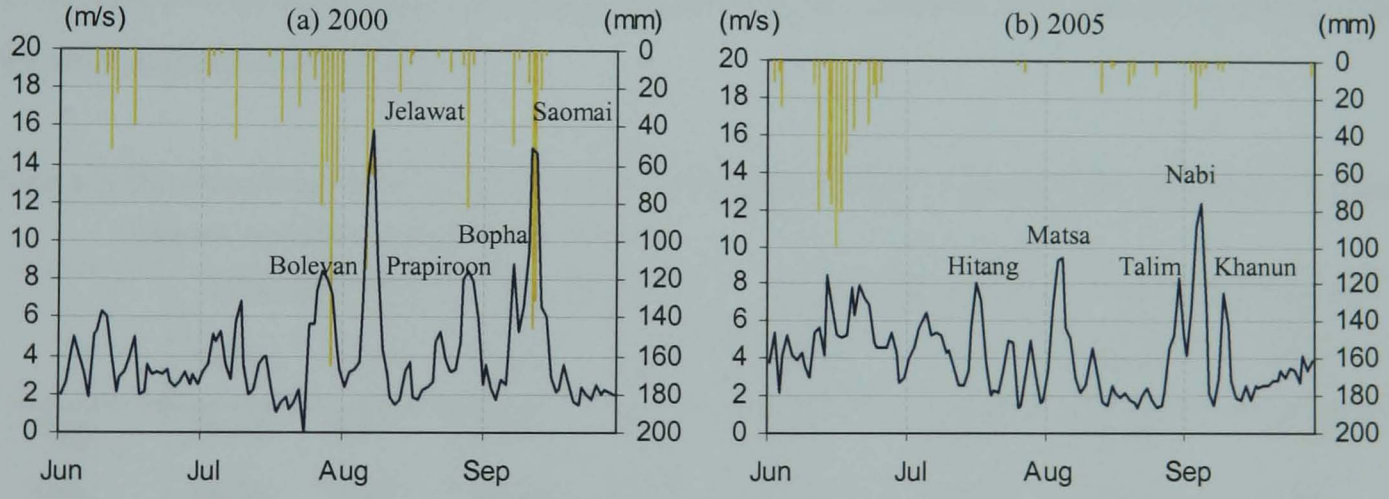

Fig. 4.30. Hyetograph from the Nago WS data from June to September in (a) 2000 and (b) 2005: daily mean wind speed in the blue line scaled by the left Y axis and daily rainfall in the yellow bar scaled by the right Y axis.

Fig. 4.30 shows the hyetograph - daily mean wind speed and rainfall measured at the Nago WS from June to September in (a) 2000 and (b) 2005. It is clear that the daily mean wind speed increases during the typhoon visits in 2000, when Jelawat in early August and Saomai in mid September crossed over Okinawa (Fig. 4.29a). Their central pressures were 965 hPa and 945 hPa respectively; the daily mean wind speed reached 15.8 m/s and 14.6 m/s respectively (Fig. 4.30a). In the case of typhoon Bolaven in late July 2000, the central pressure was relatively higher, 985 hPa, and it yielded a lower mean wind speed (8.0 m/s) than Jelawat and Saomai. In late August, some influence (7.9 m/s) can be seen from Prapiroon due to the relatively lower pressure level of 975 hPa, despite its passage 330 km southwest from Okinawa. When Bopha

approached Okinawa, on the other hand, in early September, the increase of the mean wind speed stayed at a similar magnitude (8.8 m/s) to that of Prapiroon because it was a weaker typhoon with a rather higher central pressure of 990 hPa.

In 2005 the number of the typhoons whose centres approached Okinawa within 200 km was zero (Fig. 4.29b). However, typhoon influence on the wind over Okinawa is still detectable. At a distance from Okinawa, typhoon Hitang passed 490 km away from Okinawa, but with a significant low central pressure of 935 hPa, in mid July. This caused an increase of the daily mean wind speed in Okinawa to 8.0 m/s. Similarly, Matsa in early August, Talim in late August and Khanun in early September passed far to the southwest. Nevertheless, the daily mean wind speed increased to 9.4 m/s, 8.3 m/s and 7.5 m/s respectively (Fig. 4.30b). Typhoon Nabi was closest, at 280 km north of Okinawa, with a very low central pressure of 935 hPa. It brought the highest daily mean wind speed, 12.3 m/s.

Given the difference in the daily mean wind speed in 2000 and 2005, the SST and OC4 responses at the coast of Okinawa (D3) in these periods were compared. The monthly climatology (1998 – 2006) of August and September and their standard deviations (Table 4.2) were compared with the values in August and September 2000 and 2005 that are averaged along the west and east coast (Table 4.3).

Table 4.2. The climatology (1998 – 2006) of August and September of the SST and OC4, and their standard deviation along the west and the east of Okinawa (D3).

	West SST (°C)		East SST (°C)		West OC4 (mg/m^3)		East OC4 (mg/m^3)	
	Mean	STD	Mean	STD	Mean	STD	Mean	STD
Aug	29.45	0.83	29.60	0.80	0.10	0.015	0.09	0.030
Sep	28.50	0.88	28.58	0.78	0.14	0.028	0.11	0.017

Table 4.3. The SST and OC4 along the west and the east of Okinawa (D3) in 2000 (AS) and 2005 (AS), and their difference Δ from climatology (1998 – 2006) in Table 4.2.

	SST (°C)		ΔSST (°C)		OC4 (mg/m^3)		ΔOC4 (mg/m^3)	
	West	East	West	East	West	East	West	East
Aug 00	27.88	28.06	-1.57	-1.54	0.13	0.16	0.03	0.07
Sep 00	27.04	27.31	-1.46	-1.28	0.17	0.13	0.03	0.01
Aug 05	29.40	29.40	-0.05	-0.21	0.09	0.08	-0.01	-0.01
Sep 05	28.40	28.62	-0.10	0.04	0.10	0.09	-0.04	-0.02

To both the west and east of Okinawa for these months in 2000, there were large negative anomalies in the SST compared to the climatology, generally much greater than one standard deviation. For these months, the OC4 shows positive differences from the mean values, greater than the standard deviation, except for the eastern ΔOC4 in September 2000. This suggests that the strong winds and rainfall associated with the typhoons caused vertical mixing, leading to decrease of the SST and increase of the OC4. In the same months in 2005, no significant sign of the SST decrease or the OC4 increase can be seen (Table 4.3). Although increases in the wind were caused by the strong typhoons, despite their far distance from the Island, this was insufficient to significantly alter the SST and OC4 around the Island.

Increases of the OC4 around Okinawa (D3) can be observed in June 1998, September 1999, September 2001, June 2004, and September 2006 (noted by arrows in Fig. 4.31). In all these months except June 1998 there were actually typhoons near Okinawa which most likely caused the OC4 bloom. Although there was a typhoon approaching close to Okinawa in August and September 2003, a response of the SST and OC4 does not appear in Fig. 4.31. Possible reasons may be due to inadequate spatial and temporal resolution of the data. In addition to this, the Objective Analysis for monthly mean data cannot reconstruct the response if there was cloud cover.

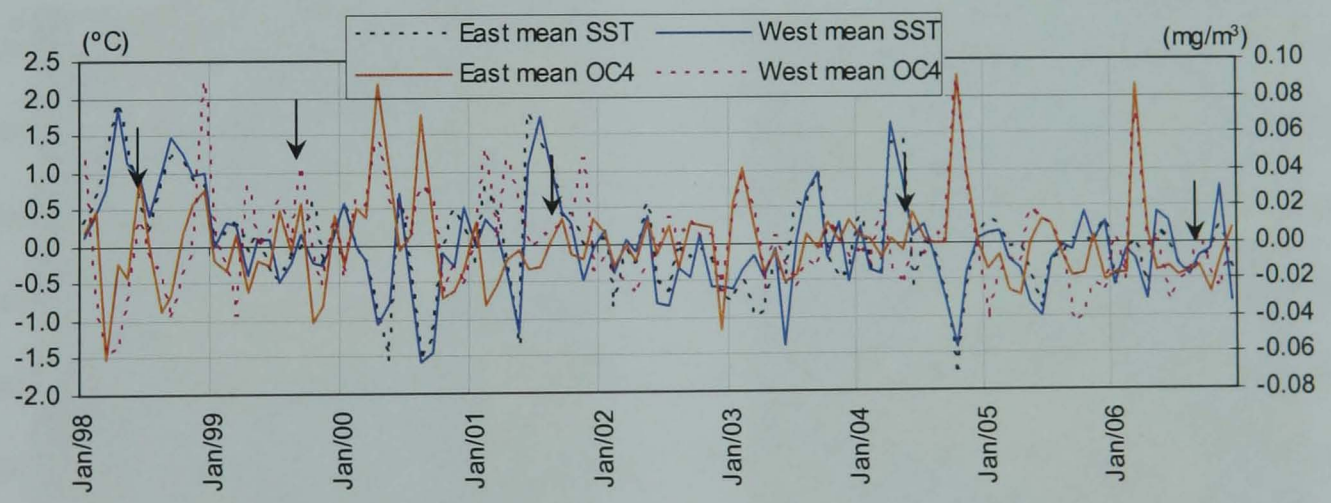

Fig. 4.31. Anomaly of the SST and OC4 averaged in the east and the west coast around Okinawa (D3).

In the case of June 1998 there was no typhoon visit or occurrence around Okinawa. That month was in the typical rainy season and substantial discharge was observed in the rivers in Okinawa which likely caused the OC4 bloom. Most of the typhoons in 2000 also brought substantial amounts of rainfall. As seen in Fig. 4.30 (a), the maximum daily rainfall associated with them was: 166 mm (Bolevan), 115 mm (Jelawat), 82.5 mm (Prapiroon), 50 mm (Bopha) and 145.5 mm (Saomai). Note that Pinazo et al. (2001) showed that the nutrients carried in freshwater run-off, together with the influence of local winds, have a significant effect in increasing the phytoplankton biomass in the Gulf of Lions in the Mediterranean. However, the

strong wind alone can affect the SST and OC4, as can be observed in the case of the typhoon visit to Okinawa in September 2006 (Fig. 4.31) that supplied only 16.5mm/day of rainfall at its maximum impact. Thus, effects of both strong winds and rainfall associated with typhoons on the coastal zone need to be evaluated, if the winds that cause upwelling and rainfall that enhances the run-off producing a terrestrial influence through the rivers have different contribution to the SST and OC4 variability. This will be discussed in the next chapter.

4.7.2 Case Study: Warm Eddy

When a warm eddy approaches the land the sea level rises higher than normal. Such abnormal sea levels were recorded along the coast of Okinawa in July 2001 and August 2003. The tidal anomaly reached up to +20 cm at the city of Naha in the southwest of Okinawa. It was reported that sea level rise was due to a warm eddy which reached Okinawa (Fukushima and Yamazaki, 2001; JMA, 2005). Fig. 4.32 is the map of the sea surface height (SSH) anomaly around Okinawa produced from TOPEX/POSEIDON satellite showing warm eddies surrounding Okinawa on 20 July 2001 and 30 August 2003.

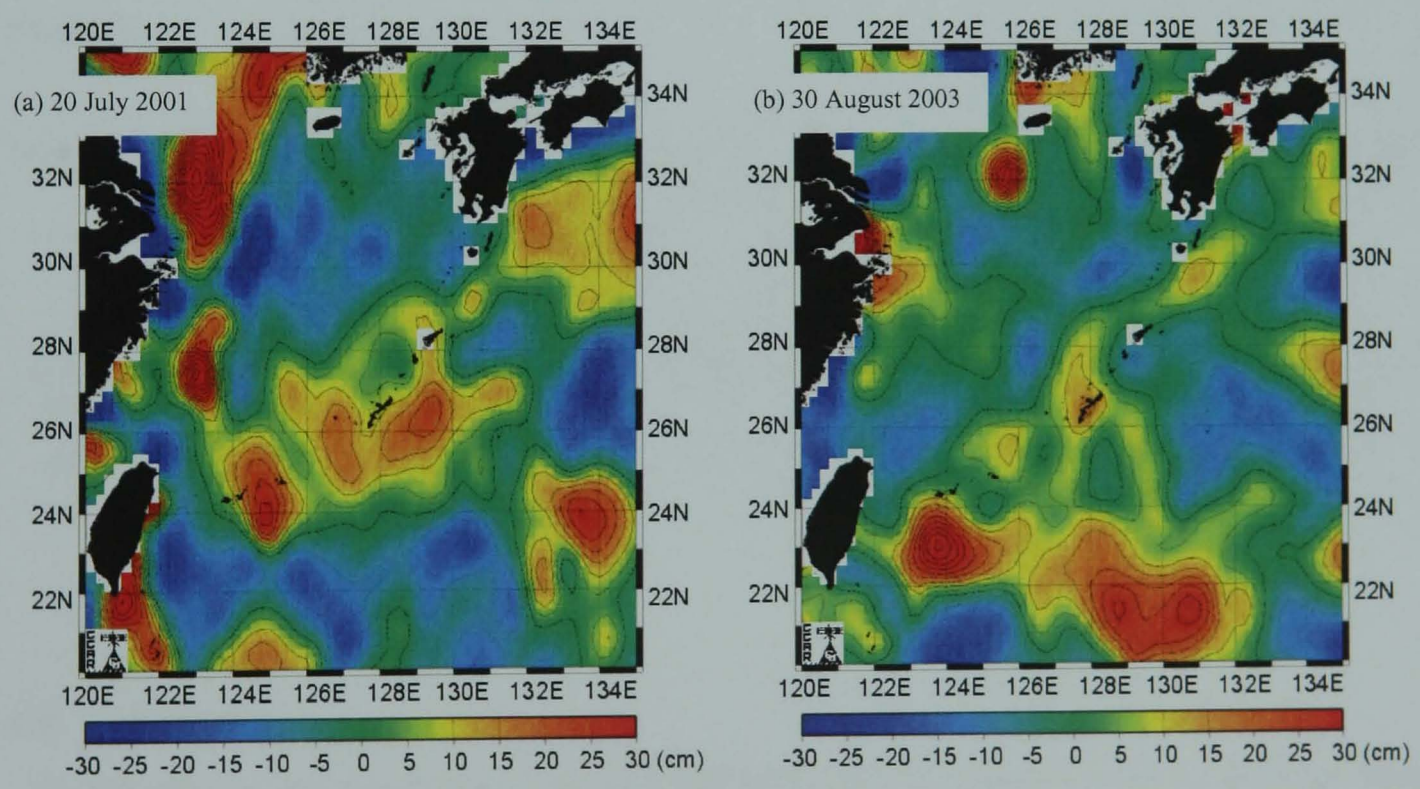

Fig. 4.32. The SSH anomaly: warm eddies surrounding Okinawa, (a) 20 July 2001 and (b) 30 August 2003.

The warm eddy in 2001, estimated to be approximately 400 km in diameter, was first seen in January at 25°N, 135°E. It then proceeded west at about 150 km/month, and reached Okinawa in July (Nozaki et al., 2003; Fig. 4.32a). The size of the warm eddy in 2003 was much smaller (Fig. 4.32b). Table 4.4 shows the SST and OC4 values during warm eddy approaches. The SSTs in these months were higher than the mean level due to the warm water mass in the eddy. In the case of July 2001 the departure from the climatological value is more significant than the case

of August 2003, consistent with the scale of the eddy (Fig. 4.32a). When these warm eddies reached Okinawa no appreciable signal of OC4 depletion was seen, either in July 2001 or August 2003. However, on both occasions the eddy occurred during the annual minimum in OC4 and hence any impact was likely to be small. Although there are negative anomalies in the OC4 in July 2001 and August 2003, they are not significant, and other regions recorded positive anomalies. The effect of the warm eddies on OC4 depletion cannot therefore be identified. While there are only a limited number of events, the downwelling of the surface in these warm eddies is insufficient to induce any biological response (McGillicuddy and Robinson, 1997). Another study described an opposite effect. Woodward and Rees (2001) suggested that in the open ocean anticyclonic warm eddies help sustain new production within the euphotic zone by transporting nutrients into the surface mixed layer. Surface aggregation of zooplankton was observed at frontal regions around the warm water tongue of the Kuroshio Current off the east ocean of Japan (Nishikawa et al., 1995). Warm eddies observed in 2001 and 2003 around Okinawa approached from the oligotrophic Western Pacific Ocean, not from the main stream of the Kuroshio in the East China Sea. Thus transport of nutrients by the warm eddies is less likely. It will require further observation and study to understand fully the effect of warm eddies on the coastal waters of Okinawa. Events occurring during time of the year with high OC4 would be desirable.

Table 4.4. The SST and OC4 averaged in the west and the east of Okinawa (D3) in July 2001 and August 2003, and their difference Δ from the climatology (1998 – 2006).

	SST (°C)		ΔSST (°C)		OC4 (mg/m^3)		ΔOC4 (mg/m^3)	
	West	East	West	East	West	East	West	East
Jul 01	30.67	30.35	1.73	1.37	0.11	0.09	0.00	-0.01
Aug 03	30.12	30.10	0.67	0.50	0.09	0.10	-0.01	0.01

4.8 Summary

In this chapter, the variability of the SST and OC4 and their controls over the ECS has been studied by using objectively analysed satellite data. The climatological SST (1985 – 2006) showed (1) a greater variation on the continent shelf than other regions, (2) the flow of the KC and its branch current, and (3) the progress of the warm SST front from the south Philippine Sea in summer and the progress of the cold SST front in the northern shelf. The climatological OC4 (1998 – 2006) showed (1) high variability on the continental shelf through the year as also seen in the SST, (2) high level concentration of 3 mg/m^3 occurring within the 100 m isobath on the shelf, extending most in winter, and (3) a plume of higher level concentration (7 mg/m^3)

occurring at the Yangtze River estuary during summer, indicating the influence of run-off from the river enhanced by the rainfall brought by the summer EAM.

Given the different variability of the SST and OC4 over the ECS, key controls at different scaled domains were investigated, to see whether the controls on the high variability on the large scale of the continental shelf region affect the local variability in the coastal environment around the Island of Okinawa. For this purpose, EOF analyses were employed over three domains in the ECS – D1: the ECS and the Philippine Sea, D2: the KC and Okinawa, and D3: the coastal zone around Okinawa.

For the SST EOF (Table 4.5), the analysis revealed that the most dominant control, the 1st mode, is driven by the solar radiation, accounting for more than 90 % of the total variance in all the domains, and it is more influential on the continental shelf region because of shallow bathymetry. The 2nd mode in D1 appeared to be related to the winter EAM, accounting for 2.6 % of the total variance. Its eigenvector suggests the cooling effect in the northern region of the shelf.

Table 4.5. The result of the EOF analysis on SST: each mode accountability in % and related controls are noted.

SST EOF	D1	D2	D3
1st mode	91.6 % solar radiation	94.6 % solar radiation	97.6 % solar radiation
2nd mode	2.6 % the winter EAM	0.7 % –	0.5 % –
3rd mode	0.6 % –	0.6 % –	0.4 % –

Table 4.6. The result of the EOF analysis on OC4: each mode accountability in % and related controls are noted.

OC4 EOF	D1	D2	D3
1st mode	13.8 % the winter EAM	58.1 % the winter EAM	62.7 % the winter EAM
2nd mode	9.5 % the Yangtze discharge involved	4.5 % –	6.2 % strong influence near the large river
3rd mode	6.3 % the Yangtze discharge involved	2.2 % –	5.5 % strong influence near the large river
4th mode	5.4 % west of Kyushu	2.0 % –	5.1 % strong influence in the north of the large river

For the OC4 EOF (Table 4.6), the results showed that the winter EAM is an important control in all the domains, but with the difference in contribution from large domain to the localised region around Okinawa. The 1st mode in D1 showed an annual cycle with pronounced peaks in the short term, and revealed that the winter EAM is responsible for the OC4 variability in D1. explaining 13.8 % of the total variance. The 2nd and the 3rd modes in D1 indicated influences of the Yangtze discharge coupled with other processes with short term periods. The high values in the 4th mode eigenvector showed its relation to the OC4 variability to the west of Kyushu, Japan. Other high values of this eigenvector suggested influences of the Chinese Coastal Water and the Yangtze River discharge along the Chinese coast. In D2 and D3, the winter EAM becomes more important, accounting for 58.1 % of the total variance in D2 and 62.7 % in D3 respectively. The 1st mode eigenvectors of D2 and D3 also show that shallower regions tend to have higher values, suggesting that a bathymetric control is also important, as seen in D1. This is because nutrients from the bottom are more available in shallower regions when the strong northerlies of the winter EAM cause upwelling in the ocean. The highest values of the 2nd and the 3rd mode eigenvectors in D3 occurred in the same location, near the largest river of the Island of Okinawa. It suggests that a terrestrial influence via this river affects the OC4 variability in that location.

Further analysis in D3 with extreme events such as typhoons showed that the strong winds associated with typhoons have an effect on the modulation of the SST and OC4. In response to the enhanced wind energy on the sea surface, entrainment, upwelling and deepening of the mixed layer occur that lead to decrease in the SST. This wind effect also causes an OC4 bloom. In addition, heavy rainfall associated with typhoons may have an important impact on the OC4 blooms through enhanced run-off, which delivers increased sediments and nutrients offshore. The influence of the Yangtze River during the rainy season was seen in the OC4 EOF in D1, indicating the importance of a rainfall control on the OC4. Although typhoons are episodic and short term events, their controls produce significant anomalies from the mean values. Typhoons' acute impacts on coral reefs are also significant, particularly when they interact with terrestrial factors that exacerbates soil run-off (Wilkinson, 1994; Omija, 1994). In Okinawa, fragile red soils have often been eroded and delivered to the adjacent coast by heavy rainfall, causing coastal environmental problems (e.g., Omija, 1992). Therefore, understanding terrestrial and typhoon control is important and needs to be examined, particularly whether typhoon rainfall will lead to an effective terrestrial control through river run-off. In the next chapter, further analysis of the coastal zone around the Island of Okinawa will be discussed with an emphasis on terrestrial influence and typhoon impact.

Chapter 5 Controls on the SST and Ocean Colour Variability around the Island of Okinawa: Terrestrial influence and a link with the coastal environment

5.1 Introduction

In the previous chapter, it was found that the winter East Asian Monsoon (EAM) is a primary control of the OC4 variability in the East China Sea and the coastal zone around the Island of Okinawa (§4.6.3). As with the noticeable influence of the Yangtze River on the OC4 variability on the continental shelf (§4.6.1), it is also conceivable that run-off from Okinawa has an effect on the OC4 variability (§4.6.3). It was also found that typhoons play an important role in decreasing the SST and the OC4 blooms around the coast of Okinawa (§4.7.1). With these findings, what can be questioned are (1) how much river run-off contributes to the OC4 variability as a terrestrial control and (2) how much typhoon rainfall and winds contribute to the SST/OC4 variability around Okinawa. In addition, with the importance of the winter EAM, its influence of the coastal sediment variability around Okinawa is investigated.

Firstly, in order to identify possible terrestrial controls through the rivers, EOF analyses were applied on an even smaller region – the 5 pixels of the western coast (W5) of Okinawa where the largest river in the Island, the Hija River, discharges. The period for the SST and OC4 variability is the same as in Chapter 4 (Fig. 5.1). The river discharge data from the Okinawa Prefectural Government (OPG) cover 1998 – 2005 (8 years, Fig. 5.1). The results show that the river discharge appeared as a secondary control on the OC4, particularly off the Hija River estuary (§5.5.2). Secondly, in order to investigate the effect of typhoons, EOF analyses were applied on the SST and OC4 anomalies in W5. The result showed that the SST anomaly is strongly influenced by the outer ocean (Domain 2) temperature, indicating the significance of a large scale control (§5.3.3). The anomaly of notheasterly wind caused by typhoons was found to be a secondary control, indicating its effect on upwelling. For the OC4 anomaly, the rainfall anomaly caused by typhoons was found to be an important factor, suggesting an enhanced terrestrial effect through increased run-off (§5.3.4). The northeasterly wind anomaly caused by typhoons has a secondary impact through the effect of upwelling.

Using the data of the Suspended Particle in Sea Sediment (SPSS) for 1995 – 2006 (12 years, Fig. 5.1), the effect of the winter EAM on the OC4 variability was also found to be responsible for sediment removal on the west side of Okinawa due to the strong northeasterly causing Ekman transport (§5.4.3). This result indicates an important linkage between the winter EAM and the coastal environment around the Island of Okinawa.

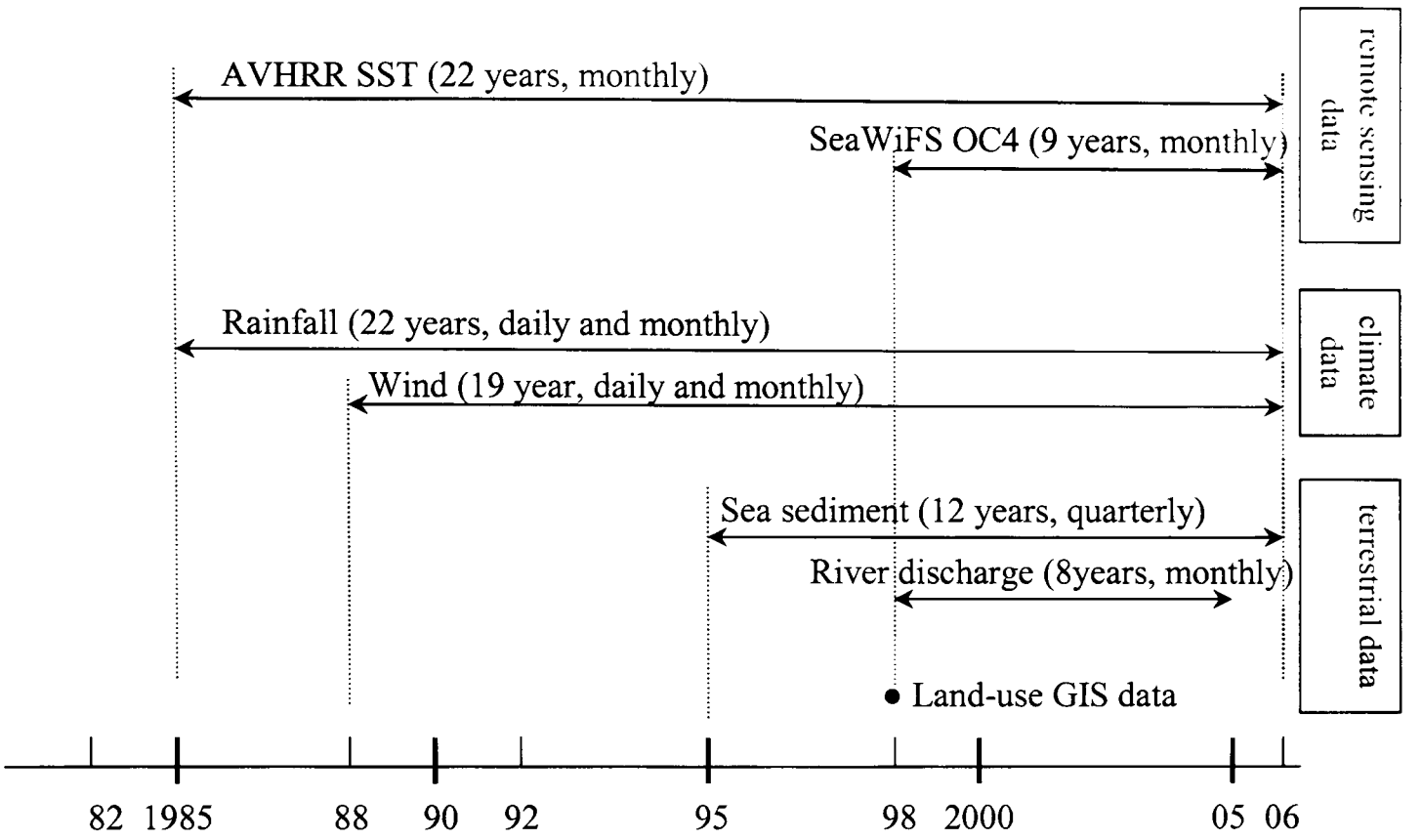

Fig. 5.1. Data used in this chapter and their temporal coverage.

5.2 Terrestrial Influence on the Coastal Zone

5.2.1 Land-use in the Catchments and Geographical Settings for EOF Analysis

In order to investigate the relationship between the SST and OC4 in the coastal zone and the terrestrial input through the river discharge, discharge data of 8 rivers out of 10 measured by the *OPG River Section* are used in this study (Fig. 5.2). These 8 rivers are flowing to the East China Sea off the west coast of Okinawa, and adjacent pixels of the SST and OC4 satellite data along the west coast were selected to compare their responses to the discharge (Fig. 5.3). Along the east coast, however, it was not possible to select pixels adjacent to other 2 rivers flowing to the east of Okinawa without covering other land or coastal zone due to the coarse resolution of the image. Therefore the eastern coastal zone was not analysed in this study. In attempting to identify terrestrial influence through run-off, 5 pixels of the SST and OC4 satellite data (R1 – R5) are selected (Fig. 5.3). These 5 pixels along the west coast (W5) are used for further EOF analyses. These cells are a sub domain of Domain 3 (26 cells around the Island: see Chapter 4 §4.4), therefore, it will enable a more focused evaluation of terrestrial control of the SST and OC4 by rivers.

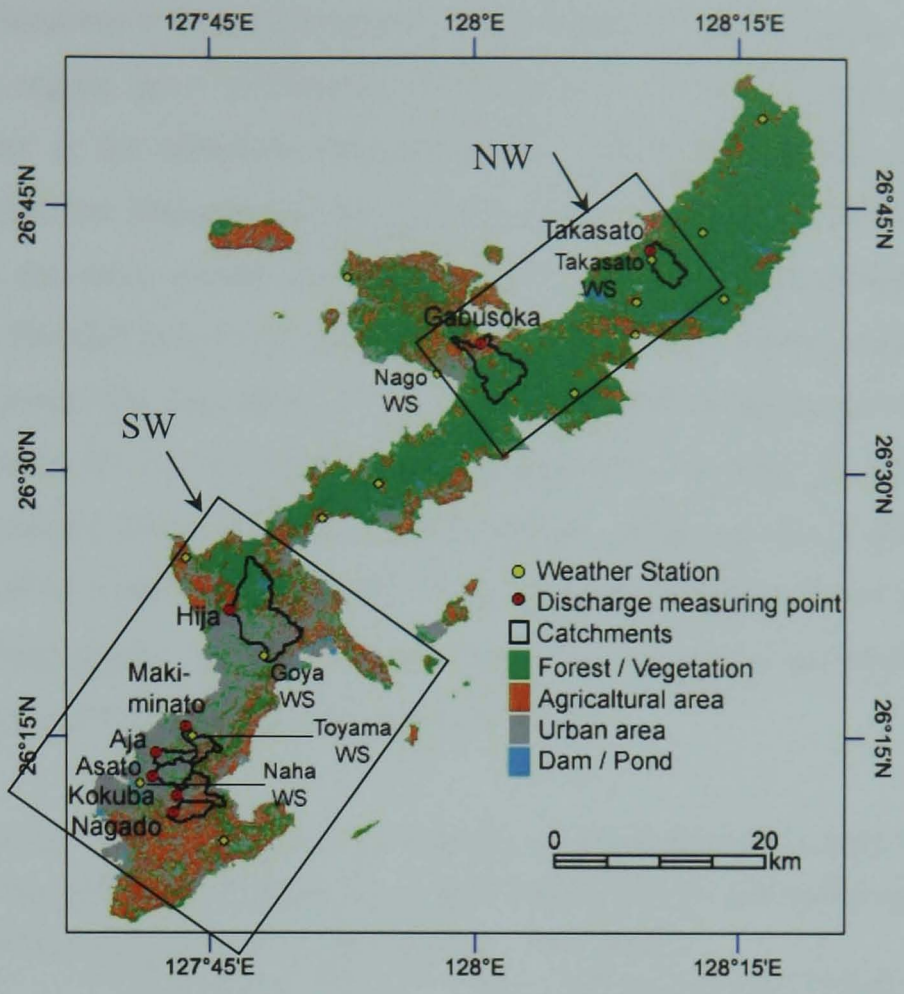

Fig. 5.2. Land use and the catchments of the 8 rivers in the west side used for the analysis.

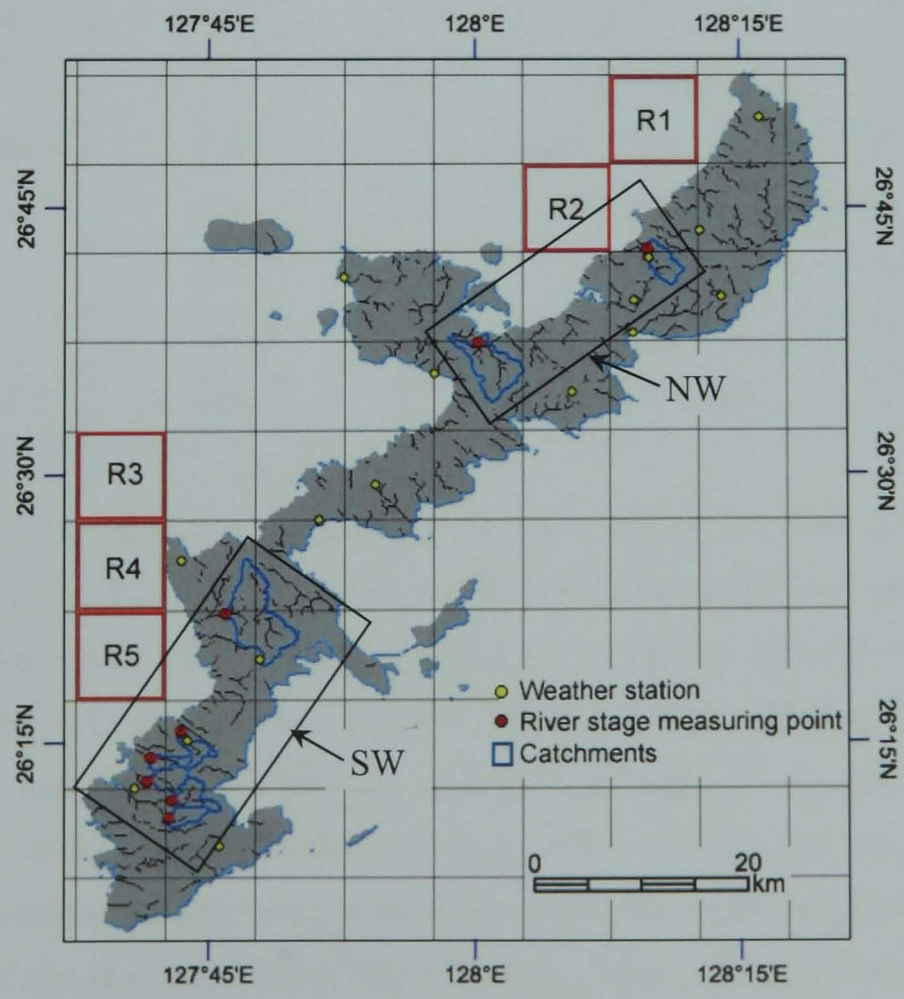

Fig. 5.3. Selected 5 cells (R1 – R5) in the west coast of Okinawa (W5). Satellite data of the SST and OC4 in W5 are used to EOF analyses to indentify terrestrial control though the rivers.

In Fig. 5.2 the land-use and the catchments of the selected 8 rivers are given. The rivers in the northwest (NW) region have catchments relatively well covered by forest and vegetation compared to those in the urbanised southwest (SW) regions, particularly those in the most southern region (SR: the Makiminato, the Aja, the Asato, the Kokuba and the Nagado Rivers). Table 5.1 shows the mean annual discharges (1998 – 2005) and the catchment areas of the selected 8 rivers. Rainfall data in the table were inserted from the nearest weather station (WS) to the discharge point. The Hija River is the largest river with a discharge of 1.63 m^3/s. Other large discharge rivers (> 0.5 m^3/s) are in the southern part; the Makiminato River, the Asato River and the Kokuba River. Rivers in the north are relatively small scale. Although the catchment areas of the Gabusoka River (19.77 km^2) and the Takasato River (8.53 km^2) are the second and the third largest catchments respectively, the discharges are smaller: 0.38 m^3/s for the Takasato River and 0.42 m^3/s for the Gabusoka River.

Table 5.1. Characteristics of the selected rivers: mean values are calculated from 1998 to 2005. The Makiminato, Aja, Asato and Kokuba Rivers are urban rivers, and greatly influenced by waste waters which often make the run-off coefficient over 100 % (*OPG River Section*, 1998 – 2005a).

	river	catchment area (km^2)	total length (km)	annual rainfall (mm, WS)	mean discharge (m^3/s)	run-off coefficient (%)
NW	Takasato	8.53	4.9	2605 (Takasato)	0.38	52.5
	Gabusoka	19.77	3.7	2243 (Nago)	0.42	28.3
SW	Hija	33.76	14.5	2217 (Goya)	1.63	66.6
	Makiminato	5.28	3.3	2247 (Toyama)	0.59	142.5
	Aja	4.32	5.2	2273 (Naha)	0.41	129.7
	Asato	7.15	7.3	2273 (Naha)	0.54	111.4
	Kokuba	7.66	9.1	2273 (Naha)	0.50	90.8
	Nagado	5.62	2.3	2273 (Naha)	0.19	44.8

Fig. 5.4 shows the area of each land-use in the catchments. With the high forest and vegetation coverage in the NW, the run-off coefficient here remains low compared to the SW. On the other hand, urban cover is a major land-use in the SR. The SR has a high run-off coefficient because of not only the land-use effect but also additional wastewater from residential areas and industries. Where a run-off coefficient in the SR exceeds 100 %, wastewater is the likely cause (OPG River Section, 1998 – 2005a), and river works in the SR e.g., flood prevention work and bank construction affect the water height. The latter leads to overestimation of the discharge (OPG River Section, 1998 – 2005a). The Hija River has a significant urban area but with large forest and vegetation area, the run-off coefficient is relatively low compared to those of the SR. Given the large discharge and the high coverage of urban area of the SW region, high nutrient concentrations may occur in run-off. The high

agriculture area of the SR could lead to high sediment concentration delivery to the adjacent ocean and hence also affect the OC4 response near SW.

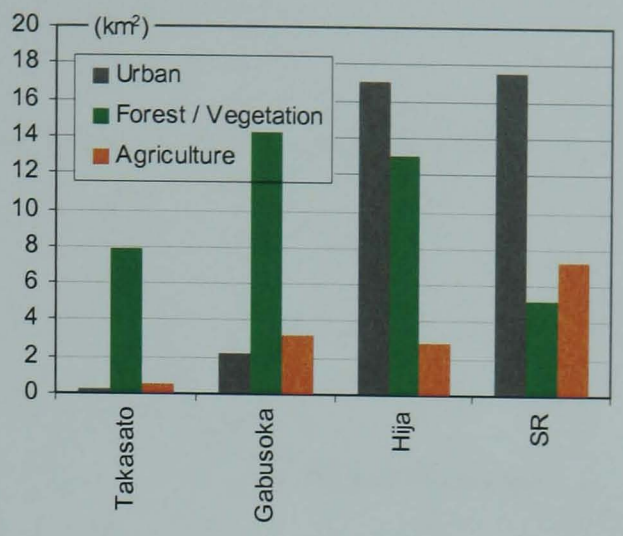

Fig. 5.4. Land-use of the selected catchments in Fig. 5.2 in 1998. The SR includes the Makiminato, Aja, Asato, Kokuba, and Nagado River.

5.2.2 EOF analysis of the SST and OC4

For the SST EOF in W5, the solar annual cycle is the dominant control appeared in the 1st mode, accounting for 97.7 % of the total variance. Basically, the result was the same as the analysis in D3 in Chapter 4. The details are presented in Appendix A1.2.

For the OC4 EOF in W5, the 1st mode, accounting for 81.2 % of the total variance (Fig. 5.5), shows again the importance of the winter EAM, as seen in D3 (Chapter 4, §4.5.3; see Appendix A1.3 for the detail). In the 2nd mode, explaining 9.6 % of the total variance, its eigenvector shows the highest value in R5 nearest to the Hija River estuary (Fig. 5.6), indicating the significant effect of the large river on the adjacent coast. On the other hand, R1 and R2 show negative eigenvectors. The discharge of NW rivers can be regarded as having an influence on R1 and R2. Their discharge contributes only 16.7 % on average to the total discharge (NW + SW). The variability in the NW discharge (STD = 0.7 m^3/s) is much lower than the SW discharge (STD = 3.1 m^3/s) and the total discharge (STD = 3.7 m^3/s). This discharge difference in the NW and SW rivers probably causes the difference in the 2nd mode eigenvectors of the NW (R1 and R2) and SW (R3 – R5) regions.

The 2nd mode temporal function has an annual cycle element in its spectra with additional 4 and 2 month cycles (Fig. 5.7). A comparison between its temporal function and the total discharge of the rivers shows a statistically significant correlation ($r = 0.31$, $p = 0.0019$). This relation shows that a terrestrial control through the rivers on the OC4 variability in W5 appears as a secondary control. Several peaks of the temporal function and the runoff coincide,

particularly in September 2001. This acute run-off was triggered by the heavy rainfall brought by Typhoon Nari. This typhoon approached Okinawa in early September and stayed for about 10 days around the Island. In the next section, the effect of typhoon rainfall and winds will be discussed.

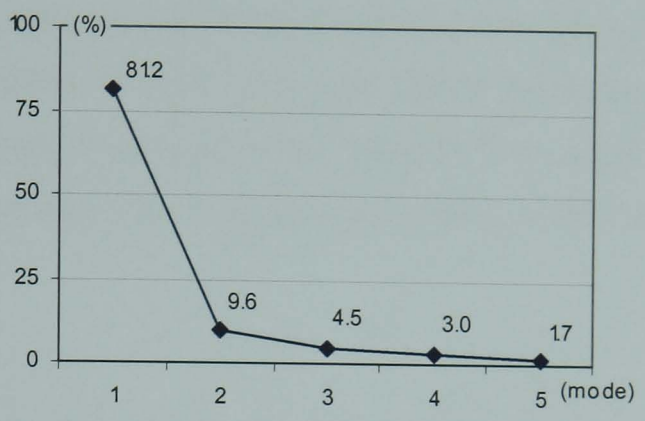

Fig. 5.5. Eigenvalues of the OC4 EOF in W5.

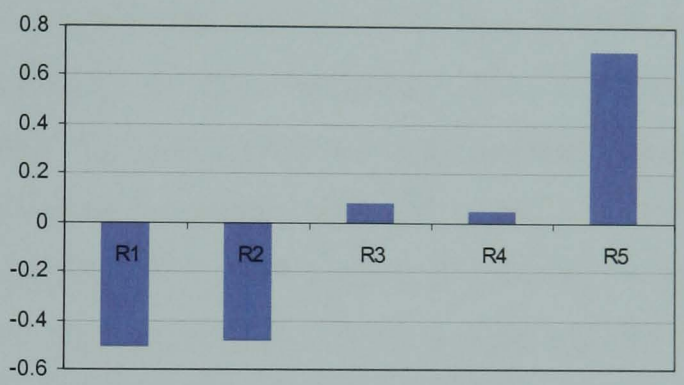

Fig. 5.6. The 2nd mode eigenvectors of the OC4 EOF in W5.

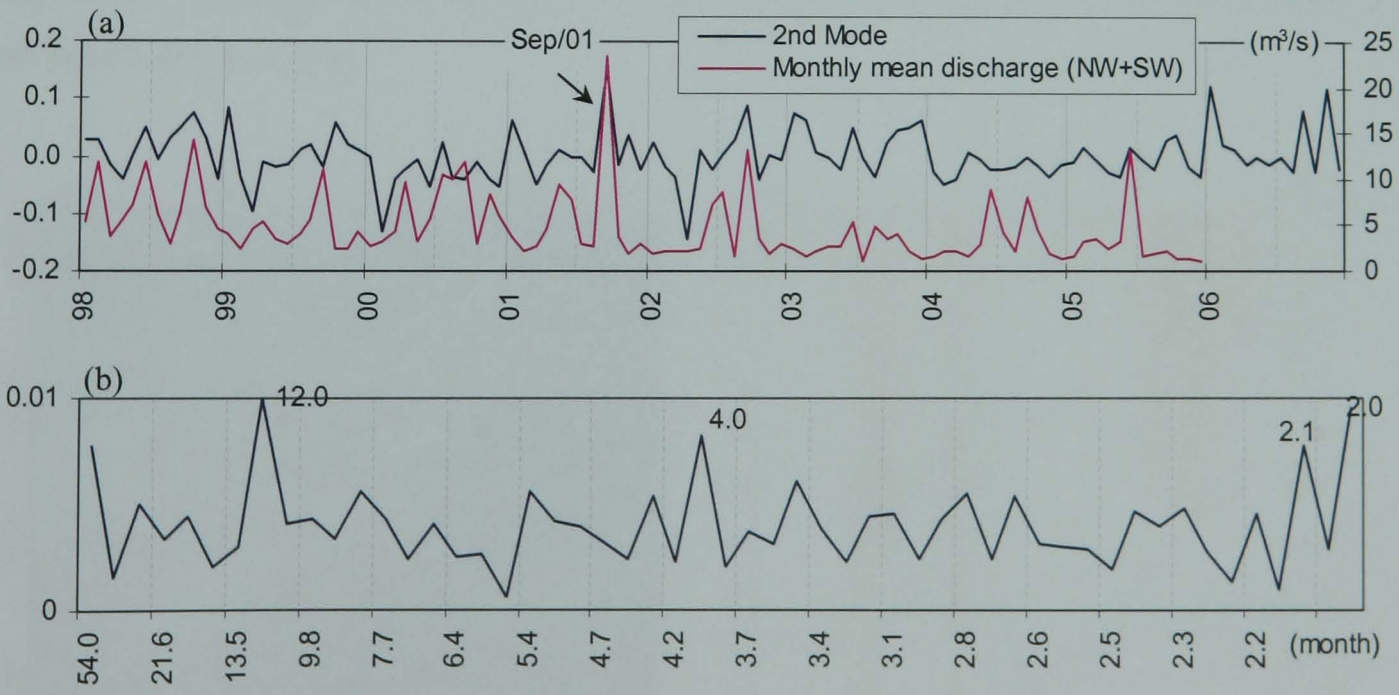

Fig. 5.7. (a) Temporal functions and (b) spectrum of the 2nd mode OC4 EOF in W5.

5.3 Typhoon Influence on the SST and OC4

Terrestrial impact through run-off was found to have a secondary control on the SST and OC4 variability. Typhoons have a significant impact on enhancing run-off and the OC4 bloom by their heavy rainfall. Typhoons are episodic events around Okinawa, but occur every year during summer to autumn. Thus, typhoon rainfall is a likely significant factor on the SST and OC4 variability. As coral reefs are significantly influenced by such short-term events providing extreme sediment and nutrient delivery, it is important to investigate typhoon control on the coastal zone. In this section, a case study of Typhoon Nari, which approached Okinawa in September 2001, and the more general typhoon contribution to SST and OC4 variability will be investigated.

5.3.1 Case study: Typhoon Nari

An extreme run-off was observed in September 2001 which coincided with a peak of the temporal function of the 2nd mode for the OC4 EOF (Fig. 5.7a). It was triggered by Typhoon Nari that approached Okinawa in early September 2001. Typhoon Nari was an abnormal typhoon in terms of its track. Fig. 5.8 (a) shows its track around Okinawa. It first approached the Island on September 6, passed through westward, made a U-turn toward the Island on September 10, and re-approached on September 11. Finally it passed to west again on September 14. These two visits are apparent in the rainfall and the wind data, providing two heavy rainfall events exceeding 180 mm/day and two wind speed maxima of over 12 m/s at the Naha WS (Fig. 5.8b). Rainfall at the Goya WS (nearest to the Hija River) was 127 mm on September 7 and 286 mm on September 8. These heavy rainfall events created the extreme run-off shown in Fig. 5.7 (a).

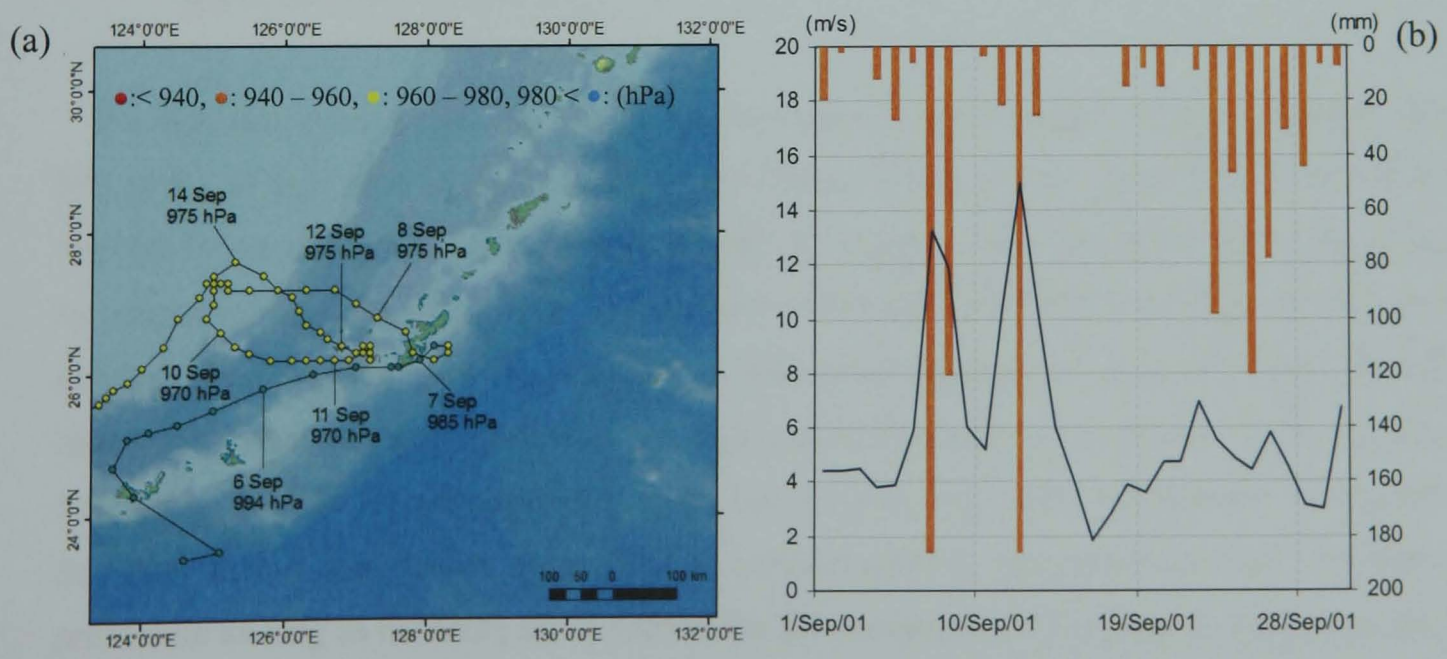

Fig. 5.8. Typhoon Nari: (a) its track, and (b) rainfall and daily mean wind speed at the Naha WS.

The SST and OC4 values for 2001 are shown in Fig. 5.9, along with averaged values of R1 – R5 and R5 values alone. For the OC4, a pronounced peak can be seen in R5 in September. much higher than the averaged value. It is a clear example of a typhoon's effect, indicating a significant impact on the OC4 bloom offshore of a large river by its heavy rainfall. A heavy rainfall not only increases river discharge but also triggers more soil erosion, hence soil run-off. Nutrient loss associated with erosion (Mihara, 2001) is transferred to the coastal zone with runoff, leading to an increase in the OC4 (Gallago et al., 1992). During the rainy season and the typhoon visits, enhanced soil run-offs are often observed, impacting coral reefs around Okinawa (Omija, 1985, Omija and Ikema, 1990; Omija et al., 1994; Onaga et al., 1999). It will lead to an OC4 bloom as shown here. Considering that rainfall is a cause of run-off, the summer EAM that brings the rainy season can be regarded as a contributor to this secondary control. The EAM, a global scale dynamical process, is therefore a major control on the OC4 response in general. It affects particularly the OC4 bloom in winter through upwelling. During the summer nutrients brought in by run-off, also contribute to the bloom but to a lesser, episodic, extent than in the winter.

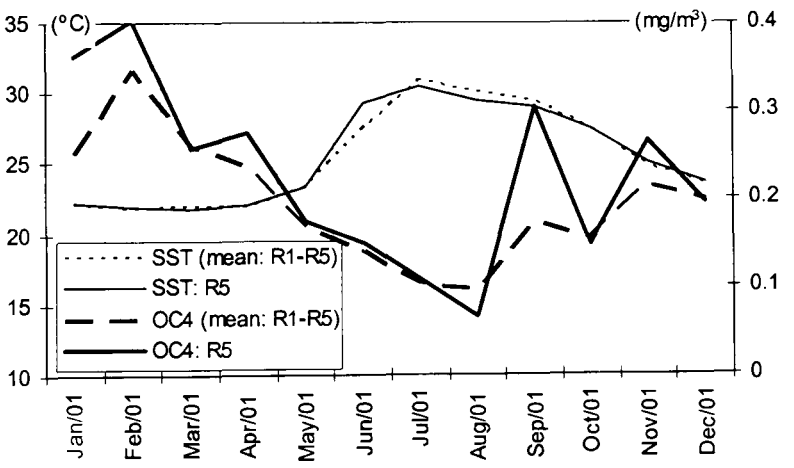

Fig. 5.9. The SST and OC4 from objectively analysed data in 2001. Averaged values of R1 – R5 are in dotted line and R5 values alone in solid line.

No sign of a lowered SST is seen during the typhoon visit for either western averaged (R1 – R5) or R5 values. This suggests that the OC4 bloom is affected by the enhanced run-off from the Hija River caused by heavy rainfall brought by Typhoon Nari, but not by upwelling induced by strong winds associated with the typhoon. However, the SST used here is objectively analysed data. Missing data are interpolated with pixels adjacent in space and time. Therefore interpolated data may not represent an event that actually occurred. In the SST here, the data in September 2001 in R5 were missing due to cloud cover, and hence interpolated. Compared to the OC4 bloom that detects chlorophyll-a concentration in phytoplankton that continues to proliferate as long as nutrients are available, the SST response to upwelling by typhoons may be a shorter event. Cloud cover associated with a typhoon will create additional problems for

detection by satellite remote sensing. Therefore, a typhoon's effect on upwelling may not be fully represented by the SST data for an episodic event.

However, effects of typhoon winds are important. The run-off effect on the OC4 bloom will be greater when strong typhoon winds occur, providing greater disturbance both on land by causing excessive sediment run-off (Milliman and Kao, 2005; Galewasky et al., 2006) and in the open ocean by initiating water mixing and upwelling (Shiah et al., 2000; Lin et al., 2003). Zheng and Tang (2007) investigated the OC4 response around the Island of Hainan to Typhoon Demrey in the South China Sea in September 2005, indicating that rain-triggered discharge and seaward advection by the wind enhanced the OC4 around the Island. Thus, it is important to assess the effect of typhoons on both rainfall and winds. These effects will be discussed, using anomaly data and EOF analyses to add a quantitative evaluation of general typhoon effects on the SST and OC4 variability off the west coast of Okinawa.

5.3.2 Definition of Typhoon Rainfall and Winds around Okinawa

To prepare anomalies of rainfall and NE wind component (northeasterly) caused by typhoons, firstly, typhoons which approached the Island of Okinawa to within 300 km were defined using typhoon track data collected from the Digital Typhoon website (http://agora.ex.nii.ac.jp/digital-typhoon/) operated by the *National Institute of Informatics*. The months when typhoons closed to Okinawa within 300 km (T300) are determined as T300 months (Fig. 5.10a).

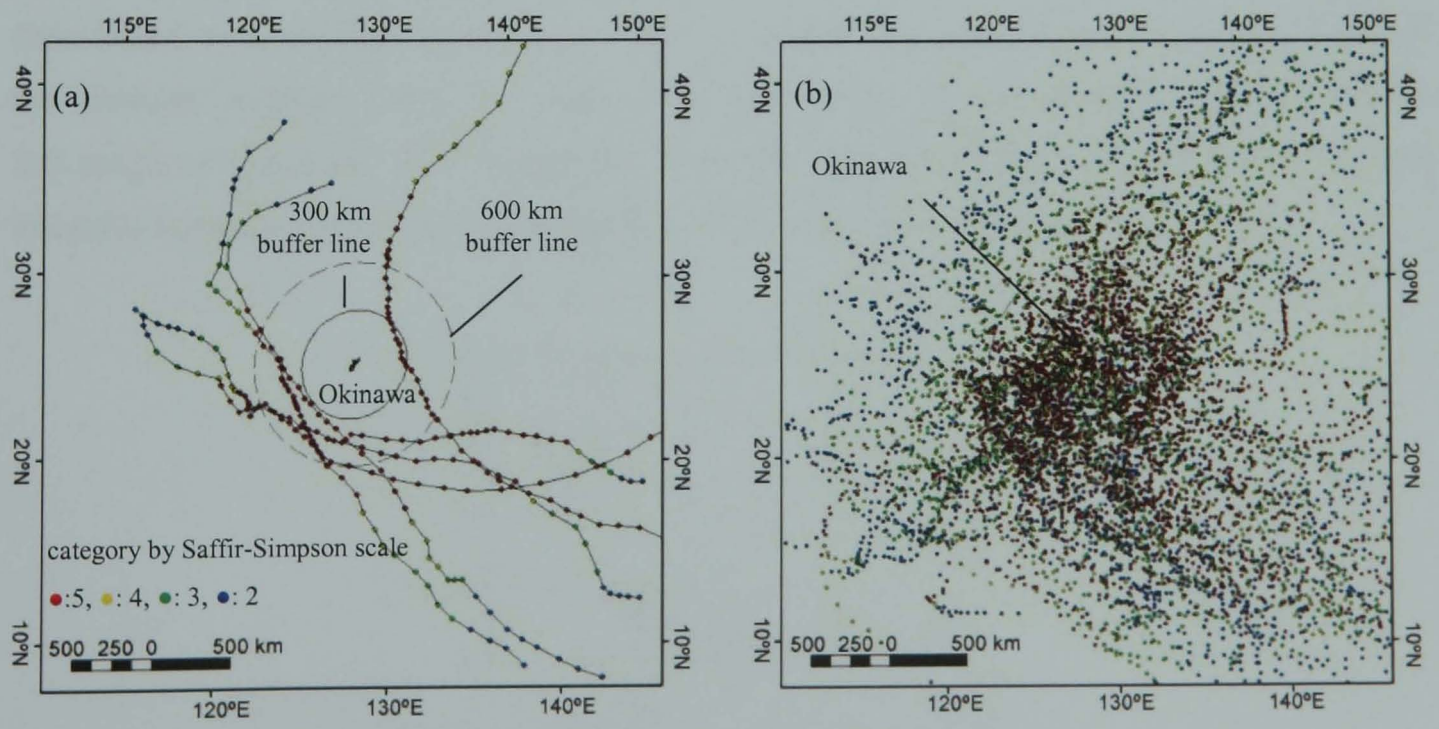

Fig. 5.10. Typhoon tracks around the Island of Okinawa for (a) Jul – Sep 2005 and (b) 1982 – 2005. Most of typhoons travel from SE to NE. Typhoons' intensity is classified according to the Saffir-Simpson scale. Solid line and dashed line in (a) indicate the buffer lines from the island of 300 km and 600 km respectively.

Typhoons which passed the Island in the distance between 300 km and 600 km are not included as typhoon events because their influence on rainfall and winds are much smaller than T300 typhoons. Fig. 5.10 (b) shows the tracks of 184 typhoons that occurred around the Island of Okinawa during 1982 – 2005. Most of them approach from the SE of Okinawa and proceed to the NE. It shows Okinawa is a hot spot for typhoon visits.

Monthly rainfall and northeasterly wind component which occurred in T300 months are determined as typhoon-driven. Rainfall and the northeasterly wind component in the remaining months are determined as events in ordinary (ORD) months (note that typhoon within 300-600 km are not included in ORD month either). Data at the Nago and Naha WS were used for the rainfall and northeasterly wind component. For a comparison with the AVHRR SST (1985 – 2006), an annual climatology of rainfall was created for 1985-2006. The annual climatology of northeasterlies used the period of 1988 – 2006 because wind measuring point in the WS in Okinawa was moved in 1987. For a comparison with the SeaWiFS OC4 (1998 – 2006), a climatology of rainfall and northeasterlies was produced over 1998 – 2006. Therefore, monthly anomalies of rainfall and northeasterlies were prepared for the AVHRR SST and SeaWiFS OC4, and anomalies caused by typhoons are determined by the occurrence in T300 months.

5.3.3 EOF analysis of the SST anomaly

EOF analyses were applied on the SST anomaly here. To create anomalies of the SST, its annual cycle was removed from the original objectively analysed monthly dataset. The eigenvalues were obtained as shown in Fig. 5.11. In this case, the 1st mode explains 72.8 % of the variance, indicating there is a major signal apart from solar annual cycle. The 2nd and the 3rd modes account for 12.3 % and 8.3 % of the variance, respectively. Eigenvectors and temporal functions explaining more than 5 % of the variance are presented here.

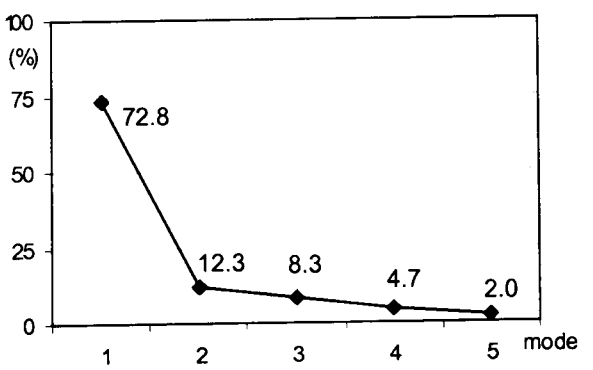

Fig. 5.11. Eigenvalues of the SST anomaly EOF in W5.

The 1st mode eigenvector shows all positive values, indicating all of R1 – R5 are positively influenced by this mode (Fig.5.12.M1). In its temporal function (Fig. 5.13), persistent positive

anomalies are seen during 1998. It was due to the strongest El Niño that brought warm sea water around Okinawa and caused a huge coral bleaching event (Yamazato, 1999). Thus external influence seems strong on the local SST. In a comparison of the SST anomaly in Domain 2 (see Chapter 4 §4.4) with this temporal function, it actually showed a strong correlation ($r = 0.84$, $p < 0.001$: Fig. 5.13.M1a). Therefore, anomalous SST around Okinawa is strongly influenced by surrounding sea water temperatures.

For the 2nd mode, its temporal function showed a statistically significant correlation with the T300 northeasterly anomaly at Naha, lagged by 1 month. It is a negative correlation ($r = -0.25$, $p = 0.042$), indicating the cooling effect of typhoon winds through upwelling. The eigenvector shows that its effect appeared to be influential in the SW region (R3 – R5: Fig. 5.12.M2).

In the 3rd mode, no correlations were found with rainfall or northeasterly anomaly in T300 or ORD months. The highest eigenvector appeared in R1 (Fig. 5.12.M3), and the temporal function showed a correlation ($r = 0.57$, $p < 0.001$) with the SST anomaly in R1. This mode is dominated by the SST variability of the local area (R1) offshore, rather than a wider effect, although not to any local discharge.

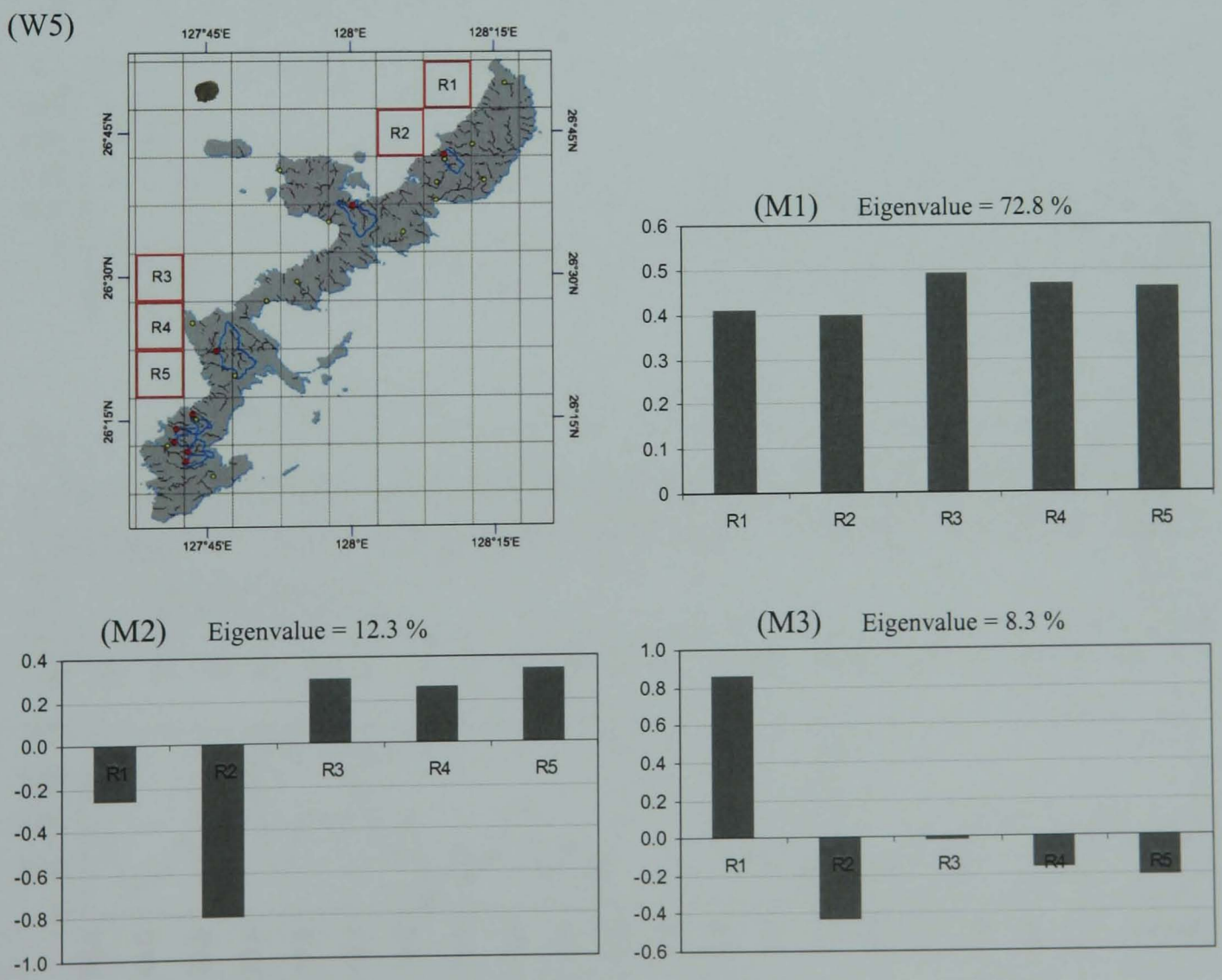

Fig. 5.12. Eigenvectors of the SST anomaly EOF in W5: (W5) location of the 5 cells in the west coast, R1 – R5, (M1) the 1st mode, (M2) the 2nd mode and (M3) the 3rd mode.

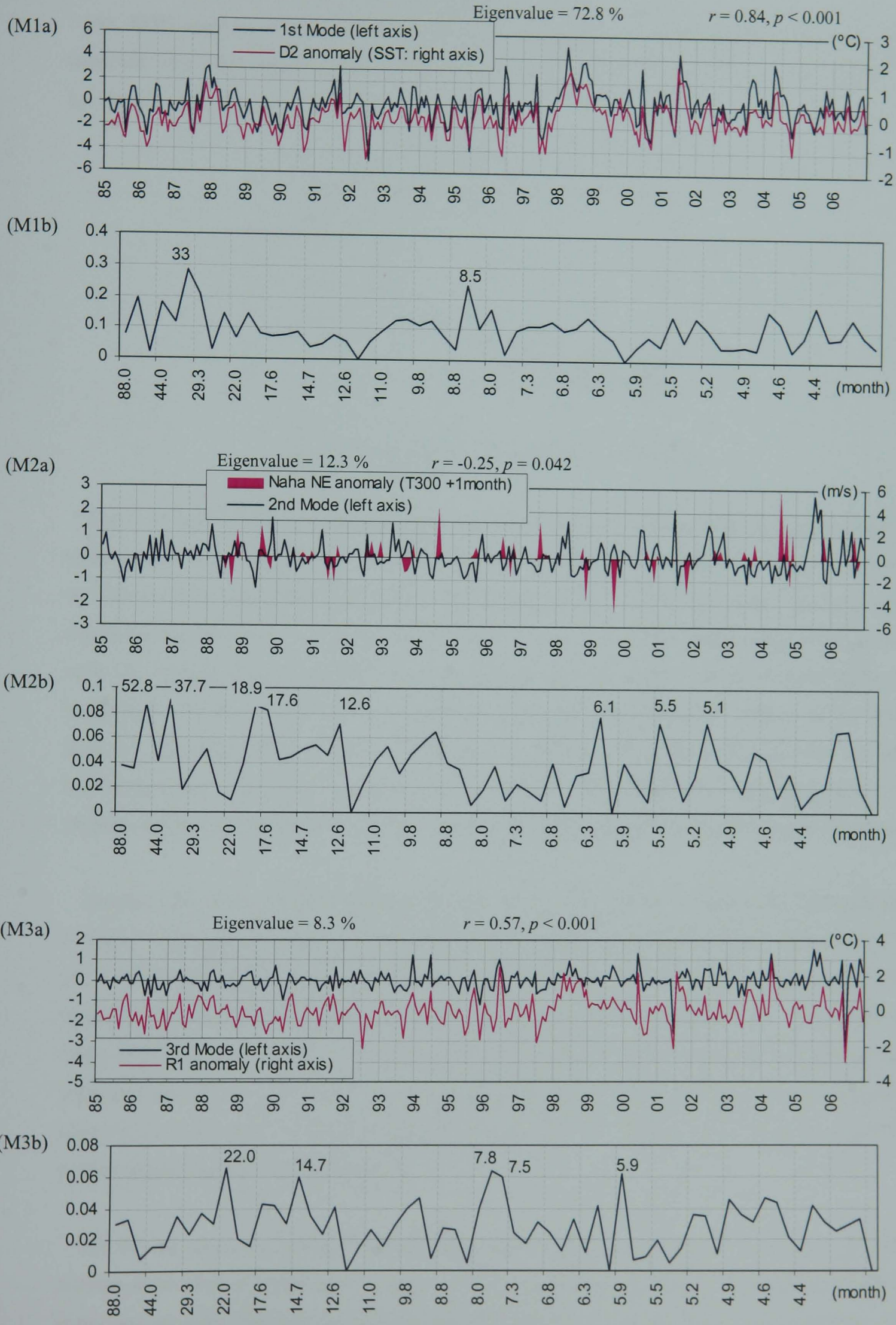

Fig. 5.13. (a) Temporal functions and (b) spectrum of the SST anomaly EOF in W5: (M1) the 1st mode, (M2) the 2nd mode and (M3) the 3rd mode.

5.3.4 EOF analysis of the OC4 anomaly

An EOF analysis was applied on the OC4 anomaly, where the annual cycle had been removed. The eigenvalue is given in Fig. 5.14. The modes greater than 5 % are discussed here i.e. the 1st, 2nd, 3rd and 4th mode.

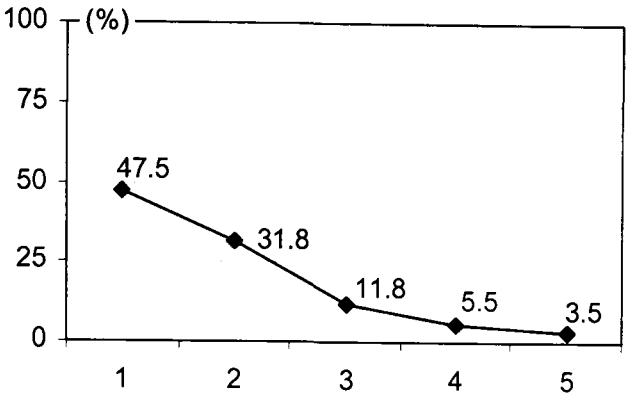

Fig. 5.14. Eigenvalues of the OC4 anomaly EOF in W5.

Fig. 5.15 and 5.16 show the eigenvectors and the temporal functions, respectively. For the 1st mode which accounts for 47.5 % of the anomalous variance, its temporal function showed correlations with the rainfall anomaly in T300 months (Fig. 5.16.M1a) at Nago and Naha with statistical significance (r = 0.38, p = 0.037 and r = 0.37, p = 0.042, respectively). Comparison with the rainfall anomaly in ORD months showed no statistically significant correlation. It suggests that typhoon rainfall is an important control that influences the variance of the OC4 anomaly. The eigenvector of the 1st mode (Fig. 5.15.M1) shows high values for R4 and R5, indicating effects from the large rivers in the Islands. This result shows the importance of typhoon rainfall and subsequent run-off from the rivers that impact the coastal zone of Okinawa.

For the 2nd mode, accounting for 31.8 % of the anomalous variance, the northeasterly anomaly at Naha was found to be correlated with the temporal functions of this mode (r = 0.24, p = 0.014), lagged by 1 month. However, greater correlations were found in a comparison with just the typhoon northeasterly anomaly (Fig. 5.16.M2a) at Nago (r = 0.43, p = 0.015) and at Naha (r = 0.51, p = 0.036). Therefore, next to typhoon rainfall, their strong winds are an important control on anomalous OC4 variability along the west coast of Okinawa. The highest eigenvector in R5 (Fig. 5.15.M3) may suggest a strong influence of typhoon winds that upwells sediments delivered from the Hija River.

For the 3rd mode, its temporal function was found to be correlated with the anomaly of ORD northeastelies (Fig. 5.16.M3a) at Nago (r = 0.45, $p < 0.001$) and at Naha (r = 0.44, $p < 0.001$), indicating an effect from an anomalous winter EAM. No correlations were found between the

temporal function of the 4th mode (Fig. 5.16.M4a) and any rainfall and norheasterly anomalies, suggesting purely local impacts at R1 and R3 (Fig. 5.15.M4).

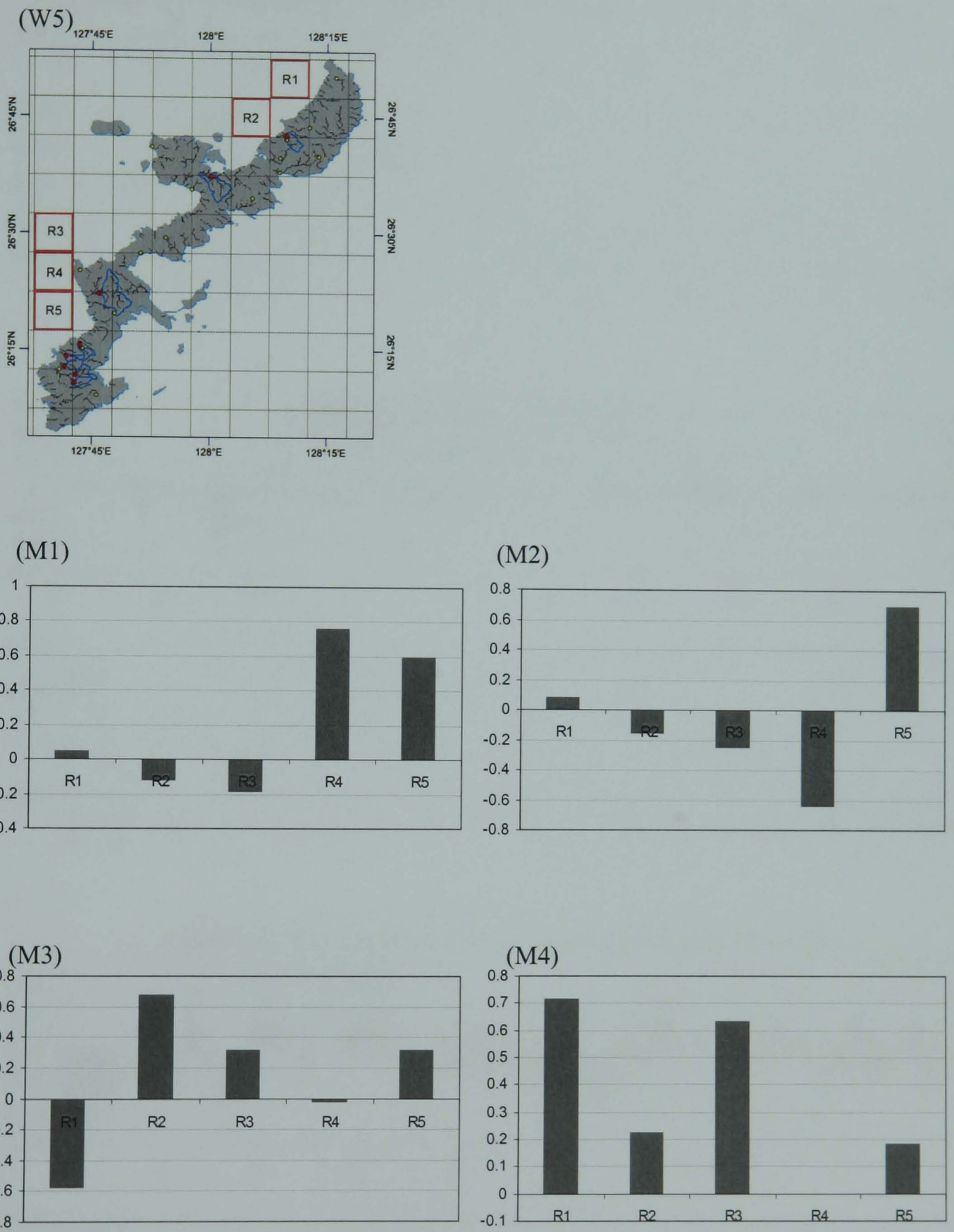

Fig. 5.15. Eigenvectors of the OC4 anomaly EOF in W5: (W5) location of the 5 cells in the west coast, R1 – R5, (M1) the 1st mode, (M2) the 2nd mode, (M3) the 3rd mode and (M4) the 4th mode.

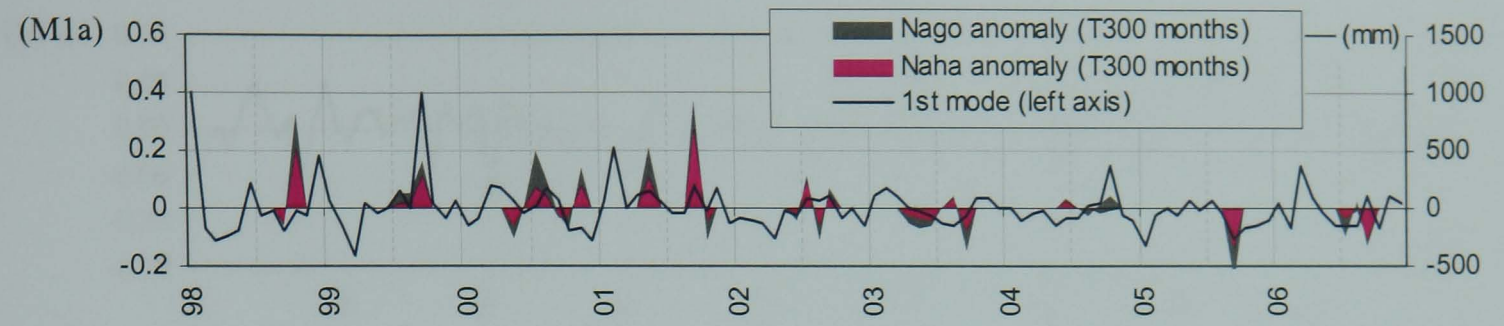

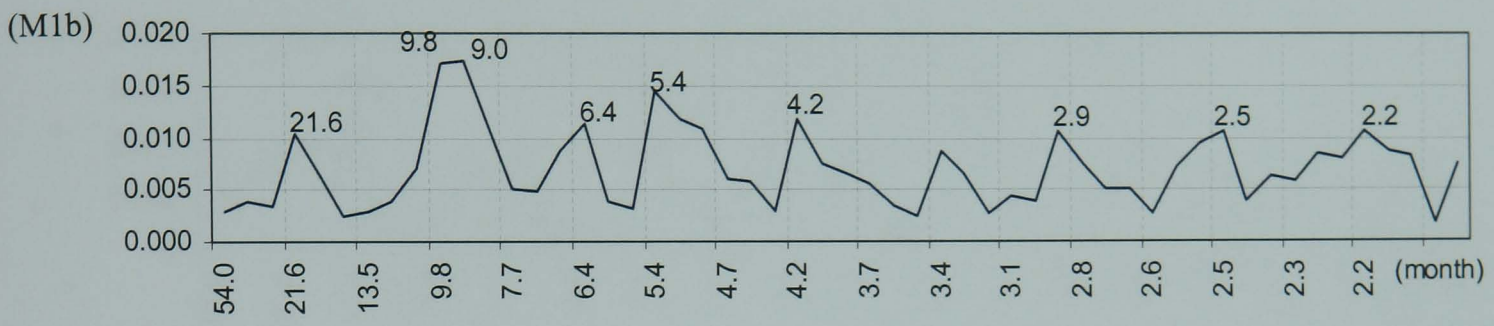

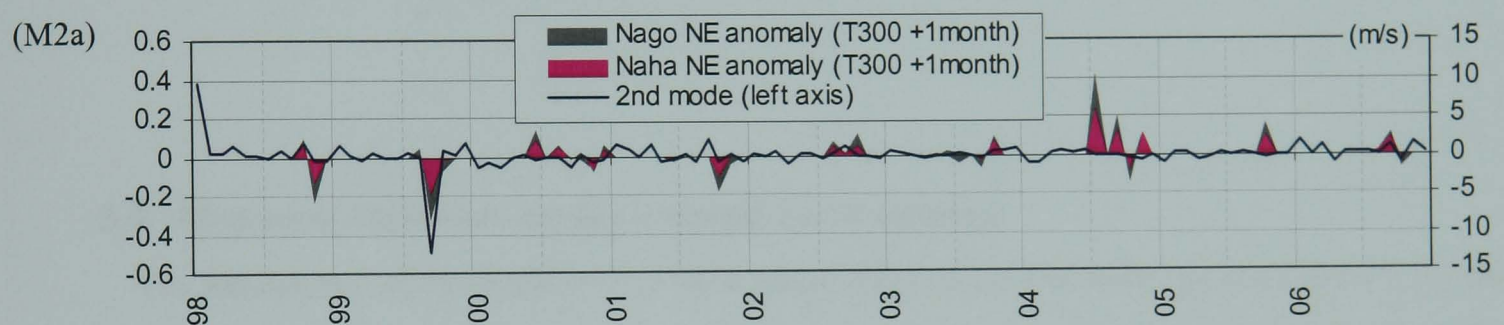

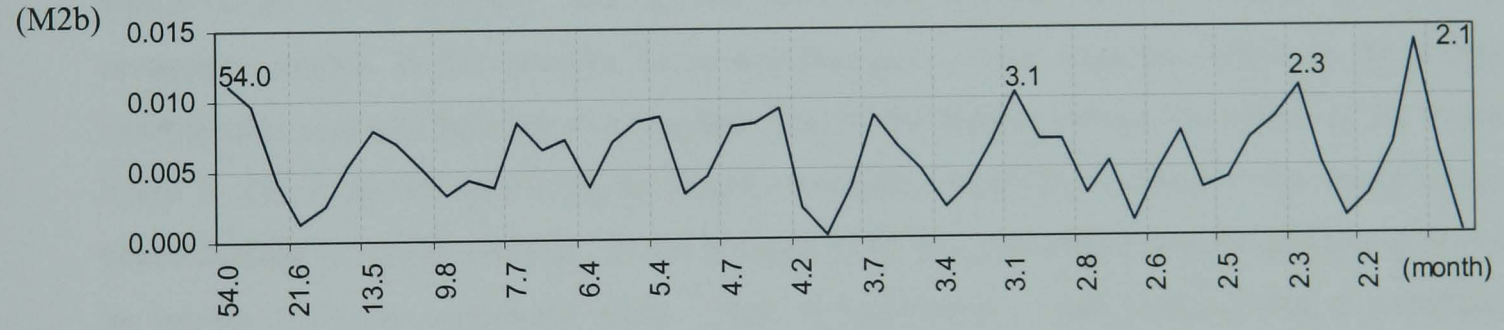

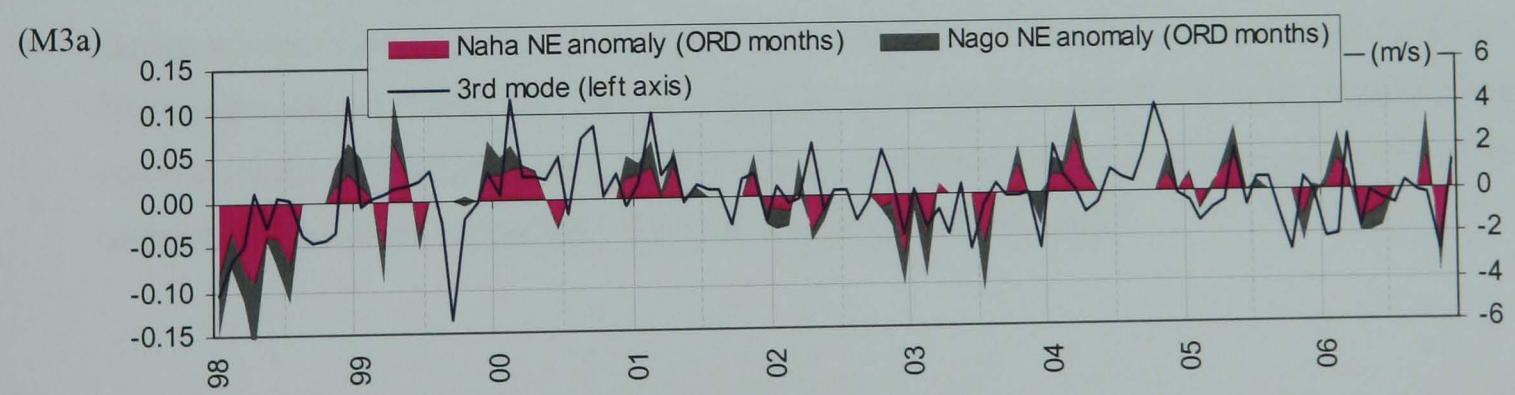

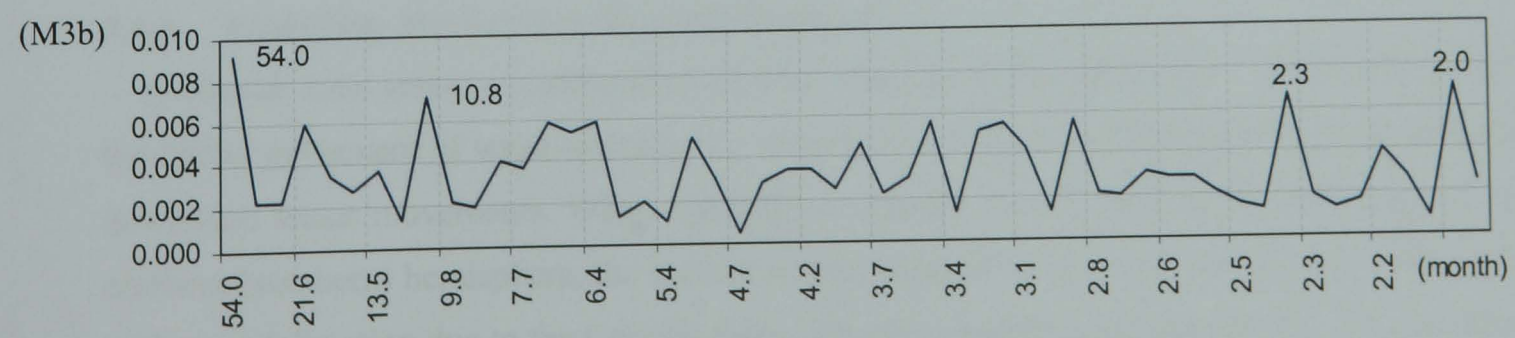

Fig. 5.16. (a) Temporal functions and (b) spectrum of the OC4 anomaly EOF in W5: (M1) the 1st mode, (M2) the 2nd mode and (M3) the 3rd mode.

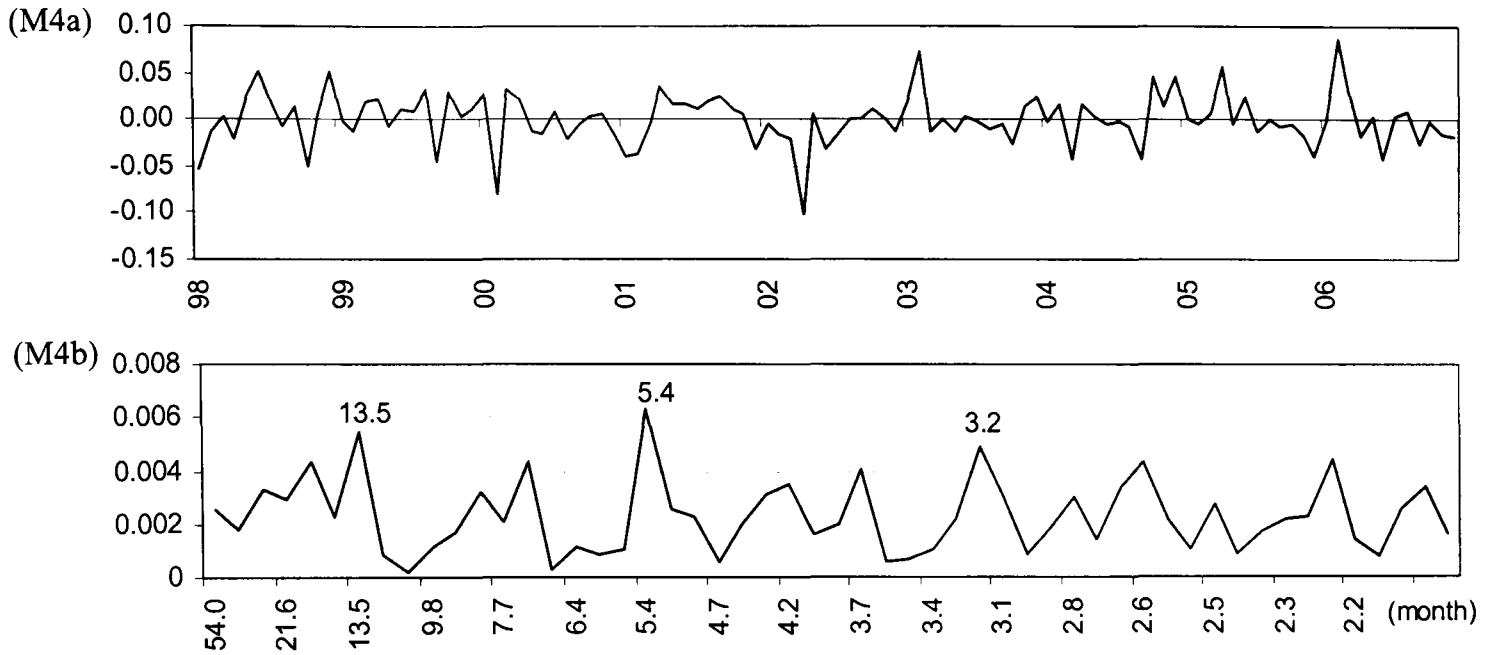

Fig. 5.16 continued. (a) Temporal functions and (b) spectrum of the OC4 anomaly EOF in W5: (M4) the 4th mode.

5.4 Monsoon Influence on the Coastal Environment

The importance of the EAM on the OC4 variability around Okinawa has been shown: (1) the winter EAM is the primary control, and (2) run-off brought by the summer EAM is the secondary control. In this section, further interpretation of the monsoon effect on the coastal environment around Okinawa is discussed. One of the findings about the effect of the winter EAM is that it causes upwelling by Ekman transport, supplying nutrient to the upper ocean, hence leading to an OC4 bloom. It can be speculated that materials from the seafloor will also be moved with the upwelling water. Here, a hypothesis is put forward that accumulated sediment offshore during the rainy season in summer may be resuspended by the northerly during winter. Therefore, the winter EAM may also act to reduce the sediment on the seafloor. During the summer EAM, soil run-off caused by associated rainfall has been an environmental issue since the 1960s in Okinawa. In this section, the contrasting effects of the winter EAM on sediment removal and the summer EAM on soil run-off are discussed.

5.4.1 Upwelling Mechanism: Ekman Transport

In coastal zone areas, a combination of wind, rotation of the Earth (the Coriolis effect), and the lateral movement of water restricted by shorelines and shallow bottoms induces upward and downward water movements. When wind blows parallel to the coast on its left (right) in the northern (southern) hemisphere, the surface water (Ekman layer) is transported to the right (left) of the wind direction due to the Coriolis force. This transportation of water by the wind is called Ekman transport. Coastal upwelling occurs where Ekman transport moves water away from the coast. Then bottom water wells up to the surface to replace it (Fig. 5.17).

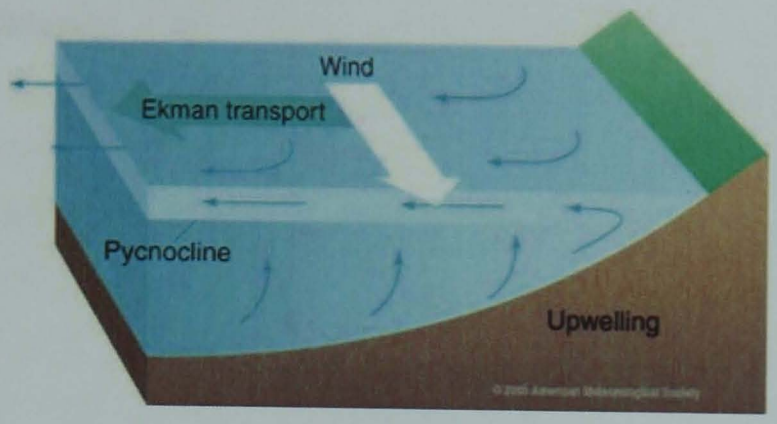

Fig. 5.17. Mechanism of Ekman transport. (from NASA Ocean Motion website http://oceanmotion.org/html/ back ground /upwelling-and-downwelling.htm).

The transported volume can be given by (Hamaya et al., 1994)

$$\tau / \rho_w f \qquad \text{(Eq. 5-1)}$$

where τ is the wind stress, ρ_w is water density and f is the Coriolis Force. τ is determined by

$$\tau = \rho_a C_D U^2 \qquad \text{(Eq. 5-2)}$$

where ρ_a is air density, C_D is the drag coefficient and U is the wind speed 10 m above sea level. Ekman transport is thus proportional to U^2.

It can be speculated that the sediment in the seafloor will also be removed with the upwelling. The amount of the reduced sediment can be estimated in relation to the amount of water moved by Ekman transport (Fig. 5.18). Therefore, the sediment will be reduced according to U^2. Because the winter EAM provides a strong northerly along the west coast of Okinawa, a comparison of the sediment difference before and after the winter EAM with the net U^2 during the winter EAM may show a link if the speculation is correct.

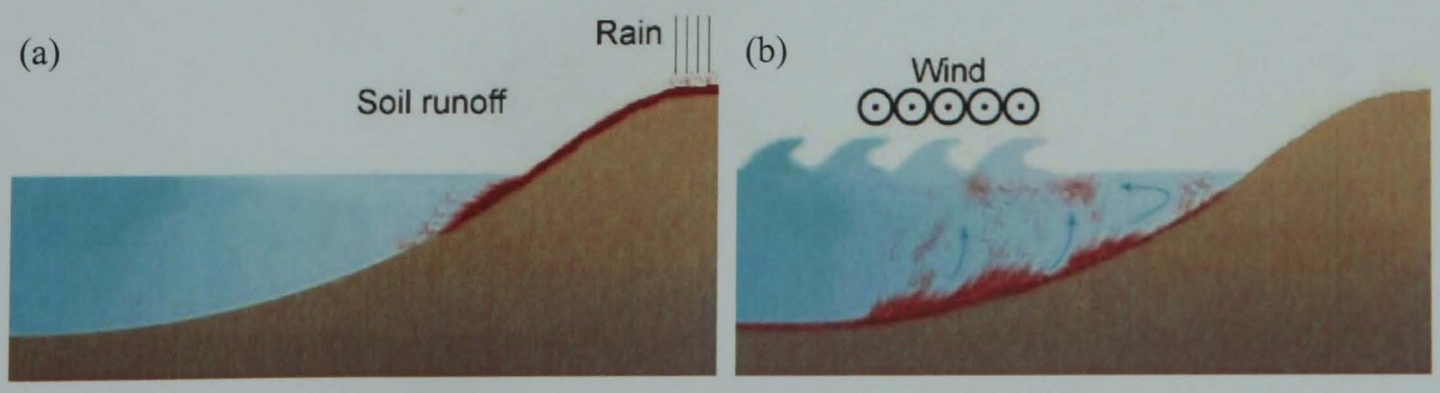

Fig. 5.18. Concept of soil run-off and sediment removal by Ekman transport. (a) soil run-off and its delivery to the sea caused by rainfall, (b) sediment resuspension and removal with upwelling water by Ekman transport.

5.4.2 Sea Sediment around Okinawa

On the Island of Okinawa, some of the geographical features are conducive to soil run-off: steep terrain, short rivers, heavy rainfall, typhoon disturbance and erodible soil, particularly the red soil type *Kunigami maji* (Onaga et al., 1983) which is predominantly distributed in the north of Okinawa (see the soil map in Fig. 2.14). Eroded soils are delivered to the coast through the rivers and then accumulated. They cause adverse impact on coral communities and fishery activities. The *OPG Institute of Health and Environment* has been surveying the deposited soil around Okinawa since 1983. In 1987, Omija (1987) developed a quick method to measure the sediment concentration on the coastal bottom. This method estimates the sediment concentration derived from the transparency measured in a cylinder filled with the diluted sample of sediment, and it is calculated in kilogram per 1 m^3. This measured value is called the concentration of Suspended Particle in Sea Sediment (SPSS). It is known that SPSS has a logarithmic normal distribution (Omija, 1987).

The SPSS survey has been carried out quarterly but not at a fixed date. Usually it is sampled once in one of the spring months (MAM) before the rainy season (June), once in summer months (JASO) or after the typhoon season, once in fall to winter (OND), and once at the end of the winter EAM when the northerly has calmed (JFM). Its sampling points are shown in Fig. 5.19. There are 3 points to the west, Henan, Genka and Akase; 4 points to the east, Taira, Kanna, Kan and Ishikawa; and 2 points to the south, Aji and Odo.

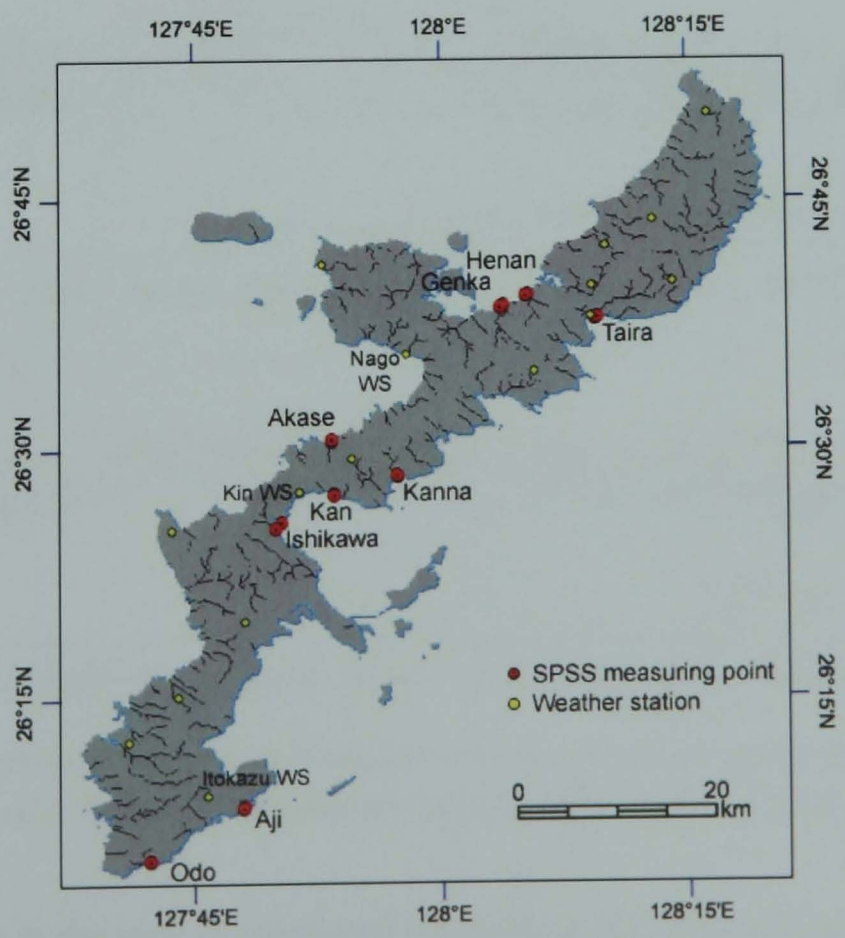

Fig. 5.19. The Suspended Particle in Sea Sediment (SPSS) sampling points around Okinawa. Sampling and measurements are carried out quarterly by the *OPG Institute of Health and Environment*.

The variation of the SPSS from 1995 to 2006 is given in Fig. 5.20. The SPSS in the west and the east are mainly composed of red coloured and highly erodible soil, *Kunigami maji*. For the SPSS in the west (Fig. 5.20a), it has a clear seasonality: high concentration in summer and low concentration in winter. In the east (Fig. 5.20b), such seasonality is not as clear as in the west. The SPSS of Taira is constantly at a high level (> 100 kg/m^3) during 1998 and 1999. This was due to abandoned pineapple fields and heavy rainfall in 1998 (Nakasone et al., 2000). The SPSS of Kanna and Kan is also somewhat higher in these periods. Ishikawa, located in a semi - enclosed bay, shows high levels of the SPSS with less variability. In the south, the SPSS is higher than the west normally, but relatively lower than Taira and Ishikawa in the east. Occasionally, the SPSS of Aji, composed of the highly erodible soil, *Jagaru*, reaches a high level of 100 kg/m^3 (Fig. 5.20c). At the most southern site, Odo, where the lowest erodible soil, *Shimaji maji*, is seen, the SPSS is lower than of Aji. A seasonal pattern is not strong at either site.

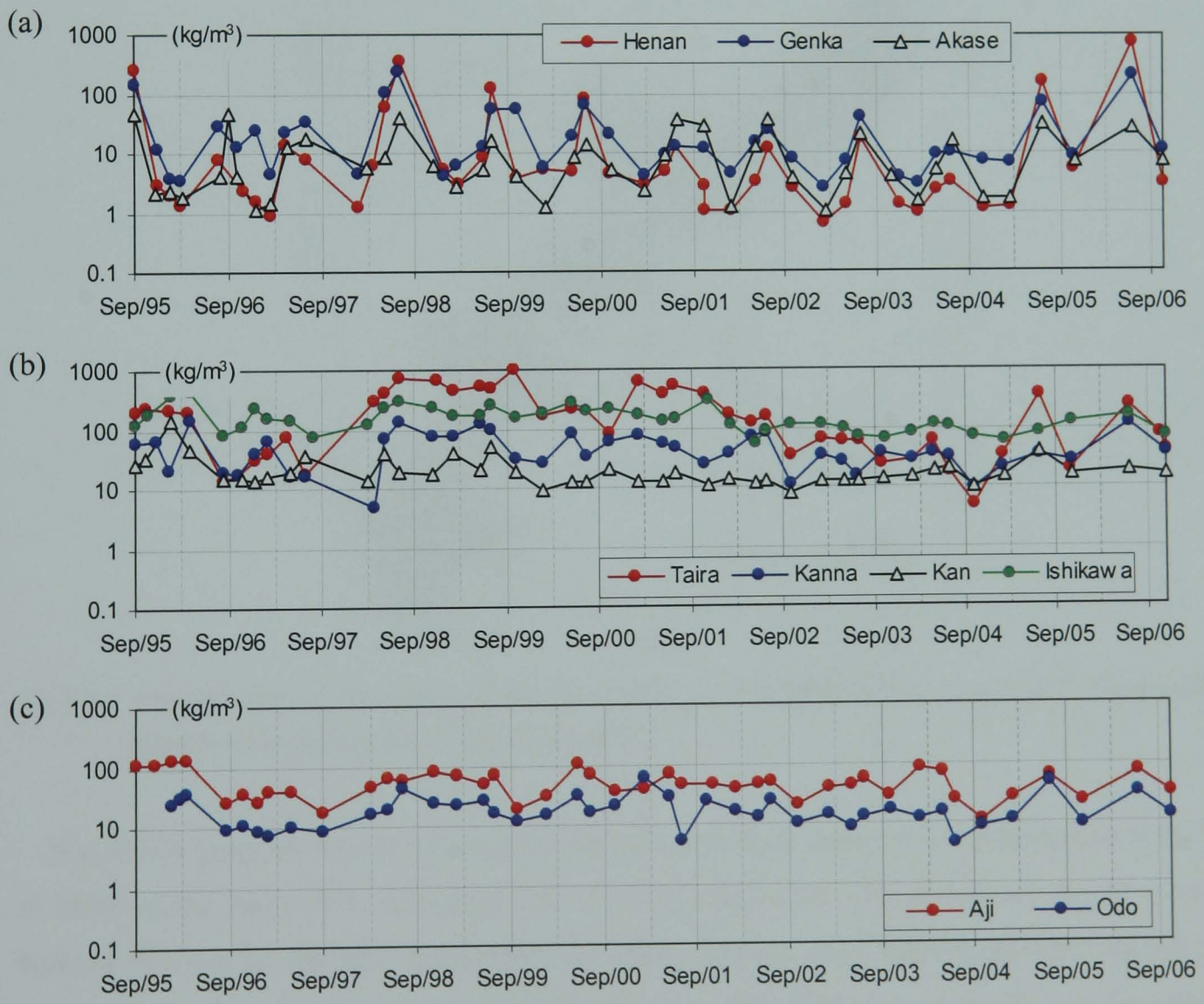

Fig. 5.20. Suspended Particle in Sea Sediment (SPSS) around Okinawa (Fig. 5.19). (a) west coast, (b) east coast and (c) southeast coast. Data are collected and provided by the *OPG Institute of Health and Environment*.

Seasonality seen in the west is considered to be due to the rainy season in summer and the strong northerly in winter (Omija et al., 1992; Nakasone et al., 2000). Although such a clear

seasonal pattern is not visible in the east and the south, Omija et al (2002) calculated that the average SPSS around the entire Island reaches its highest at 46.8 kg/m^3 in summer (MJJA), starts to decrease in fall (SON, 23.7 kg/m^3), drops to its lowest at 15.4 kg/m^3 in winter (DJF), and then starts to increase in spring (MAM, 45.9 kg/m^3).

5.4.3 Monsoon Influences on Sea Sediment around Okinawa

As described in section 5.4.1, if the coastal sediment follows the water moved by Ekman transport, the amount of sediment along the coast will be reduced by the end of the winter EAM. To the west of Okinawa, such an effect can be expected when the wind blows from the northeast, and from the southwest for the east coast (Fig. 5.21).

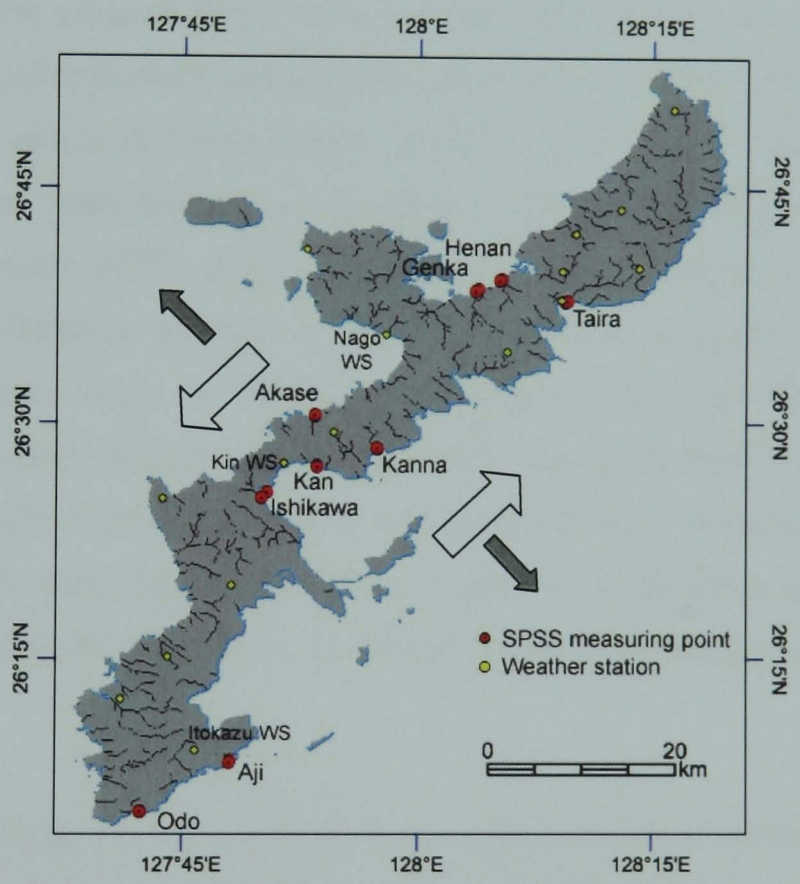

Fig. 5.21. Wind direction (⇨) causing the Ekman transport off shore (➡) which can expectedly resuspend the sediment by upwelling, hence reducing the SPSS.

Fig. 5.22 (a) shows the climatology of the NE wind component speed and rainfall from 1998 to 2006 at the Nago WS. Similarly Fig. 5.22 (b) shows the climatology at the Kin and the Itokazu WS but for the SE wind component speed. On the west side (Nago WS), the NE wind starts to prevail in October, and lasts until February. This is the winter EAM. On the east side (Kin WS), the SW wind blows in June and July. It originates from the summer EAM. Sediment removal by the Ekman transport can be expected from October to February for the west coast, and from June to July for the east coast. However, sediment delivery by soil run-off also occurs during the rainy and typhoon season, June – September. Thereby a decrease of SPSS on the east coast by the SW wind in summer may not occur.

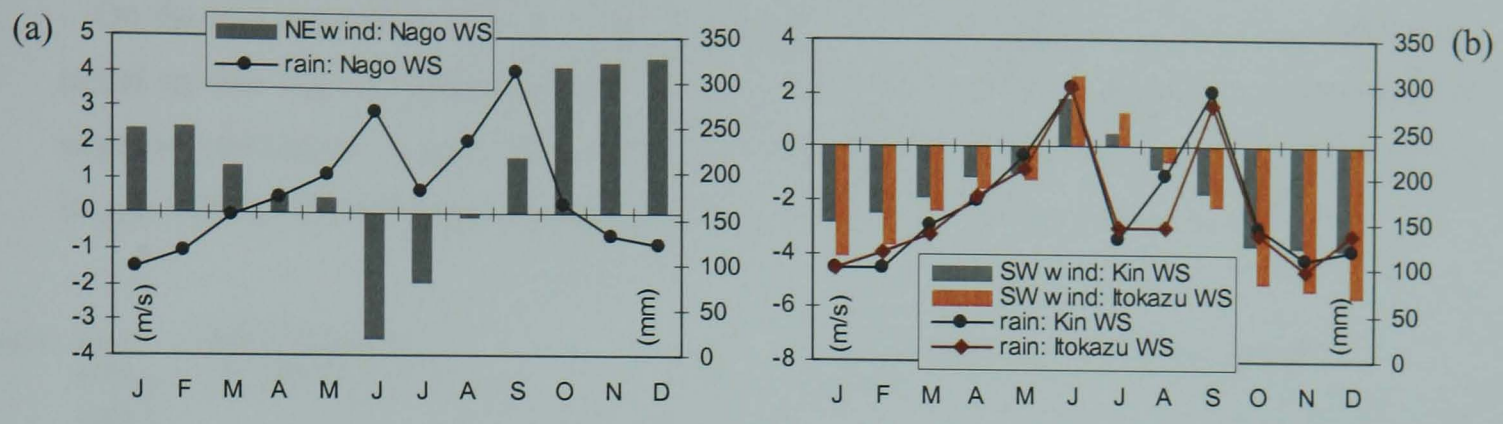

Fig. 5.22. Climatology (1995 – 2006) of wind speed and rainfall. (a) NE wind at the Nago WS and (b) SW wind speed at the Kin WS and the Itokazu WS.

Fig. 5.23 shows a comparison of the difference of the SPSS (ΔSPSS) and the sum of the squared wind speed using daily data. On the west coast, the ΔSPSS is determined by the difference between the summer SPSS and the winter SPSS in the next year. For the summer SPSS, available data after the rainy season (MJ) was chosen i.e. JAS. Since the SPSS sampling in winter is usually carried out from January to February, the winter SPSS was chosen from these months. For the wind, the sum of the squared NE daily wind component ($\sum NE^2$) from November to the winter SPSS sampling month (January or February) in the next year is compared. Because typhoons can still occur in October, the squared wind is summed from November. On the east coast, the ΔSPSS was determined from the difference between the spring month (Apr or May) and the next available date in a month from summer to autumn. The sum of the squared SW wind component is calculated ($\sum SW^2$) during the same period of the ΔSPSS. For the south coast, the Itokazu WS is located at 128 m above sea level which is not appropriate to determine the wind stress for Ekman transport as being too high. Therefore, it is not discussed here.

On the west coast (Fig. 5.23 a1 – a3), the most northern point at Henan shows a significant correlation between ΔSPSS and $\sum NE^2$ ($r = 0.72$, $p = 0.02$), suggesting sediment removal by Ekman transport caused by the winter EAM. At Genka, the highest correlation is obtained in the comparison with the NE wind speed over 5 m/s ($r = 0.59$) but with only a weak statistical significance ($p = 0.07$). At Akase, no significant relationship is observed. Possible reasons for non-correlation are: (1) coastal geographical features e.g., inner bay and shallow tidal flat; (2) a local orographic effect on the wind distribution; and (3) terrestrial conditions where anthropogenic activities are responsible for soil run-off and sediment off the coast that exceeds the natural reduction effect. Actually, Akase is in a small inner bay, less influenced by the outer ocean compared to Henan and Genka where the coast line is relatively open and more directly influenced by the ocean (Nakasone et al., 2000). Henan is likely to be least affected by these complexities, which makes the relationship between the ΔSPSS and $\sum NE^2$ most clear.

On the east coast (Fig. 5.23 b1 – b4), as expected, no statistically significant correlations are found in this region. Although there is not a statistical significance, all the points show a negative correlation. It may suggest that when the SW wind prevails in summer, it brings an increase of the SPSS through rainfall from the summer EAM or typhoons.

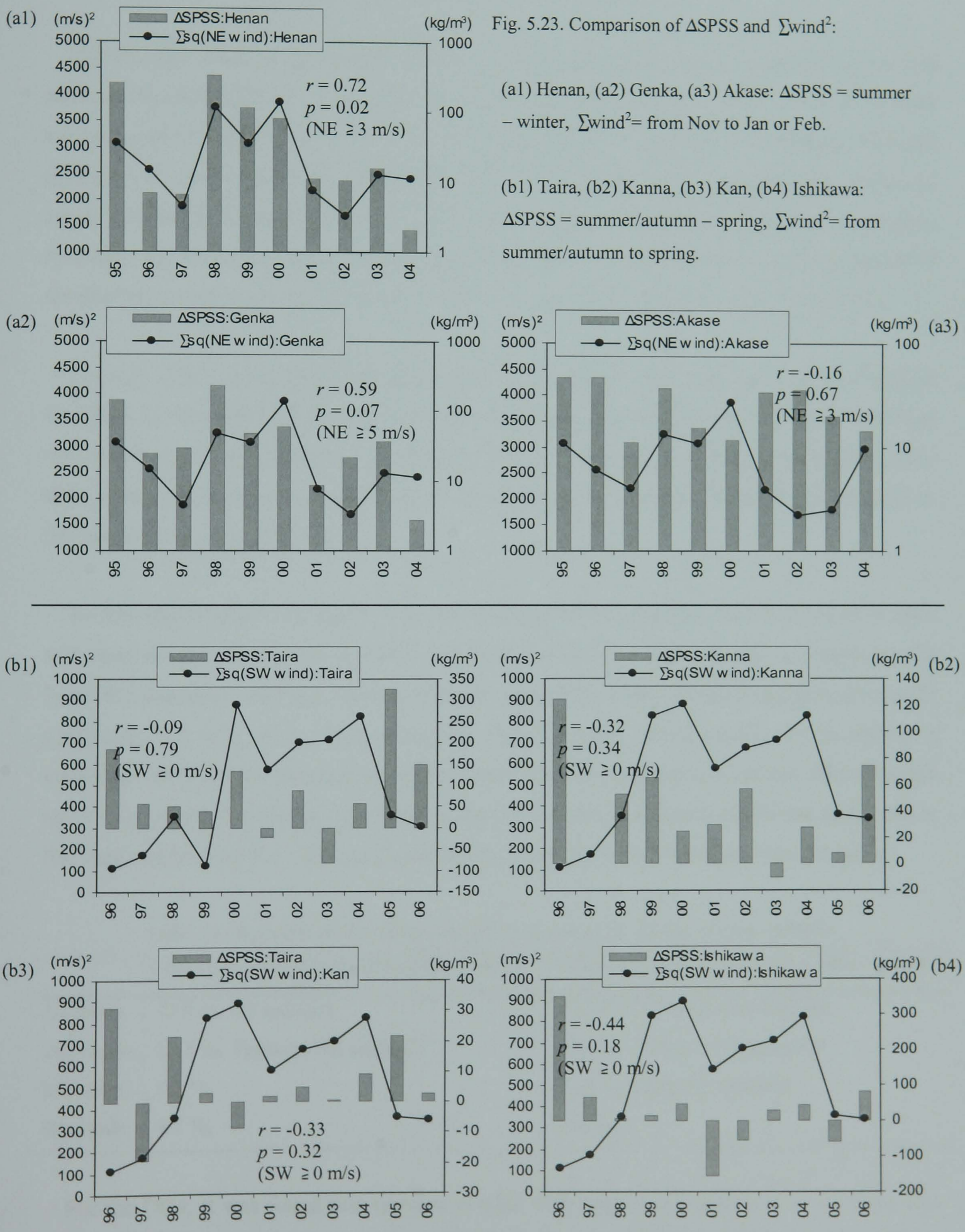

Fig. 5.23. Comparison of ΔSPSS and $\sum wind^2$:

(a1) Henan, (a2) Genka, (a3) Akase: ΔSPSS = summer – winter, $\sum wind^2$= from Nov to Jan or Feb.

(b1) Taira, (b2) Kanna, (b3) Kan, (b4) Ishikawa: ΔSPSS = summer/autumn – spring, $\sum wind^2$= from summer/autumn to spring.

5.5 Summary

This chapter has investigated (1) how much does river run-off contribute to on the OC4 variability as a terrestrial control and (2) how much does typhoon rainfall and wind contribute to the SST/OC4 variability around Okinawa? The relationship between the winter EAM and the sediment variability off the coast of Okinawa was also investigated.

Off the west coast of the Island of Okinawa (W5), terrestrial control appeared as the 2nd mode of the OC4 EOF that correlates with the river discharge, accounting for 9.6 % of the total variance, below the primary control of the winter EAM. Its influence is strongly imposed offshore near the outflow from the largest river of Hija in the Island, indicating the impact of run-off. Although the analysis does not uniquely define the effects of run-off, since sediments, nutrients, and contaminants are potentially confounding variables within run-off, the amount of the discharge itself appears to be a control affecting the OC4 on the west coast of Okinawa.

In a case study of Typhoon Nari that occurred in September 2001 and stayed around Okinawa for about 10 days, the influence of its heavy rainfall was clearly indicated in the OC4 bloom in the estuary of the Hija River by its enhanced run-off. Although typhoons are episodic events, their annual occurrences around the Island are important as typhoons bring extreme impacts to the coastal zone and coral reefs.

To investigate effects of typhoons on the SST and OC4 variability, the SST and OC4 data, with their annual cycles removed were examined. For the SST, the 1st mode indicated that the local SST anomaly is strongly influenced by the variability in the surrounding ocean (Domain2), explaining 72.8 % of the anomalous variance. The 2nd mode, accounting for 12.3 %, showed a correlation with the NE anomaly associated with typhoons, suggesting a cooling effect through upwelling and mixing (Table 5.2). There is therefore a strong influence of climate and ocean at the large scale on the SST, leaving little impact of local terrestrial influence from the Island.

Table 5.2. The Result of EOF analysis on SST/OC4 anomaly in the west coast of Okinawa.

	SST anomaly EOF in W5 (1986 – 2006)	OC4 anomaly EOF in W5 (1998 – 2006)
1st mode	72.8 %, D2 anomaly	42.5 %, Typhoon rain anomaly
2nd mode	12.3 %, Typhoon NE anomaly	31.8 %, Typhoon NE anomaly
3rd mode	8.3 %, –	11.8 %, ORD NE anomaly
4th mode	4.7 %, –	5.5 %, –

For the OC4, it was found that typhoon rainfall is an important control on its anomaly that correlates with the 1st mode, accounting for 42.5 % of the anomalous variance, and typhoon winds (NE component) that cause upwelling are a secondary control, accounting for 31.8 %

(Table 5.2). The NE anomaly during ORD months showed a correlation with the 3rd mode. This result indicates the importance of typhoons on OC4 both directly and through terrestrial feedbacks.

As an important link between the OC4 variability and the winter EAM was found, the relationship between the northeasterlies and the variability of coastal sediments (SPSS) around Okinawa was examined. It was found that the variability of the SPSS on the coast of Okinawa is also affected by both the winter EAM, particularly at Henan on the northwest coast where the winter EAM acts to reduce SPSS. On the east and the south coast on the other hand, the SPSS removal does not occur because the summer EAM has a relatively low wind speed from the appropriate direction (SW) for upwelling to occur.

In the previous chapter, it was described how climatic and oceanographic processes at the large scale influence the SST and OC4 in the East China Sea and the coastal zone around the Island of Okinawa. Under the interaction between atmospheric and terrestrial processes, a local scale effect is also seen through the local events of run-off and coastal upwelling. Given these results, a question can be raised: is there any trend in the winter EAM and rainfall, particularly typhoon-driven extreme winds and rainfall under warming environment that could increase or decrease the impact on coral reefs around Okinawa? In the next chapter, the changes in both wind and rain brought by the EAM and typhoons will be examined, attempting to view future perspectives for the coastal environment of Okinawa.

Chapter 6 Spatial-Temporal Changes in Wind and Rainfall Patterns around Okinawa

6.1 Introduction

The terrestrial influence of Okinawa Island was revealed as a secondary control on the OC4 variability though run-off from the rivers, indicating the influence of rainfall on the coastal environment of Okinawa (Chapter 5, §5.3). It was also found that the winter EAM, a primary control of the OC4 variability along the coast of Okinawa, is responsible for sediment removal by its associated upwelling (Chapter 5, §5.5). Therefore, wind and rainfall are important atmospheric factors over the coastal zone of Okinawa. Given the trend of a globally warming environment in recent years, as reported in the IPCC FAR (Solomon et al., 2007), a question can be raised: Are wind and rainfall around Okinawa increasing or decreasing under climate change, suggesting a possible change in importance of the identified controls? To answer this question, changes in wind (the winter EAM for 1988 – 2005) and rainfall over Okinawa (for 1982 – 2005) will be investigated in this chapter. Under influences of atmospheric and terrestrial controls on the coastal environment, this study will also provide an important understanding of how the coast of Okinawa will likely respond in the future. However, it should be noted that changes in wind and rainfall for the period of this study (24 years) related to global warming is too short to be properly assessed. The result may show only marginal changes compared to a longer-term analysis.

The EAM is an annual event but non-stationary. It is also coupled with a global scale phenomena e.g., El Niño. In this chapter it is shown that intensity of the winter EAM over Okinawa is also affected by the Southern Oscillation Index (§6.2), indicating the coastal environment of Okinawa is coupled with the SOI, but no statistically significant increasing or decreasing trend of the winter EAM was found. The local SST around Okinawa is also affected by El Niño – Southern Oscillation (ENSO), showing a correlation with the SOI. The coral reef around the Island will not only suffer acute stress from high sea temperature brought by a strong El Niño, such as in 1997/98, but also a weak winter EAM, which coincided with this El Niño, will leave more sediment in place leading to a combined impact on the coral reefs around Okinawa.

In order to investigate changes in rainfall, probability distribution functions (PDF) of daily rainfall data in Okinawa (1982 – 2005) were used. An increasing trend of strong typhoon occurrence in the Pacific Ocean has been reported (Webster et al., 2005). The number of strong

typhoons approaching Okinawa (1982 – 2005) was also analysed (§6.5). In addition to this rainfall change analysis, spatial distribution of these changes over the Island was investigated.

In this chapter, the impact of typhoon will be discussed. Although typhoons and heavy rainfall are episodic events, lack of appropriate land management may delay natural recovery of the coastal ecosystem around the Island of Okinawa, degrade its resilience, and lead to permanent change into a barren marine environment.

Data used in this chapter and their temporal coverage are given in Fig. 6.1. The latest year of the data is aligned to the rainfall data coverage (1982 – 2005) recorded by the Okinawa General Bureau which is used for an investigation of rainfall distribution over the Island. Typhoon data include the track and intensity. While this period is relatively short it covers a time of regional climate parameters in many places around the world (Solomon et al., 2007).

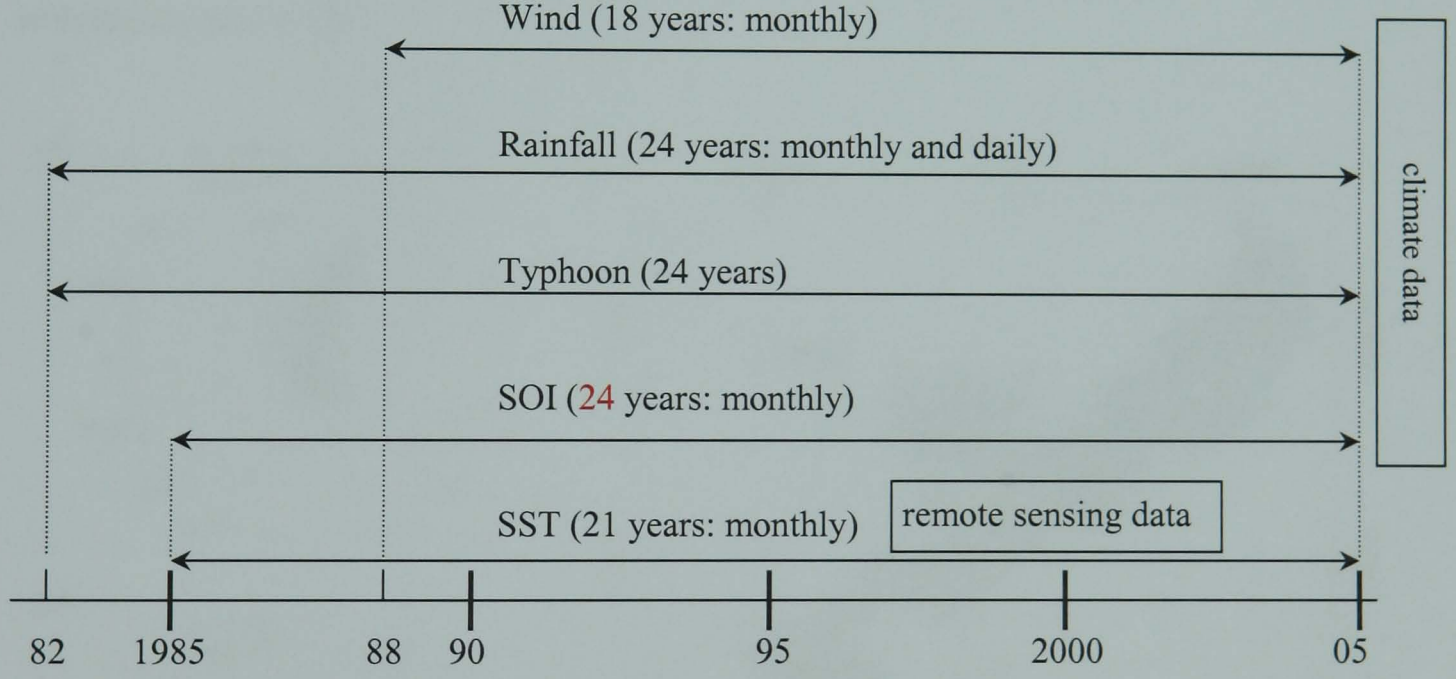

Fig. 6.1. Data used in this chapter and their temporal coverage. The latest year of the data is aligned to the rainfall data recorded by the Okinawa General Bureau which are available until 2005.

6.2 The Winter East Asian Monsoon in Okinawa

It was found in §5.3 that the winter East Asian Monsoon (EAM) is a major control on the OC4 variability and responsible for sediment removal along the western coast of Okinawa through associated upwelling. Changes in the winter EAM will thus affect the status of the coastal zone around Okinawa, so it is important to investigate its trend in considering the possible future for the coastal environment of Okinawa.

The winter EAM, accompanied by a strong Siberian high and active cold surges, is among one of the most energetic monsoon circulation systems (Zhang et al., 1997). It is also known that the EAM is linked to El Niño – Southern Oscillation (ENSO) (e.g., Lau and Chang, 1987; Li, 1990). Zhang et al. (1997) showed that strong winter wind seasons are associated with La Niña and high Southern Oscillation Index (SOI) years, and weak wind seasons are associated with El Niño and low SOI years. Therefore, changes in the SOI will affect the winter EAM, and hence affect the coast of Okinawa. To quantify the winter EAM variability in Okinawa, firstly the direction of the most frequent winter EAM was determined at the Nago WS (6.1 m above sea level) and the Naha WS (28.1 m above sea level). Secondly, the relationship of their DJF values with the SOI, and associated trends, were examined. Fig. 6.2 shows the wind rose for 1988 – 2005 measured at Nago and Naha. Data used in the wind rose are the direction for which maximum wind speed (maximum of the 10 minutes-averaged) occurred on each day. Both WS records indicate that the most frequent wind is northerly, NNE at Nago and N at Naha, originating in the winter EAM. The secondary but more directionally broad peak is associated with the summer EAM.

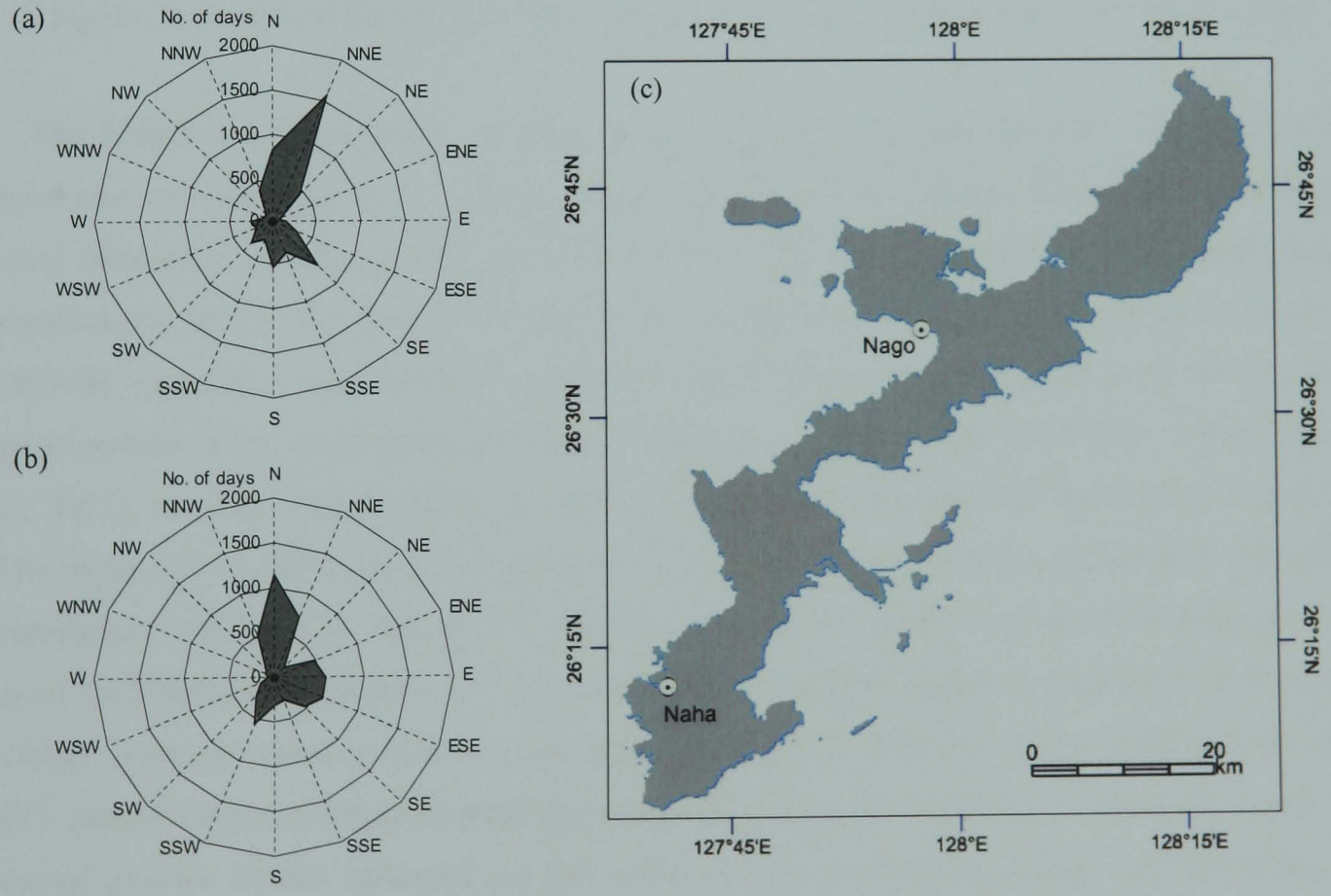

Fig. 6.2. Wind rose (1988 – 2005) in. (a) Nago WS, (b) Naha WS and (c) their location. Wind measurement points of both WS were moved in 1987, therefore the data after 1988 was used.

During the period of 1988 – 2005, both NNE at Nago and N at Naha showed a statistically significant correlation with the SOI (DJF), suggesting that the coastal environment of Okinawa is coupled with the SOI (Fig. 6.3). In low SOI years, the winter EAM over Okinawa becomes weak and vice versa. It means a major control of sediment removal along the coast of Okinawa

will be less (more) influential in low (high) SOI seasons. A linear trend fitted to the data of the SOI, NNE at Nago and N at Naha for 1988 – 2005 showed no significant trend. It suggests that no change in the contribution of a primary control for the OC4 variability and sediment removal has been occurring in Okinawa during this period. But the variability due to ENSO is dominant.

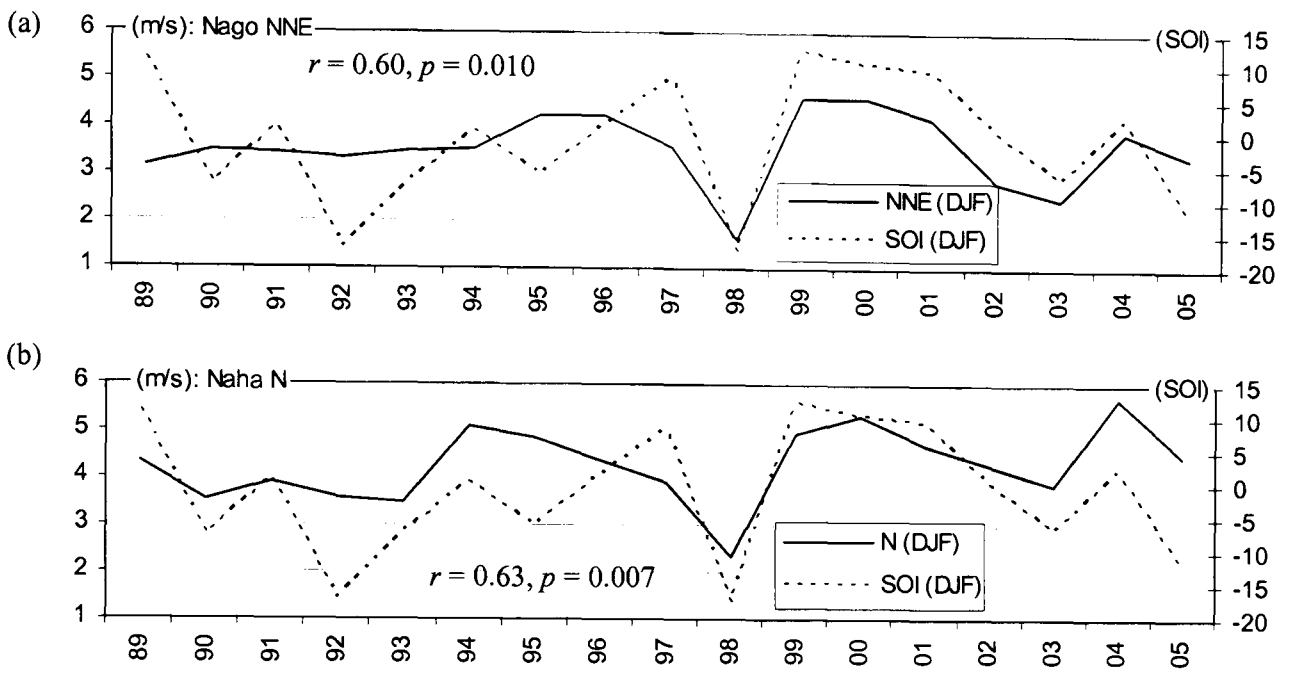

Fig. 6.3. The local northerlies in Okinawa and the SOI for (a) NNE winds at Nago and (b) N winds at Naha.

The ENSO is a phenomenon centred in the tropical Pacific, and therefore significant to the coral reef environment in the tropical and subtropical Pacific Ocean. For example, extensive coral bleaching associated with the 1982/83 El Niño was attributed to water temperatures significantly above the normal average high temperature range (Glynn, 1993). El Niño in 1997/98 triggered a wide range of coral bleaching around the world (Wilkinson, 2001), and a great portion of the coral coverage around Okinawa was diminished (Yamazato, 1999; Loya et al., 2001). A relationship between the SST around Okinawa and the SOI can be given in Fig. 6.4. The mean SST in Domain 2 (D2 defined in Chapter 4, § 4.4) shows a statistically significant correlation with the SOI, lagged by 5 months ($r = 0.17$, $p = 0.007$), and the SST along the west coast (W5 defined in Chapter 5, § 5.3) also shows a 5-month lagged correlation ($r = 0.14$, $p = 0.029$). Although these correlations are weak, it shows an influence of the ENSO on the local SST around Okinawa likely through the north equatorial and Kuroshio Currents. In Fig. 6.3 is shown another ENSO influence on the winter EAM, particularly during 1997/98 when the strong El Niño led to a significant decrease in the winter EAM. The results here suggest that ENSO also has an effect on the coral reef environment through altering atmospheric forcing. El Niño in 1997/98, which triggered acute stress on corals through high sea temperature, appeared to weaken the winter EAM, reduce its effect on sediment removal, and hence imposed a combined stress on coral reefs around Okinawa.

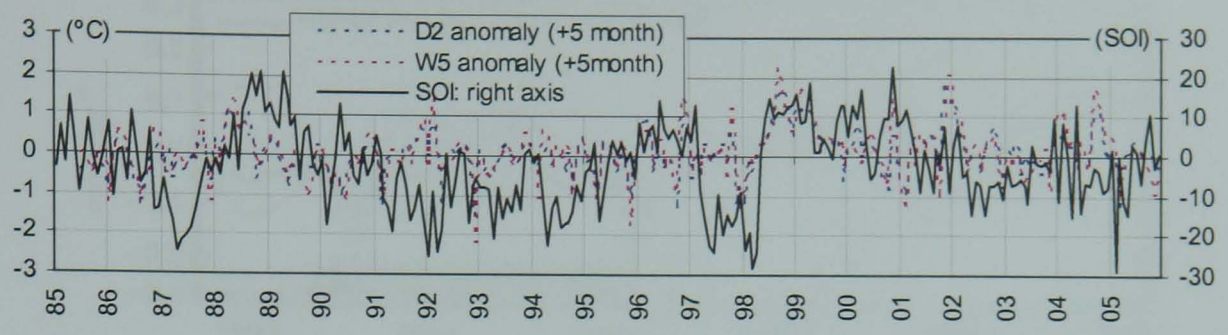

Fig. 6.4. The SST anomalies in D2 and W5 and the SOI (1985 – 2005).

6.3 Rainfall in the Tropical Region

Is rainfall increasing? Sine the 1990s, studies have reported increasing rainfall in some areas, apparently due to global warming (e.g., Houghton et al., 1990; Hennessy, 1997). In the Islands of Japan during 1998 – 2004, the frequency of extreme high rainfall has been higher than the frequency of extreme low rainfall (Japan Meteorological Agency, 2005). If rainfall over the Island of Okinawa shows an increasing trend, the terrestrial influence on the coastal zone may also be increasing, which would increase the importance of a secondary control on the OC4 variability discussed in the previous chapter. If heavy rainfall is a driver for an increasing trend, soil erosion and run-off will be greatly enhanced and the impact on the coastal zone will be stronger. Therefore, it is of importance to investigate changes in rainfall over Okinawa. The trend of rainfall in the tropical region generally and in Okinawa specifically will be discussed in this section and the next section, respectively.

6.3.1 Trend in the Tropical Region

Gu et al. (2007) examined tropical rainfall variations using the Global Precipitation Climatology Project (GPCP) monthly dataset from 1979 to 2005. GPCP is an analysis of global precipitation under the support of the World Climate Research Programme from 1979 to the present. The data are produced over a global 2.5° × 2.5° grid from a merged analysis that incorporates precipitation estimates from satellite microwave data, satellite infrared data and surface rain gauges (Adler et al., 2003). Although the global linear change of precipitation in the dataset is near zero during the time period they investigated, an increase in tropical rainfall was observed. Fig. 6.5 shows the result from Gu et al. (2007) focusing on the tropical region (25 °S – 25 °N). It indicated an upward linear trend (0.06 mm/day/decade) over the oceans, with a 99 % confidence level. There was a downward linear trend (-0.01 mm/day/decade) over land, though it was not statistically significant (about 88 % confidence level). However, over the whole tropical band, the rainfall showed an upward trend (0.04 mm/day/decade) which reached to the 98 % confidence level (Gu et al., 2007).

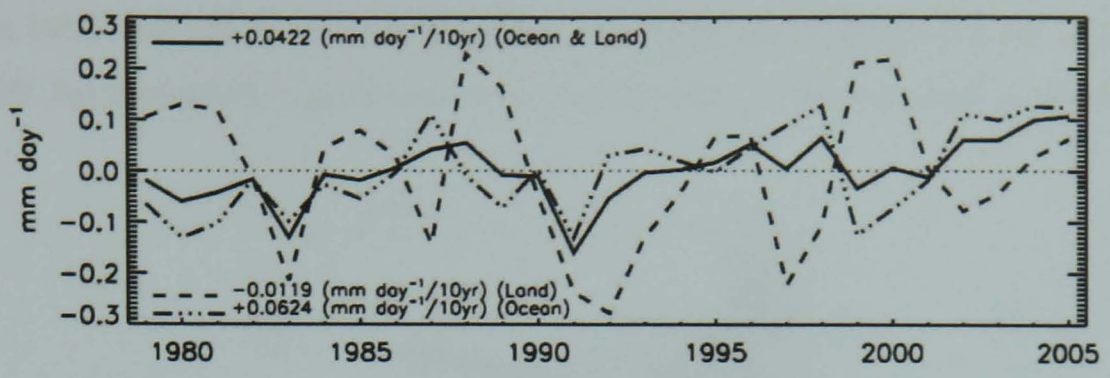

Fig. 6.5. Rainfall anomaly trend in the tropical region 25 °S – 25 °N (adapted from Gu et al., 2007).

A possible cause of this increase in the tropical rainfall is that there is an intensifying hydrological cycle in the tropical region given a warming environment (e.g., Yang et al., 2003; Wentz et al., 2007). During the last 50 years, SST over the tropical oceans has been increasing, which is likely to influence the atmospheric circulation (Kumar et al., 2004). Kumar et al. (2004) explained that warmer SST will lead to an increase in evaporation, thereby an increase in precipitation, however, an increased hydrological cycle does not necessarily imply that all regions will experience an increased rainfall because an increased precipitation and associated vertical mass transport over one region has to be balanced by more descending motion in other regions, leading to a reduction in rainfall.

In the case of the Island of Okinawa, it is located at 26 °N, just outside the study band of Gu et al. (2007). In the Third Assessment Report (TAR) of the Intergovernmental Panel on Climate Change (IPCC), it was reported that rainfall has increased by 0.5 % per decade over most mid and high latitudes of the Northern Hemisphere over the 20th century but it has decreased in sub-tropical (10 °N – 30 °N) land areas by about 0.3 % per decade (Houghton et al., 2001). However, Okinawa is a small island in the western North Pacific Ocean. Rainfall may be in an upward trend because of a greater influence from ocean. Or it may possibly show no significant trend, just fluctuating in the balancing of rainfall variation between the tropical and sub-tropical regions.

6.4 Rainfall in Okinawa

6.4.1 Changes in Monthly and Annual Rainfall

To investigate the rainfall variability in Okinawa, 14 WS daily records were used (Fig. 6.6). Some of the WS moved their rain gauges in 1981. To homogenise the dataset, a 24-year dataset (1982 – 2005) was used. Fig. 6.7 shows the variability of the averaged rainfall of the 14 WS, (a) the monthly rainfall, (b) rainy season (Baiu), MJ mean and (c) annual rainfall. The monthly rainfall often shows pronounced peaks because of typhoon events. For MJ (Baiu), an oscillating pattern can be seen about every 3 – 4 years after 1994. For annual rainfall, the wettest year

occurred in 1998 with 165 % of the mean value. A similar, but slightly reduced, peak was also seen in 2000. No statistically significant trend was obtained for these rainfalls or for each WS.

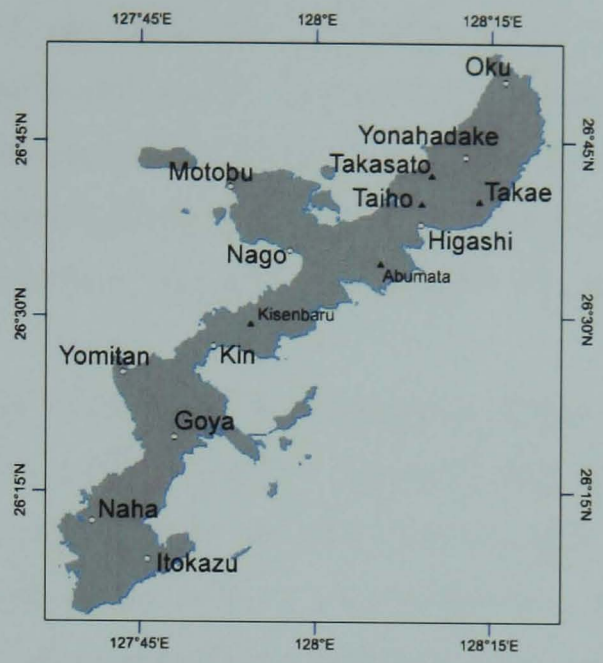

Fig. 6.6. The 14 weather stations (WS) used for rainfall analysis in Okinawa for 1982 – 2005. The WS are operated by the Japan Meteorological Agency (○: JMA) and the Okinawa General Bureau (▲: OGB).

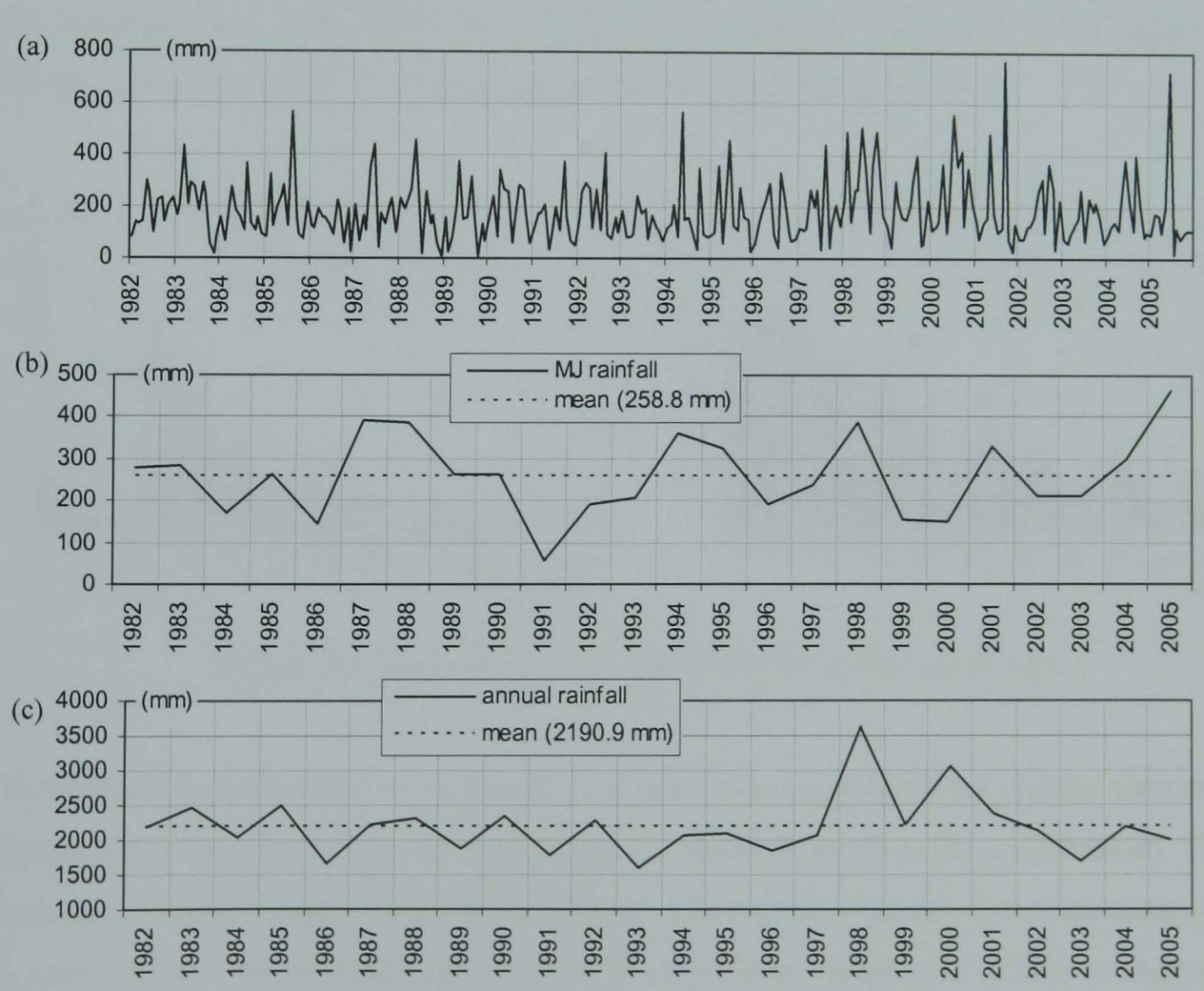

Fig. 6.7. Rainfall (1982– 2005) averaged of 14 WS in Okinawa. (a) monthly, (b) MJ mean rain and (c) annual.

It is worth noted that annual rainfall is correlated with annual mean air temperature at Naha (r = 0.54, $p < 0.01$) and Oku (r = 0.61, $p < 0.01$). This suggests that the annual rainfall over Okinawa may increase along with the warming scenario (Solomon et al., 2007).

6.4.2 Probability Distribution Function of Rainfall

Major environmental events on Okinawa are episodic e.g., typhoons. So there may be a change in the frequency distribution of associated events, particularly heavy rainfall. Although there is no significant trend seen in the MJ and annual rainfall in Okinawa, it is possible to investigate trends according to the rainfall intensity using a probability distribution function (PDF). Here, the analysis is based on the premise that a trend in rainfall PDF associated with changing rainfall characteristics is likely to be more sensitive to the change at a larger scale than the total rainfall, and would be more detectable (Lau and Wu, 2007).

To create the rainfall PDF of Okinawa, the probability of rainfall according to its intensity (mm/day) was calculated for 1982 – 2005. The number of days was counted according to the rainfall intensity by a 1 mm/day interval. Dividing these data by the total days of the period 1982 – 2005 yields the probability of a particular daily intensity, or the frequency of occurrence (FOC). Multiplying the number of days by the rainfall intensities gives the accumulated rainfall amount (ARA) for that intensity. By these processes, PDFs for FOC and ARA can be obtained. Averaging the data of the 14 WS (Fig. 6.6), the climatological PDF for (a) FOC and (b) ARA were obtained (Fig. 6.8). The FOC shows an exponential distribution. The highest FOC (25.0 %) is achieved by 0 – 1 mm/day rainfall (0 mm/day not included).

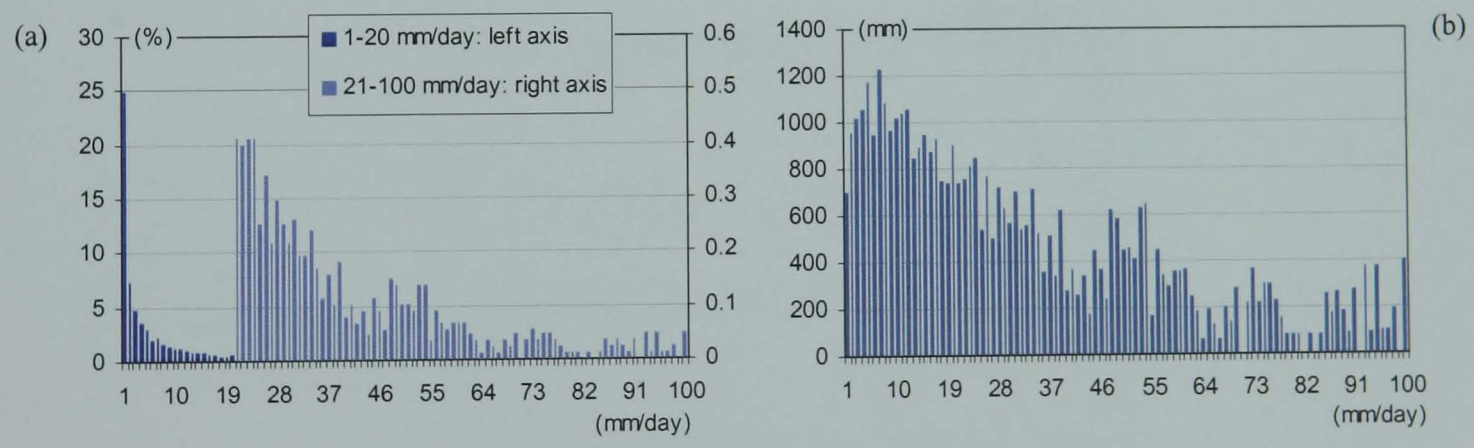

Fig. 6.8. The climatological (1982 – 2005) PDF for (a) FOC and (b) ARA.

The ARA shows that the 2 – 12 mm/day rainfall range contributes the highest amount (> 900 mm for each band), indicating that light rainfall contributes most to the total amount. The ARA decreases relatively linearly until 44 mm/day (~ 174 mm in amount), but it increases again (> 400 mm) for 48 – 54 mm/day ranges as the FOC in these ranges also shows a small increase. ARA decreases again until 67 mm/day (~ 67 mm). There is a small increase (> 200 mm) for 72 – 77 mm/day as well as a similar rise in the FOC in these intensities. Since the impact of very heavy rainfall over 90 mm/day is significant, a few occurrences yield over a few hundred mm of rainfall.

6.4.3 Trend and Spatial Distribution of the Rainfall

Considering the yearly PDF of FOC and the accumulated rain amount for each of 24 years (1982 – 2005), linear regressions can be calculated for each intensity, and hence the trend can be obtained. Fig.6.9 shows the results, namely, the trend of (a) FOC, (b) same as in (a) except being normalised by the mean in each rain rate and (c) ARA. Trends with a confidence level > 95 % are presented in red coloured bars. For the FOC trend, a statistically significant decreasing trend is seen in 3 of the light to mid-heavy rainfall intensities and an increasing trend in 2 heavy rainfall intensities (Fig. 6.9a). Although statistically significant trends occur sporadically with the 1 mm/day resolution, combining rainfall intensities may provide stronger signals.

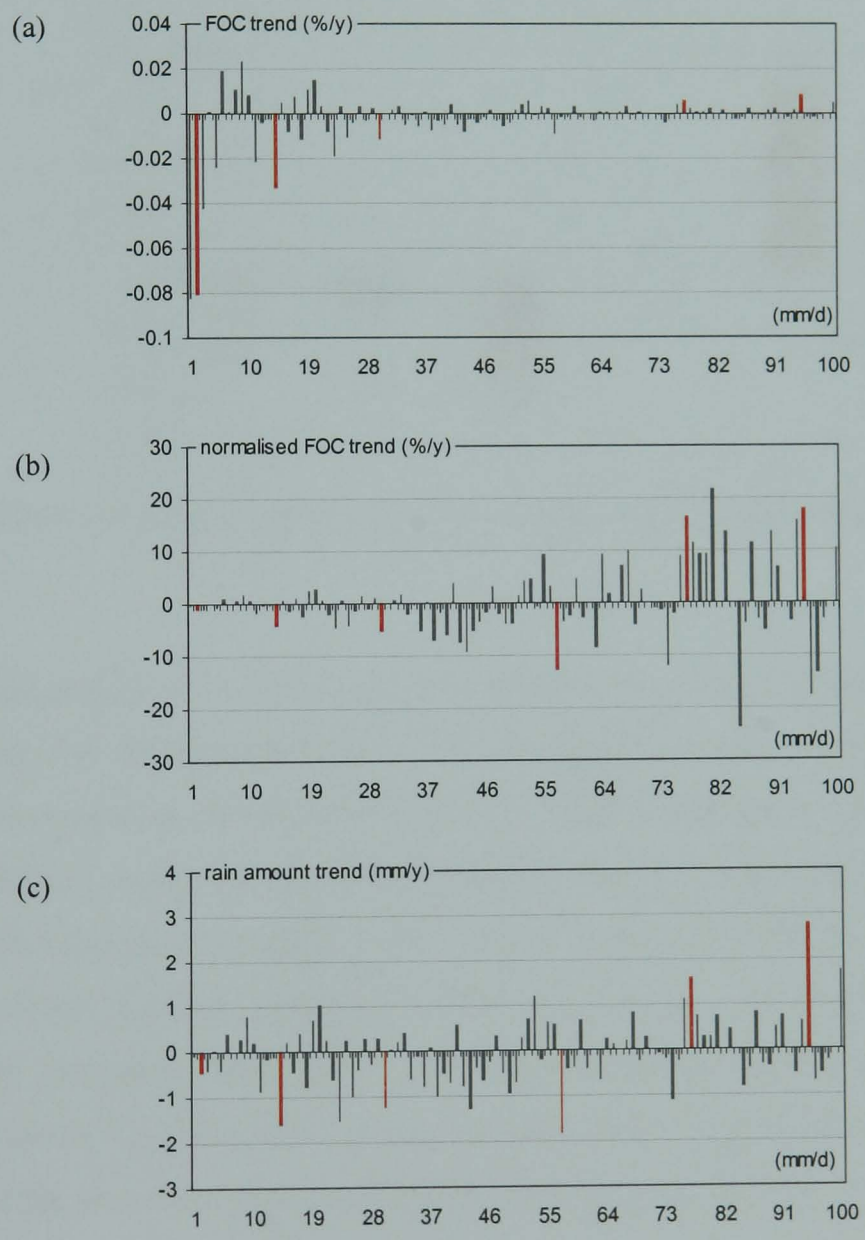

Fig. 6.9. Linear trend of (a) FOC, (b) normalised FOC and (c) ARA. The red bars with confidence level > 95 %.

By clustering the rainfall intensity into 5 ranges: 0 – 3 mm/day, 4 – 25 mm/day, 26 – 50 mm/day, 51 – 75 mm/day, and > 75 mm/day (Fig. 6.10), three rainfall ranges of light rainfall (0 – 3 mm/day), mid-heavy rainfall (26 – 50 mm/day) and heavy rainfall (> 75 mm/day) show trends with a statistical significance > 95 % (Fig. 5.10) both in FOC (Fig. 6.10a) and ARA (Fig. 6.10b). The FOC indicates that light and mid-heavy rainfall are decreasing at a greater rate than the increasing rate heavy rainfall (Fig. 6.10a). In contrast, in the trend of ARA, heavy rainfall

has the largest increasing trend compared to decreasing trends of light and mid-heavy rainfall (Fig. 6.10b). It indicates the significance of high intensity rainfall on the rainfall amount.

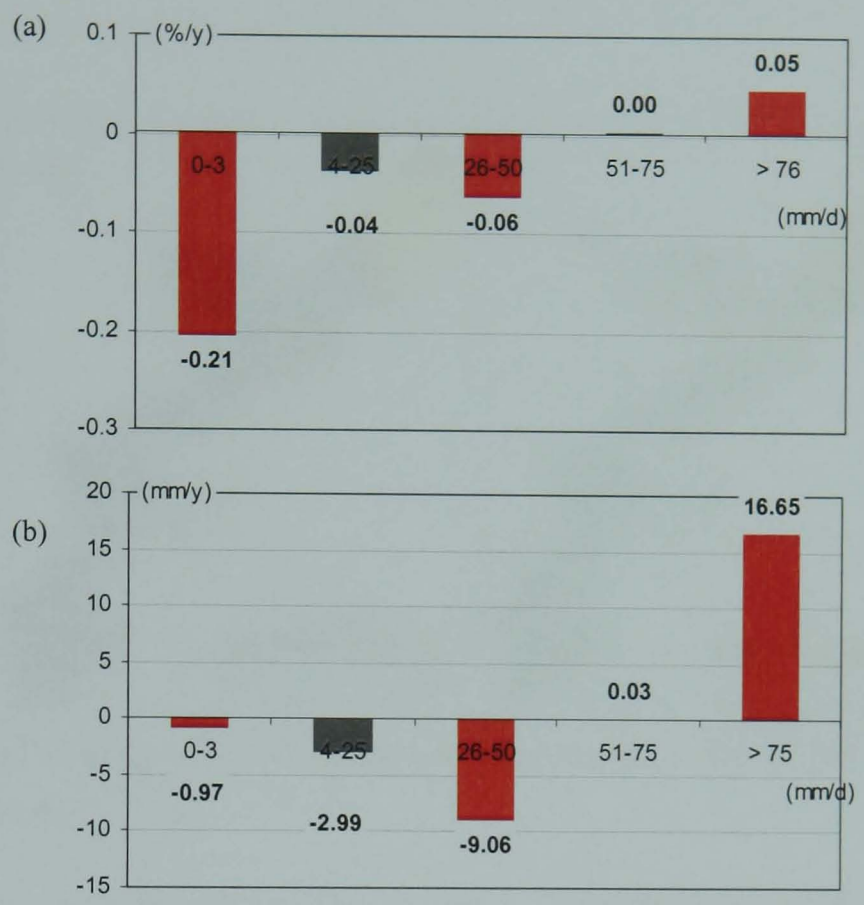

Fig. 6.10. Linear trend in the clustered rainfall for (a) FOC and (b) ARA. The red bars indicate statistical significance > 95 %.

Whether a decreasing or an increasing trend occurs, knowing their geographical distribution is important e.g., for understanding the likely occurrence of soil run-off, flood and landslide. Particularly, heavy rainfall will potentially have a notable influence on the coastal environment, enhancing terrestrial control on the OC4 variability. Fig. 6.11 shows (a) the spatial distribution of the climatological annual rainfall (1982 – 2005) using the 14 WS and (b) the topography of the Island. It is clear that high rainfall (> 2500 mm/y) occurs over the high elevation region in the north due to orographic enhancement. The mid-east coast also receives high rainfall. This is because the summer EAM blows from the southeast and brings moist air which interacts with the east side of the mountain ridge, thus giving more rainfall than the west side. The difference between the highest and the lowest rainfall seen in the west and the south is about 1200 mm/year.

Fig. 6.12 shows the spatial distribution of FOC for clustered rainfall intensity (a) light rain (0 – 3 mm/day), (b) mid-heavy rain (26 – 50 mm/day) and (c) heavy rain (> 75 mm/day). As seen in the climatological rain distribution (Fig. 6.11), mid-heavy and heavy rain occur more often in the north and the east of Okinawa (Fig. 6.12 (b) and (c), respectively). For heavy rainfall, other high FOC (~ 1.4 %) regions are seen not only in the north and the east but also in the mid-south

of the Island. Interestingly, the light rainfall FOC shows a different distribution from the climatology and other rain types (Fig. 6.12a). Its highest frequency (> 18 %) occurs in the mid-north region of the Island. The second highest FOC (~ 17 %) regions are seen in the southwest of the Island.

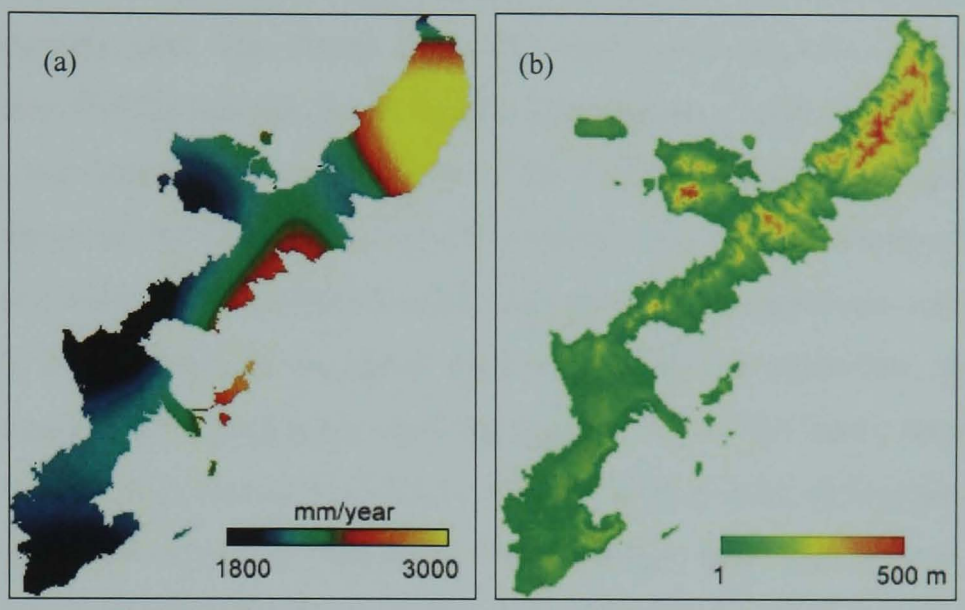

Fig. 6.11. (a) spatial distribution (spline fitting applied) of the climatological rainfall (1982 – 2005) in Okinawa and (b) topography.

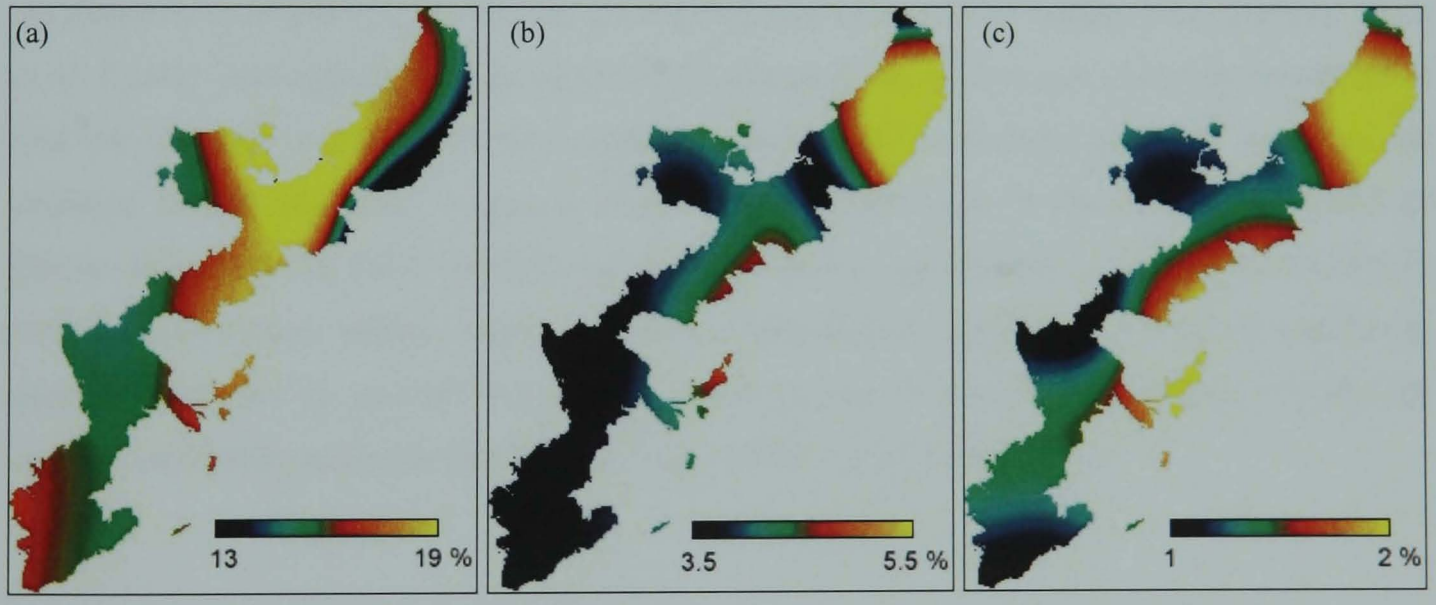

Fig. 6.12. Spatial distribution (spline fitting applied) of rainfall FOC in Okinawa. (a) light rain (0 – 3 mm/day), (b) mid-heavy rain (26 – 50 mm/day) and (c) heavy rain (> 75 mm/day).

In the analysis of the tropical region by Gu et al. (2007), the rainfall over land showed a decreasing trend without statistical significance but the rainfall over the ocean, and the total (ocean plus land), showed a significant increasing trend. It was not statistically clear if the rainfall in Okinawa was increasing or decreasing until the rainfall was classified according to its intensity.

6.5 Changes in Typhoons affecting Okinawa

Using a PDF for GPCP rain data during the period 1979 – 2003 over tropical and sub-tropical region (30 °S – 30 °N), Lau and Wu (2007) indicated that there is an increasing trend in the FOC of light (< 1 mm/day) and heavy rainfall (> 20 mm/day) and a decreasing trend in the FOC of intermediate rain (4 – 14 mm/day). Light rainfall was found mainly over the tropical oceans. Intermediate intensity rain was found over the warm pool regions and the Intertropical Convergence Zone (ITCZ) and the South Pacific Convergence Zone (SPCZ) adjacent regions, and heavy rain was seen in the cores of the ITCZ and the SPCZ. They speculated that the increased light rain over the large regions in the tropical ocean induces a reduction in cloudiness, which increases cooling by loss of heat to space. For the tropical region as a whole, an increased cooling needs to be balanced by increased condensation heating elsewhere, most probably in moisture convergence and topographic uplifting regions, hence the heavy rainfall increases in the ITCZ and the SPCZ (Lau and Wu, 2007). The ITCZ is an area of low pressure where the Northeast Trade Winds meet the Southeast Trade Winds near the equator. As the winds converge, moist air is forced upward. It causes water vapour to condense, resulting in a band of heavy precipitation. This band moves seasonally, being drawn toward the most intense solar heating area or the warmest surface temperatures. It moves north during the high-sun season of the northern hemisphere and south during the high-sun season in the southern hemisphere. Chen et al. (2004) investigated the role of the ITCZ and tropical cyclones in monsoon precipitation over the east Asia and western Pacific regions, and pointed out that monsoon rain revival in the southern part of east Asia is caused either by tropical cyclones or the ITCZ. The Island of Okinawa is located at about 26 °N in the western Pacific, thus influence of the ITCZ itself may be indirect and small. Rather, tropical cyclones (typhoons) are most likely associated with heavy rainfall. Analyses on rainfall will be continued in this section by classifying rainfall into ordinary and typhoon-driven rainfall, and their trends will be investigated.

6.5.1 Probability Distribution Function of Ordinary and Typhoon Rainfall

Rainfall from typhoons was determined using daily rainfall data averaged over the 14 WS in Okinawa during 1982 – 2005 (Fig. 6.6) and using typhoon track data. Generally, relatively small rainfall events occur a few days before and after the peak rainfall event as typhoons come close to the Island and then depart. Therefore, rainfall 2 – 3 days before and after the rainfall peak during a typhoon's approach was classified as typhoon rainfall. This typhoon rainfall is further classified according to the distance between the typhoon centre and the Island: rainfall from typhoons that approached within 300 km of the Island (typhoon rainfall < 300 km: TR300) and from typhoons in the 300 – 600 km range (TR600) from the Island (see Chapter 5 §5.3.2). Typhoons further than 600 km from the Island are likely to be less influential, and thus are not

classified as yielding typhoon rainfall. Subtracting typhoon rainfall from all the rainfall data, the remaining will be classified as ordinary rainfall (OR) here.

Using the daily rainfall data averaged over the 14 WS, the PDFs for FOC and ARA of OR, TR300 and TR600 during 1982 – 2005 are shown in Fig. 6.13, 6.14 and 6.15, respectively. Total rainfall events are 6356 days and total rainfall amount is about 52.7 m. Most rainfall events are from OR (92.4 %) and they contribute 77.4 % to the total amount of rainfall. Typhoon rainfall events occupy only 7.6 % (FOC of TR300 + TR600) of all rainfall events, but their amounts provide 22.6 % of rainfall over Okinawa. The PDF of OR FOC (Fig. 6.13a) indicates that light rainfall (< 10 mm/day) events are the most frequent, and make up most of the OR amount (Fig. 6.13b).

The PDF of TR300 FOC (Fig. 6.14a) shows that occurrence of all the rainfall intensities is lower than 0.2 % and the FOC distribution is relatively skewed to higher rainfall intensity compared to OR FOC. The PDF of TR300 ARA (Fig. 6.14b) shows the low contribution of light rainfall (0 – 10 mm/day) and relatively constant contribution of heavy rainfall (> 50 mm/day). It shows the significance of heavy rainfall from typhoons that can influence the rainfall amount to a greater extent with a small number of occurrences.

The PDF of TR600 FOC (Fig. 6.15a) shows the high frequency in light rainfall similar to the FOC distribution of OR and the low frequency in heavy rainfall compared to TR300. The total occurrence of TR600 is 3.3 % (Fig. 6.15b), just 1 % lower than the total of TR300 events (4.3 %), but the total of TR600 accumulated amount is 4.0 %, significantly lower than that of TR300 (18.6 %). Thus typhoon rainfall can be more clearly represented by TR300, using OR and TR300 will better provide a difference in changes in ordinary and typhoon rainfall over time. Therefore, OR and TR300 will be used and compared in the analysis here.

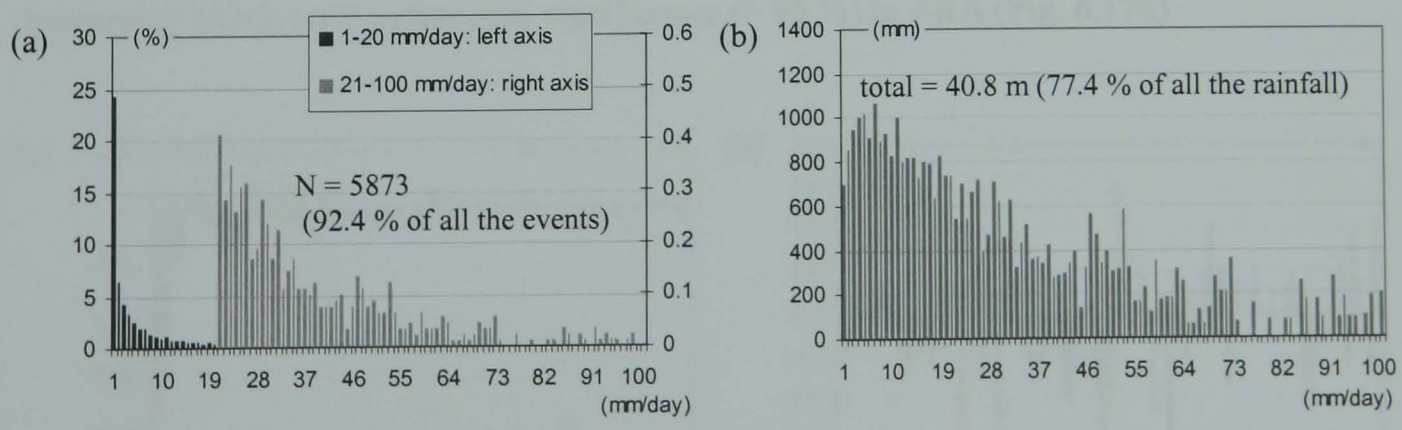

Fig. 6.13. PDFs during 1982 – 2005 of OR for (a) FOC and (b) ARA.

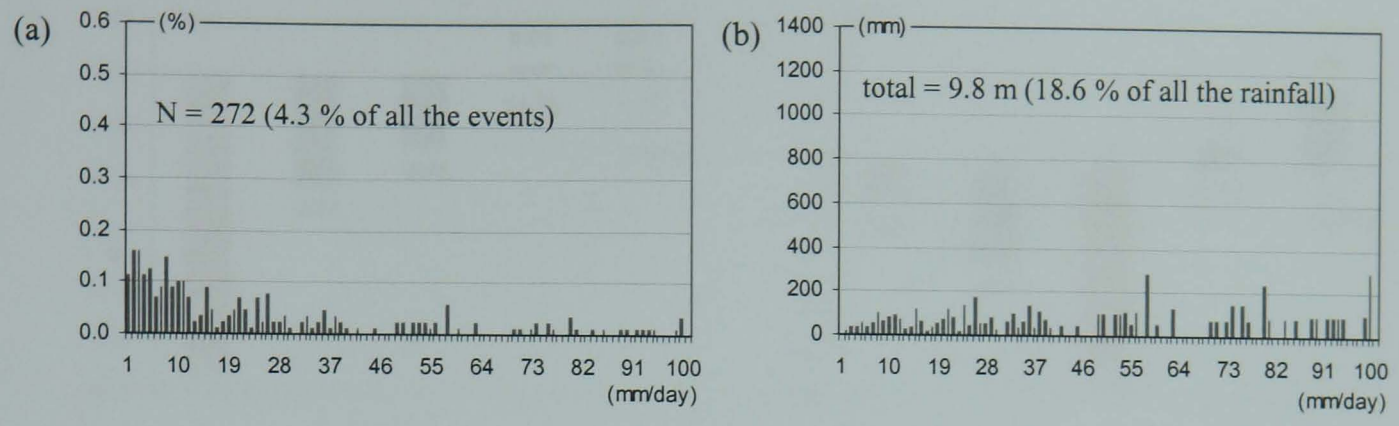

Fig. 6.14. PDFs during 1982 – 2005 of TR300 for (a) FOC and (b) ARA.

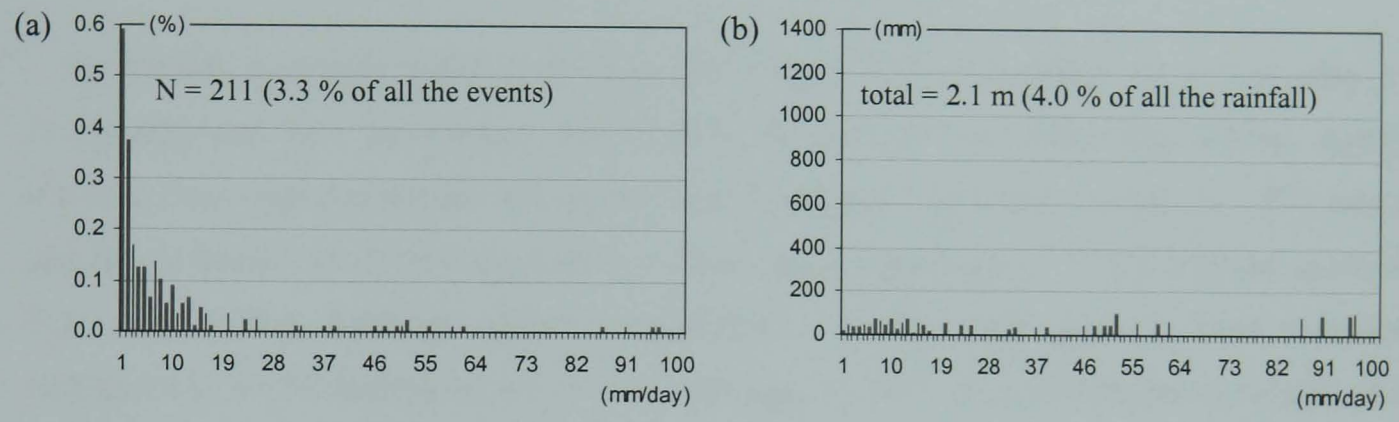

Fig. 6.15. PDFs during 1982 – 2005 of TR600 for (a) FOC and (b) ARA.

In order to investigate trends in FOC and ARA for OR and TR300, linear trends of FOC and ARA over 1982 – 2005 were calculated by creating PDFs for each year. Fig. 6.16 shows the result of the trend of OR. The red and blue bars indicate a statistical significance > 95 % and > 94 %, respectively. A decreasing trend appears in light rainfall (1 – 2 mm/day) and moderate rainfall (22 – 23 mm/day) both in FOC (Fig. 6.16a) and ARA (Fig. 6.16b). There is an increasing trend in heavy rainfall (51 – 52 mm/day) in both FOC and ARA, but a weak statistical significance. These signals were made clearer by clustering the rainfall intensity into 5 ranges: 0 – 3 mm/day, 4 – 25 mm/day, 26 – 50 mm/day, 51 – 75 mm/day, and > 75 mm/day. Two ranges, light (0 – 3 mm/day) and mid-heavy rainfall (26 – 50 mm/day), show clear decreasing trends with a statistical significance (> 95 %) in ARA (Fig. 6.17b).

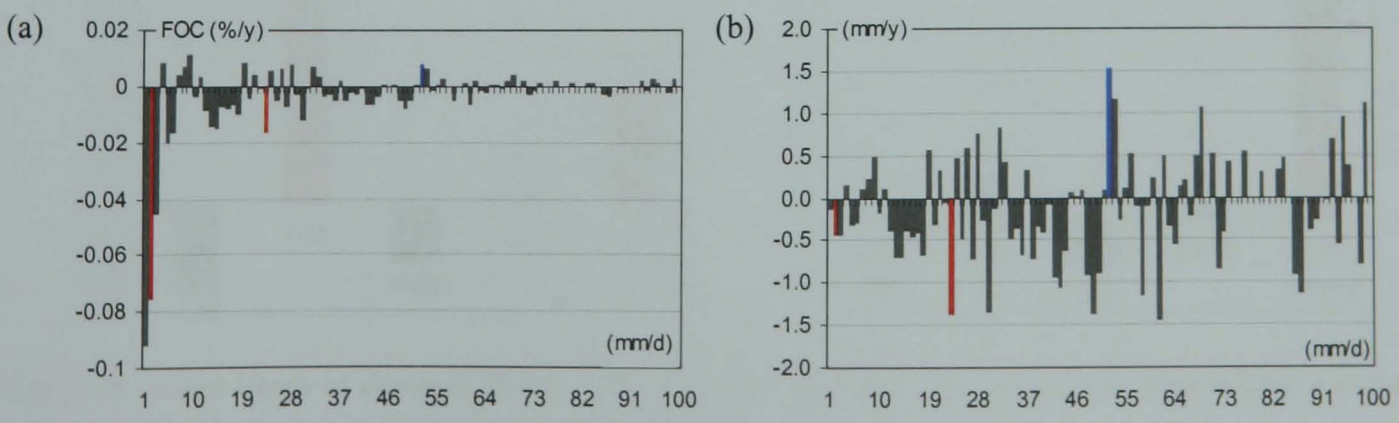

Fig. 6.16. Linear trends of OR for (a) FOC and (b) ARA. The red and blue bars indicate a statistical significance > 95 % and > 94 %, respectively.

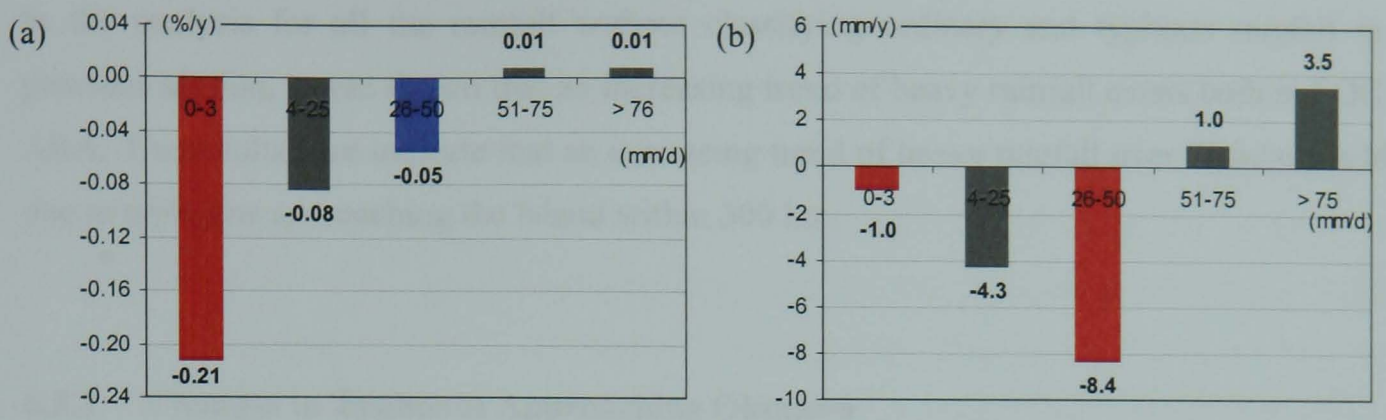

Fig. 6.17. Linear trends of clustered OR for (a) FOC and (b) ARA. The red and blue bars indicate a statistical significance > 95 % and > 94 % respectively.

For TR300, increasing trends (> 94 % or 95 %) occur in 3 – 4 mm/day, 14 – 15 mm/day, 18 – 19 mm/day and 79 – 80 mm/day both in FOC (Fig. 6.18a) and ARA (Fig. 6.18b). Again to enhance these signals, rainfall intensities were clustered. Light-mid rainfall (4 – 25) mm/day and heavy rainfall (> 75 mm/day) show a statistically significant (> 95 %) increasing trend in FOC (Fig. 6.19a). Although light-mid rainfall (4 – 25 mm/day) shows a weak statistically significant (> 94 %) increasing trend (+2.0 mm/year) in ARA (Fig. 6.19b), heavy rainfall shows a considerably greater trend (+10.8 mm/year).

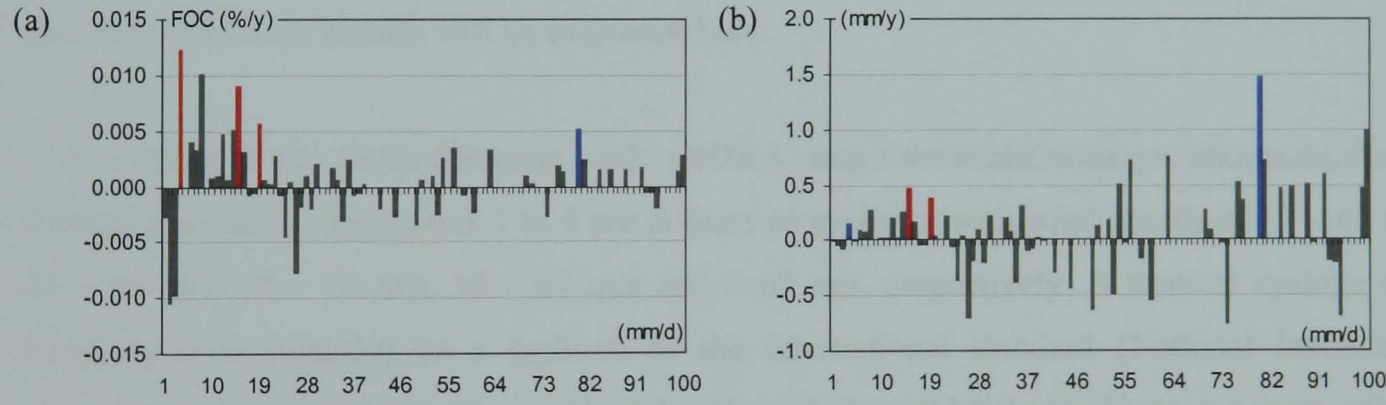

Fig. 6.18. Linear trends of TR300 for (a) FOC and (b) ARA. The red and blue bars indicate a statistical significance > 95 % and > 94 % respectively.

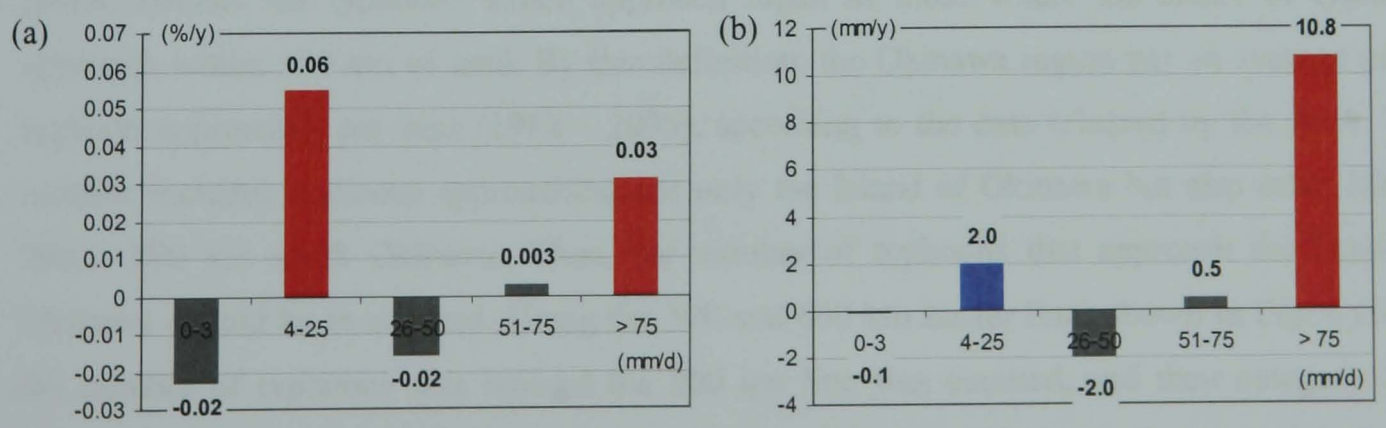

Fig. 6.19. Linear trends of clustered TR300 for (a) FOC and (b) ARA. The red and blue bars indicate a statistical significance > 95 % and > 94 % respectively.

In the analysis for all the rainfall without classifying ordinary and typhoon rainfall in the previous section, it was shown that an increasing trend of heavy rainfall exists both in FOC and ARA. The results here indicate that an increasing trend of heavy rainfall over Okinawa is likely due to typhoons approaching the Island within 300 km.

6.5.2 Changes in Typhoons Approaching Okinawa

A reason for an increase of typhoon rainfall over Okinawa could be because the number of typhoons approaching Okinawa may have increased, leading to increases in the FOC of heavy rainfall. IPCC TAR indicated that the variation of tropical and extra-tropical storm showed regional increase in the North Pacific, parts of North America, and Europe over the past several decades (Houghton et al., 2001). Further study by Webster et al. (2005) showed that increases have been observed in the North Atlantic, North Pacific, Indian and Southwest Pacific Ocean (1970 – 2004). They indicated that the number of storms remained approximately constant, but the numbers of storms in the strongest categories have been increasing. These changes occur in all the ocean basins and the largest increase occurred in the North Pacific, Indian and Southwest Pacific Oceans. Therefore, it is conceivable that an increased number of strong typhoons have affected heavy rainfall occurrence in Okinawa. The number of typhoons approaching Okinawa and their effects on rainfall will be examined here.

According to the Saffir-Simpson scale (NOAA, http://www.nhc.noaa.gov/aboutsshs.shtml), tropical cyclones in categories 1 to 5 are defined as cyclones with wind speeds of 33 – 43 m/s, 43 – 50 m/s, 50 – 56 m/s, 56 – 67 m/s and > 67 m/s, respectively. A tropical cyclone over Category 2 is regarded as a typhoon in the international standard (National Institute of Informatics, http://agora.ex.nii.ac.jp/digital-typhoon/help/unit.html.en). These cyclones will be referred to as typhoons in this section. The period of 1982 – 2005 examined in the rainfall analysis will also be used for the typhoon approach analysis. The *Japan Meteorological Agency* (JMA) defines the typhoons which approach Japan as those where the centre of typhoons approach within 300 km of land. By this definition, the Okinawa region has an average of 7.7 typhoon approaches per year (1982 – 2005), according to the data released by the JMA. This number includes typhoons approaching not only the Island of Okinawa but also other islands 200 – 300 km south Okinawa. Thus, the number of typhoons that approach the Island of Okinawa should be re-counted. Using the 300 and 600 km buffer lines shown in Fig. 6.13 (a), the number of typhoons that crossed the 300 km line was counted, and their category (CT) occurring within the 300 km line was used to classify their CT i.e. typhoons that had CT5 outside of the 300 km range will not be counted as typhoons with CT5 because it will not have affected rainfall in Okinawa with CT5 intensity.

Fig. 6.20 shows the number of typhoons that approached the Island of Okinawa (1982 – 2005), for CT4, CT5 and the total of these typhoons. The averages of typhoon approach per year for CT4, CT5 and the total are 1.4, 2.4 and 3.8 respectively. Their linear trends were -0.004, 0.05 and 0.05 per year, respectively. However, they are not statistically significant. Typhoon approach and associated rainfall occurs mostly during Aug – Sep (as Fig. 6.21). Rather than the total number of typhoons in the year, the number of AS typhoons seems to be more influential for rainfall. Changes in the number of typhoon in CT4 and CT5 for MJJ, Aug, Sep, and ON are given in Fig. 6.22, but none of these division shows a statistically significant trend. The number of storms of CT4 and 5 in the North Pacific has been increasing in accordance with warming sea temperature over 1970 – 2004 (Webster et al., 2005). However, this has not led to more strong typhoons coming close to Okinawa.

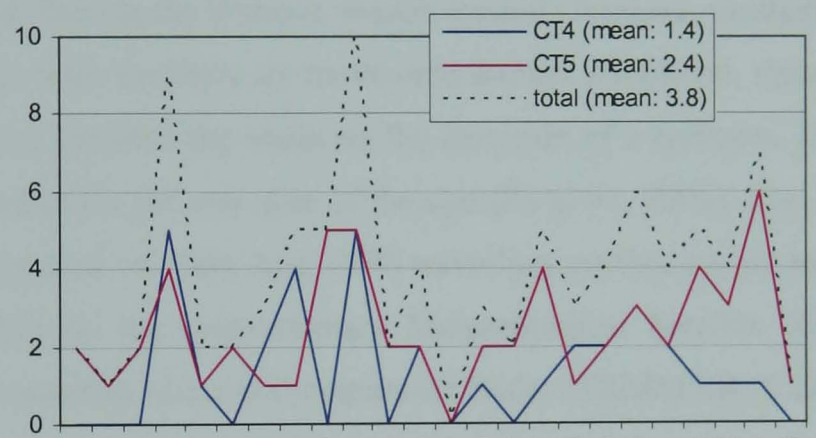

Fig. 6.20. No. of typhoon approached Okinawa within 300 km according to their categories.

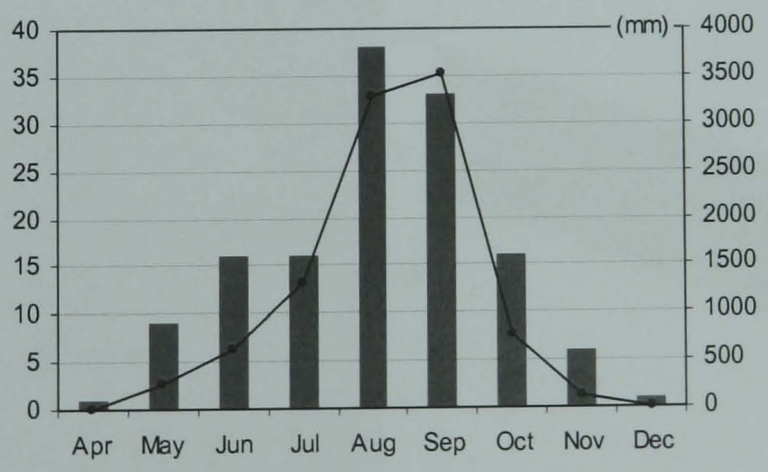

Fig. 6.21. Total number of typhoons (CT4 and CT5) approached Okinawa and rainfall (right y-axis) per month (Apr – Dec) for 1982 – 2005.

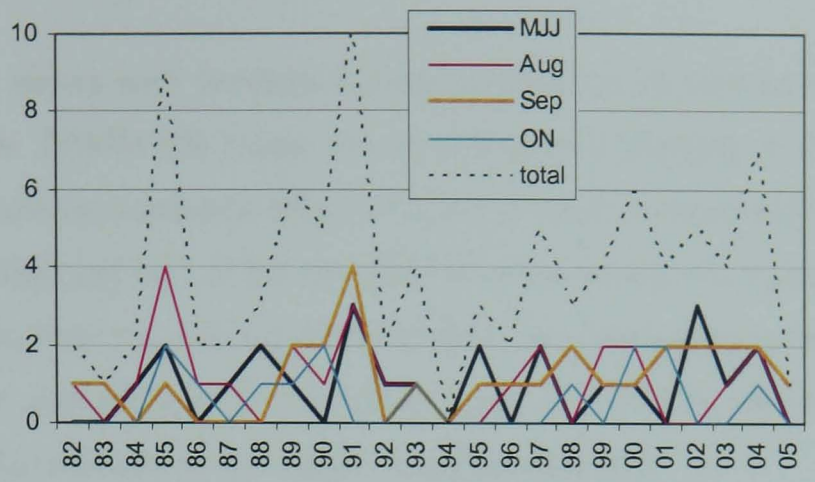

Fig. 6.22. No. of typhoon (CT4 and 5) approached the Island of Okinawa within 300 km for MJJ, Aug, Sep, ON.

Another possibility for increased typhoon rainfall over Okinawa is that typhoons approached even closer to the Island, or typhoons predominantly occurred such that their east side involve Okinawa. Winds and rainfall are at their highest intensities around 30 – 100 km from a typhoons centre (Ogura, 1990). During the typhoon season around Okinawa, southerlies prevail and move typhoons northward. With cyclonic air movement around a typhoon, these southerlies enhance wind speed and moist air from the south on the east side of a typhoon. Thus intense wind and rainfall are concentrated on the east side of the eye (Pu et al., 2002). Fig. 6.23 shows an image of Typhoon Rex acquired on 30th Aug 1998 travelling northeastward and approaching Japan (Bessho et al., 2001) by the Geostationary Meteorological Satellite (GMS: 6.22a) and the Tropical Rainfall Measuring Mission Precipitation Radar (TRMM PR: 6.22b).

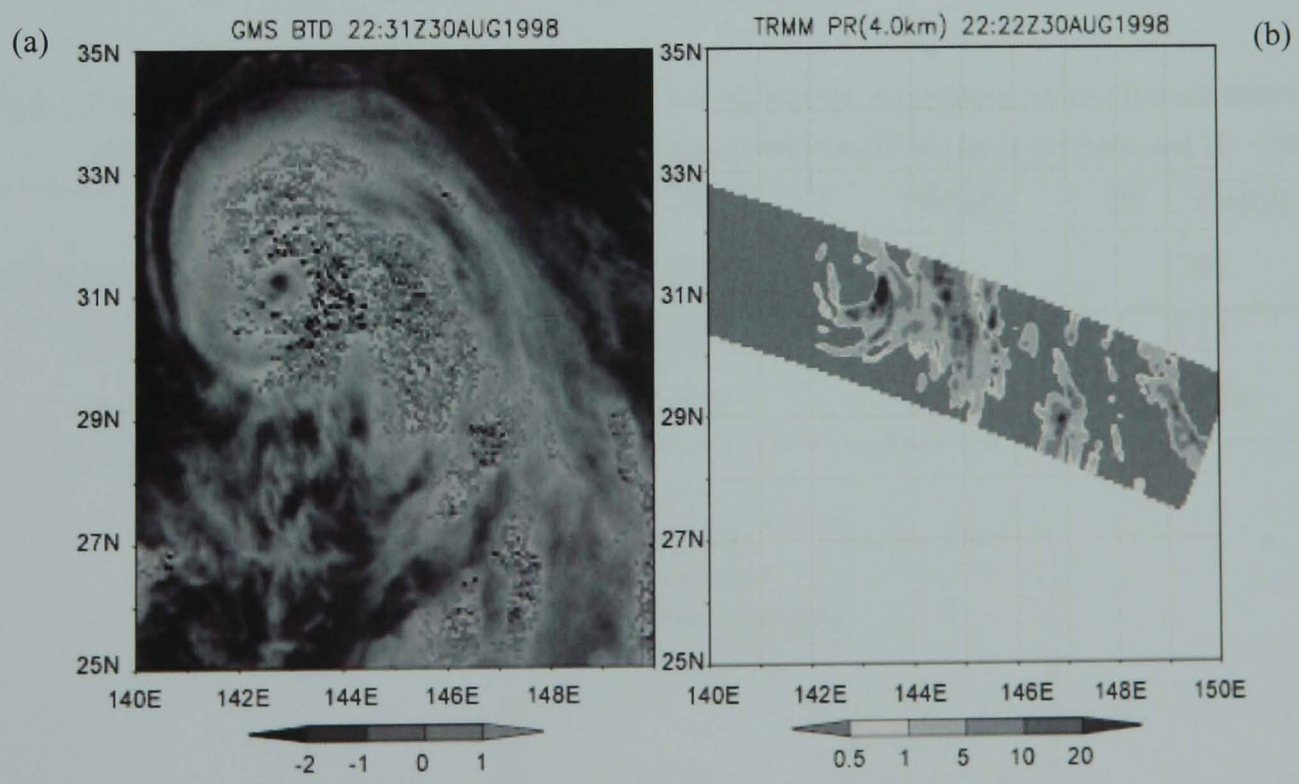

Fig. 6.23. (a): Image of Typhoon Rex travelling northeastward observed by GMS at 22:31 (UTC) 30 Aug 1988, indicating brightness temperature difference (BTD) between brightness temperature of infrared and water vapour channel. BTD is used to identify cumulonimbus for estimating the typhoon intensity. (b): Image of rain intensity (mm/hr) in the same typhoon at the 4 km altitude observed by TRMM PR at 22:22 (UTC) 30 Aug 1988 (Image from Bessho et al., 2001).

The GMS image shows well developed cumulonimbus in the east to southeastern sector of the typhoon and the TRMM PR image shows strong rain intensity in the same area. These images clearly indicate the combined effect of cyclonic air movement and inflow of air from the south intensifying wind and rain in the east and southeast sector of a typhoon. If typhoons pass Okinawa to the west, they will provide more rainfall than if they pass to the east. Therefore, the number of typhoons approaching to even closer range (< 100 km) and their course should be considered in helping understanding changes in typhoon rainfall.

The number of typhoons was classified according to (1) the distance within 100 km from Okinawa (TN100), (2) typhoons which touched Okinawa on their west side (TW) and (3) east side (TE). TW or TE typhoons which closed less than 100km to Okinawa were counted as TN100, so there is no overlapping between these classifications. With a comparison with the typhoon rainfall (TR300), TE yields a higher correlation, with statistical significance, than TW (Table 6.1). The number of typhoons that closed within 100 km distance from Okinawa (TN100) has an even stronger relation to TR300 than TE, and the total of TN100 and TE produces the highest correlation and statistical significance. Therefore, typhoons that were counted as TE and TN100 provide a better reason for an increasing trend of typhoon rainfall. However, in investigation of changes in the number of TE, TN100 and TE + TN100 for 1982 – 2005 (Fig. 6.24), none of these typhoons has a statistical significant linear trend for this period. Their changes with season show no statistical significant trend either (Fig. 6.25).

Table 6.1. Correlation between typhoon rainfall (TR300) and the number of typhoons which involved Okinawa by their west sector (TW) and east sector (TE), approached within 100 km range (TN100), and TE + TN100.

	TW	TE	TN100	TE + TN100
(no. of typhoon)	(36)	(35)	(41)	(76)
correlation	0.20	0.43	0.54	0.72
p-value	0.355	0.035	0.007	< 0.001

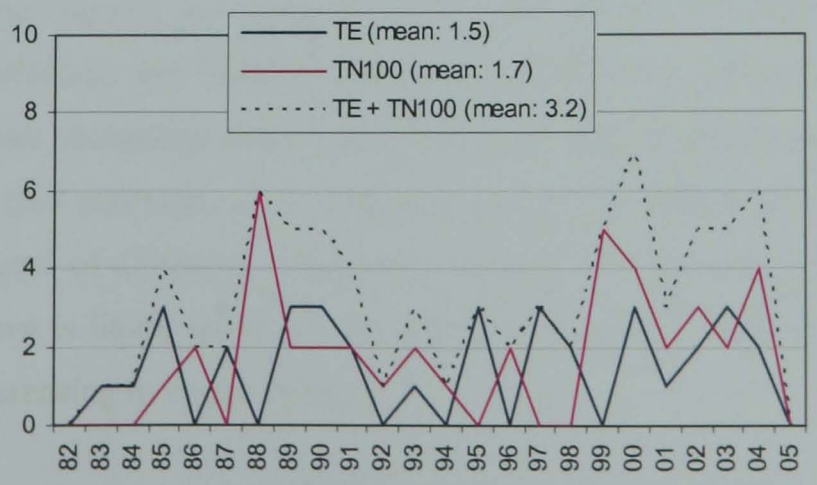

Fig. 6.24. No. of typhoon, TE, TN100 and their total.

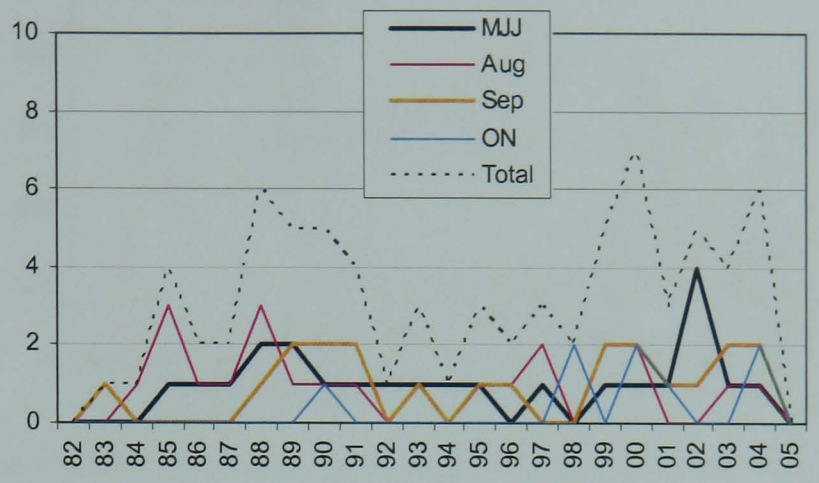

Fig. 6.25. No. of typhoon (TE and TN100) for MJJ, Aug, Sep and ON.

Another possibility is that rainfall per typhoon is increasing. Under a warming trend in surface temperature (Levitus et al., 2000), there will be increased evaporation and atmospheric moisture availability, leading to an intensifying hydrological cycle (Yang et al., 2003; Kumar et al., 2004). Fig. 6.26 shows typhoon rainfall (TR300) for MJJ, Aug, Sep, ON and the total amount over 1982 – 2005. In this figure, an increasing linear trend with a statistical significance was derived for MJJ (5.8 mm/year, $p = 0.046$) and Sep (8.5 mm/year, $p = 0.031$).

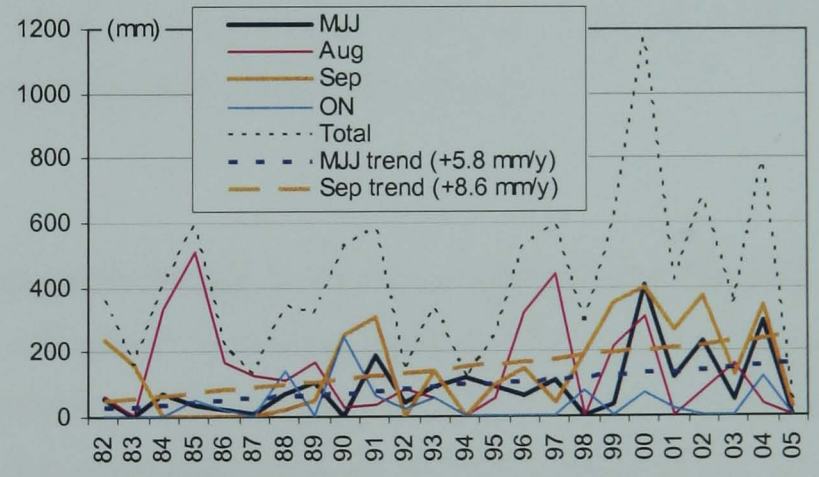

Fig. 6.26 Typhoon rainfall (TR300) for MJJ, Aug, Sep and ON.

Dividing TR300 given in Fig. 6.26 by the number of TE + TN100 in Fig. 6.25 will provide an estimation of rainfall amount per typhoon in TE and TN100. By this calculation, typhoon rainfall (TR300) provided per typhoon (TE and TN100) was obtained (Fig. 6.27), and a statistically significant increasing trend was obtained for MJJ (5.9 mm/year, 26% increase, $p = 0.040$) and for Sep (6.5 mm/year, 33 % increase, $p = 0.028$). Although this rainfall analysis is confined to the Island of Okinawa, the result suggests that an increasing trend of typhoon rainfall over Okinawa is likely attributed to typhoons (TE and TN100) in MJJ and Sep whose rainfall supply is increasing in recent years.

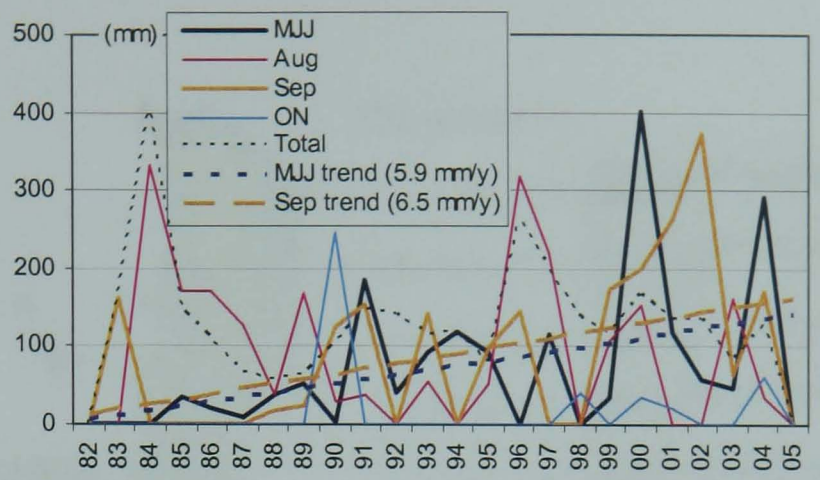

Fig. 6.27. Typhoon rainfall (TR300) amount per typhoon (TE and TN100) for MJJ, Aug, Sep and ON.

Under a warming ocean environment, Rodgers et al. (2000) found a positive correlation (0.52) between monthly typhoon rainfall and the SST anomaly in the western North Pacific for the period of 1987-89 and 1991-98. This supports the result of increasing typhoon rainfall indicated in Fig. 6.27. In analyses of rainfall over tropical and subtropical regions (1979 – 2003), Lau and Wu (2007) found an increasing trend of heavy rainfall areas in the cores of the ITCZ and SPCZ. In terms of typhoon formation, most of the initial disturbances from which typhoons later develop, originate on the poleward side of the Equatorial Trough of the ITCZ (Aoki, 1985). Typhoons are not generated without any cyclonic disturbances originated from the ITCZ (Nakazawa, 2000). Thus, a trend towards more heavy rainfall in the ITCZ could enhance moisture content in typhoons, and supply more rainfall.

6.5.3 Spatial-Temporal Changes in Ordinary and Typhoon Rainfall

With the results indicating a decreasing trend in OR and an increasing trend in TR300 for 1982 – 2005, investigating spatial-temporal changes in these rainfall over Okinawa will be useful to estimate the geographical bias of terrestrial influence on the coastal environment. Ordinary rainfall (OR < 50 mm/day) and typhoon rainfall (TR300: all intensities) will be used here. Their differences are also studied for an earlier period (1982 – 1993) and later period (1994 – 2005).

Fig. 6.28 shows the locations of the 14 WS in Okinawa and the total amount of OR (< 50mm/day) and TR300 at the WS for 1982 – 2005. Although the OR used here is at the rate less than 50mm/day, Fig. 6.28 indicates that OR is the major rainfall over Okinawa. Rainfall amounts and the altitude of the WS are plotted in Fig. 6.29 (a) for OR (< 50mm/day) and (b) for TR300.

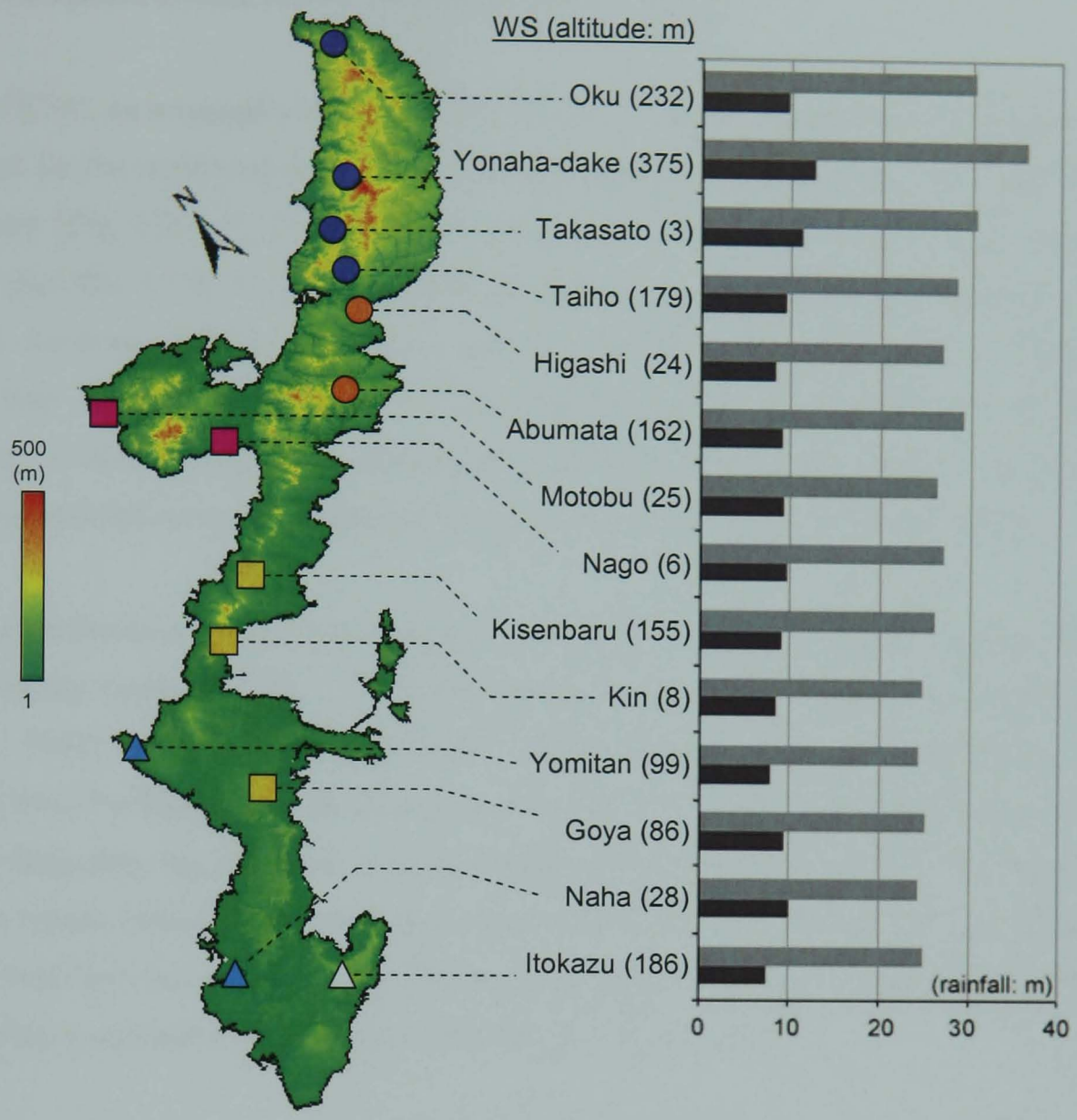

Fig. 6.28. Rainfall (1982 -2005) for OR (< 50 mm/day) (■) and TR300 (■) at the WS in Okinawa.

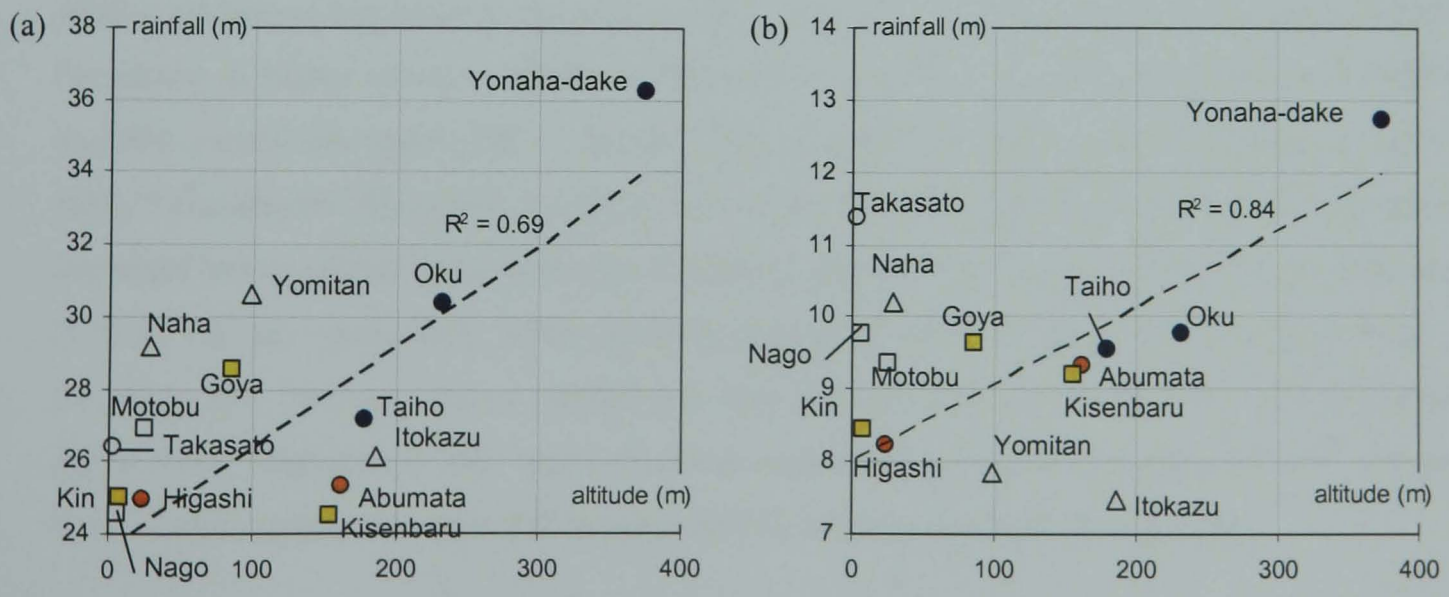

Fig. 6.29. Plots of total rainfall (1982 – 2005) at the WS in Okinawa and their altitudes for (a) OR (< 50 mm/day) and (b) TR300. Dashed lines are linear regressions derived from the WS in N (•, except Takasato WS), NE (•)and E (■).

For OR (< 50mm/day), the northern WS with high altitude have high rainfall amounts. A linear regression against altitude shows this (Fig. 6.29a: $R^2 = 0.69$).

For TR300, an orographic effect can also be seen. A linear regression derived from the same WS used for the regression in OR (< 50mm/day) indicates a closer relation between TR300 and orography (Fig. 6.29 (b): $R^2 = 0.84$). Abumata and Kisenbaru are closer to the regression in TR300 than that in OR (< 50mm/day), suggesting the orographic effect is enhanced in typhoon rainfall. However, Itokazu still shows very low rainfall in TR300 despite its altitude being higher than Abumata and Kisenbaru. There may be regional factors other than altitude itself affecting Itokazu rainfall e.g., mountain configuration and semi-enclosed coastline. The significant rainfall amount of Takasato is again consistent with its high surroundings.

To see differences in the amount of OR (< 50mm/day) in a decreasing trend and TR300 with an increasing trend for 1982 – 2005, differences between their amounts in an earlier period (1982 – 1993) and in a later period (1994 – 2005) were determined by subtracting the latter amount from the former amount (Fig. 6.30). For OR (< 50mm/day), all the WS shows negative values, indicating the influence of a decreasing trend in OR. For TR300, all the WS show positive values, indicating an increasing trend of TR300 all over the Island. Fig. 6.30 shows that the WS with less (more) decrease in OR (< 50mm/day) has more (less) increase in TR300. This relation has a statistically significant correlation ($r = 0.65$, $p = 0.013$).

Fig. 6.31 shows the variation of rainfall change between the later and earlier period, in relation to WS altitude, for (a) OR and (b) TR300. Generally, orographic enhancement on rainfall is clearer in TR300 than in OR, as the altitude-rainfall regression shows less scatter. With a relation of less (more) decrease in OR (< 50mm/day) and more (less) increase in TR300, the places in higher (lower) altitude in Okinawa will likely have more (less) increased TR300 and less (more) decreased OR (< 50 mm/day), although there are some exceptions (Yonaha-dake, Takasato and Abumata). It implies that orographically influenced regions will experience increased heavy rainfall from typhoons. Enhanced erosion and run-off will also occur frequently in these regions, particularly in the northern regions where the fragile soil "*Kunigami-maji*" is the main soil. Not only heavy rainfall but also strong winds associated with typhoons could cause forest degradation and hence decrease vegetation cover, which enhances soil erosion. Subsequently, adjacent coasts will be impacted by enhanced terrestrial influences.

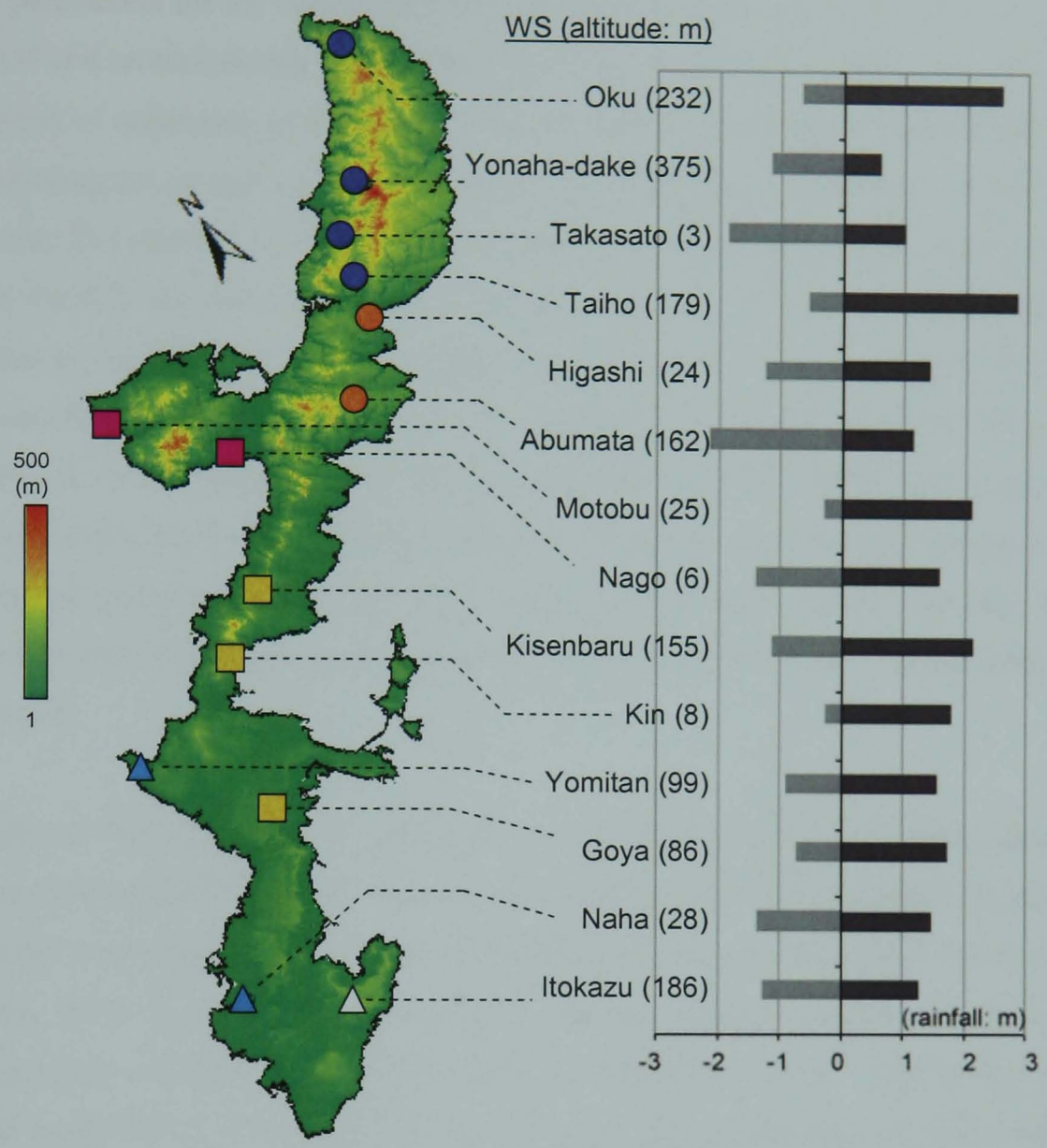

Fig. 6.30. Difference in rainfall amount [1994 – 2005 minus 1982 – 1993] for OR (< 50 mm/day) (■) and TR300 (■) at the WS in Okinawa.

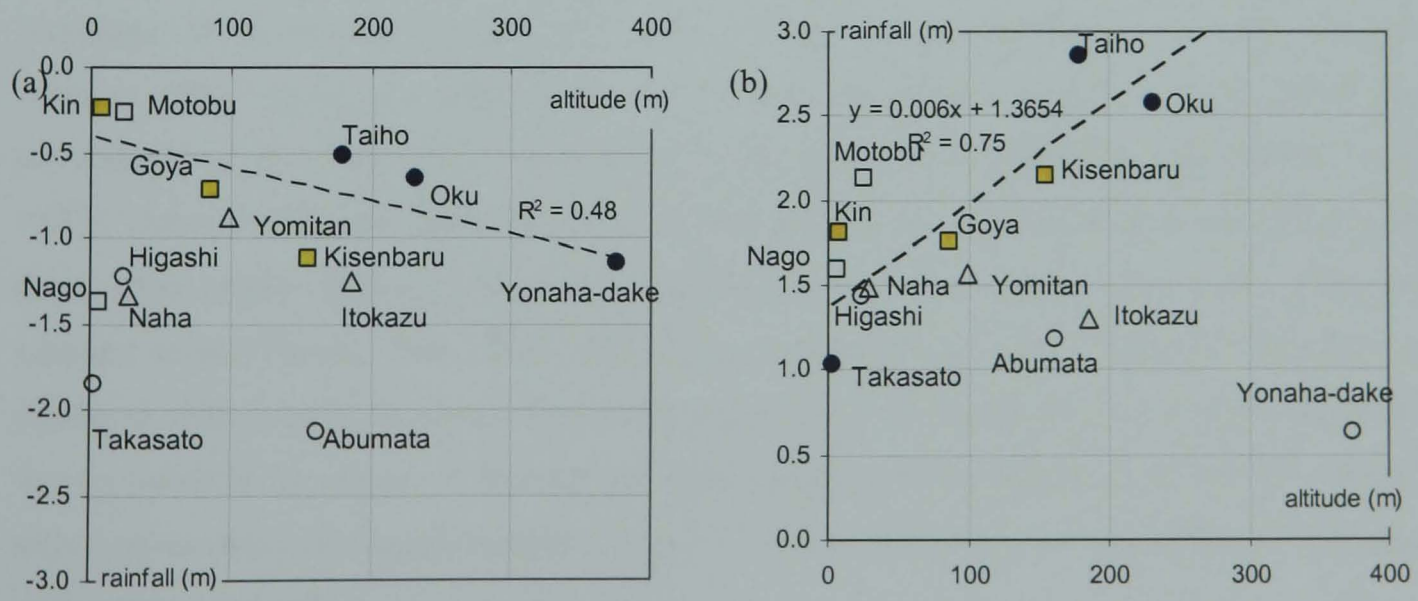

Fig. 6.31. Plots of rainfall amount difference [1994 – 2005 minus 1982 – 1993] at the WS in Okinawa and their altitudes for (a) OR (< 50 mm/day) and (b) TR300. Linear regression (dashed line) for (a) is derived from the WS in N (●, except Takasato WS) and E (■), and for (b) from WS in N (●, except Yonaha-dake WS) and E (■).

6.6 Local Significance of Findings

As key parameters for the coastal environment around the Island of Okinawa, changes in the winter EAM and rainfall during 1982 – 2005 were examined. For the winter EAM which affects the dispersion of sediments on the west coasts, its intensity indicates no statistically significant trend, suggesting no natural increasing or decreasing tendency in sediment reduction along the western coast. For rainfall, it was found that ordinary rainfall (OR) has a statistically significant decreasing trend in the rain rate of 0 – 3 mm/day and 22 – 50 mm/day, and typhoon rainfall (TR300) has an increasing trend with a statistical significance in the rain rate of 3 -22 mm/day and > 62 mm/day. While the occurrence of the number of strong typhoons (≥CT4) is increasing in North Pacific in the warming ocean environment (Webster et al., 2005), this is not true for the Island of Okinawa itself. The increasing trend of TR300 is due to an increasing trend in the rainfall amount per typhoon over Okinawa, particularly typhoons in MJJ and Sep. Orographic effects on OR and TR300 are evident over the Island, providing high rainfall amounts in the northern region.

Although the FOC of typhoons (≥CT4) shows no trend, one has to take due account of the importance of associated heavy rainfall which does have an increasing trend. Having frequent heavy rainfall means more potential for soil erosion, run-off and sediment delivery to the coast of Okinawa. With an orographic effect on rainfall, the northern region will be more likely affected by heavy rainfall. The northern region has erodible red soil, "*Kunigami-maji*", which has caused a coastal environmental problem in the history of Okinawa. A local ordinance has been in place since 1995 to mitigate the problem. According to this ordinance the upper limit of the sediment concentration from development sites is set at 200 mg/l in the run-off. Other countermeasures are check dams to trap sediments. These check dams were designed with an estimation of the heaviest rainfall rate with a probability of occurrence once every ten years (Omija, 1992). However, inflow rate to the check dams often exceeds the estimated rate, particularly around bare lands that deliver large quantities of sediments (Yoshinaga, 1986, 1987). These overflowed check dams cannot hold sediments, and accumulated sediments in the dams often release high concentration of sediments when overflows occur to the rivers and adjacent coasts (Omija, 1986, 1988, 1991). Given an increasing trend of heavy rainfall over the Island, in order to keep the upper limit of the sediment concentration regulated in the Ordinance and to maintain the health of the coastal environment, greater protection at the development sites may be required. Specifications of the check dams may also need modification to prepare for increased run-off.

Increasing heavy rainfall may influence the frequency of sediment-related disasters on land such as debris flow, landslide and slope failure. According to the sediment-related hazard map

of Okinawa (OPG River section, 2005b: Fig. 6.32), danger zones of debris flow are often seen in the northern and northwestern region. Geographical conditions in these regions with erodible soil and orographically affected heavy rainfall are conducive for destabilisation of the land. But even greater attention may be required in these regions, preparing for frequent heavy rainfalls to come. Danger zones of debris flow and steep slopes can be seen in the southwestern region where urban rivers flow westward. Nutrient input from these rivers is highly influenced by the dense population. Debris flow and slope failure on land will have an impact on more nutrient supply by increased sediment transport into the rivers (Milliman and Kao, 2005). Although typhoons and land disasters are episodic events, the combined effect of erosion, land degradation and run-off will likely be increasing and it will be an aggravating factor for the coastal environment.

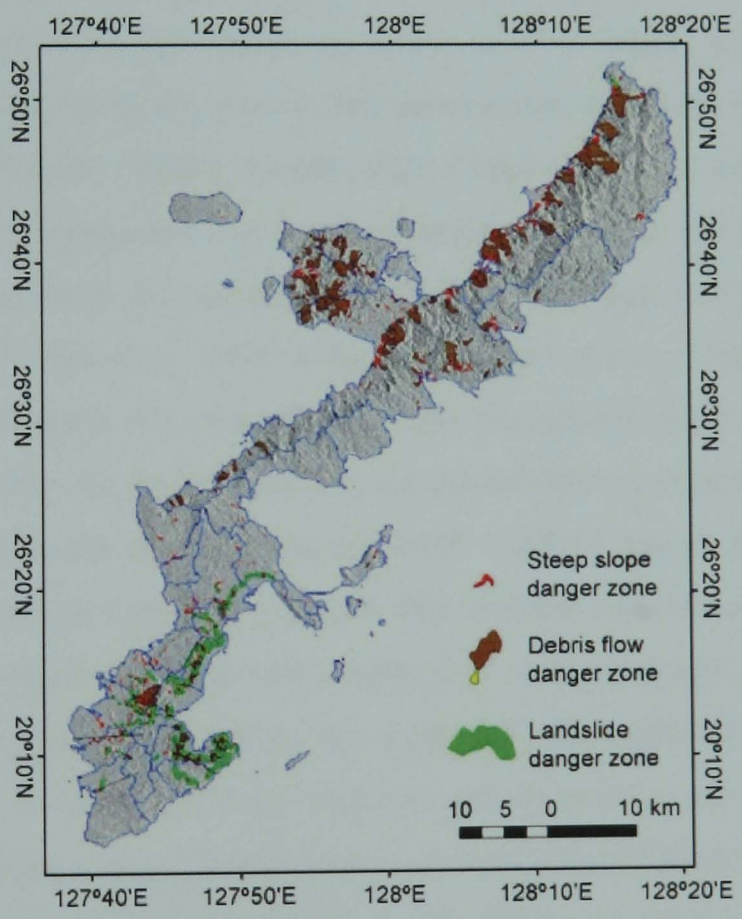

Fig. 6.32. Sediment-related hazard map of Okinawa (OPG River Section, 2005b).

With increased sea temperature under warming environment, coral bleaching has been frequently occurring on the global scale in the post-1990 period, and the impact of climate change on coral reefs has been discussed (Wilkinson and Buddemeier, 1994; Yamazato, 1999; Wilkinson, 2001). However, the terrestrial influence has to be considered with increasing heavy rainfall that may be related to climate change. Increased sediments in run-off accompanied by heavy rainfall will likely expand unsuitable environments for coral reef. There are at least three adverse effects on corals from sediments: (1) unconsolidated sediment with no hard bottom is an unstable substrate for new coral settlement or reef formation, (2) acute stress can result from the smothering effects of rapid sediment deposition by terrestrial run-off and resuspension, and

(3) chronic stress can result from an enhanced suspended load which reduces water clarity and light levels, hampering photosynthetic activities (McLaughlin et al., 2003). Damage to corals by red soil run-off and deposited sediments around Okinawa has been a major environmental problem, and their impact has been decreasing coral coverage and degrading ecosystem (Sakai and Nishihira, 1991; Omija et al., 1999; Kinjo et al., 2005). Considering the combined impact of high SST occurred in 1998 due to strong El Niño and the weakened winter EAM which has more influence on sediment removal the west coastal zone than the east of Okinawa, corals along the west coast may have more greatly impacted compared to those on east. This may be a reason that corals on west more severely degraded by the 1998 El Niño, as shown in Fig. 1.4.

Increase in rainfall will also change not only the sediment stress of coral reefs but also the flux of nutrients and contaminants (Wilkinson and Buddemeier, 1994). Under oligotrophic water, corals can conduct photosynthetic activities in clear water. Increased nutrient input causes phytoplankton blooms which lead to decreased clarity of water and light availability for coral photosynthesis. Nakano (2002) reported that a high nutrient concentration also impacts metabolism of symbiotic algae and coral insects in corals, and hence inhibits corals from growth. Around Okinawa, it has been shown that coastal zones with high nutrient concentrations are inhospitable to corals (Omija et al., 2003; Kinjo et al., 2006). Heavy rainfall will likely provide high nutrient run-off, but there will be additional input brought by the strong winds of typhoons. Xu et al. (2004) found that the highest nutrient concentrations are achieved in forest soil in the north of Okinawa during the typhoon season (1996 – 2001) due to increased leaf litterfall, caused by associated strong winds. It suggests that nutrient concentrations in run-off during typhoons will contain additional nutrients compared to ordinary heavy rainfall without strong winds. Typhoons' heavy rainfall therefore has these potential combined effects on the coastal zone around Okinawa. If these effects are added to already stressed coral reefs due to high sea temperatures from climate change, it will make the coral's environment difficult to regenerate due to adverse sediments and nutrient impacts. According to JMA (2007), the SST in the southern East China Sea including the Island of Okinawa has been increased by 1.1 °C in the last 100 years (1900 – 2006). Annual SST data around Okinawa (the mean value of Domain 3 determined in Chapter 4, §4.4) used in this study for 22 years (1985 – 2005) are given in Fig. 6.33, showing a quasi biennial cycle. Although no statistically significant linear trend was derived, low SST years in the cycle appears to be increasing their temperature. It suggests that the SST around Okinawa has been influenced by increasing temperature in the southern East China Sea. This influence from the surrounding ocean on the local SST was described in §5.4.

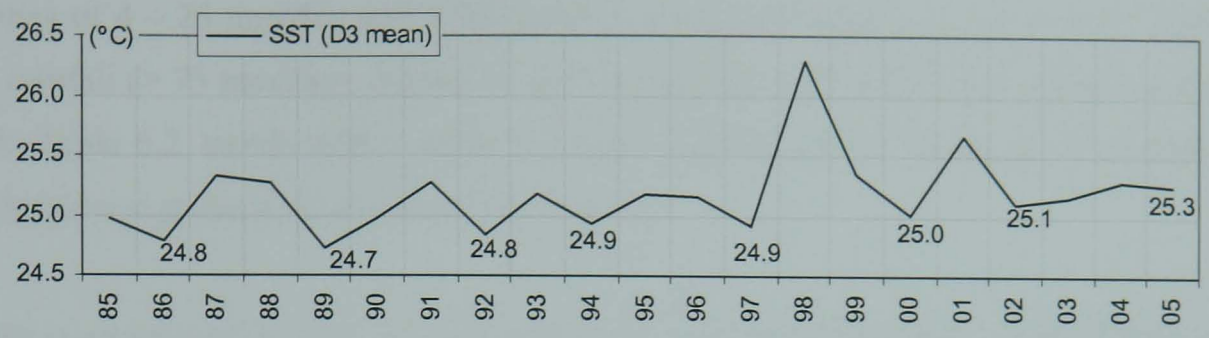

Fig. 6.33. Annual SST around Okinawa (the mean value of D3 determined in Chapter 4) during 1985 – 2005.

Although rising temperature will not endanger coral survival, frequent episodes of temperature extremes will increase coral bleaching and mortality, thereby degrading the health of corals and increasing vulnerability to other stresses (Wilkinson and Buddemeier, 1994). Damage to coral reefs will lead to decrease in the reef fish and detraction of the landscape (Bellwood et al., 2004), impacting on fisheries and tourism which are major industries of Okinawa. Although typhoons are episodic events, lack of appropriate mitigation for land degradation will delay natural recovery of coral reefs, degrade their resilience, and may result in permanent change into a barren marine ecosystem. Omija et al. (1999) and Kinjo et al. (2005) reported that the maximum value of the sea sediments recorded in a year is more influential on coral coverage on site rather than its annual mean value. It suggests an episodic acute stress of sediments has to be mitigated, if corals are to be preserved.

6.7 Summary

Changes in the winter EAM (1988 – 2005) and rainfall (1982 – 2005) over the Island of Okinawa have been investigated in this chapter. Intensity of the winter EAM (DJF) in Okinawa is linked to the SOI (DJF): the winter EAM is high (low) during high (low) SOI. It indicates that the coastal environment of Okinawa is coupled with a global scale process, the SOI. However, no statistically significant increasing or decreasing trend of the winter EAM was found.

In analyses of rainfall, it was found that light (0 – 3 mm/day) and mid-heavy (26 – 50 mm/day) rainfall has a statistically significant decreasing trend but heavy rainfall (> 75 mm/day) has an increasing trend with a statistical significance. Due to orographic enhancement, high FOC of heavy rainfall (> 75 mm/day) occurs in the northern regions of Okinawa. To investigate a cause of the increasing trend of heavy rainfall, the OR, TR300 and number of typhoons approaching Okinawa (1982 – 2005) were studied. The OR and TR300 contribute 92.4 % and 4.3 % respectively to all the rainfall events, but 77.4 % and 18.6 % respectively to the total rainfall over Okinawa. For OR, rainfall intensities of 0 – 3 mm/day and 26 – 50 mm/day were found to have a decreasing trend in ARA (Table 6.2). For TR300, rainfall

intensities of 4 – 25 mm/day and > 75 mm/day have an increasing trend in FOC. Particularly, heavy rainfall (> 75 mm/day) showed a clear increasing trend (+10.8 mm/year) in ARA (Table 6.2). In Table 6.2, trends with a weak statistical significance (> 94 %) are also shown. They likely become significant in a longer-term analysis.

There is an increasing trend towards strong typhoons over the Pacific basin (Emanuel, 2005; Webster et al, 2005), however, this does not lead to a greater number of strong typhoons approaching Okinawa. Rather, rainfall supplied by typhoons for MJJ and Sep was found to be increasing (5.9 mm/year and 6.5 mm/year respectively: Table 6.3), which is likely a cause of increasing heavy rainfall over Okinawa. Orographic effect on rainfall was seen in a decrease of OR and an increase of TR300. It implies that orographically influenced regions will likely experience more heavy rainfall which will enhance soil erosion and run-off.

Table 6.2. Trend of FOC and ARA for OR and TR300 (1982 – 2005).

	OR		TR300	
rainfall (mm/day)	0 – 3	26 – 50	4 – 25	> 75
trend of FOC (%/year)	- 0.21	(- 0.05)	+ 0.06	+ 0.03
trend of ARA (mm/year)	- 1.0	- 8.4	(+ 2.0)	+ 10.8

* ( ) indicates a statistical significance > 94 %

Table 6.3. Trend of TR300 per typhoons TE and TN100 for MJJ and Sep (1982 – 2005).

	MJJ	Sep
rainfall trend	+ 5.9 mm/year (26 %)	+6.5 mm/year (33 %)

Given the results obtained, answers for the question mentioned in the introduction can be as follows: The winter EAM showed a coupling of the SOI, but no increasing or decreasing trend. In addition, the ENSO also affects the local SST around Okinawa. Rainfall showed a decreasing trend in OR and an increasing trend in TR300 due to increased rainfall supply per typhoon. It suggests that contribution of the winter EAM control to the coastal zone of Okinawa will likely remain at the same level on average, although there will be interannual variability affected by the ENSO. Heavy rainfall from typhoons will provide more run-off and sediment delivery to the coast, but natural removal of sediments by the winter EAM will be relatively constant. Hence sediment accumulation occurs off the coast. Heavy rainfall and strong winds associated with typhoons will also cause landslide and forest disturbance, providing additional sediment and nutrient supply to the coast, impacting coral reefs.

Chapter 7 Discussion and Implications

7.1 Introduction

This chapter draws together the research discussed in this thesis. To begin it is appropriate to remind ourselves of the original objective and aims. These are set out below.

Overall objective

To understand key controls on the coastal environment around the Island of Okinawa at both regional to local scale, and to understand their changes and impacts on coral reefs in the western Pacific.

Aim 1

To identify key climate controls on the SST and ocean colour in the western Pacific and the coastal zone around Okinawa.

Aim 2

To identify impacts of the terrestrial controls on the SST and ocean colour on the coastal zone around Okinawa.

Aim 3

To assess impacts of typhoons on the SST and ocean colour on the coastal zone around Okinawa.

Aim 4

To clarify relationships between key controls and the variability of sediment concentration in the coastal zone around Okinawa.

Aim 5

To clarify how observed changes over time in key controls, and impact on the coral reefs around Okinawa.

The following sections provide the conclusions corresponding to the objectives 1 to 5, and discuss implications derived from this thesis for management of coral reefs in the western Pacific. Possible future work is also described in order to further develop an understanding of the relationship between the key controls and the coastal zone, and the impact of climate change on the coral reef environment.

7.2 Discussion

7.2.1 Overview of time series data findings: controls and effects

Key controls on the variability of both SST and OC4 around the Island of Okinawa under climate and local terrestrial processes have been investigated in this study. Monthly satellite data were objectively analysed to interpolate data gaps within both AVHRR SST (1985 – 2006) and SeaWiFS OC4 time series data (1998 – 2006). The climatological SST showed an annual cycle over the ECS associated with the warm Kuroshio Current (KC) flowing northward in the Okinawa Trough. Higher variability in the SST was observed over the continental shelf region than off-shelf. The climatological OC4 showed that high OC4 concentrations generally occur during winter and decrease in summer within the East China Sea (ECS). Input of sediments and nutrients from the Yangtze River is significant. The highest concentration in OC4 occurs around the Yangtze Estuary, also demonstrating much higher variability than in the off-shelf region. The climatological ocean surface wind processed from the SeaWinds satellite data archive (2000 – 2006) showed the East Asian Monsoon (EAM) with its seasonal wind shift: strong northerlies in winter and relatively weak southeasterlies in summer. Using these remote sensing data and local climate date, main findings of this thesis were derived as following:

(1) Solar radiation is a dominant control on the SST variability (1985 – 2006) in large (ECS) and local (Okinawa) scales.

(2) The EAM is a primary control on the OC4 variability (1998 – 2006) in large (ECS) and local (Okinawa) scale, with various contributions at different scales.

(3) Run-off from the rivers was a terrestrial impact appeared as a secondary control on OC4 variability around Okinawa.

(4) Typhoon rainfall and wind were important factors affecting OC4 anomalies around Okinawa,

(5) The SST anomalies around Okinawa were strongly influenced by outer ocean,

(6) The winter EAM also contributed to the sediment removal along the western coastal zone of Okinawa,

(7) The northerlies brought by the winter EAM (1988 – 2005) showed no statistical trend (i.e. increasing or decreasing) but a link with the ENSO,

(8) Changes in rainfall (1982 – 2005) over Okinawa showed a decreasing trend in light and mid-heavy rainfall and an increasing trend of heavy rainfall,

(9) An increasing trend of heavy rainfall was attributed to rainfall from typhoons approaching Okinawa; despite the occurrence of strong typhoons approaching Okinawa has shown no tendency to increase over the study period (1982 – 2005).

7.2.2 Aim 1: Climate control on the ocean at three scales in the ECS

Three different-sized domains over the ECS were defined from large to small scale as follows (Chapter 4, §4.4):

Domain 1 (D1) - a region covering the East China Sea and the Philippine Sea.

Domain 2 (D2) - a sub region of D1 - around Okinawa, including the KC.

Domain 3 (D3) - a sub region of D2 - near the coastline of the Island of Okinawa.

7.2.2.1 Domain 1 Findings

In D1, the 1st mode of the SST EOF showed its clear annual cycle related to the solar radiation, accounting for 91.6 % of the total variance (1985 – 2006). Its eigenvector showed higher values over the shallower shelf region, indicating effects of shallow bathymetry. The 2nd mode of the SST EOF (2.6 % of the total variance) was correlated with the winter EAM, lagged by 2 months, suggesting its cooling effect. Other higher modes accounted for less than 1 %. The 1st mode of the OC4 EOF, accounting for 13.8 % for the total variance (1998 – 2006), showed an annual cycle in its temporal function: high values in winter and low values in summer, showing a relation with the winter EAM whose northerlies prevail during winter. The 1st mode eigenvector showed high positive values generally over the continental shelf, but negative values off the Yangtze River. Eigenvectors of the 2nd (9.5 %) and 3rd (6.3 %) modes showed high positive values around the Yangtze River estuary, suggesting a strong influence of the Yangtze run-off which provides a tremendous quantity of sediment and nutrients during the rainy season brought by the summer EAM. The temporal functions of the 2nd and 3rd mode were not directly linked to the variation of the Yangtze discharge, suggesting these modes are coupled with other processes on the shelf. Although it is known that OC4 concentration is generally high over the continental shelf during winter to spring (Kiyomoto et al., 2001; Gong et al., 2003), multiple processes integrated in the ECS produce a complex OC4 variations both in space and time, e.g., the Yangtze River run-off (Milliman, 1985), the Kuroshio water intrusion into the shelf (Lin et al., 1992; Tang and Yang, 1993), the variation of other waters of the Yellow Sea Warm Current and Chinese Coastal Water (Beardsley et al., 1985). Eigenvectors of the principal modes (the 1st to 3rd modes) occur over the continental shelf and off the Yangtze River, and their influence is small around Okinawa.

7.2.2.2 Domain 2 Findings

Off the continental shelf, the analysis in D2 showed that the 1st mode of the SST EOF is driven by the solar heating cycle, explaining 94.6 % of the total variance. The highest values of its eigenvector appeared over the shallow regions and a tongue of the KC was seen with low values. The 2nd and 3rd modes accounted for less than 1 %, showing little significance. In the OC4 EOF, the accountability for the total variance of the 1st mode increased to 58.1 %, much

higher than that for D1. Its eigenvector showed the highest values over the shelf edge and other high eigenvectors occurred in the shallower region off northwest Okinawa. As the 1st mode temporal function showed a statistical relation with the strong northerlies in winter, lagged by 2 months, the influence of the winter EAM was a clearer primary control in D2. The eigenvector and the temporal function of this mode imply that the OC4 variability off the shelf region is less influenced from the shelf, suggesting sediment and nutrient deposition into the Okinawa Trough (Kao et al., 2003). The 2nd and 3rd mode account for 4.5 % and 2.2 % of the total variance respectively and their temporal functions showed the strong influence of one pixel on the shelf edge, suggesting a contaminated signal.

7.2.2.3 Domain 3 Findings

In a local analysis in D3, the 1st mode of the SST EOF around Okinawa accounted for 97.6 % of the total variance, with a strong annual cycle related to solar radiation. The 2nd mode and the 3rd mode explained little (0.5 % and 0.4 % respectively of the total variance). The 1st mode of the OC4 EOF revealed that the winter EAM was a distinctive primary control, accounting for 62.7 % of the total variance, showing a correlation with the temporal function of this mode, again lagged by 2 months. It was found that the smaller the domain size, the higher the accountability of the total variance of the 1st mode of the OC4 EOF, which represents the effect of the winter EAM. This was highlighted on the west coast of Okinawa where the strong northerlies of the winter EAM cause coastal upwelling, and so supply nutrients to the ocean surface. The 2nd mode of the OC4 EOF, accounting for 6.2 % of the total variance, its eigenvector showed the highest value in the pixel nearest to the largest river in the Island. The 3rd mode (5.5 %) eigenvector showed the highest value in the same pixel as the 2nd mode. Their temporal functions showed some pronounced peaks that are influenced by the OC4 variation of this point. It suggests that these modes are affected by terrestrial control through the river, just as the Yangtze River influenced the OC4 around its estuary.

7.2.2 Aim 2: Terrestrial control on the coastal zone around Okinawa

In order to identify a possible terrestrial control from the rivers in Okinawa, the study region was focused to the west coast of the Island where the large rivers drain, and EOF analyses were applied on this region (Chapter 5, §5.2.2). The results showed that a terrestrial control on the OC4 variability through the rivers appeared to be a secondary control, accounting for 9.6 % of the total variance (1998 – 2006), below the primary control linked to the winter EAM that accounted for 81.2 % of the total variance. An OC4 bloom from enhanced run-off has been reported by many studies (e.g., Pinazo et al., 2001; West and van Woesik, 2001; McLaughlin et

al., 2003; Zheng and Tang, 2007). This study confirmed such an effect and quantified its correlation to the OC4 variability.

From the results obtained for Objective 1 and 2, a schematic representing the controls on variability of the SST and OC4 over the ECS, including the Island of Okinawa (D1 – D3), can be shown in Fig. 7.1. This presents a cross-section from China in the left (west), the ECS, Okinawa Trough, Okinawa Island to the Ryukyu Trench to the right (east). The Kuroshio Current (KC) flows into the Okinawa Trough from south to north.

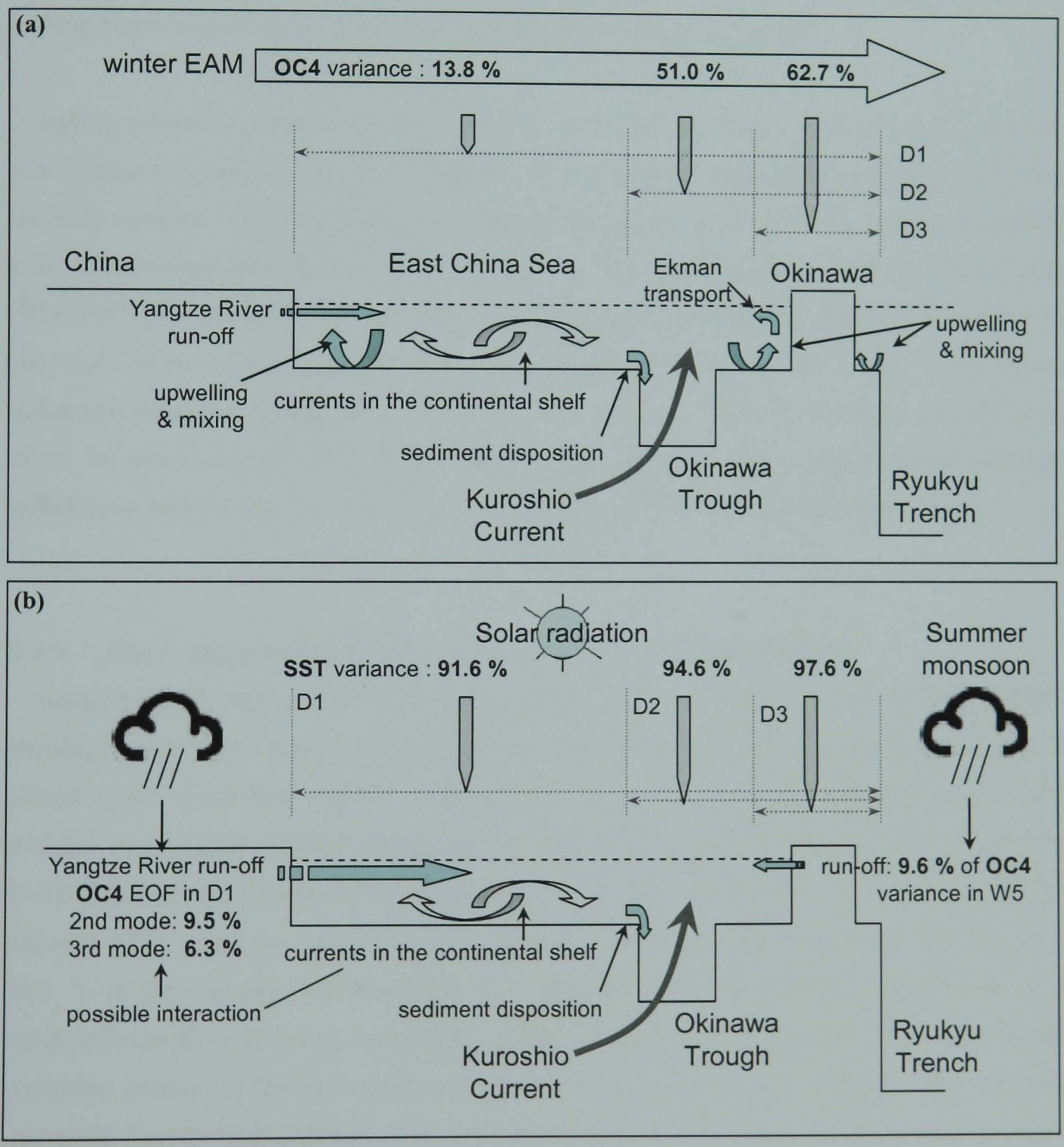

Fig. 7.1. Schematic of the controls on the variability of the SST and OC4 over the ECS and the Island of Okinawa for (a) winter and (b) summer. See text for the detail.

During winter months (Fig. 7.1a), the northerly EAM is a primary control on the OC4 variability. It causes upwelling and mixing over the ECS, resulting in a decreasing SST and

increasing surface OC4 concentrations. Such effects have greater influence in the shallower regions. But the OC4 variability is complex over the continental shelf due to a variety of processes including the Yangtze River run-off and interactions with other currents. The winter EAM effect explained by the 1st mode OC4 EOF contributes increasingly to the variability as the scale is reduced: by 13.8 % in D1, 51.0 % in D2 and 62.7 % in D3. Sediments from the continental shelf are apparently deposited into the deep depression of the Okinawa Trough (Ujiie et al., 1991; Kao et al., 2003), hence there is less variability off the shelf compared to the inner shelf. Around the Island of Okinawa, the west coast experiences a greater effect of the winter EAM on coastal upwelling than the east side. Along with the upwelling, coastal sediments are resuspended and transported offshore by Ekman transport.

During summer months (Fig. 7.1b), the SST increases with intensified solar radiation which is a dominant control on the SST variability in all domains, contributing greater than 90 % to the total variance. The summer EAM brings warm and most air from the south and southeast with weaker wind than the winter EAM. It brings the rainy season over China known as the "Mei-Yu" and over Japan as the "Baiu", increasing run-off from the Yangtze River and the rivers in Okinawa. Eigenvectors of the 2nd and 3rd mode of the OC4 EOF in D1 showed influences from the Yangtze River. Off the west coast of Okinawa, enhanced run-off has an effect on increasing the OC4 through associated sediments and nutrients, demonstrating a terrestrial control on the OC4 variability, accounting for 9.6 % of the total OC4 variance.

7.2.3 Aim 3: Impact of typhoons on the coastal zone around Okinawa

Because the extreme impact from typhoons may have a link to the observed SST and OC4 variability, the higher modes of the SST and OC4 EOF were investigated by removing the annual cycles from their signals, creating SST and OC4 anomalies, and then another EOF analysis was applied on the anomaly dataset off the west coast of Okinawa (W5, Chapter 5, §5.3). Typhoon rainfall showed its significance in the temporal function of the 1st mode of OC4 anomaly EOF through a correlation with rainfall anomaly caused by typhoons, accounting for 42.5 % of the anomaly variance (Fig. 7.2). This indicates the terrestrial influence through enhanced run-off to the coast, supplying sediment and nutrients. This result shows that the most important control on the OC4 anomaly variance originates from the terrestrial influence which interacted directly with typhoons. The 2nd mode appeared to be linked to the northeasterly wind component anomaly caused by typhoons, accounting for 31.8 % of the variance. Less than the effect of the typhoon rainfall anomaly, the typhoon wind anomaly is an important control on anomalous OC4 variability along the west coast of Okinawa. The highest eigenvector in the nearest point to the Hija River suggests a strong influence of typhoon winds that uplift

sediments delivered from the large river. The 3rd mode temporal function showed a relation with the ordinary northeasterly wind component anomaly, accounting for 11.8 %. This indicates the effect of coastal upwelling caused by the winter EAM anomaly.

The SST anomaly EOF suggests the strong influence of the outer ocean by showing a correlation between the temporal function of the 1st mode (accounting for 72.8 %) and the SST anomaly in D2, indicating the significance of the larger scale effect on local SST (Fig. 7.2). The 2nd mode showed an influence of the northeasterly component anomaly caused by typhoons, accounting for 12.3 %. This suggests the effect of the typhoon wind anomaly that causes upwelling, bringing colder water to the surface. Although typhoons are episodic and short-term events around Okinawa, the results here indicated their significance to function of the coastal environment around the Island.

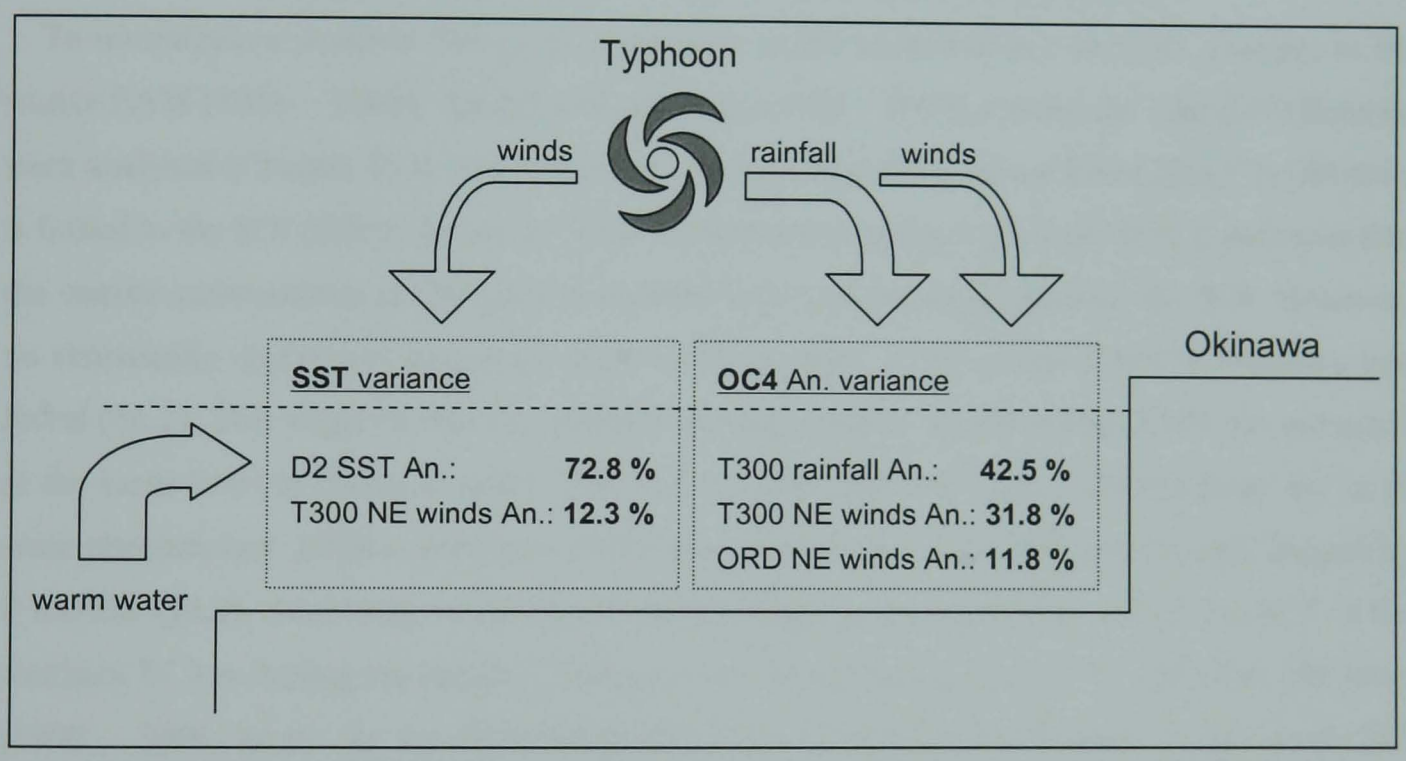

Fig. 7.2. Impact of typhoons on the west coast of Okinawa derived from EOF analyses applied on the SST (1985 – 2006) and OC4 (1998 – 2006) anomaly (AN). Distance between the typhoon centre and Okinawa less than 300 km (T300) was used to determine the month influenced by typhoon rainfall and winds. Rest of the month were defined as ordinary month (ORD).

7.2.4 Aim 4: Relationship between the winter EAM and sediments in the coast around Okinawa

It was also found that the influence of the winter EAM extends to the concentrations of the suspended particles in sea sediments (SPSS) off the west coast of Okinawa (Chapter 5, §5.4). The EAM's strong northerlies induce Ekman transport along the west coast of the Island, leading to resuspension of bottom sediments, and transport offshore, and hence a decrease in the sediment supply to the seafloor. The winter EAM, therefore, is a primary control, being

responsible for modulating the SPSS along the west coast of Okinawa. On the east coast, on the other hand, such an effect was not found because of the weak summer EAM's southeasterlies. Instead, rainfall brought by the summer EAM contributes to increasing the SPSS by increased soil erosion and run-off from the Island. Given the anomalous SPSS in Okinawa, studies have been rather concentrated on the terrestrial and coastal zones, e.g., soil loss estimation (Higa et al., 1995b; Nakasone et al., 1998), sediment yield modelling (Paringit and Nadaoka, 2003; Sakai and Osawa, 2005) and monitoring sediment (Nadaoka and Tamura, 1992; Higa et al., 2001; Omija et al., 2002). In this study, the statistical relationship between the SPSS loss and the winter EAM indicated a cycle of sediment input through terrestrial processes and sediment reduction via an atmospheric process.

7.2.5 Aim 5: Changes in key controls on the coastal zone around Okinawa

To investigate a possible change in importance of the identified key controls, changes in the winter EAM (1988 – 2005), rainfall and typhoons (1982 – 2005) around the Island of Okinawa were analysed (Chapter 6). It was found that the intensity of the winter EAM (DJF) in Okinawa is linked to the SOI (DJF): the winter EAM is high (low) during high (low) SOI. It indicates that the coastal environment of Okinawa is coupled with a global scale process, the SOI. However, no statistically significant long term trend in the strength of the winter EAM at Okinawa was found (§6.2). This suggests that the natural sediment removal by the winter EAM has remained at the same level in recent decades. The SST around Okinawa is also influenced by the large scale phenomenon, ENSO, showing a correlation between the local SST and the SOI, lagged by 5 months (§6.2). According to the *Japan Meteorological Agency* (JMA, 2007), the SST in the southern ECS including the Island of Okinawa has been increased by 1.1 °C in the last 100 years (1900 – 2006, §6.6). As the ECS temperature has a significant influence on the local SST around Okinawa, the coral reefs around the Island have experienced a combined climate impact: no changes in sediment removal by the winter EAM but increasing sea temperature, raising the risk of coral bleaching.

An analysis using a probability distribution function of daily rainfall data in Okinawa (1982 – 2005) revealed that light (0 – 3 mm/day) and mid-heavy (26 – 50 mm/day) rainfall has a statistically significant decreasing trend but heavy rainfall (> 76 mm/day) has an increasing trend with a statistical significance (Chapter 6, §6.4). It was found that heavy rainfall increase is due to rainfall (TR300) brought by typhoons which approached less than 300 km from the Island. Ordinary rainfall (OR) and TR300 contribute 92.4 % and 4.3 % respectively to all the rainfall frequency of occurrence (FOC), respectively, but 77.4 % and 18.6 % respectively to the accumulated rainfall amount (ARA) over Okinawa. For OR, rainfall intensities of 0 – 3 mm/day

and 26 – 50 mm/day were found to have a statistically significant decreasing trend in ARA: -1.0 mm/year and -10.1 mm/year respectively. For TR300, rainfall intensities of 4 – 25 mm/day and > 75 mm/day have a statistically significant increasing trend in FOC, particularly heavy rainfall (> 75 mm/day) showed a clear increasing trend (+10.8 mm/year) in ARA (§6.5). This result indicates the importance of typhoon rainfall despite its limited occurrence.

The cause of the typhoon rainfall increase was found not to be an increase in the number of strong typhoons but a result of the amount of rainfall provided per typhoon; particularly typhoons during MJJ and Sep, which showed a statistically significant trend of 5.9 mm/year and 6.5 mm/year respectively. Although it has been reported that the occurrence of strong storms in the Pacific Ocean has been increasing (Webster et al., 2005), this is not the case for the region around Okinawa. Increasing rainfall from typhoons and warming SST around Okinawa are shown schematically in Fig. 7.3.

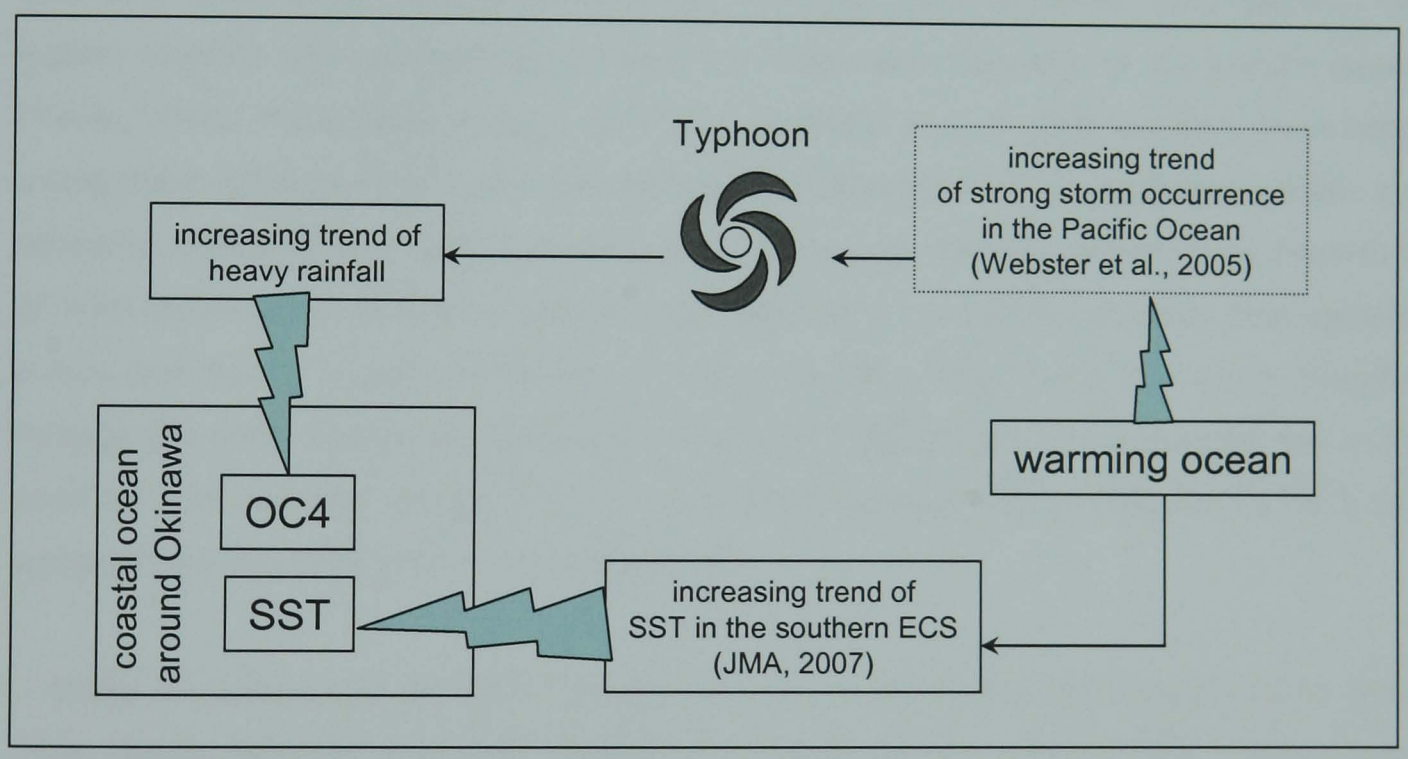

Fig. 7.3. Impact of a warming ocean on the coastal zone around Okinawa through typhoons and surrounding ocean.

An orographic effect on rainfall over Okinawa was also observed, showing expected higher rainfall over the hilly northern regions of the Island, particularly for TR300 (§6.5.3). This implies that orographically influenced regions will likely experience more heavy rainfall which will enhance soil erosion and run-off. Increasing heavy rainfall over the Island of Okinawa will influence soil run-off to coastal coral reefs around the Island. Its adverse effects, such as smothering corals, have already damaged the coastal environment of Okinawa significantly. To mitigate soil run-off problems, the *Red-soil Ordinance* was legislated in 1995 by the Okinawa Prefecture Government (OPG) which set the upper limit of the sediment concentration at 200 mg/l in the run-off from the developing sites. Other counter-measures included the use of check dams to trap sediments. These check dams were designed with an estimation of the heaviest

rainfall rate with a probability of occurrence once every ten years (Omija, 1992). Given an increasing trend of heavy rainfall over the Island, in order to keep the upper limit of the sediment concentration regulated in the Ordinance and to maintain the health of the coastal environment, greater protection at the development sites may be required. Specifications of the check dams may also need modification to prepare for increased run-off. Increasing heavy rainfall may influence the frequency of sediment-related disasters on land such as debris flow, landslide and slope failure. Danger zones may need careful attention, including a preparation for frequent heavy rainfalls to come.

7.3 Implications of This Study for Management of Coral Reefs in the Western Pacific

As mentioned in Chapter 1 (§1.1), coral reefs in the western Pacific Ocean are known for their rich biodiversity (Wilkinson, 2002, 2004). Particularly, Southeast Asia harbours the highest diversity and productivity of corals and associated organisms in the world's oceans (Veron, 1993). These corals occupy 32.3 % of the global total of coral reef area. For a better management of coral reefs in the coastal zone, the importance of understanding climate and terrestrial effects on the coastal zone has been noted because management needs an assessment of both long-term stress from climate control and short-term (but acute) stress from episodic events and human impact (Wilkinson and Buddemeier, 1994). From the results achieved through this study focused on the Island of Okinawa, implications for the management of the coral reefs in the wider western Pacific region under the same climate influence of the EAM, typhoons and terrestrial threats will be discussed.

Under the influence of the EAM, strong northerlies prevail in the region during winter and a rainy season develops over East Asia. It was found that the winter EAM causes coastal upwelling and enhances OC4 concentrations; particularly along the western coast of Okinawa (Chapter 4, §4.5.3). For the coastal zone around islands in South Asia the winter EAM, therefore, is an important climate control that can selectively increase the surface OC4 concentration. This suggests that a seasonal stress of sediments and nutrient around the coastal zone during winter will be apparent, providing favourable conditions for algal bloom but negative conditions for corals because of increased turbidity from abundant plankton and resuspension of sediments. However, the strong northerlies provided by the winter EAM also acts to remove some sediments from the seafloor off appropriately oriented coasts (Chapter 5, §5.4.2). This winter EAM effect of clearing sediments from the reefs may be more important than the seasonal increase in OC4 concentration. Indeed if the sediments are not removed from the reefs they may form a chronic stress from the smothering effects, and could hamper coral

recruitment through less of a hard bottom (McLaughlin et al., 2003). In fact, Hu et al. (2000) investigated the winter EAM response to global warming using a coupled general circulation model, and reported that winter northeasterlies along the Pacific coast of the Asian continent are weakened due to less difference in the sea level pressure and surface temperature between the Asian continent and the Pacific Ocean. This means that sediment removal by the winter EAM will be reduced in the coastal zone of the western Pacific under this scenario or in the future. Subsequently, sediments in the coastal zone will accumulate as a result of reduced removal and increasing input as heavy rainfall increases.

During summer months, the EAM provides a regional rainy season. This, combined with existing human impacts, exacerbates sediment and nutrient delivery from land to the coastal zone. In South East Asia, one of the major problems, that damages 88 % of their coral reefs, is increasing sedimentation and pollution from industrial and agricultural waste, and poor land-use practices (Wilkinson, 2002, 2004). Off the Island of Okinawa, the coastal zone near the largest river, the Hija River, is influenced from run-off delivering sediment and nutrients (Chapter 5, §5.2.2). For the islands of South East Asia, this terrestrial impact should be assessed, as this is a major cause of sediment and nutrient delivery to the coastal zone, which can be controlled by effective land management. The events originated from this type of terrestrial source provide short-term but acute impacts on coral reefs. If this effect exceeds the natural process of sediment removal by the winter EAM, sediments will be accumulated over the coral reefs adjacent to the rivers. For coastal zones near the large rivers, such terrestrial influence will be greater as the expected discharge volume from nearby catchments becomes larger.

Fig. 7.4 shows the ocean surface winds in Jan 2000 over Southeast Asia derived from the QuickSCAT satellite data (Chapter 3, §3.2.2). This shows the wind pattern of the winter EAM, strong northeasterlies over the South China Sea and Philippine Sea. With these prevailing winds, the sediment removal effect will be most apparent along the northeast to southwest oriented coasts in this region, which are marked in circles by Fig. 7.5. Fig. 7.5 also shows the estimated threat level of sedimentation and pollution from terrestrial sources on the coral reefs in Southeast Asia (Burke et al., 2002). Within the circled zones in Fig. 7.5, the coasts with a high sedimentation threat level are the likely regions where the natural sediment removal will act to counter the rising sedimentation problems, if heavy rainfall occurs more frequently (high sediment input) and the winter EAM becomes weaker (low sediment removal). Other high risk coasts will need greater management of soil erosion and run-off during heavy rainfall periods because the effect of the winter EAM is small. These regions will likely keep high levels of sedimentation as seen in the eastern coast of Okinawa that shows little seasonal pattern.

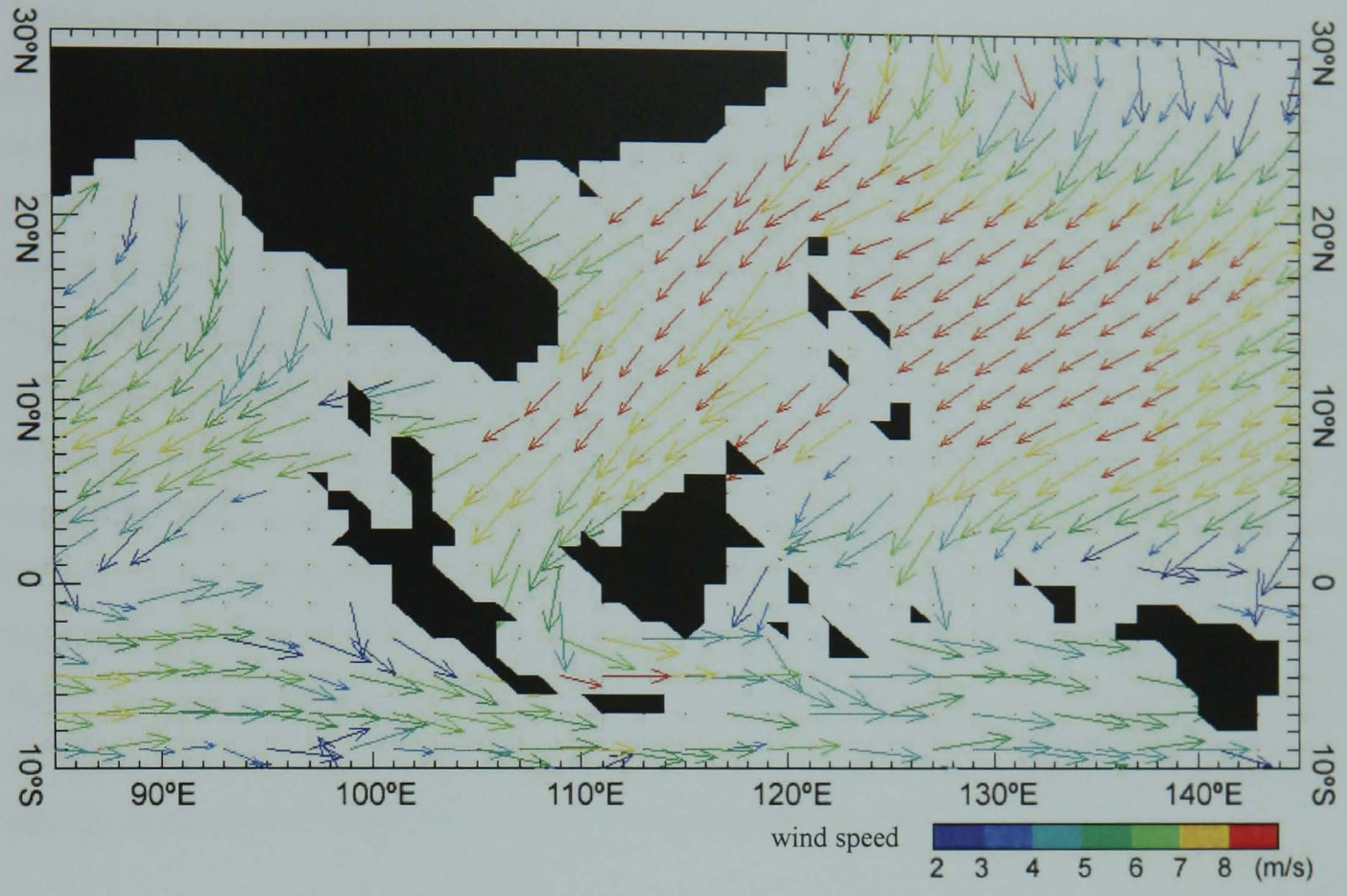

Fig. 7.4. Ocean surface wind (the winter EAM) over Southeast Asia in Jan 2000. Processed from SeaWinds data, same data source described in Chapter 3, §3.2.2.

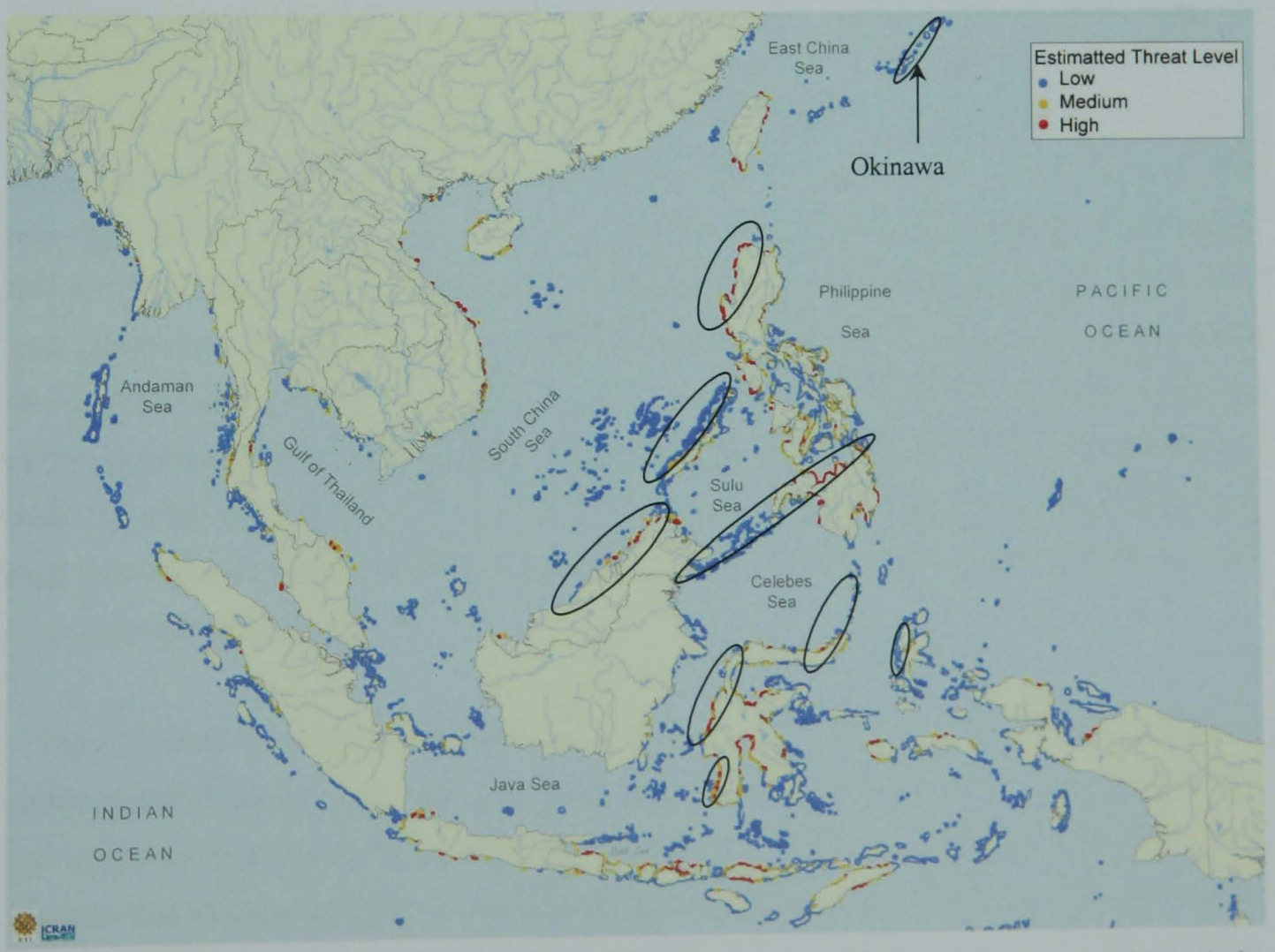

Fig. 7.5. Southeast Asia reefs threatened by sedimentation and pollution from terrestrial sources (adapted from Burke et al., 2002). The circles indicate the reef zones where the influence of the winter EAM is likely to be high and contribute to the OC4 variability and thus sediment removal.

Although the occurrence of strong typhoons appeared not to be increasing around Okinawa (Chapter 6, §6.5.2), Webster et al. (2005) showed an increasing trend for strong tropical storms in the Pacific Ocean. This trend is likely to be more applicable to South East Asia, as a whole, rather than a local study in a small island of Okinawa. Thus, there is a possibility of an additional increase in terrestrial impact due to frequent typhoon visits over South East Asia. Terrestrial influences through the rivers will be greater not only from the scale of rivers but also under the trend of a globally warming environment in recent years (Solomon et al., 2007). As the analysis of rainfall trend over Okinawa indicated (Chapter 6, §6.5.1), heavy rainfall has been increasing. Importantly, this increasing trend of heavy rainfall is brought by typhoons; not because of more frequent typhoons approaching Okinawa but rainfall per typhoon was found to be increasing. Importantly, if this is also true for typhoons in other regions, heavy rainfall over South East Asia is likely to be influenced by typhoons (tropical cyclones), and their impact will be even more severe due to associated strong winds that cause disturbances over land surfaces, leading to increased vulnerability to soil erosion in some regions.

It has to be mentioned that the EAM is a large scale phenomenon linked to the ENSO (Lau et al., 2001; Wang et al., 2000; Hui, 2007, Chapter 6, §6.2). The impact of the strong El Niño of 1997/98 provided a clear event which brought anomalously high ocean temperatures, causing a significant coral bleaching event around Okinawa (Yamazato, 1999; Loya et al., 2001). Fig. 7.6 shows the SST anomaly in 1998 and the extent of coral bleaching observed in Southeast Asia (Burke et al., 2002). Most of the regions experienced high SST in this period and many bleaching events were observed in the Gulf of Thailand and Sulu Sea. The winter EAM in 1998 was considerably weakened due to this El Niño (Chapter 6, §6.2), which enhanced the Hadley cell and the westerlies in the mid-latitudes, resulting in movement of the polar front zone in East Asia northward, hampering cold air breakouts southward (Li, 1990). This event demonstrates the combined impact of the oceanic (high sea temperature) and climatic (low sediment removal) on the coral reefs. Thus, in this region soil erosion and run-off must also be well controlled to take into account extreme events such as ENSO, in order to minimise coral degradation from high SST and low natural sediment removal, particularly for the coasts with a high threat level of sedimentation in Fig. 7.5.

Future trends in ocean temperature are a very important factor for sustainable coral reef environments (Chapter 1, §1.1.2). The JMA (2007) reported that the SST in the southern ECS has increased by as much as 1.1 °C in the last 100 years (1900 – 2006; Chapter 6, §6.6). This suggests that a serious increase in coral bleaching events under high ocean temperatures is likely. This warming sea environment is not just a problem for the coral reefs of the ECS and South East Asia, but a global threat (Wilkinson and Buddemeier, 1994; Wilkinson, 2004). Coral reefs

in the western Pacific will more likely share similar warming conditions to Okinawa. This is therefore an issue that needs a global and international cooperation to tackle climate change. Terrestrial control is an issue that can be dealt with at a local level, for example via implementing of an appropriate land management plan to reduce soil erosion and sediment delivery. Under the warming trend of global environment and increasing trend of terrestrial influence on the coastal zone, assessment and planning of land management will be very crucial (Chapter 6, §6.6). Given the impacts of high sea temperature, heavy rainfall, typhoons' strong winds, sediments delivery, actions are needed both globally and locally in the western Pacific to secure coral reef biodiversity and avoid further coral mortality.

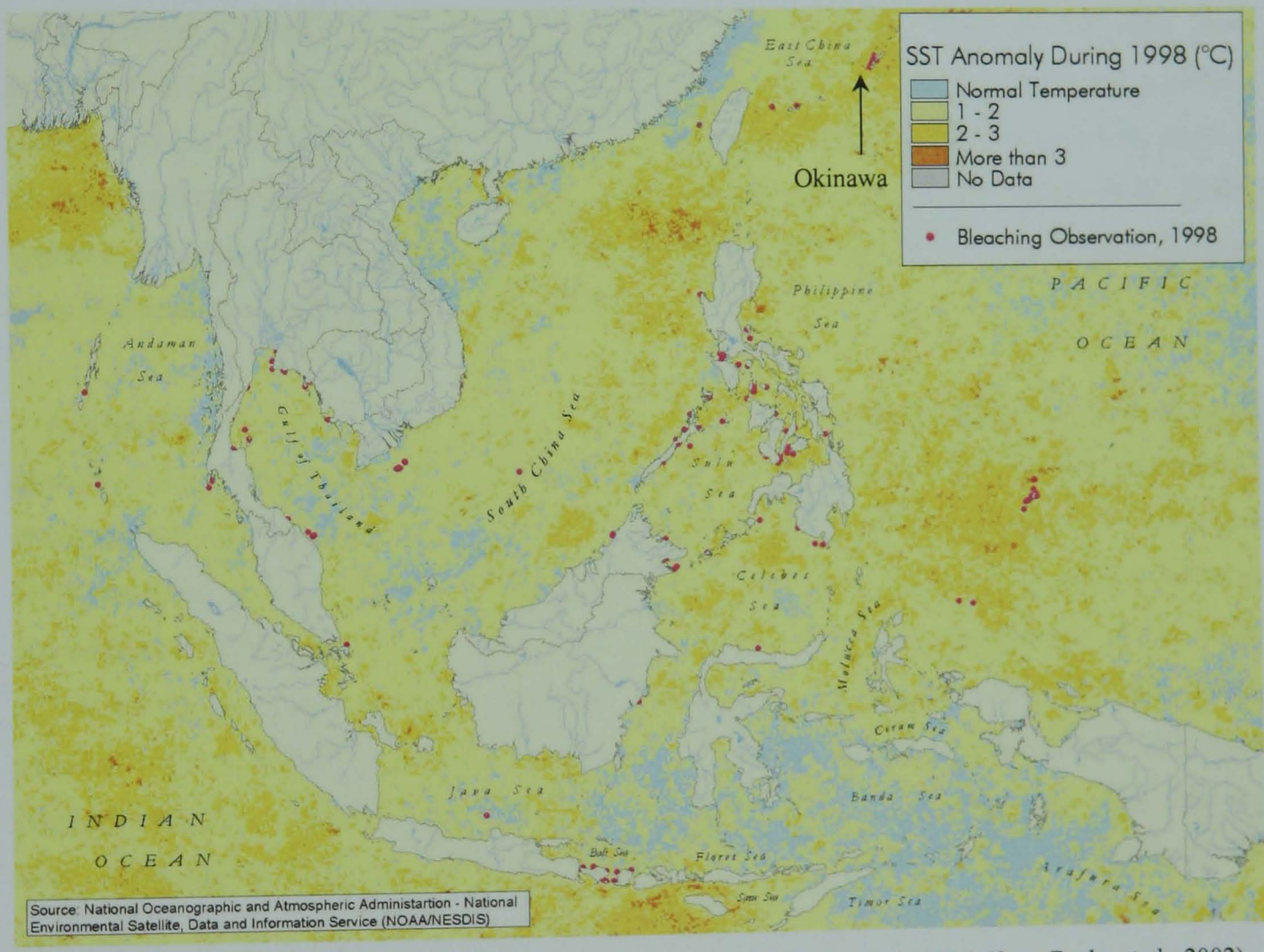

Fig. 7.6. The SST anomalies and observations of coral bleaching in Southeast Asia, 1998 (from Burke et al., 2002).

7.4 Future Work

7.4.1 Climate Studies

In this study, key controls on the stakes of the coastal zone have been investigated through basic stochastic approaches that sought to derive empirical relations between climate, terrestrial, and decomposed signals from EOFs. For future work, one of the next steps will be some additional modelling work based on relations between these variables both in space and time. In essence this should be within a physical model, particularly one which couples a hydrodynamic

model involving ocean current movement and flows from the land. In the ocean around the Island of Okinawa, there are active ocean dynamics; the KC to the west, and warm eddy approaches to the east of Okinawa. This physical modelling work could advance understanding of water movement not only for horizontal surface flows but also for a three-dimensional interpretation, which is important to estimate oceanic upwelling and downwelling. Linking a biogeochemical component to the physical model (e.g., Liu et al., 2002) is also a challenge which requires a range of biological parameters to be determined e.g., chlorophyll growth/mortality rate dependency on temperature, nitrogen and light in a future work. Understanding the links between climate, ocean, and biogeochemical processes will make it possible to draw scenarios with climate change and provide detailed information for environmental managers. Modelling and forecasting of typhoons will also become more important since the warming trend appears likely to increase occurrence of strong typhoons (Webster et al., 2005). In addition, interaction with warm eddies around Okinawa may need to be investigated to evaluate the local cause of increasing typhoon intensity, as Lin et al. (2005) reported that Super Typhoon Maemi's intensity rapidly increased when it encountered a warm eddy in the western Pacific in September 2003.

A research issue which needs to be addressed in order to better understand a local scale process is the generation of more detailed spatial information related to the coastal zone around small islands like Okinawa. In this study, the spatial resolution used to analyse the SST and OC4 variability was about 9 km. With this resolution, it was difficult to select pixels adjacent to the coastlines in the east side of Okinawa (Chapter 5, §5.3.1). To overcome this problem, an option would be to use the Moderate Resolution Imaging Spectrometer (MODIS) data which provide 250 m, 500 m and 1000 m resolution for both SST and ocean colour. Although continued MODIS observations are available only after 2002, it is worth using these data for local scale assessments and case studies. Field work will also be needed, particularly for calibration, validation of remote sensing data, and for investigation of extreme events of heavy rainfall or El Niño. Together with field data, remote sensing using new sensors will contribute to assess the efficiency of water policies through the observation (Gohin et al., 2008). It is difficult to conduct in-situ surveys over the long-term, but short-term studies are still important in order to identify localised characteristics, e.g., different tendencies in sediment removal by the winter EAM along the west coast of Okinawa (Chapter 5, §5.5.3).

7.4.2 Terrestrial Studies

In order to advance the understanding of terrestrial processes that influence the coastal environment, high quality and high frequent monitoring of sediment flux is desirable. Although

the *OPG Environment Conservation Section* monitors the concentration of suspended matter in river discharges to assess their water quality, this measurement is implemented once a month in fine weather (i.e. no rain). It is therefore extremely difficult to estimate the impact of rainfall on sediment and nutrient flux in the discharge. If using these data with suspended matter and discharge volume at higher temporal resolution, it would be possible to model a rating curve and to estimate sediment concentration; and hence estimate the amount of sediment delivery to the coast. Rating curves can be also used to estimate the change in sediment concentration caused by an individual event (e.g., typhoon and landslide) by comparison of two curves from pre- and post-event data. The development of a distributed model for soil erosion in Okinawa would be very useful, not only to understand the terrestrial process of sediment delivery, but also for a better land management to effectively implement erosion protection and to plan the placement of check dams.

7.4.3 Possible Future Impacts

Rising SST is a crucial issue for the survival of coral reefs. The global extent of coral bleaching observed during the 1997/98 ENSO foreshadows the likely serious consequences of increasing SST associated with climate change (Burke et al., 2002). The SST have been raised so close to coral thermal limits that the fluctuations of temperatures within natural climatic events such as ENSO can cause massive coral bleaching (Hoegh-Guldberg, 1999). In fact, reports of mass coral bleaching have increased greatly since 1979 (Logh, 2000). Therefore monitoring changes in SST is essential both at global scale (to watch the occurrence of the ENSO) and local scale (to reduce additional terrestrial impact). In addition to the effect of high SST on coral bleaching, its impact on chlorophyll growth may need to be considered under a warming environment to interpret the OC4 variability. An in-situ survey of phytoplankton biomass during 1998 – 1999 off the east coast off Sesoko Island located northwest of Okinawa by Tada et al. (2003) suggested that the high sea temperature in 1998 (which was caused by the strong El Niño event) reduced the total phytoplankton biomass significantly. It is known that beyond the optimum temperature at which maximum growth is obtained, the growth rate of phytoplankton decreases drastically with increasing temperatures (Eppley, 1972). As Tada et al. (2003) indicated the effect of anomalous sea temperature on phytoplankton in a site around Okinawa, an extreme event of high sea temperature will be a limiting factor on the OC4 variability. In this consideration, it is likely that not only an El Niño event but also warm eddies may decrease the OC4 concentration. Although the effect of warm eddies on OC4 was not observed directly in this study (Chapter 4, §4.7.2), a decreasing signal may occur if the warm water of the eddy exceeds the optimum temperature for phytoplankton growth and persists for long enough around Okinawa to impact on survival of corals.

Under global warming, impacts on the coral ocean will come not only from increased sea temperatures but also increased atmospheric CO_2 concentrations. This will result in more dissolved CO_2 in the ocean and acidification of the sea. Dissolved CO_2, when combined with water, produces carbonic acid, which releases ionised hydrogen that combines with a carbonate ion. This decreases the concentration of carbonate, therefore slowing calcification rates in corals. Acidification combined with high water temperature will create a combined stress on coral reefs, and the result will more likely be less diverse reef communities and carbonate reef structures (Hoegh-Guldberg et al., 2007). Therefore, understanding the changes in CO_2 concentration both in the atmosphere and ocean will be important for assessing the climate impact on the coral ocean.

In this study, climate controls on the coastal zone were found to be the primary factor influencing its characteristics, and the terrestrial factor was found to be secondary; but with an important short-term impact. Under global changes in climate, it is important to understand the behaviour of these key controls. The combined effect of climate change and terrestrial impacts will more likely exacerbate stresses on coral reefs at both global and local scales, driving reefs increasingly toward the tipping point of functional collapse (Hoegh-Guldberg et al., 2007). Multi-scaled management intervention and decisive action are required if coral ecosystems are to be preserved (Hoegh-Guldberg et al., 2007); and at the same time a multi-scaled and inter-disciplinary research programme is important to advance the science of the coastal environment and to apply the gained knowledge more broadly.

Reference

Acker, J. G., Vasilkov, A., Nadeau, D. and Kuring, N. (2004). "Use of SeaWiFS ocean color data to estimate neritic sediment mass transport from carbonate platforms for two hurricane-forced events." Coral Reefs 23(1): 39-47.

Adler, R. F., Huffman, G. J., Chang, A., Ferraro, R., Xie, P.-P., Janowiak, J., Rudolf, B., Schneider, U., Curtis, S., Bolvin, D., Gruber, A., Susskind, J., Arkin, P. and Nelkin, E. (2003). "The Version-2 Global Precipitation Climatology Project (GPCP) Monthly Precipitation Analysis (1979-Present)." Journal of Hydrometeorology 4(6): 1147-1167.

Ahagon, N., Tanaka, Y. and Ujiie, H. (1993). "Florisphaera profunda, a possible nannoplankton indicatro of late Quaternary changes in sea-water turbidity at the northwestern margin of the Pacific." Marine Micropaleontology 22: 255-273.

Ahn, Y.H., Moon, J.E., Gallegos, S. (2001). "Development of suspended particulate matter algorithms for ocean color remote sensing." Korean journal of remote sensing 17: 285-295.

Alcala, A. C., Gomez, E. D. and Yap, H. T. (1987). "Phillipine coral reefs: status and human response to changes." Resource Management and Optimization 4: 297-340.

Andréfouët, S., Mumby, P., McField, M., Hu, C. and Muller-Karger, F. (2002). "Revisiting coral reef connectivity." Coral Reefs 21(1): 43-48.

Aoki, S., Imawaki, S. and Ichikawa, K. (1995). "Baroclinic disturbances propagating westward in the Kuroshio Extenstion region as seen by satellite altimeter and radiometer." Journal of Geophysical Research 100: 839-855.

Babin, S. M., Carton, J. A., Dickey, T. D. and Wiggert, J. D. (2004). "Satellite evidence of hurricane-induced phytoplankton blooms in an oceanic desert." Journal of Geophysical Research 109: C03043, doi:10.1029/2003JC001938.

Barnes, R. A., Holmes, A. W., Barnes, W. L., Esaias, W. E., McClain, C. R. and Svitek, T. (1994). SeaWiFS Prelaunch Radiometric Calibration and Spectral Characterization. NASA Technical Memo 104566. S. B. Hooker, E. R. Firestone and J. G. Acker. Greenbelt, Maryland, NASA Goddard Space Flight Center. 23: 55.

Barton, Ian (1995). "Satellite-derived sea surface temperatures: Current status." Journal of Geophysical Research, 100 (C5): 8777-8790.

Beardsley, R. C. R., Limeburner, H. Y. and Cannon, G. A. (1985). "Discharge of the Changjiang (Yangtze River) into the East China Sea." Continental Shelf Research 4: 57-76.

Beaufort, L., de Garidel-Thoron, T., Linsley, B., Oppo, D. and Buchet, N. (2003). "Biomass burning and oceanic primary production estimates in the Sulu Sea area over the last 380 kyr and the East Asian monsoon dynamics." Marine Geology 201(1-3): 53-65.

Bellingham, P. J., Kohyama, T. and Aiba, S. (1996). "The effects of a typhoon on Japanese warm-temperate rain forests." Ecological Research 11: 229-247.

Bellwood, D. R., Hughes, T. P., Folke, C. and Nystrom, M. (2004). "Confronting the coral reef crisis." Nature 429(6994): 827-833.

Bessho, K., Tanaka, Y. and Nakazawa, T. (2001). Validation of GMS brightness temperature difference technique for estimate of cumulonimbus in typhoon by TRMM PR data. 11th Conference on Satellite Meteorology and Oceanography, Madison, WI.

Bigg, G. R. and Inoue, M. (1992). "Rossby waves and El Nino during 1935-46." Quartery Journal of the Royal Meteorological Society 118: 125-152.

Bingham, F. M. (1992). "The formation and spreading of subtropical mode water in the North Pacific." Journal of Geophysical Research 97: 11 177- 11 189.

Bray, J. R. and Gorham, E. (1964). "Litter production in forests of the world." Advances in Ecology Research 2: 229-247.

Brown, B. E. and Ogden, J. C. (1993). "Coral bleaching." Scientific American 268: 64-70.

Burke, L., Selig, L. and Spalding, M. (2002). Reefs at Risk in Southeast Asia, World Resources Institute.

Campbell, J. and Aarup, T. (1992). "New production in the North Atlantic derived from seasonal patterns of surface chlorophyll." Deep Sea Research 39(10A): 1669-1694.

Carter, E. F. (1983). The Statistics and Dynamics of Ocean Eddies. Division of Applied Science. Cambridge, Massachusetts, Harvard University. PhD thesis.

Carter, E. F. and Robinson, A. R. (1987). "Analysis Models for the Estimation of Oceanic Fields." Journal of Atmospheric and Oceanic Technology 4(1): 49-74.

Chang, C. P. and Lau, K. M. (1980). "Northeasternly cold surges and near-equatorial disturbances over the Winter-MONEX area during 1974. Part II: Planetary scale aspects." Monthly Weather Review 108: 293-312.

Chen, C., Beardsley, R. C., Limeburner, R. and Kim, K. (1994). "Comparison of winter and summer hydrographic observations in the Yellow and East China Seas and adjacent Kuroshio during 1986." Continental Shelf Research 14(7-8): 909-929.

Chen, G. J. J. and Chang, C.-P. (1980). "The structure and vorticity budget of an early summer monsoon trough (Mei-Yu) over South China and Japan." Monthly Weather Review 108(942-953).

Chen, T.-C., Wang, S.-Y., Huang, W.-R. and Yen, M.-C. (2004). "Variation of the East Asian Summer Monsoon Rainfall." Journal of Climate 17(4): 744-762.

Chou, L. M. (1991). "Community structure of sediment stressed reefs in Singapore." Galaxea 7: 101-111.

Chuang, W.-S. (1985). "Dynamics of subtidal flow in the Taiwan Strait." Journal of the Oceanographic Society Japan 41: 65-72.

Chuang, W.-S. (1986). "A note on the driving mechanism of current in the Taiwan Strait." Journal of the Oceanographic Society Japan 42: 355-361.

Chuang, W.-S. and Liang, W.-D. (1994). "Seasonal variability of intrusion of the Kuroshio water across the continental shelf northeast of Taiwan." Journal of Oceanography 50(5): 531-542.

Chung, Y. C. and Chang, W. C. (1995). "210Pb fluxes and sedimentation rates on the lower continental slope between Taiwan and the South Okinawa Trough." Continental Shelf Research 5(149-164).

Chung, Y.-C. and Hung, G.-W. (2000). "Particulate fluxes and transports on the slope between the southern East China Sea and the South Okinawa Trough." Continental Shelf Research 20(4-5): 571-597.

Clark, D. W. (1981). Phytoplankton pigment algorithms for the Nimbus-7 CZCS. Oceanography From Space. J. F. R. Gower. New York, Plenum.

Clarke, G. L., Ewing, G. C. and Lorenzen, C. J. (1970). "Spectra of Backscattered Light from the Sea Obtained from Aircraft as a Measure of Chlorophyll Concentration." Science 167(3921): 1119-1121.

Dippner, J., Nguyen, K., Hein, H., Ohde, T. and Loick, N. (2007). "Monsoon-induced upwelling off the Vietnamese coast." Ocean Dynamics 57(1): 46-62.

Doty, M. S. and Oguri, M. (1956). "The Island Mass Effect." ICES J. Mar. Sci. 22(1): 33-37.

Dunbar, R. S., Hsiao, S. V., Kim, Y. J., Pak, K. S., Weiss, B. H. and Zhang, A. (2001). Science Algorithm Specifications for SeaWinds on QuickSCAT and SeaWinds on ADEOS-II.

JPL D-21978. Pasadena, CA, Jet Propulsion Laboratory, California Institute for Technology.

Ebuchi, N. and Hanagawa, K. (2001). "Trajectory of mesoscale eddies in the Kuroshio recirculation region." Journal of Oceanography 57: 471-480.

Eppley, R. W. (1972). "Temperature and phytoplankton growth in the sea." Fishery Bulletin 70: 1063-1085.

Eppley, R. W. and GRenger, E. H. (1988). "Nanomolar increase in surface layer nitrate concentration following a small wind event." Deep-Sea Research 35: 1119-1125.

Erickson, D. J., Hemandez, J. L., Ginoux, P., Gregg, W. W., McClain, C. and Christian, J. (2003). "Atmospheric iron delivery and surface ocean biological activity in the Southern Ocean and Patagonian region." Geophysical Research Letters 30(12): 1609.

Falkowski, P. G., Jokiel, P. L. and Kinzie III, R. A. (1990). Irradiance and corals. Coral Reefs: Ecosystems of the World 25. D. Z. New York, Elsvier: 89-107.

Fairbridge, R. W. (1980). The estuary: Its definition and geodynamic cycle. Chemistry and Biochemistry of Estuaries. E. Olausson and I. Cato. New York, John Willey.

Fukushima, S. and Yamazaki, T. (2002). "Abnormal High Sea Level in the Vicinity of the Okinawa Island." Techinical Bullein on Hydrography 20: 7-10.

Galewsky, J., Stark, C. P., Dadson, S., Wu, C.-C., Sobel, A. H. and Horng, M.-J. (2006). "Tropical cyclone triggering of sediment discharge in Taiwan." Journal of Geophysical Research 111: F03014, doi:10.1029/2005JF000428.

Gallegos, C. L., Jordan, T. E. and Correll, D. L. (1992). "Event-Scale Response of Phytoplankton to Watershed Inputs in a Subestuary: Timing, Magnitude, and Location of Blooms." Limnology and Oceanography 37(4): 813-828.

Gibo, S., Zhao, T., Karashima, M., Sasaki, K. and Yoshizawa, M. (1998). "Slope failures in the Kunigami-maaji (red) soil area in Okinawa." Bulletin of Faculty of Agriculture, University of the Ryukyus 4: 157-166.

Gitelson, A. (1992). "The peak near 700 nm on radiance spectra of algae and water: relationships of magnitude and position with chlorophyll concentration." International Journal of Remote Sensing 13(17): 3367-3373.

Glynn, P. W. (1993). "Coral reef bleaching: ecological perspectives." Coral Reefs 12: 1-18.

Gohin, F., Saulquin, B., Oger-Jeanneret, H., Lozac'h, L., Lampert, L., Lefebvre, A., Riou, P. and Bruchon, F. (2008). "Towards a better assessment of the ecological status of coastal

waters using satellite-derived chlorophyll-a concentrations." Remote Sensing of Environment 112(8): 3329-3340.

Gong, G.-C., Lee Chen, Y.-L. and Liu, K.-K. (1996). "Chemical hydrography and chlorophyll a distribution in the East China Sea in summer: implications in nutrient dynamics." Continental Shelf Research 16(12): 1561-1590.

Gong, G.-C., Shiah, F.-K., Liu, K.-K., Chuang, W.-S. and Chang, J. (1997). "Effect of the Kuroshio intrusion on the chlorophyll distribution in the southern East China Sea during spring 1993." Continental Shelf Research 17(1): 79-94.

Gong, G.-C., Wen, Y.-H., Wang, B.-W. and Liu, G.-J. (2003). "Seasonal variation of chlorophyll a concentration, primary production and environmental conditions in the subtropical East China Sea." Deep Sea Research Part II: Topical Studies in Oceanography 50(6-7): 1219-1236.

Gordon, H. R., Brown, O. B., Evans, R. H., Brown, J. W., Smith, R. C., Baker, K. S. and Clark, D. K. (1988). "A semianalytic radiance model of ocean color." Journal of Geophysical Research 93: 909-924.

Gordon, H. R., Clark, D. K., Mueller, J. L. and Hovis, W. A. (1980). "Phytoplankton Pigments from the Nimbus-7 Coastal Zone Color Scanner: Comparisons with Surface Measurements." Science 210(4465): 63-66.

Gray, W. M. (1968). "Global view of the origin of tropical disturbances and storms." Monthly Weather Review 96: 669-700.

Great Barrier Reef Marine Park Authority (1989). The Great Barrier Reef: Reef Notes. Townsville, Great Barrier Reef Marine Park Authority.

Grigg, R. W. and Dollar, S. J. (1990). Natural and anthropogenic disturbances on coral reefs. Coral reefs: Ecosystem of the World 25. Z. Dubinsky (Ed.). Amsterdam, Elsevier: 439-452.

Gross, M. G. (1990). Oceanography. Columnbus, Merrill.

Gu, G., Adler, R. F., Huffman, G. J. and Curtis, S. (2007). "Tropical Rainfall Variability on Interannual-to-Interdecadal and Longer Time Scales Derived from the GPCP Monthly Product." Journal of Climate 20(15): 4033-4046.

Hallock, P. (1988). "The role of nutrient availability in bioerosion: consequences to carbonate buildups." Palaeogeography, Palaeoclimatology, Palaeoecology 63: 275-291.

Hama, T., Shin, K. H. and Handa, N. (1997). "Spatial Variability in the Primary Productivity in the East China Sea and Ita Adjacent Waters." Journal of Oceanography 53: 44-51.

Hamaya, T., Nishida, Y., Setani, T. and Koga, M. (1994). Physics of the Earth. Tokyo. Gakujutsutosho Press.

Han, L. (1997). "Spectral reflectance with varying suspended sediment concentrations in pure and algal-laden waters." Photogrammetric Engineering & Remote Sensing 63(6): 701-705.

Hanawa, K. and Kamada, J. (2001). "Variability of Core Layer Temperature (CLT) of the North Pacific Subtropical Mode Water." Geophysical Research Letters 28(11): 2229-2232.

Hanawa, K., Watanabe, T., Iwasaka, N., Suga, T. and Toba, Y. (1998). "Surface thermal conditions in the western North Pacific during the ENSO events." Journal of the Meteorological Society of Japan 66: 445-456.

Hannachi, A., Jolliffe, I. T. and Stephenson, D. B. (2007). "Empirical orthogonal functions and related techniques in atmospheric science: A review." International Journal of Climatology 27(9): 1119-1152.

Hashizume, H., Xie, S.-P., Fujiwara, M., Shiotani, M., Watanabe, T., Tanimoto, Y., Liu, W. T. and Takeuchi, K. (2002). "Direct Observations of Atmospheric Boundary Layer Response to SST Variations Associated with Tropical Instability Waves over the Eastern Equatorial Pacific." Journal of Climate 15(23): 3379-3393.

Hatcher, B. G., Imberger, J. and Smith, S. V. (1987). "Scaling analysis of coral reef systems: an approach to problems of scale." Coral Reefs 5(4): 171-181.

Haunting, S., Z., Chao, X. C. and Jianrong, Z. (1998). Change of the discharge and sediment flux to estuary I Changjing River. Seoul, The Earth Love Publication Association.

Hayes, S. P., McPhaden, M. J. and Wallace, J. M. (1989). "The influence of sea surface temperature on surface wind in the eastern equatorial Pacific." Journal of Climate 2: 1500-1506.

Hennessy, K. J., Gregory, J. M. and Mitchell, J. F. B. (1997). "Changes in daily precipitation under enhanced greenhaouse conditions." Climate Dynamics 13: 667-680.

Higa, E., Hanashiro, K., Omija, T. and Mitsumoto, H. (1995b). "Source of Soil Run-Off on Okinawa Island." Annual Report of Okinawa Prefectural Institute of Health and Environment 29: 89-98.

Higa, E., Mitsumoto, H., Nakasone, K. and Omija, T. (1998). "Study on Soil Erosion of the Main Soils of Okinawa." Annual Report of Okinawa Prefectural Institute of Health and Environment 32: 83-95.

Higa, E., Nakasone, K., Omija, T. and Hiroaki, M. (2001). "Pollutants Run-off from Mouth of Rivers to Sea in Okinawa Island." Annual Report of Okinawa Prefectural Institute of Health and Environment 35: 111-119.

Higa, E., Omija, T., Hanashiro, K. and Mitsumoto, H. (1995a). "Quantity of Soil Run-Off on Okinawa Island." Annual Report of Okinawa Prefectural Institute of Health and Environment 29: 83-88.

Highsmith, R. C. (1982). "Reproduction by fragmentation in corals." Marine Ecology - Progress Series 7: 207-226.

Ho, C.-R., Zheng, Q. and Kuo, N.-J. (2004). "SeaWiFS observations of upwelling south of Madagascar: long-term variability and interaction with East Madagascar Current." Deep Sea Research Part II: Topical Studies in Oceanography 51(1-3): 59-67.

Hoegh-Guldberg, O. (1999). "Climate change, coral bleaching and the future of the world's coral reefs." Marine and Freshwater Research 50(8): 839-866.

Hoegh-Guldberg, O., Mumby, P. J., Hooten, A. J., Steneck, R. S., Greenfield, P., Gomez, E., Harvell, C. D., Sale, P. F., Edwards, A. J., Caldeira, K., Knowlton, N., Eakin, C. M., Iglesias-Prieto, R., Muthiga, N., Bradbury, R. H., Dubi, A. and Hatziolos, M. E. (2007). "Coral Reefs Under Rapid Climate Change and Ocean Acidification." Science 318(5857): 1737-1742.

Houghton, J. T., Ding, Y., Griggs, D. J., Noguer, M., van der Linden, P. J., Dai, X., Maskell, K. and Johnson, C. A. (2001). Climate Change 2001: The Scientific Basis. Cambridge, Cambridge University Press.

Houghton, J. T., Jenkins, G. J. and Ephraums, J. J. (1990). Climate change: the IPCC scientific assessment. Cambridge, UK, Cambridge University Press.

Hu, Z.-Z., Bengstton, L. and Arpe, K. (2000). "Impact of global warming on the Asian winter monsoon in a coupled GCM." Journal of Geophysical Research 105(D4): 4607-4624.

Huang, C. Y., Wu, S. F., Zhao, M., Chen, M. T., Wang, C. H., Tu, X. and Yuan, P. B. (1997). "Surface ocean and monsoon climate variability in the South China Sea since the last glaciation." Marine Micropaleontol 32: 71-94.

Huang, S., Yang, J., Ji, W., Wang, X. and Chen, G. (1983). Silicon, nitrogen and phosphorus in the Changjian River Mouth water. Proceedings of International Symposium on Sedimentation on the Continental Shelf with Special Reference to the East China Sea, Beijing, China Ocean Press, Beijin, 220-228.

Huddleston, J. N. and Stiles, B. W. (2007). Multidimensional Histogram (MUDH) Rain Flag Product Description Version 2.1, Jet Propulsion Laboratory.

Hughes, T. P., Baird, A. H., Bellwood, D. R., Card, M., Connolly, S. R., Folke, C., Grosberg, R., Hoegh-Guldberg, O., Jackson, J. B. C., Kleypas, J., Lough, J. M., Marshall, P., Nystrom, M., Palumbi, S. R., Pandolfi, J. M., Rosen, B. and Roughgarden, J. (2003). "Climate Change, Human Impacts, and the Resilience of Coral Reefs." Science 301(5635): 929-933.

Hui, G. (2007). "Comparison of East Asia winter monsoon indices." Advances in Geosciences 10: 31-37.

Hwang, C., Wu, C. R. and Kao, R. (2004). "TOPEX/Poseidon observations of mesoscale eddies over the subtropical counter-current: Kinematic characteristics of an anticyclonic eddy and of a cyclonic eddy." Journal of Geophysical Research 109: C08013, doi:10.1029/2003JC002026.

Ichikawa, H. and Beardsley, R. C. (2002). "The Current System in the Yellow and East China Seas." Journal of Oceanography 58: 77-92.

International Ocean Color Coordinating Group (2000). Remote sensing of ocean colour in coastal, and other optically complex, waters. Report on 3. Dartmouth, IOCCG: 140.

Iseki, K., Okamura, K. and Kiyomoto, Y. (2003). "Seasonality and composition of downward particulate fluxes at the continental shelf and Okinawa Trough in the East China Sea." Deep Sea Research Part II: Topical Studies in Oceanography 50(2): 457-473.

Ito, Y. (1997). "Diversity of forest tree species in Yanbaru, the northern part of Okinawa Island." Plant Ecology 133: 125-133.

Jan, S., Wang, J., Chern, C.-S. and Chao, S.-Y. (2002). "Seasonal variation of the circulation in the Taiwan Strait." Journal of Marine Systems 35(3-4): 249-268.

Japan Meteorological Agency (2005). Extreme Weather Report 2005. Japan Meteorological Agency: 110-114.

Japan Meteorological Agency (2007). Long term changes in the SST around Japan. Press release material (May/15/2007), Japan Meteorological Agency: 1-6.

Japan Weather Association (1973). Typhoon Tracks for 30 Years (1940 - 1970).

Jensen, J. R. (2000). Remote sensing of the environment: an earth resource perspective. Prentilce-Hall, Inc.

Jhun, J.-G. and Lee, E.-J. (2004). "A New East Asian Winter Monsoon Index and Associated Characteristics of the Winter Monsoon." Journal of Climate 17(4): 711-726.

Jickells, T. D., An, Z. S., Andersen, K. K., Baker, A. R., Bergametti, G., Brooks, N., Cao, J. J., Boyd, P. W., Duce, R. A., Hunter, K. A., Kawahata, H., Kubilay, N., laRoche, J., Liss, P. S., Mahowald, N., Prospero, J. M., Ridgwell, A. J., Tegen, I. and Torres, R. (2005). "Global Iron Connections Between Desert Dust, Ocean Biogeochemistry, and Climate." Science 308(5718): 67-71.

Johnson, R. H., Wang, Z. and Bresch, J. F. (1993). "Heat and moisture budgets over China during the early summer monsoon." Journal of the Meteorological Society of Japan 71(137-152).

Jokiel, P. L. and Coles, S. J. (1990). "Response of of Hawaiian and other Indo-Pacific reeef corals to elevated temperature." Coral Reefs 8: 115-162.

Kao, S. J., Lin, F. J. and Liu, K. K. (2003). "Organic carbon and nitrogen contents and their isotopic compositions in surficial sediments from the East China Sea shelf and the southern Okinawa Trough." Deep Sea Research Part II: Topical Studies in Oceanography 50(6-7): 1203-1217.

Kataoka, K. (2003). "Tracks of Tropical Cyclones in the Mid-latitudes of the Western North Pacific." Tenki 50(9): 5-14.

Kilpatrick, K. A., Podestá, G. P. and Evans, R. (2001). "Overview of the NOAA/NASA advanced very high resolution radiometer Pathfinder algorithm for sea surface temperature and associated matchup database." Journal of Geophysical Research 106(C5): 9179-9197.

Kinjo, K., Higa, E. and Oshiro, Y. (2006). "Nutrients State in Coral Reef Coastal Sea Area around Okinawa." Annual Report of Okinawa Prefectural Health and Environmental Institute 40: 107-113.

Kinjo, K., Higa, E. and Uehara, M. (2005). "Transition of Sediment of Red Soil on Seabed and Its Impact on Corals." Annual Report of Okinawa Prefectural Health and Environmental Institute 39: 63-74.

Kiyomoto, Y., Iseki, K. and Okamura, K. (2001). "Ocean Color Satellite Imagery and Shipboard Measurements of Chlorophyll a and Suspended Particulate Matter Distribution in the East China Sea." Journal of Oceanography 57: 37-45.

Kobashi, F. and Kawamura, H. (2001). "Variation of sea surface height at periods of 65-220 days in the subtropical gyre of North Pacific." Journal of Geophysical Research 106(26): 817-831.

Kochi, R. (2003). River in Okinawa. Vanishing mountains, rivers and ocean in Okinawa. Okinawa Education Culture Center and Environment and Pollution Education Committee, Okinawa Jiji Shuppan.

Kumar, A., Yang, F., Goddard, L. and Schubert, S. (2004). "Differing Trends in the Tropical Surface Temperatures and Precipitation over Land and Oceans." Journal of Climate 17(3): 653-664.

Lau, K. M. and Weng, H. (2001). "Coherent Modes of Global SST and Summer Rainfall over China: An Assessment of the Regional Impacts of the 1997-98 El Nino." Journal of Climate 14: 1294-1308.

Lau, K. M. and Wu, H. T. (2001). "Principal Modes of Rainfall-SST Variability of the Asian Summer Monsoon: A Reassessment of the Monsoon-ENSO Relationship." Journal of Climate 14(13): 2880-2895.

Lau, K. M. and Yang, S. (1996). "The Asian monsoon and predictability of the tropical ocean-atmosphere system." Quarterly Journal - Royal Meteorological Society 122: 945-957.

Lau, K.-M. and Chang, C.-P. (1987). Planetary scale aspects of the winter monsoon and atmospheric teleconnections. Monsoon Meteorology, Oxford University Press: 161-201.

Lau, K.-M. and Li, M.-T. (1984). "The Monsoon of East Asia and its Global Associations - A Survey." Bulletin of the American Meteorological Society 65(2): 114-125.

Lau, K.-M. and Wu, H.-T. (2007). "Detecting trends in tropical rainfall characteristics, 1979-2003." International Journal of Climatology 27: 979-988.

Lee, H.-J. and Chao, S.-Y. (2003). "A climatological description of circulation in and around the East China Sea." Deep Sea Research Part II: Topical Studies in Oceanography 50(6-7): 1065-1084.

Levitus, S., Antonov, J. I., Boyer, T. P. and Stephens, C. (2000). "Warming of the World Ocean." Science 287(5461): 2225-2229.

Li, C. (1990). "Interaction between anomalous winter monsoon in East Asia and El Niño events." Advances in Atmospheric Science 7: 36-46.

Lighthill, J., Holland, G., Gray, W., Landsea, C., Craig, G., Evans, J., Kurihara, Y. and Guard, C. (1994). "Global climate change and tropical cyclone." Bulletin of the American Meteorological Society 75: 2147-2157.

Lillesand, Thomas (1999). Remote sensing and image interpretation, Ralph W. Kiefer, 4th ed, John Wiley & Sons, Inc.

Limsakul, A., Saino, T., Midorikawa, T. and Goes, J. I. (2001). "Temporal variations in lower trophic level biological environments in the northwestern North Pacific Subtropical Gyre from 1950 to 1997." Progress In Oceanography 49(1-4): 129-149.

Lin, C.-Y., Shyu, C.-Z. and Shih, W.-H. (1992). "The Kuroshio fronts and cold eddies off northeastern Taiwan observed by NOAA-AVHRR imageries." Terrestrial Atmospheric and Oceanic Science 3: 225-242.

Lin, I., Liu, W. T., Wu, C.-C., Wong, G. T. F., Hu, C., Chen, Z., Liang, W.-D., Yang, Y. and Liu, K.-K. (2003b). "New evidence for enhanced ocean primary production triggered by tropical cyclone." Geophysical Research Letters 30(13): 1718, doi:10.1029/2003GL17141.

Lin, I.-I., Liu, W. T., Wu, C.-C., J.C.H.Chiang and Sui, C.-H. (2003a). "Satellite observations of modulation of surface winds by typhoon-induced upper ocean cooling." Geophysical Research Letters 30(3): 1131,doi:10.1029/2002GL015674.

Lin, I.-I., Wu, C.-C., Emanuel, K. A., Lee, I.-H., Wu, C.-R. and Pun, I.-F. (2005). "The Interaction of Supertyphoon Maemi (2003) with a Warm Ocean Eddy." Monthly Weather Review 133: 2635–2649.

Lindzen, R. S. and Nigam, R. S. (1987). "On the role of sea surface temperature gradients in forcing low level winds and convergence in the tropics." Journal of the Atmospheric Sciences 44: 2418-2436.

Liu, K. K., Chao, S. Y., Shaw, P. T., Gong, G. C., Chen, C. C. and Tang, T. Y. (2002). "Monsoon-forced chlorophyll distribution and primary production in the South China Sea: observations and a numerical study." Deep Sea Research Part I: Oceanographic Research Papers 49(8): 1387-1412.

Lough, J. M. (2000). Perspectives on Global Climate Change and Coral Bleaching: 1997-1998 Sea Surface Temperature at Local to Global Scales. Proceedings of the Japanese Marine Science and Technology Center International Coral Reef Symposium, Yokosuka, Japan.

Loya, Y., Sakai, K., Yamazato, K., Nakano, Y., Sambali, H. and van Woesik, R. (2001). "Coral bleaching: the winners and the losers." Ecology Letters 4(2): 122-131.

Lungu, T., Ed. (2006). SeaWinds Science Data Product User's Manual Version 2.0, Jet Propulsion Laboratory.

Marra, J., Bidigare, R. R. and Dickey, T. D. (1990). "Nutrients and mixing, chlorophyll and phytoplankton growth." Deep-Sea Research 37: 1427-1450.

Martinez, J. I., De Deckker, P. and Chivas, A. R. (1997). "New estimates for salinity changes in the Western Pacific Warm Pool during the Last Glacial Maximum: Oxygen-isotope evidence." Marine Micropaleontol 32: 311-340.

Mask, A. C. and O'Brien, J. J. (1998). "Wind-driven effects on the Yellow Sea Warm Current." Journal of Geophysical Research 103(C13): 30,713-30,729.

Massel, S. R. and Done, T. J. (1993). "Effects of cyclone waves on massive coral assemblages on the Great Barrier Reef: meteorology, hydrodynamics and demography." Coral Reefs 12: 153-166.

Matsumoto, S., Yoshimizu, S. and Takenchi, M. (1970). "On the structure of "Baiu" front and the associated intermediate scale disturbances in the lower atmosphere." Journal of the Meteorological Society of Japan 48: 479-491.

McClain, E. P., Pichel, W. G. and Walton, C. C. (1985). "Comparative performance of AVHRR-based multichannel sea surface temperatures." Journal of Geographical Research 90(11): 587-11, 601.

McGillicuddy, D. J. and Robinson, A. R. (1997). "Eddy-induced nutrient supply and new production in the Sargasso Sea." Deep Sea Research Part I: Oceanographic Research Papers 44(8): 1427-1450.

McLaughlin, C. J., Smith, C. A., Buddemeier, R. W., Bartley, J. D. and Maxwell, B. A. (2003). "Rivers, runoff, and reefs." Global and Planetary Change 39(1-2): 191-199.

McMillin, L. M. (1975). "Estimation of sea surface temperatures from two infrared window measurements with different absorption." Journal of Geographical Research 80: 5113-5117.

Mesaki, S. (1985). Coral reefs and Karsts. Explore the Ryukyu Arc, Okinwa Aki-shobo: 69-138.

Meskhidze, N., Chameides, W. L., Nenes, A. and Chen, G. (2003). "Iron mobilization in mineral dust: Can anthropogenic SO2 emissions affect ocean productivity?" Geophysical Research Letters 30(21): 2085.

Michaels, A. F., Knap, A. H., Dow, R. L., Gundersen, K., Johnson, R. J., Sorensen, J., Close, A., Knauer, G. A., Lohrenz, S. E., Asper, V. A., Tuel, M. and Bidigare, R. (1994). "Seasonal patterns of ocean biogeochemistry at the U.S. JGOFS Bermuda Atlantic time-series study site." Deep Sea Research Part I: Oceanographic Research Papers 41(7): 1013-1038.

Mihara, M. (2001). "SW--Soil and Water: Nitrogen and Phosphorus Losses due to Soil Erosion during a Typhoon, Japan." Journal of Agricultural Engineering Research 78(2): 209-216.

Milliman, J. D. and Kao, S.-J. (2005). "Hyperpycnal Discharge of Fluvial Sediment to the Ocean: Impact of Super-Typhoon Herb (1996) on Taiwanese Rivers." Journal of Geology 113: 503-516.

Milliman, J. D., Shen, H.-T., Yang, Z.-S. and Meade, R. H. (1985). "Transport and deposition of river sediment in the Changjiang estuary and adjacent continental shelf." Continental Shelf Research 4(37-45).

Ministry of Education, Culture, Sports, Science and Technology (2006). High precision and resolution climate modelling. Research and Development Bureau.

Mitchell, B. G. (1994). "Coastal zone color scanner retrospective." Journal of Geophysical Research 99: 7291-7292.

Mitchell, B. G. and Holm-Hansen, O. (1991). "Bio-optical properties of Antarctic Peninsula waters: Differentiation from temperate ocean models." Deep Sea Research 38(39): 1009-1028.

Morales, C. E., Blanco, J. L., Braun, M., Reyes, H. and Silva, N. (1996). "Chlorophyll-a distribution and associated oceanographic conditions in the upwelling region off northern Chile during the winter and spring 1993." Deep Sea Research Part I: Oceanographic Research Papers 43(3): 267-289.

Nadaoka, Nadaoka, K., Nihei, Nihei, Y., Wakaki, Wakaki, K., Kumano, Kumano, R., Kakuma, Kakuma, S., Moromizato, Moromizato, S., Omija, Omija, T., Iwao, Iwao, K., Shimoike, Shimoike, K., Taniguchi, Taniguchi, H., Nakano, Nakano, Y., Ikema and Ikema, T. (2001a). "Regional variation of water temperature around Okinawa coasts and its relationship to offshore thermal environments and coral bleaching." Coral Reefs 20(4): 373-384.

Nadaoka, K., Nihei, Y., Kumano, R., Yokobori, T., Omija, T. and Wakaki, K. (2001b). "A field observation on hydrodynamic and thermal environments of a fringing reef at Ishigaki Island under typhoon and normal atmospheric conditions." Coral Reefs 20(4): 387-398.

Nadaoka, K. and Tamura, H. (1992). "LANDSAT/TM-Based Analysis of the Problems Related to the Red-Silt Outflow from the Okinawa Island." Journal of the Remote Sensing Society of Japan 12(3): 3-19.

Naderi, F. M., Freilich, M. H. and Long, D. G. (1991). "Spaceborne Radar Measurement of Wind Velocity Over the Ocean - An Overview of the NSCAT Scatterometer System." Proc. IEEE 79: 6.

Nakamoto, S., Kumar, S. P., Oberhuber, J. M., Ishizaka, J., Muneyama, K. and Frouin, R. (2001). "Response of the equatorial Pacific to chlorophyll pigment in a mixed layer

isopycnal ocean general circulation model." Geophysical Research Letters 28(10): 2021-2024.

Nakano, Y. (2002). Physiological response of hermatypic corals to environmental loads. Coral Reef Studies in Japan. T. Nakamori. Tokyo, Japanese Coral Reef Society: 43-50.

Nakano, Y. (2004). Global environmental change and coral bleaching. Coral Reef of Japan, Japan Wildlife Research Center: 42-28.

Nakasone, K., Higa, E., Mitsumoto, H. and Omija, T. (1998). "Estimation of Soil Loss in Okinawa Prefecture (II)." Annual Report of Okinawa Prefectural Institute of Health and Environment 32: 67-71.

Nakasone, K., Omija, T., Mitsumoto, H., Uehara, M. and Oshiro, T. (2000). "Monitoring Water Pollution Caused by Reddish Soil Run-off." Annual Report of Okinawa Prefectural Institute of Health and Environment 34: 85-95.

Nakazawa, T. (2000). "MJO and tropical cyclone activity during 1997/98 ENSO." Advances in Space Research 25(5): 953-958.

Nicol, S., Pauly, T., Bindoff, N. L., Wright, S., Thiele, D., Hosie, G. W., Strutton, P. G. and Woehler, E. (2000). "Ocean circulation off east Antarctica affects ecosystem structure and sea-ice extent." Nature 406(6795): 504-507.

Ning, X., Liu, Z. and Cai, Y. (1998). "Physicobiological oceanographic remote sensing of the East China Sea: Satellite and in situ observations." Journal of Geophysical Research 103(C10): 21,623-26,635.

Nishikawa, J., Tsuda, A., Ishigaki, T. and Terazaki, M. (1995). "Distribution of euphausiids in the Kuroshio front and warm water tongue with special reference to the surface aggregation of Euphausia pacifica." Journal of Plankton Research 17(3): 611-629.

Norris, E. A. (1993). Global marine biological diversity: a strategy for building conservation into decision making. Washington, Island Press.

Nozaki, F., Higaki, M. and Kono, N. (2003). "Unusual Tides induced by Mesoscale Eddy at Nansei Islands." Umi to Sora 79(1): 39-49.

Ogura, Y. (1999). General Meteorology, University of Tokyo Press.

Ohnuki, Y. and Shimizu, A. (2004). "Experimental studies on rain splash erosion of forest soils after clearing in Okinawa using an artificial rainfall apparatus." Journal of Forest Research 9(2): 101-109.

Okinawa Construction Technology Center (2003). Rivers and Ocean in Okinawa. OPG River Section, OPG Dam Bureau, Northern Civil Engineering Bureau, Okinawa Construction

Technology Center (2003). Rivers and Ocean in Okinawa. OPG River Section, OPG Dam Bureau, Northern Civil Engineering Bureau.

Okinawa Prefecture Government (2004). "White Paper of the Environment of Okinawa."

Okinawa Prefecture Government (2006). Annual Population Estimates. Statistic Section: 1-14.

Okinawa Prefecture Government Department of Agriculture Forestry Fisheries (2007). "Agriculture, Forestry and Fisheries in Okinawa."

Okinawa Prefecture Government River Section (1998). "Report on the observation of the hydrology."

Okinawa Prefecture Government River Section (1999). "Report on the observation of the hydrology."

Okinawa Prefecture Government River Section (2000). "Report on the observation of the hydrology."

Okinawa Prefecture Government River Section (2001). "Report on the observation of the hydrology."

Okinawa Prefecture Government River Section (2002). "Report on the observation of the hydrology."

Okinawa Prefecture Government River Section (2003). "Report on the observation of the hydrology."

Okinawa Prefecture Government River Section (2004). "Report on the observation of the hydrology."

Okinawa Prefecture Government River Section (2005a). "Report on the observation of the hydrology."

Okinawa Prefecture Government River Section (2005b). "Okinawa Landslide Hazard Map."

Okinawa Prefecture Government Statistic Section (1999). "Okinawa Prefecture Statistics FY1999."

Okinawa Prefecture Government Statistic Section (2001). "Okinawa Prefecture Statistics FY2001."

Okinawa Prefecture Government Statistic Section (2005). "Okinawa Prefecture Statistics FY2005."

Omija, T. (1985). "Survey on Water Pollution by Reddish Soil in Okinawa -The Present Situation of Water Pollution in Northern Okinawa Island-." Annual Report of Okinawa Prefectural Institute of Health and Environment 18: 71-86.

Omija, T. (1986). "Red soil pollution in the cobalt blue Okinawan ocean." Nature Preservation 289: 8-11.

Omija, T. (1987). "Survey on Pollution by Reddish Soil in Okinawa - A Convenient Measuring Method for Reddish Soil in Sediment and Reddish Soil Levels in Okinawa." Annual Report of Okinawa Prefectural Institute of Health and Environment 20: 100-110.

Omija, T. (1991). Present status on red soil problem. Symposium on Creating Prosperous Okinawan Ocean, Naha City, Okinawa Prefecture Government Fishery Industry Association.

Omija, T. (1992). "Water Pollution Caused by Reddish Soil Erosion on the Okinawa Island." Annual Report of Okinawa Prefectural Institute of Health and Environment 26: 87-96.

Omija, T. (2004). Terrestrial inflow of soils and nutrients. Coral Reefs of Japan. The Japanese Coral Reef Society and Ministry of the Environment. Tokyo, Ministry of the Environment: 64-68.

Omija, T., Furugen, K. and Futenma, T. (1994). "The Movement of Accumulated Reddish Soil in The Coastal Sea Caused by Waves of Typhoons and Monsoon." Proceedings of the 28th Annual Meeting of Japan Society on Water Environment: 168-169.

Omija, T., Higa, E., Nakasone, K. and Hiroaki, M. (2002). "Comparison of the Accumulated Soil in Okinawa Coastal Sea before and after the Enforcement of Red Soil Erosion Prevention Ordinance." Annual Report of Okinawa Prefectural Institute of Health and Environment 36: 77-84.

Omija, T. and Ikema, N. (1990). "Present Situation of Red Soil Pollution around the Island of Okinawa." Journal of Okinawa Public Health 21: 1-15.

Omija, T., Nakasone, K., Mitsumoto, H. and Higa, E. (2003). Monitoring of Terrestrial Pollutants into Coral Reef. Report on Coral Reef Survey (contract research of the Cabinet Office), Research Institute for Subtropics: 86-102.

Omija, T., Nakasone, K., Mitsumoto, H. and Kobayashi, T. (1999). "Effect of Accumulated Reddish Soil on Coral II." Annual Report of Okinawa Prefectural Institute of Health and Environment 33: 111-120.

Omija, T., Nakasone, K., Mitsumoto, H., Uehara, M. and Oshiro, T. (2000). "Comparison of Sediment-resistance of Corals with Bleaching-resistance." Annual Report of Okinawa Prefectural Institute of Health and Environment 34: 69-76.

Onaga, K., Komesu, R. and Arakaki, A. (1999). "The Outline of Red Soil Loss and Erosion Control Measure in Okinawa." The Science Bulletin of the Faculty of Agriculture, University of the Ryukyus 46: 71-82.

Onaga, K. and Yoshinaga, A. (1983). Survey on the mechanism of red soil run-off, Okinawa Association: 68-69.

O'Reilly, J. E., Maritorena, S., Mitchell, B. G., Siegel, D. A., Carder, K. L., Garver, S. A., Kahru, M. and MacClain, C. (1998). "Ocean color chlorophyll algorithms for SeaWiFS." Journal of Geophysical Research 103(No. C11): 24,937-24,953.

Otero, M. P. and Siegel, D. A. (2004). "Spatial and temporal characteristics of sediment plumes and phytoplankton blooms in the Santa Barbara Channel." Deep Sea Research Part II: Topical Studies in Oceanography 51(10-11): 1129-1149.

Pan, Y. Q., Su, J. L. and Xu, D. R. (1991). "Oceanographic features on the northern shelf of Taiwan in summer and winter." The Research Issue on Kuroshio Project (2), China Ocean Press: 126-135.

Paringit, E. C. and Nadaoka, K. (2003). "Sediment yield modelling for small agricultural catchments: land-cover parameterization based on remote sensing data analysis." Hydrological Processes 17(9): 1845-1866.

Penaflor, E. L., Villanoy, C. L., Liu, C.-T. and David, L. T. (2007). "Detection of monsoonal phytoplankton blooms in Luzon Strait with MODIS data." Remote Sensing of Environment 109(4): 443-450.

Perry, K. L., Ed. (2000). QuikSCAT science data product user's manual ver.2.0. Pasadena, CA, Jet Propulsion Laboratory, California Institute of Technology.

Pinazo, C., Millet, B., Marsaleix, P., Estournel, C., Kondrachoff, V. and Vehil, R. (2001). "Phytoplankton variability in summer in the northwestern Mediterranean: Modelling of the wind and freshwater impacts." Journal of Coastal Research 17(1): 146-161.

Pu, Z., Tao, W.-K., Braun, S., Simpson, J., Jia, Y., Halverson, J., Olson, W. and Hou, A. (2002). "The Impact of TRMM Data on Mesoscale Numerical Simulation of Supertyphoon Paka." Monthly Weather Review 130(10): 2448-2458.

Qiu, B. (1999). "Seasonal Eddy Field Modulation of the North Pacific Subtropical Countercurrent: TOPEX/Poseidon Observations and Theory." Journal of Physical Oceanography 29(10): 2471-2486.

Ramage, C. S. (1971). Monsoon meteorology. New York, Academic Press.

Richman, M. B. (1986). "Rotation of principal components." International Journal of Climatology 6(3): 293-335.

Roberts, C. M., McClean, C. J., Veron, J. E. N., Hawkins, J. P., Allen, G. R., Mcallister, D. E., Mitterrneier, C. G., Schueler, F. W., Spalding, M., Wells, F., Vynne, C. and Werner, T. B. (2002). "Marine Biodiversity Hotspots and Conservation Priorities for Tropical Reefs." Science 295: 1280-1284.

Rodgers, E. B., Adler, R. F. and Pierce, H. F. (2000). "Contribution of Tropical Cyclones to the North Pacific Climatological Rainfall as Observed from Satellites." Journal of Applied Meteorology 39(10): 1658-1678.

Ryan, B. F., Watterson, I. G. and Evans, J. L. (1992). "Tropical cyclone frequencies inferred from Gray's yearly genesis parameter: validation of GCM tropical climates." Geophysical Research Letters 19: 1831-1834.

Sakai, K. and Nishihira, M. (1991). "Immediate effect of terrestrial runoff on a coral community near a river mouth in Okinawa." Galaxia 10(2): 125-134.

Sakai, K. and Osawa, K. (2005). "Soil Runoff Analysis Using the WEPP Model in Okinawa, Japan." American Society of Agricultural and Biological Engineering Annual Meeting: 052015.

Shen, S. and Lau, K.-M. (1995). "Biennial oscillation with the East Asian summer monsoon and tropical sea surface temperatures." Journal of the Meteorological Society of Japan 73: 105-124.

Shiah, F.-K., Chung, S.-W., Kao, S.-J., Gong, G.-C. and Liu, K.-K. (2000). "Biological and hydrographical responses to tropical cyclones (typhoons) in the continental shelf of the Taiwan Strait." Continental Shelf Research 20(15): 2029-2044.

Smith, S. V. and Buddemeier, R. W. (1992). "Global change and coral reef ecosystems." Annual Reviews - Ecology, Evolution, and Systematics 23: 89-118.

Smith, T. M., Reynolds, R. W., Livezey, R. E. and Stokes, D. C. (1996). "Reconstruction of Historical Sea Surface Temperatures Using Empirical Orthogonal Functions." Journal of Climate 9(6): 1403-1420.

Solomon, S., Qin, D., Manning, M., Marquis, M., Averyt, K., Tignor, M. M. B., Miller, H. L. and Chen, Z. (2007). Climate Change 2007: The Physical Scientific Basis. Cambridge, Cambridge University Press.

Son, S., Platt, T., Bouman, H. and Lee, D. (2006). "Satellite observation of chlorophyll and nutrients increase induced by Typhoon Megi in the Japan/East Sea." Geophysical Research Letters 33: L05607.

Statistics Bureau (2000). "Annual Report of National Census." Director-General for Policy Planning (Statistical Standards) & Statistical Research and Training Institute.

Statistics Bureau (2005). "Annual Report of National Census." Director-General for Policy Planning (Statistical Standards) & Statistical Research and Training Institute.

Steele, M., Morley, R. and Ermold, W. (2001). "PHC: A Global Ocean Hydrography with a High-Quality Arctic Ocean." Journal of Climate 14(9): 2079-2087.

Strass, V. (1992). "Chlorophyll patchiness caused by mesoscale upwelling at fronts." Deep Sea Research 39(1A): 75-96.

Suga, T. and Hanawa, K. (1995). "Interannual Variations of North Pacific Subtropical Mode Water in the 137° Section." Journal of Physical Oceanography 25(5): 1012-1017.

Tada, K., Sakai, K., Nakano, Y., Takemura, A. and Montani, S. (2003). "Size-fractionated phytoplankton biomass in coral reef waters off Sesoko Island, Okinawa, Japan." J. Plankton Res. 25(8): 991-997.

Tan, C.K., Ishizaka, J., Matsumura, S., Yusoff, F., Mohamed, M., I., H. (2006) "Seasonal variability of SeaWiFS chlorophyll a in the Mallaca Strait in relation to Asian monsoon." Continental Shelf research 26: 168-178.

Tang, D. L., Kawamura, H. and Guan, L. (2004). "Long-time observation of annual variation of Taiwan Strait upwelling in summer season." Advances in Space Research 33(3): 307-312.

Tang, T. Y. and Yang, Y. J. (1993). "Low frequency current variability on the shelf break northeast of Taiwan." Journal of Oceanography 49: 193-210.

The Japanese Coral Reef Society and Ministry of the Environment (2004). Coral Reefs of Japan. Tokyo, Ministry of the Environment.

Thomas, A. C. (1999). "Seasonal distributions of satellite-measured phytoplankton pigment concentration along Chilean coast." Journal of Geophysical Research 104(NO. C11): 25,877-25,890.

Thomas, A. C., Carr, M.-E. and Strub, P. T. (2001). "Chlorophyll variability in eastern boundary currents." Geophysical Research Letters 28(18): 3421.

Thunell, R. C., Anderson, D., Gellar, D. and Miao, Q. (1994). "Sea surface temperature estimates for the tropical western Pacific during the last glaciation and their implications for the Pacific warm pool." Quaternary Research 41: 255-264.

Tsai, W., Graf, J. E., Winn, C., Huddleston, J. N., Dunbar, R. S., Freilich, M. H., Wentz, F. J., Long, D. G. and Jones, W. L. (1999). "Postlaunch Sensor Verification and Calibration of the NASA Scatterometer." IEEE Transactions Geoscience and Remote Sensing 37: 1517-1542.

Ujiie, H. (1991). History of the Ryukyu Arc. Coral Reefs of Okinawa. M. Nishihira (ed.). Urasoe, Okinawa Environmental Science Center: 16-34.

Ujiie, H., Tanaka, Y. and Ono, T. (1991). "Late Quaternary paleoceanographic record from the middle Ryukyu Trench slope." Marine Micropaleontology 18: 115-128.

Ujiie, H. and Ujiie, Y. (1999). "Late Quaternary course changes of the Kuroshio Current in the Ryukyu Arc region, northwestern Pacific Ocean." Marine Micropaleontology 37(1): 23-40.

United Nation Environment Programme (2004). Fifty key facts about seas and oceans. World Environment Day: Wanted! Seas and Oceans: Dead or Alive?, Barcelona, Spain.

United Nation Environment Programme World Conservation Monitoring Centre (2006). In the front line: shoreline protection and other ecosystem services from mangroves and coral reefs. Cambridge, UK, Cambridge Printers.

Veron, J. E. N. (1993). Corals of Australia and the Indo-Pacific, University of Hawaii Press.

Walker, N. D., Leben, R. R. and Balasubramanian, S. (2005). "Hurricane-forced upwelling and chlorophyll a enhancement within cold-core cyclones in the Gulf of Mexico." Geophysical Research Letters 32: L18610.

Walton, C. C. (1988). "Nonlinear multichannel algorithm for estimating sea surface temperature with AVHRR satellite data." Journal of Applied Meteorology 27: 115-124.

Walton, C. C., McClain, E. P. and Sapper, J. F. (1990). Recent changes in satellite based multichannel sea surface temperature algorithms. paper presented at Marine Technology Society Meeting MTS' 90, Washington, D. C.

Walton, C. C., Pichel, W. G. and Sapper, J. F. (1998). "The development and operational application of non-linear algorithms for the measurement of sea surface temperature

with the NOAA polar-orbiting environmental satellites." Journal of Geographical Research 103: 27, 999-28, 012.

Wang, B., Wu, R. G. and Fu, X. H. (2000). "Pacific-East Asian teleconnection: how does ENSO affect East Asian climate?" Journal of Climate 13(9): 1517-1536.

Wang, J. and Chern, C.-S. (1988). "On the Kuroshio branch in the Taiwan Strait during wintertime." Progressive Oceanography 21: 469-491.

Wang, S. and Shi, W. (1992). Different impacts of two kinds of ENSO events on the summer rainfall in China. On the Roles of the Oceans Regulating and Controlling Climate Variablity. Y. Zhang, et al. (ed.), Ocean Press: 76-87.

Webster, P. J. (1987a). The Elementary Monsoon. Monsoons. J. S. Fein and P. L. Stephens (eds.). Washington, D.C., John Wiley & Sons: 3-32.

Webster, P. J. (1987b). The Variable and Interactive Monsoon. Monsoons. J. S. Fein and P. L. Stephens (eds.). Washington, D.C, John Wiley & Sons: 269-330.

Webster, P. J., Holland, G. J., Curry, J. A. and Chang, H. R. (2005). "Changes in Tropical Cyclone Number, Duration, and Intensity in a Warming Environment." Science 309(5742): 1844-1846.

Webster, P. J. and Yang, S. (1992). "Monsoon and ENSO: Selectively interactive systems." Quarterly Journal - Royal Meteorological Society 118: 877-926.

Wentz, F. J., Ricciardulli, L., Hilburn, K. and Mears, C. (2007). "How Much More Rain Will Global Warming Bring?" Science 317(5835): 233-235.

West, K. and van Woesik, R. (2001). "Spatial and Temporal Variance of River Discharge on Okinawa (Japan): Inferring the Temporal Impact on Adjacent Coral Reefs." Marine Pollution Bulletin 42(10): 864-872.

Wilkinson, C. (2001). The 1997-1998 Mass Bleaching Event Around The World. Status of Coral Reefs of The World. C. Wilkinson, (ed.). Queensland, Australian Institute of Marine Science: 15-38.

Wilkinson, C. (2002). Status of Coral Reefs of the World: 2002. Townsville, Australia, Australian Institute of Marine Science.

Wilkinson, C. (2004). Status of Coral Reefs of the World: 2004 Volume 1. Townsville, Australia, Australian Institute of Marine Science.

Wilkinson, C. R. and Buddemeier, R. W. (1994). Global Climate Change and Coral Reefs: Implications for People and Reefs. Report of the UN EP-IOC-ASPEI-UCN Global Task Team on the Implications of Climate Change on Coral Reefs.

Woodward, E. M. S. and Rees, A. P. (2001). "Nutrient distributions in an anticyclonic eddy in the northeast Atlantic Ocean, with reference to nanomolar ammonium concentrations." Deep Sea Research Part II: Topical Studies in Oceanography 48: 775-793.

Xie, S.-P., Hafner, J., Tanimoto, Y., Liu, W. T., Tokinaga, H. and Xu, H. (2002). "Bathymetric effect on the winter sea surface temperature and climate of the Yellow and East China Seas." Geophysical Research Letters 20(24): 2228.

Xie, S.-P., Ishiwatari, M., Hashizume, H. and Takeuchi, K. (1998). "Coupled ocean-atmospheric waves on the equatorial front." Geophysical Research Letters 25: 3863-3866.

Xu, X., Hirata, E. and Shibata, H. (2004). "Effect of typhoon disturbance on fine litterfall and related nutrient input in a subtropical forest on Okinawa Island, Japan." Basic and Applied Ecology 5(3): 271-282.

Yamazato, K. (1999). "Coral bleaching in Okinawa, 1980 vs 1998." Galaxia 1: 83-87.

Yanagi, T., Takahashi, S., Hoshika, A. and Tanimoto, T. (1996). "Seasonal variation in the transport of suspended matter in the East China Sea." Journal of Oceanography 52(5): 539-552.

Yang, F., Kumar, A., Schlesinger, M. E. and Wang, W. (2003). "Intensity of Hydrological Cycles in Warmer Climates." Journal of Climate 16(14): 2419-2423.

Yasuda, I., Okuda, K. and Hirai, M. (1992). "Evolution of a Kuroshio warm-core ring - Variability of the hydrographic structure." Deep-Sea Research 39: 131-161.

Yoshinaga, A. (1986). Run-off mechanisms in constructed agriculture lands. Investigations on red soil run-off mechanisms and their countermeasures, Okinawa Association: 35-45.

Yoshinaga, A. (1987). Countermeasures for red soil run-off: from their run-off characteristics in rain water. Investigations on red soil run-off mechanisms and their countermeasures, Okinawa Association: 32-41.

Yuan, Y., J. Su. and Xia, S. (1987). "Diagnostic calculation of three-dimensional circulation in the East China Sea (summer 1984)." in Kuroshio Symposium Series, edited by X. Sun, pp. 45-53, China Ocean Press, Beijing.

Yuxiang, T. (1996). "Distributional Features and Seasonal Variations of Temperature Fronts in the East China Sea." Oceanologia Et Limnologia Sinica 27: 12-29.

Zhang, Y., Sperber, K. R. and Boyle, J. S. (1997). "Climatology and Interannual Variation of the East Asian Winter Monsoon: Results from the 1979-95 NCEP/NCAR Reanalysis." Monthly Weather Review 125(10): 2605-2619.

Zhao, B. (1991). "Mechanism on the direction turning of the Changjiang plume." Acta Oceanologica Sinica. 13: 600-610.

Zhao, M., Huang, C.-Y. and Wei, K.-Y. (2005). "A 28,000 Year Uk-37 Sea-Surface Temperature Record of ODP Site 1202B, the Southern Okinawa Trough." Terrestrial, Atmospheric and Oceanic Sciences 16(1): 45-56.

Zheng, G. M. and Tang, D. (2007). "Offshore and nearshore chlorophyll increases induced by typhoon winds and subsequent terrestrial rainwater runoff." Marine Ecology Progress Series 333: 61-74.

Zheng, Q. A. and Klemas, V. (1982). "Determination of winter temperature patterns, fronts, and surface currents in the Yellow Sea and East China Sea from satellite imagery." Remote Sensing of Environment 12: 201-218.

Zhou, Y., Gibo, S., Egashira, K., Onaga, K. and Maruyama, K. (1996). "Strength Characteristics of the Fractured-Mudstone and the Softened-Mudstone from Landslides in the Shimajiri-Group Area, Okinawa - Comparison of the Urasoe and the Yamakawa landslides -." Landslides, Journal of Japan Landslide Society 32(4): 26-33.

Zhu, C., Lee, W.-S., Kang, H. and Park, C.-K. (2005). "A proper monsoon index for seasonal and interannual variations of the East Asian monsoon." Geophysical Research Letters 32, L02811, doi: 10.1029/2004GL021295.

Appendix

A1.1 SST comparison between in-situ data and AVHRR

Fig. A1.1 shows the location of the sea temperature measurement location carried out by the OPG Department of Culture and Environment and corresponding pixel of the AVHRR SST data.

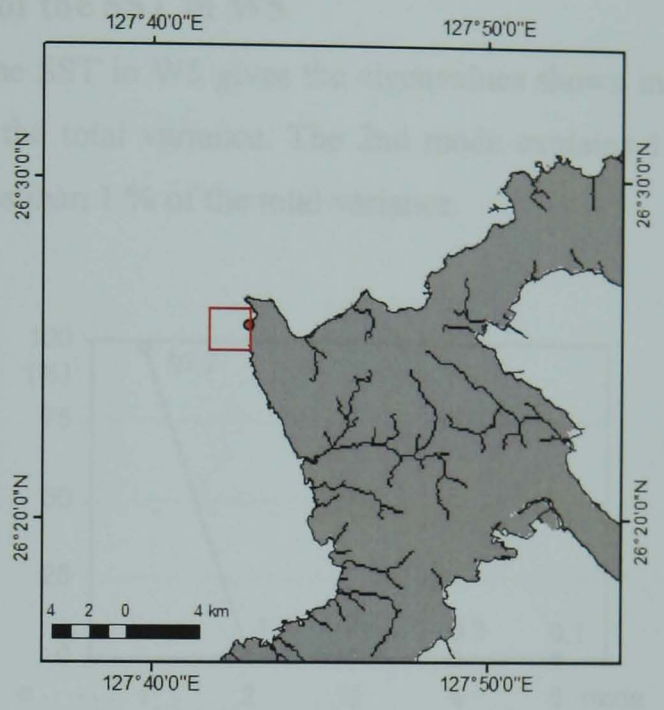

Fig. A1.1. Location of sea temperature measurement: the circle dot for the in-situ temperature measurement by the OPG Department of Culture and Environment and the square for a pixel of the AVHRR SST.

Table A1.1. SST difference between in-situ and AVHRR.

date	*A*: in-situ (°C)	In-situ measuring depth (m)	*B*: AVHRR SST (°C)	ΔT (°C) = *A* – *B*
12/05/1998	27.1	1	27.2	-0.1
11/08/1998	30.1	1	30.2	-0.1
16/06/1999	27.0	1	27.9	-0.9
10/10/2000	26.5	0.5	27.5	-1.0
13/03/2001	21.0	0.5	21.5	-0.5
01/07/2003	28.2	0.5	28.6	-0.4
29/09/2003	27.6	0.5	27.5	0.1
04/12/2003	23.7	0.5	23.9	-0.2
19/02/2004	21.0	0.5	21.4	-0.4
14/04/2005	22.0	0.5	22.6	-0.6
08/09/2005	28.0	0.5	28.7	-0.7
06/03/2006	21.6	0.5	21.9	-0.3

Mean ΔT = -0.4 °C, STD ΔT = 0.3 °C

In-situ measurement is carried out once a month at about noon ± 2 hours, at the depth of 0.5 1 m (grid reference is not available). In the comparison between this in-situ data and daily AVHRR SST for 1988 – 2006, there are 12 days which both measurement dates coincide (Table A1.1). The AVHRR SST is generally higher than the in-situ temperature, giving the mean difference (in-situ – AVHRR SST) of -0.4 °C.

A1.2 EOF analysis of the SST in W5

An EOF analysis of the SST in W5 gives the eigenvalues shown in Fig. A1.2. The 1st mode accounts for 97.8 % of the total variance. The 2nd mode explains 1.1 %, and the rest of the higher modes explain less than 1 % of the total variance.

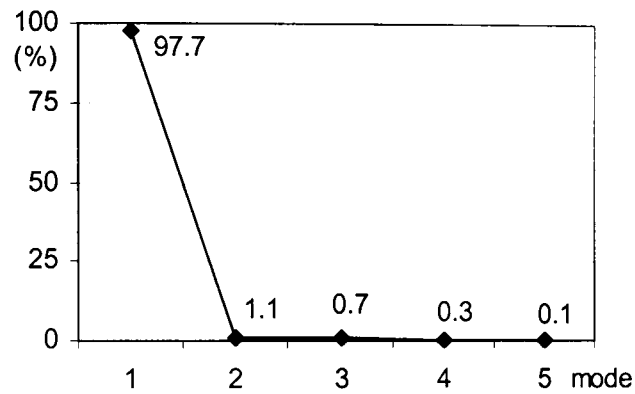

Fig. A1.2. Eigenvalues of the EOF SST in W5.

The eigenvectors and the temporal functions are shown in Fig. A1.3 and A1.4 respectively. As seen from the temporal function, the 1st mode has a clear annual cycle, indicating that solar radiation is a strong control on the SST variability in W5, as seen in other domains in Chapter 4. For the 2nd mode, the highest eigenvector of this mode is seen in R5 which is the closest point off the estuary of the largest river of Hija. However, a comparison between its temporal function and the monthly mean discharge of the NW and SW rivers does not show a correlation (Fig. A1.4.M2a). Other comparisons with northeasterly and its anomaly show no correlated relation, either. The 3rd mode, accounting for only 0.7 %, has several peaks in the spectra (Fig. A1.4.M3b) though, its temporal function shows a rather white noisy pattern (Fig. A1.4.M3a).

(W5)

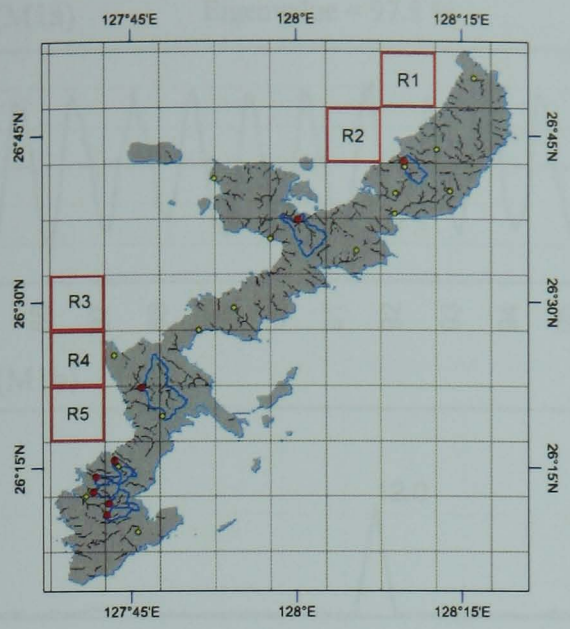

(M1)

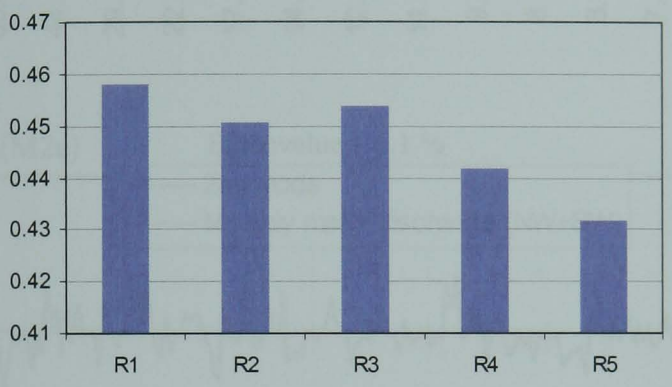

Eigenvalue = 97.7 %

(M2)

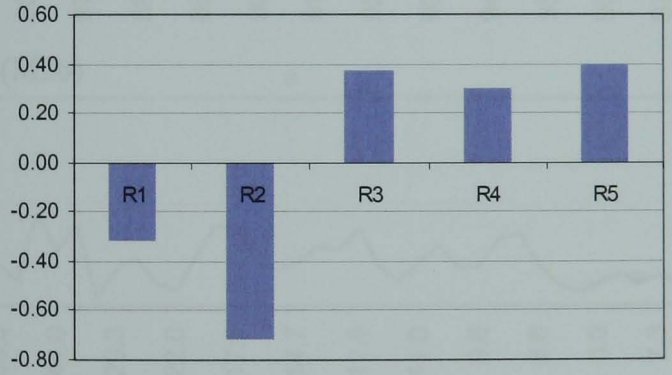

Eigenvalue = 1.1 %

(M3)

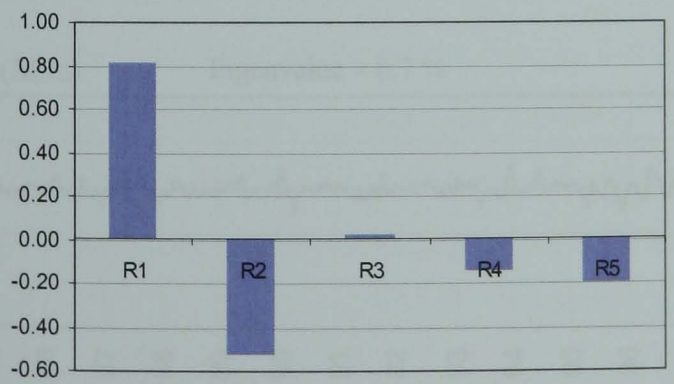

Eigenvalue = 0.7 %

Fig. A1.3. Eigenvectors of the SST EOF in W5: (W5) location of the 5 cells (R1 – R5) in the west coast, (M1) the 1st mode, (M2) the 2nd mode and (M3) the 3rd mode.

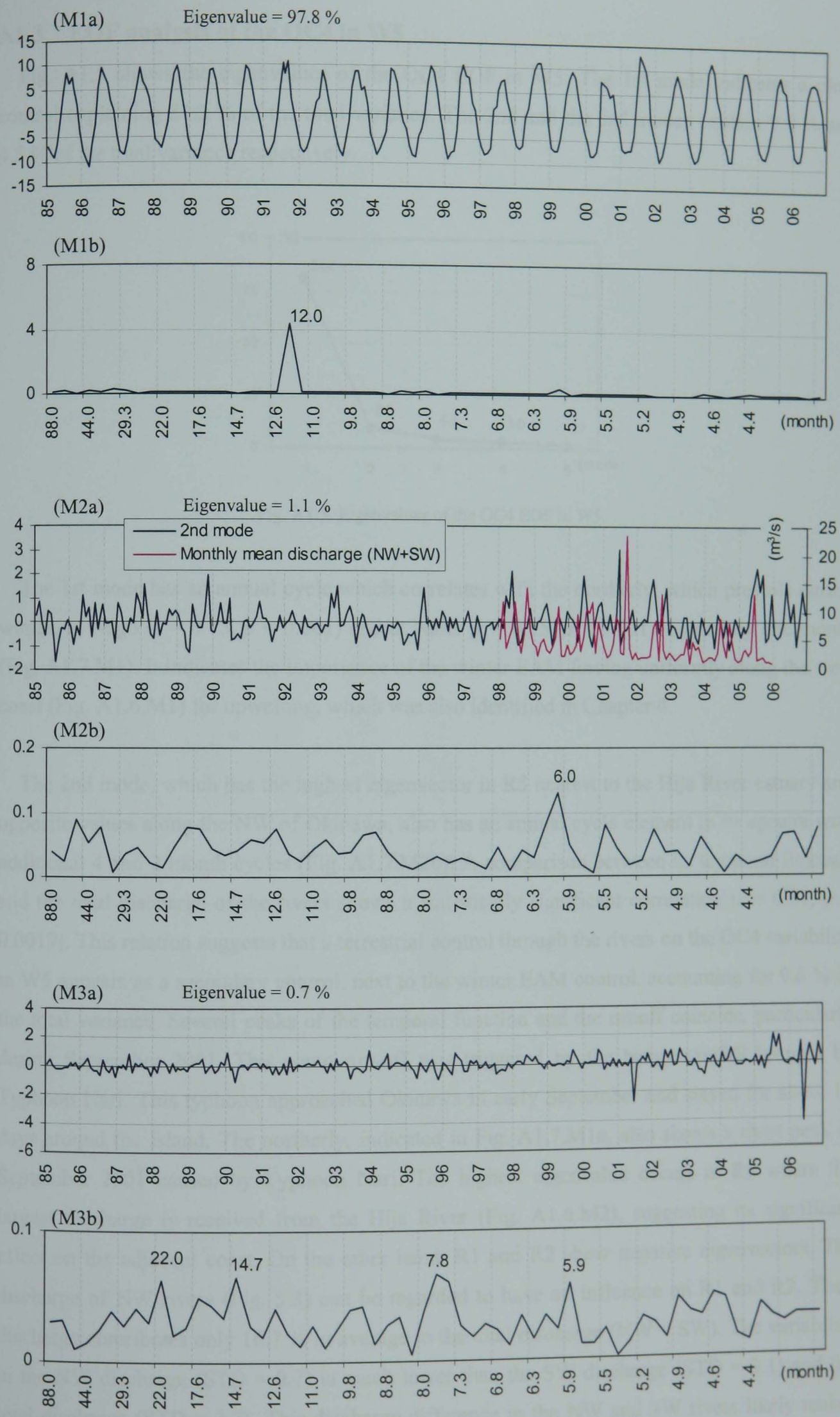

Fig. A1.4. (a) Temporal functions and (b) spectrum of the SST EOF in W5: (M1) the 1st mode, (M2) the 2nd mode and (M3) the 3rd mode.

A1.3 EOF analysis of the OC4 in W5

Fig. A1.5 shows the eigenvalues of the OC4 EOF in W5. The 1st mode indicates a clear control explaining 81.2 % of the total variance. The 2nd and the 3rd modes explain 9.6 % and 4.5 % of the total variance respectively.

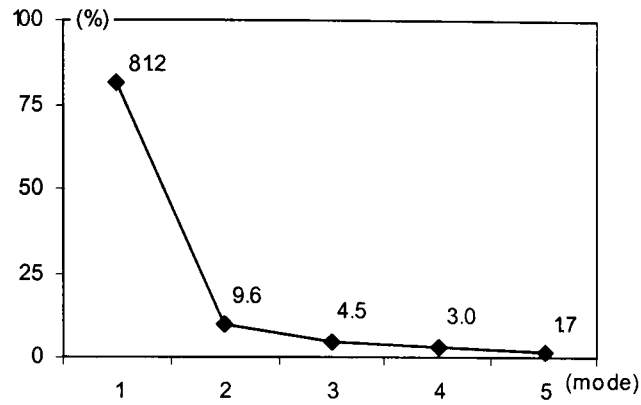

Fig. A1.5. Eigenvalues of the OC4 EOF in W5.

The 1st mode has an annual cycle which correlates with the northerly, which prevails during winter, at Nago ($r = 0.73$, $p < 0.001$) and at Naha ($r = 0.75$, $p < 0.001$), lagged by one month (Fig. A1.7.M1). It indicates the importance of the winter EAM forcing uniformly along the west coast (Fig. A1.6.M1) for upwelling, which was also identified in Chapter 4.

The 2nd mode, which has the highest eigenvector in R5 nearest to the Hija River estuary and opposite values along the NW of Okinawa, also has an annual cycle element in its spectra with additional 4 and 2 month cycles (Fig. A1.7.M2b). A comparison between its temporal function and the total discharge of the rivers shows a statistically significant correlation ($r = 0.31$, $p = 0.0019$). This relation suggests that a terrestrial control through the rivers on the OC4 variability in W5 appears as a secondary control, next to the winter EAM control, accounting for 9.6 % of the total variance. Several peaks of the temporal function and the runoff coincide, particularly during September 2001. This acute run-off was triggered by the heavy rainfall brought by Typhoon Nari. This typhoon approached Okinawa in early September and stayed for about 10 days around the Island. The northerly, indicated in Fig. A1.7.M1a, also shows a short peak in September 2001 caused by Typhoon Nari. The highest eigenvalue occurs in R5 where the largest discharge is received from the Hija River (Fig. A1.6.M2), suggesting its significant effect on the adjacent coast. On the other hand, R1 and R2 show negative eigenvectors. The discharge of NW rivers (Fig. 5.3) can be regarded to have an influence on R1 and R2. Their discharge contributes only 16.7 % in average to the total discharge (NW + SW). The variability in the NW discharge (STD = 0.7) is much lower than the SW discharge (STD = 3.1) and the total discharge (STD = 3.7). This discharge difference in the NW and SW rivers likely makes the difference in the 2nd mode eigenvectors of the NW (R1 and R2) and SW (R3 – R5) regions.

For the 3rd mode (4.5 % accountability), its temporal function shows no correlation with discharge or the winter EAM, suggesting other local effects offshore.

(W5)

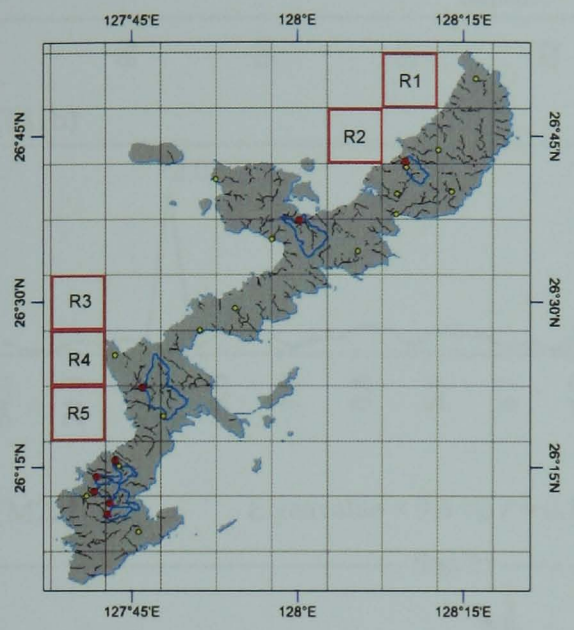

(M1)

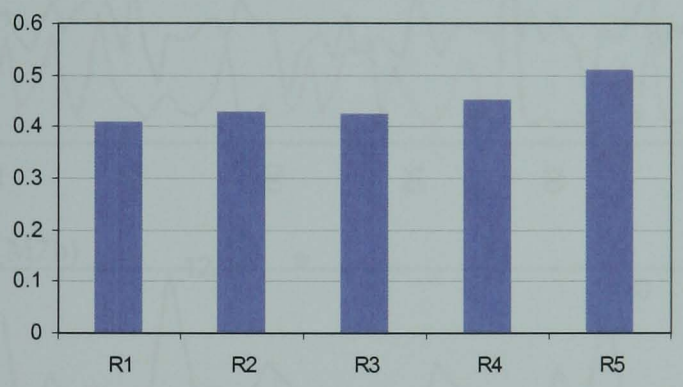

Eigenvalue = 81.2 %

(M2)

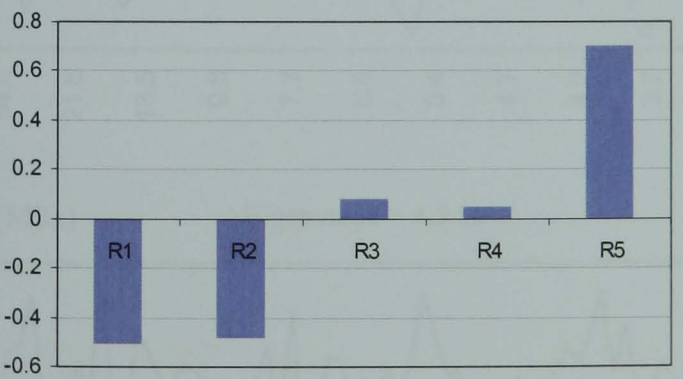

Eigenvalue = 9.6 %

(M3)

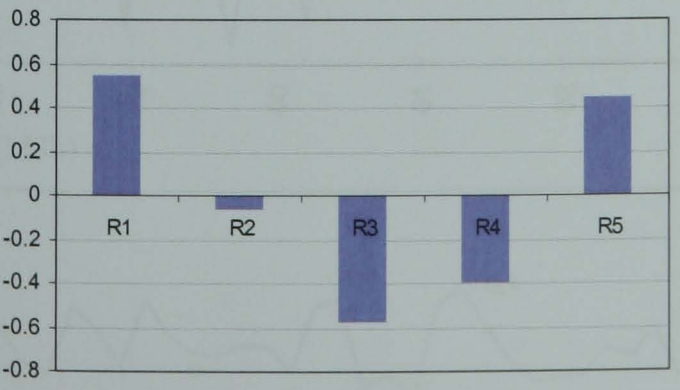

Eigenvalue = 4.5 %

Fig. A1.6. Eigenvectors of the OC4 EOF in W5: (W5) location of the 5 cells (R1 – R5) in the west coast, (M1) the 1st mode, (M2) the 2nd mode and (M3) the 3rd mode.

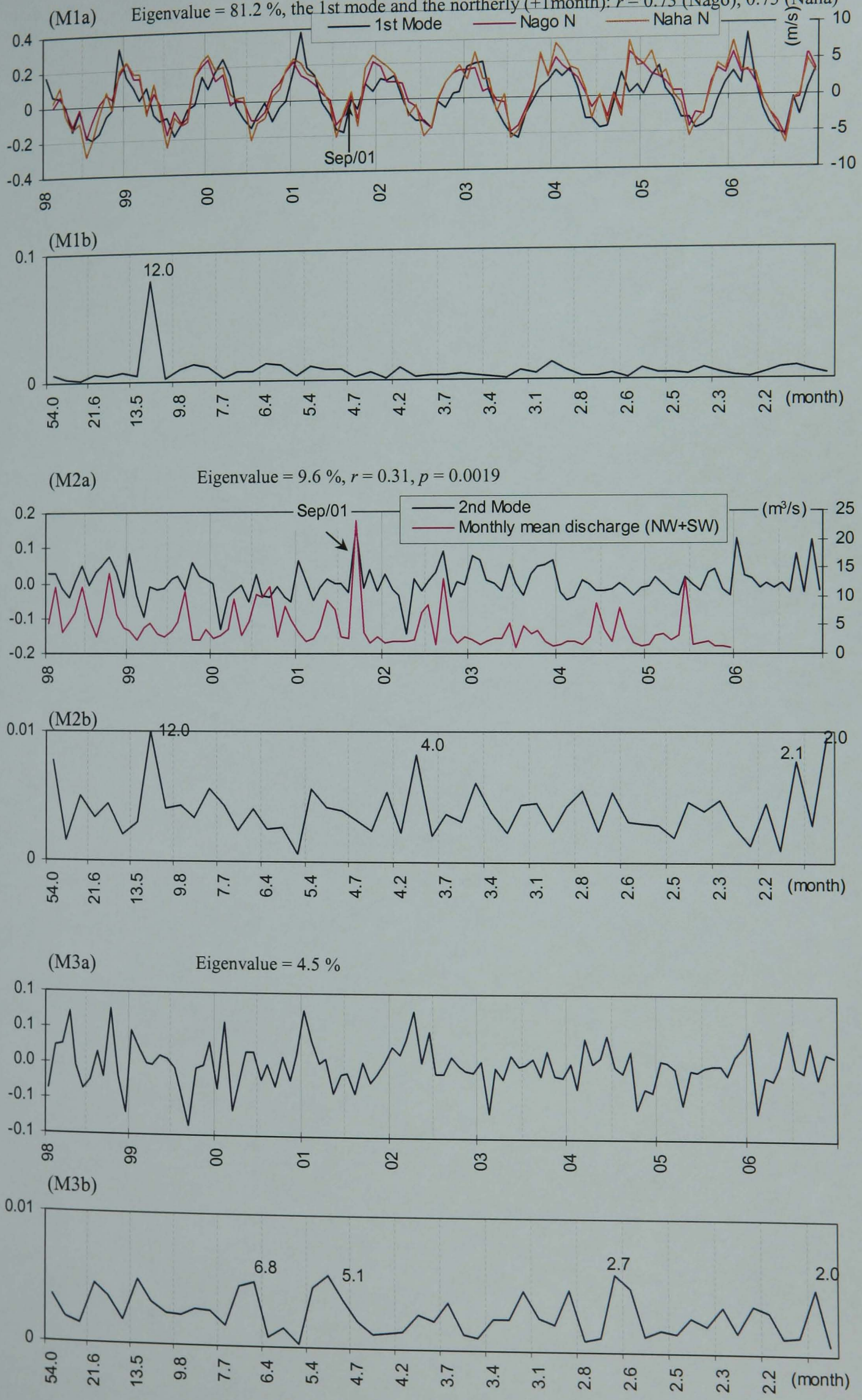

Fig. A1.7. (a) Temporal functions and (b) spectrum of the OC4 EOF in W5: (M1) the 1st mode, (M2) the 2nd mode and (M3) the 3rd mode.